# Local Calibration of the Mechanistic Empirical Pavement Design Guide for Kansas

by

Abu Ahmed Sufian

B.S., Bangladesh University of Engineering and Technology, 2013

A THESIS

submitted in partial fulfillment of the requirements for the degree

MASTER OF SCIENCE

Department of Civil Engineering
College of Engineering

KANSAS STATE UNIVERSITY
Manhattan, Kansas

2016

Approved by:

Major Professor
Dr. Mustaque Hossain

# Copyright

# Abstract

The Kansas Department of Transportation is transitioning from adherence to the 1993 American Association of State Highway and Transportation Officials (AASHTO) Pavement Design Guide to implementation of the new AASHTO Mechanistic-Empirical Pavement Design Guide (MEPDG) for flexible and rigid pavement design. This study was initiated to calibrate MEPDG distress models for Kansas. Twenty-seven newly constructed projects were selected for flexible pavement distress model calibration, 21 of which were used for calibration and six that were selected for validation. In addition, 22 newly constructed jointed plain concrete pavements (JPCPs) were selected to calibrate rigid models; 17 of those projects were selected for calibration and five were selected for validation. AASHTOWare Pavement ME Design (ver. 2.2) software was used for design analysis, and the traditional split sampling method was followed in calibration. MEPDG-predicted distresses of Kansas road segments were compared with those from Pavement Management Information System data. Statistical analysis was performed using the Microsoft Excel statistical toolbox. The rutting and roughness models for flexible pavement were successfully calibrated with reduced bias and accepted null hypothesis. Calibration of the top-down fatigue cracking model was not satisfactory due to variability in measured data, and the bottom-up fatigue cracking model was not calibrated because measured data was unavailable. AASHTOWare software did not predict transverse cracking for any projects with global values. Thus thermal cracking model was not calibrated. The JPCP transverse joint faulting model was calibrated using sensitivity analysis and iterative runs of AASHTOWare to determine optimal coefficients that minimize bias. The IRI model was calibrated using the generalized reduced gradient nonlinear optimization technique in Microsoft Excel Solver. The transverse slab cracking model could not be calibrated due to lack of measured cracking data.

# Table of Contents

# List of Figures

# List of Tables

# Acknowledgements

At the very beginning, I would like to pay my absolute homage to Almighty Allah for bestowing me with ability and courage to carry out this work and to live.

I acknowledge my sincerest appreciation and due gratitude to my major professor Dr. Mustaque Hossain for his continuous academic guidance, incredible mentorship, and relentless encouragement throughout my graduate studies.

I would like to thank Dr. Robert W. Stokes and Dr. Eric J. Fitzsimmons for being part of my thesis committee and for their inspirations.

I earnestly appreciate the financial support provided by the Kansas Department of Transportation (KDOT) for this unique research study.

I sincerely want to thank Shuvo Islam, my senior fellow graduate student, for all his help and support while conducting this study.

I am also very thankful to my graduate colleagues for their support and encouragement.

Last but not least, I wish to express my deepest respect and gratitude to my parents for their understanding, blessings, and love that helped me to be the human what I am today.

# Dedication

This thesis is dedicated to my parents, Mohammad Jahangir Alam and Mrs. Jotsna Jahangir, my elder sister, Dr. Yeasmin Sultana, and my cute little younger sister, Rifat Sultana.

# Preface

This thesis is authentic, unpublished and independent work by the author, Abu Ahmed Sufian. 

# Chapter 1 - Introduction

## 1.1 Background

The transportation infrastructure of the United States is comprised of a vast network of roads and highways. Paved roads, or pavements, account for the significant portion of this network. From the pavement structure design guide published by the American Association of State Highway and Transportation Officials (AASHTO) in 1993 to modern-day sophisticated AASHTOWare Pavement ME Design, all design procedures have been established and carried out to increase accuracy and reliability of the pavement design method.

### 1.1.1 Pavement Types

Historically, pavements have been classified into two broad categories. One category is flexible pavements, or hot-mix asphalt (HMA) pavements because a main constituent of this pavement is asphalt concrete. Another category is rigid (concrete) pavements, constructed primarily from Portland cement concrete (PCC). Rigid pavements can also be classified as jointed plain concrete pavement (JPCP), jointed reinforced concrete pavement (JRCP), continuously reinforced concrete pavement (CRCP), and prestressed concrete pavement (PCP) (Huang, 2009). Composite pavements, which are basically asphalt overlays on top of concrete pavements, are composed of both HMA and PCC. The HMA overlay is placed either as the final stage of initial construction or as a rehabilitation measure or safety treatment (TxDOT, 2011).

The United States currently has approximately 4.2 million miles of public roads, of which more than 1.4 million miles are unpaved and approximately 1.8 million miles are paved local roads with unknown pavement types. Of the remaining 960,000 miles of paved roads, approximately 794,000 miles are asphalt, 58,000 miles are concrete, and 108,000 miles are composite pavements (FHWA, 2014). Therefore, approximately 93 percent of paved roads are surfaced with asphalt and the remaining 7 percent are rigid pavements (NAPA, 2016).

The primary difference between flexible and rigid pavements is the mechanics of load distribution on the subgrade. Flexible pavements are composed of several layers of bituminous/aggregate materials that can effectively accommodate flexing so that the pavements can bend or deflect due to traffic load. However, in rigid pavements, applied load is distributed over a relatively wide area of soil due to the high modulus of elasticity and rigidity of the PCC

slab. Rigid pavements are considerably stiffer than flexible pavements due to high stiffness of the concrete slab (Khanum, 2005). Figures 1-1 and 1-2 show cross sections of flexible and rigid pavements, respectively.


**Figure 1-1: Components of a typical flexible pavement (TxDOT, 2011)**

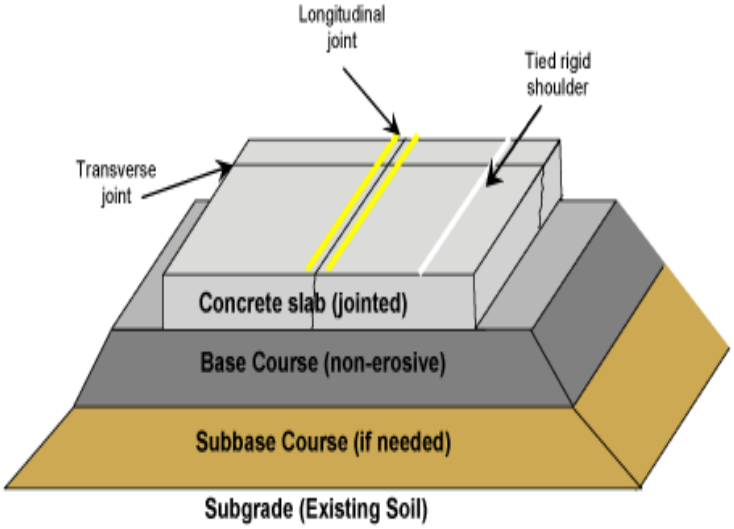


**Figure 1-2: Components of a typical rigid pavement (TxDOT, 2011)**

### 1.1.2 Pavement Design

In 1958 the American Association of State Highway Officials (AASHO) sponsored a multimillion dollar construction project in Ottawa, Illinois, known as the AASHO road test. The purpose of the project was to study the performance of asphalt and PCC pavements under different traffic loading and speed conditions. The project also quantified the amount of damage on the test sections caused by trucks for tax purposes. Valuable information derived from the project increased knowledge of pavement structural design and performance, load equivalencies, and climate effects. However, limitations such as use of a single subgrade layer material type and a

single climatic region, as well as truck axle configurations and tire pressure of 1958 necessitated careful, regulated use of these information.

Based on AASHO road test output, AASHTO developed an empirical structural design tool to design flexible and rigid pavements. This tool was known as the AASHTO pavement design guide. The first version of this guide was published in 1972, and three subsequent versions were developed in 1986, 1993, and 1996. The 1993 AASHTO pavement design guide was considered as a valuable design tool and adopted by 48 state highway agencies (Abdullah, 2015).

The design system of the 1993 AASHTO guide was purely empirical and established only on material properties, traffic, and climatic of the test location. So various extrapolations were required to modify and improve the empirical equation. Therefore, the AASHTO Joint Task Force on Pavements (JTFP), (responsible for the development and implementation of pavement design technologies) initiated an effort in 1996 to develop an improved AASHTO pavement design guide by the end of year 2002 (Kim, 2011). The outcome of that effort was National Cooperative Highway Research Program (NCHRP) Project 1-37 A, "Development of the 2002 Guide for Design of New and Rehabilitated Pavement Structures: Phase II." The primary objective was to develop a design guide that incorporated existing state-of-the-practice mechanistic-based models and design procedures.

The first edition of the Mechanistic-Empirical Pavement Design Guide (MEPDG) became available in 2004. The mechanistic portion of the MEPDG estimates pavement critical responses, such as stresses, strains, and deflections. This is based on traffic loading, layer material properties, and climatic conditions. The empirical portion of the design method, however, links the performance between laboratory and field. Thereby reflecting local construction practices and other field-related variables (Kim, 2011).

NCHRP conducted a formal review of MEPDG under project 1-40A, resulting in MEPDG software version 1.1 with extensive improvements from the design guide. MEPDG 1.1 was released to the public for implementation and evaluation in 2007. The MEPDG software is currently known as AASHTOWare Pavement ME Design, or AASHTOWare. AASHTOWare Pavement ME Design version 2.2 is the latest version of the AASHTOWare series.

Because distress prediction is the fundamental basis of pavement design by AASHTOWare, increasingly accurate distress prediction will lead to more reliable design solutions. However, performance or distress prediction models in AASHTOWare Pavement ME

Design must be recalibrated to local conditions in order to accurately and reliably predict distresses.

## 1.2 Problem Statement

The Kansas Department of Transportation (KDOT) is transitioning from use of the 1993 AASHTO Pavement Design Guide to implementation of the new AASHTOWare Pavement ME Design. However, because the distress prediction models in MEPDG were calibrated and validated using pavement performance data derived from the long-term pavement performance (LTPP) database (NCHRP, 2009), nationally calibrated performance models in the MEPDG do not necessarily reflect climate and materials specific to Kansas. These distress prediction models must be calibrated to local conditions in order to predict accurate, dependable pavement performance in Kansas.

## 1.3 Objectives

The primary purpose of this study was to enhance the accuracy of MEPDG performance prediction models through local calibration so that the AASHTOWare ME design can more reliably predict pavement performances in Kansas and the calibrated models can be more effectively used for future pavement design. This study included the following summarized objectives:

- Locally calibrate distress prediction models of flexible pavements in AASHTOWare Pavement ME Design 2.2 to Kansas conditions.
- Locally calibrate distress prediction models of JPCP in AASHTOWare Pavement ME Design 2.2 to Kansas conditions.
- Validate all locally calibrated performance prediction models.

## 1.4 Organization of Thesis

This thesis contains a total of six chapters, including the introduction chapter. Chapter 2 includes a literature review of MEPDG performance prediction models, AASHTOWare ME design inputs, and previous local calibration research studies by state highway agencies. Chapter

3 provides a systematic local calibration and validation procedure. Chapter 4 presents calibration and statistical analysis results of flexible pavement performance prediction models, and Chapter 5 presents calibration and statistical analysis results of JPCP performance prediction models. Study conclusions and recommendations for future study are summarized in Chapter 6.

# Chapter 2 - Literature Review

## 2.1 Introduction

This chapter contains detailed information about mechanistic empirical pavement design guide (MEPDG) distress prediction models and hierarchical levels of input typically used in the AASHTOWare pavement ME design software, including brief descriptions of MEDPG local calibration studies conducted by various states.

## 2.2 Brief Overview of the MEPDG

MEPDG is a mechanistic based pavement design procedure which includes factors that are directly related to the pavement performance such as traffic loadings, climatic effects, material properties, and existing soil condition (NCHRP, 2014). As the name of the design method implies, it has two distinct part for analysis and design – mechanistic and empirical. The mechanistic part is established on elementary physics and estimate pavement response to the wheel loads or environmental conditions in terms of stress, strain, and displacement. Then the empirical portion of the design uses the computed pavement response to predict the life of the pavement based on actual field performance (Timm et. al, 1988).

### 2.2.1 Advantages of Mechanistic-Empirical Method over Empirical Design Procedure

There are certain advantages of mechanistic-empirical (ME) design over traditional empirical procedures (FHWA, 2011). Those are listed below:

- Design is based on agency established performance criteria which can track down during the use phase.
- Enhanced ability to consider newer materials.
- Interaction between traffic, materials, climate, pavement structure, and construction parameters is easily understandable.
- Has the capability to evaluate additional damage caused by unique truck loading configurations or increased truck weights.

- Not only just pavement thickness but also it can consider additional design features and strategies.
- It can determine most cost-effective design strategies and output can also be used in life cycle cost analysis.

### 2.2.2 ME Design Principles

ME design approach is not just a thickness-based design procedure since a designer has total flexibility over all other design features like pavement structure, pavement materials, climatic conditions, season, soil conditions and traffic loading. The principal components of the ME design are listed below (NHI, 2002).

- Inputs – Pavement structure, materials, traffic and climate.
- Structural response model – to compute critical responses like stress, strain and deflection.
- Performance prediction models or transfer functions – to predict the performance of the pavement over the design life.
- Performance criteria – A fixed target of failure criteria like distresses based on which the pavement performance will be judged.
- Design reliability – User specified level of probability to tackle design variations.

Figure 2-1 presents a graphical approach of ME design principle.

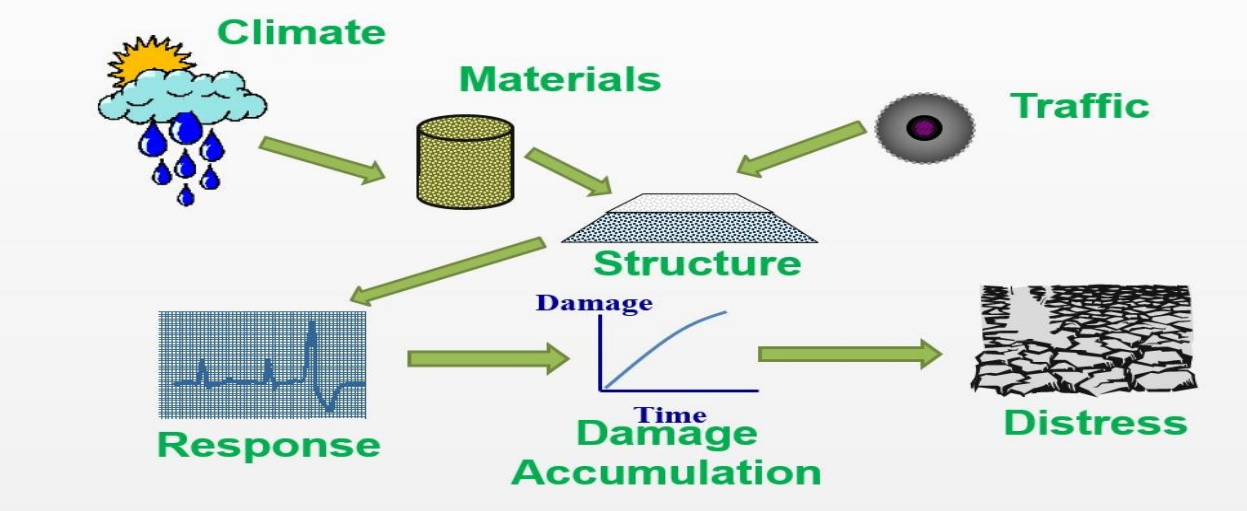


**Figure 2-1: Simplified ME design principle**

### 2.2.3 AASHTOWare Pavement ME Design Software

Structural response models was always one of the weakest links in the ME design procedure until modern computers and computational power had arrived. After the advent of different computer programs which were capable of solving complex pavement problems, pavement responses were effectively estimated from the structural response model based on the applied loadings, material properties and pavement thicknesses (Khanum, 2005).

Since flexible and rigid pavements response to applied load in pretty much different ways, different theoretical models have been developed over the recent years and based on those models, a number of computer programs have emerged to perform the analysis of both types of pavements. Due to the finite nature of concrete pavement slabs, finite element programs like ILLI-SLAB, JSLAB, WESLIQID, WESLAYER, RISC, AND 3-D EVERFE had been invented and used over the past few years to perform rigid pavement analysis (NHI, 2002). On the other hand, considering the layered system behavior of HMA pavements, multi-layer computer programs like KENLAYER, ELSYM5, CHEVRON, EVERSTRS, WESLA, ILLI-PAVE, DAMA, MnPAVE, BISAR, CIRCLY5 and MICHPAVE had been used over the past years for flexible pavement analysis (Elshaer, 2009).

In ME design procedure, the target is to keep the critical stresses and strains in the pavement below a certain acceptable limit. So the load related distresses become the main focus in the design process as they can be regulated directly by altering the structural section to reduce critical pavement stresses and strains. Common load – related and other distresses for the flexible pavements and JPCP are listed in the Table 2-1 below.

**Table 2-1: Common distresses included in the MEPDG**

| Asphalt Pavements | Concrete Pavements |
|---|---|
| • Rut depth - total, asphalt, unbound aggregate layers, and subgrade (inches).<br>• Transverse (thermal) cracking (non-load related) (feet/mile).<br>• Alligator (bottom-up fatigue) cracking (percent lane area).<br>• Longitudinal cracking (top-down) (feet/mile).<br>• Reflective cracking of asphalt overlays over asphalt, semi-rigid, composite, and concrete pavements (percent lane area).<br>• IRI predicted based on other distresses (inches/mile). | • Transverse cracking (JPCP) (percent slabs).<br>• Mean joint faulting (JPCP) (inches).<br>• Punchouts (CRCP) (number per mile).<br>• IRI predicted based on other distresses (JPCP and CRCP) (inches/mile). |

The AASHTOware pavement ME design software was developed according to the guidelines and practices described in the MEPDG. So it is comprised of a series of modules that assist the designer to go through the analysis procedure. This software provides an interface of the input design variables, computational engines for mechanistic analysis and performance prediction, and results and outputs derived from the analysis in suitable electronic format (NCHRP, 2004). Various modules of the AASHTOware pavement ME design is listed below (AASHTO, 2014):

- **General design inputs**: Include information like pavement design type, pavement type, design life, and time of construction and opening to traffic.
- **Performance criteria**: Designer specified threshold value of performance prediction models and level of reliability.
- **Traffic**: Input data to determine the vehicle loadings on the pavement structure. These data can be derived from weigh-in-motion (WIM) sites, automatic vehicle classification (AVC) sites, statewide averages, or national averages. National default values are available for the majority of inputs.
- **Climate** – This type of inputs are required to assess the environmental effects on material responses and pavement performance. Besides the data from 1,083 US and Canadian weather stations in the software (AASHTO, 2011), virtual weather stations can also be created from existing weather stations and new weather stations can be added.
- **Asphalt layer design properties** - Comprises of surface shortwave absorptivity, fatigue endurance limit (if used), and the interface friction.
- **Concrete layer design properties** - for JPCP, this information includes, joint spacing and sealant type, dowel diameter and spacing, use of a widened lane or tied shoulders, and instruction related to the erodibility of the underlying layer. For CRCP, design properties include, percent steel, bar diameter, and bar placement depth.
- **Pavement structure** – This particular module allows the designer to enter the material types, asphalt mix volumetrics, concrete mix information, mechanical properties, strength properties, thermal properties, and thickness for each layer of the pavement section.

- **Calibration factors** – There are two options of specifying calibration coefficients of the performance prediction models. One is nationally calibrated program level calibration coefficients and another is designer specified project-specific calibration coefficients. Unless otherwise mentioned, AASHTOWare will utilize the program-level calibration coefficients in the analysis.
- **Sensitivity** – This option allows the designer to define minimum and maximum values for different parameters like air voids, percent binder or layer modulus to determine the impact on the predicted condition.
- **Optimization** - This feature is utilized to determine the minimum layer thickness of a single layer that satisfies the performance criteria. In this mode, the designer inputs the minimum and maximum layer thickness for the layer to be analyzed. Then the software iterates the layer thickness within the specified range while all other inputs remain constant and the software determines the minimum layer thickness required to meet the selected performance criteria.
- **Reports** – The input summary, traffic loading prediction charts, climatic summary, material properties summary and other design tables and charts can be extracted as a PDF file and also in Microsoft Excel format.

A graphical overview of the flexible pavement and JPCP design procedure by the AASHTOWare ME design software is presented in Figure 2-2 and 2-3 respectively.

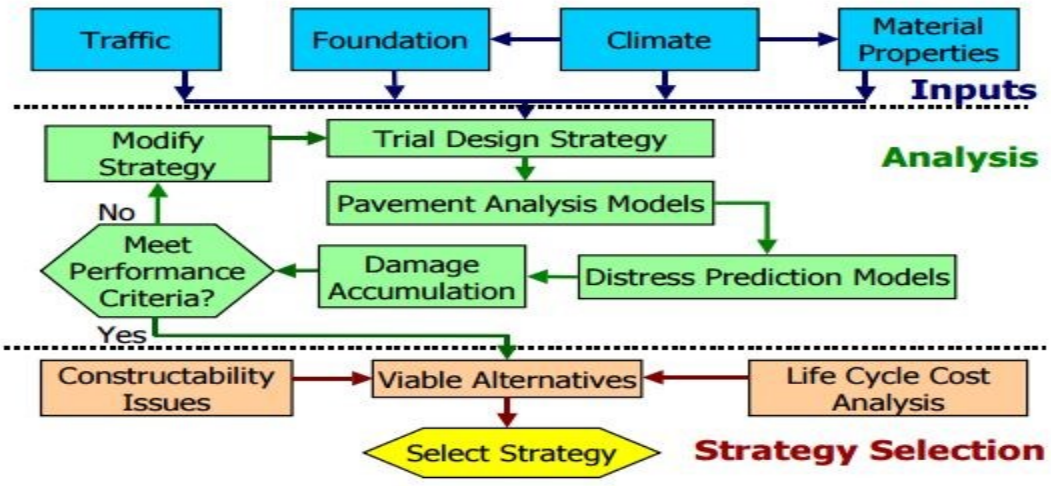


**Figure 2-2: Overview of flexible pavement design (NCHRP, 2004)**

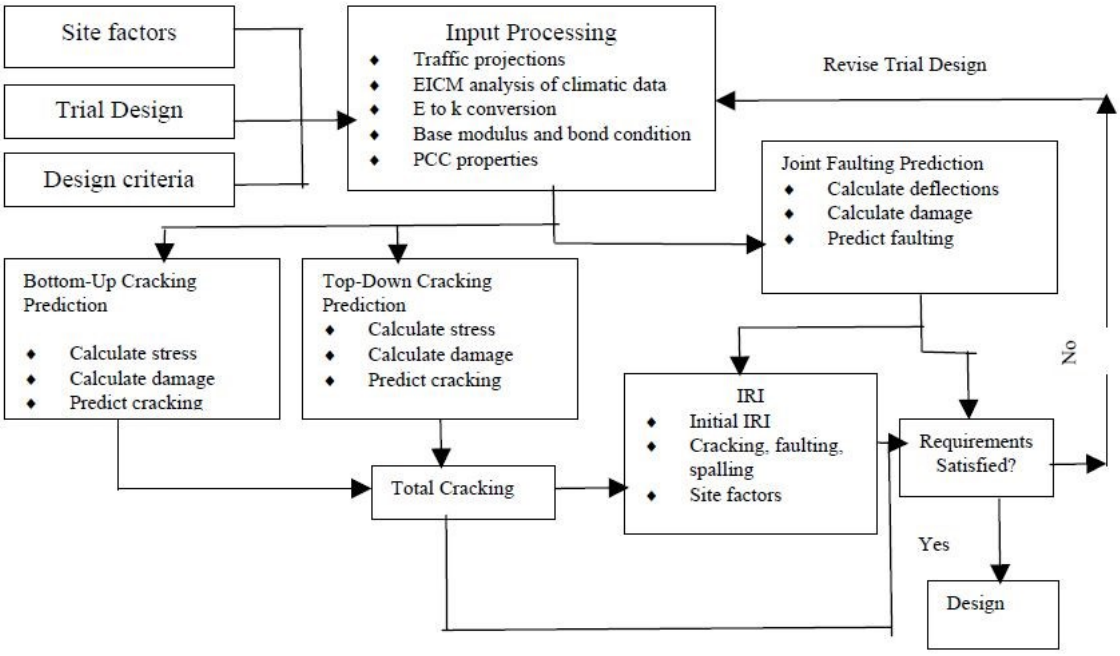


**Figure 2-3: Overview of JPCP design (Khanum, 2005)**

## 2.3 AASHTOWare MEPDG Performance Prediction Models

Pavement responses such as stress, strain, and deflection are computed based on the input of traffic load and materials by the elastic layer program model Jacob Uzan Layered Elastic Analysis (JULEA) in order to analyze pavement structure. The Integrated Climatic Model (ICM) uses climatic inputs to accurately predict pavement structure response by adjusting resilient modulus of unbound structures, effective dynamic k-value of the subgrade, and the dynamic modulus of the asphalt concrete layer. Performance models use obtained pavement responses to compute pavement damage and predict pavement damage or pavement distress over the design life.

AASHTOWare pavement ME design version 2.2 is the most recent version of the AASHTOWare software series. The performance prediction models, or transfer functions, embedded in this version of the software are briefly described in this section. Detailed descriptions of all prediction models are included in the AASHTO MEPDG Manual of Practice (AASHTO, 2015).

### 2.3.1 Performance Prediction Models for New Flexible Pavements

This section describes performance models used to calculate fatigue damage, thermal cracking damage, permanent deformation, and smoothness degradation of new flexible pavement.

#### 2.3.1.1 Rut Depth

Plastic or permanent vertical deformation in the hot mix asphalt (HMA), unbound layers, and foundation soil causes rutting in the form of surface distortion. Rut depth can be defined as the maximum vertical difference in elevation between the transverse profile of the HMA surface and a wire-line across the lane width (AASHTO, 2015). Plastic deformation for any given season of the year is the sum of plastic vertical deformation within each layer. Repeated Load Permanent Deformation (RLPD) triaxial tests are typically performed in the laboratory for HMA mixtures and unbound materials in order to measure the rate of accumulation of permanent deformation. MEPDG calculates incremental distortion or rutting within each sublayer. For all types of HMA mixtures the MEPDG field-calibrated form of the laboratory-derived relationship from RLPD tests is shown in Equation 2.1.

$$\Delta_{p(HMA)} = \varepsilon_{p(HMA)} h_{HMA} = \beta_{1r} K_z \varepsilon_{r(HMA)} 10^{K_{1r}} n^{k_{2r}\beta_{2r}} T^{k_{3r}\beta_{3r}} \quad \textbf{(2.1)}$$

Where:

$\Delta_{p(HMA)}$ = accumulated permanent or plastic vertical deformation in the HMA layer/sublayer (inches);

$\varepsilon_{p(HMA)}$ = accumulated permanent or plastic axial strain in the HMA layer/sublayer (inches);

$\varepsilon_{r(HMA)}$ = resilient or elastic strain calculated by the structural response model at the mid-depth of each HMA layer (inches);

$h_{HMA}$ = thickness of the HMA layer/sublayer (inches);

$n$ = number of axle-load repetitions;

$T$ = mix or pavement temperature (°F);

$K_z$ = depth confinement factor;

$K_{1r}, k_{2r}, k_{3r}$ = global field calibration parameters ($K1r$ = -3.35412, $K_{2r}$ = 0.4791, $K_{3r}$ = 1.5606); and

$\beta_{1r}, \beta_{2r}, \beta_{3r}$ = local or mixture field calibration constants.

$K_z$ can be calculated as

$K_z = (C1 + C_2D)\ 0.328196^{\ D}$

Where:

$C_1$ = -0.1039 $(H_{HMA})^2$ + 2.4868 $H_{HMA}$ -17.342;

$C_2$ = 0.0172 $(H_{HMA})^2$ – 1.733 $H_{HMA}$ + 27.428;

$D$ = depth below the surface (inches); and

$H_{HMA}$ = total HMA thickness (inches).

MEPDG uses the field-calibrated mathematical equation shown in Equation 2.2 to calculate plastic vertical deformation within all unbound pavement sublayers and the foundation or embankment soil.

$$\Delta_{p(soil)} = \beta_{s1} k_{s1} \varepsilon_v h_{soil} \left(\frac{\varepsilon_0}{\varepsilon_r}\right) e^{-\left(\frac{\rho}{n}\right)^{\beta}} \qquad \textbf{(2.2)}$$

Where:

$\Delta_{p(soil)}$ = permanent or plastic vertical deformation in the unbound layer/sublayer (inches);

$n$ = number of axle-load applications;

$\varepsilon_0$ = intercept determined from laboratory-repeated load permanent deformation tests (inches);

$\varepsilon_r$ = resilient strain imposed in laboratory test to obtain material properties (inches);

$\varepsilon_v$ = average vertical resilient or elastic strain in the unbound layer calculated by the structural response model (inches);

$h_{soil}$ = thickness of the unbound layer/sublayer (inches);

$k_{s1}$ = global calibration coefficients ($k_{s1}$= 2.03 for granular materials and 1.35 for fine-grained materials);

$\beta_{s1}$ = local calibration constant for rutting in the unbound layers (1.0 for global calibration); and

Log$\beta$ = -0.61119-0.017638 ($W_c$)

$$\rho = 10^9 \left(\frac{C_0}{(1-(10^9)^{\beta})}\right)^{\frac{1}{\beta}}$$

$$C_0 = Ln\left(\frac{a_1 M_r^{b_1}}{a_9 M_r^{b_9}}\right)$$

Where:

$W_c$ = water content (%);

$M_r$ = resilient modulus of the unbound layer or sublayer;

$a_{1,9}$ = regression constants ($a_1$ = 0.15 and $a_9$= 20.0,); and

$b_{1,9}$ = regression constants ($b_1$ = 0.0 and $b_9$= 0.0).

### 2.3.1.2 Load Related Cracking

AASHTOWare pavement ME design predicts two types of load-related cracking: alligator cracking, or bottom-up fatigue cracking, and longitudinal cracking, or top-down fatigue cracking. MEPDG assumes that alligator or area cracks initiate at the bottom of HMA layers and propagate to the surface with continued truck traffic, and longitudinal cracks are presumed to originate from the surface. In order to predict both types of load-related cracks, AASHTOWare MEPDG uses the allowable number of axle-load applications needed for the incremental damage index approach. The mathematical form of the model is shown in Equation 2.3.

$$N_{\text{f-HMA}} = K_{\text{f1}}(C)(C_{\text{H}})\beta_{\text{f1}}(\varepsilon_{\text{t}})^{\text{Kf2}\beta\text{f2}}(E_{\text{HMA}})^{\text{Kf3}\beta\text{f3}} \qquad \textbf{(2.3)}$$

Where:

$N_{f\text{-}HMA}$ = allowable number of axle-load applications for a flexible pavement and HMA overlays;

$\varepsilon_t$ = tensile strain at critical locations, calculated by the structural response model (inches);

$E_{HMA}$ = dynamic modulus of HMA measured in compression (psi);

$K_{f1}, K_{f2}, K_{f3}$ = global field calibration coefficients ($K_{f1}$ = 0.007566, $K_{f2}$ =+3.9492, and $K_{f3}$ = +1.281);

$\beta_{f1}, \beta_{f2}, \beta_{f3}$ = local or mixture-specific field calibration constants (1.0 for global calibration); and

$C = 10^M$

$$M = 4.84\left(\frac{V_{\text{be}}}{V_{\text{a}}+V_{\text{be}}} - 0.69\right)$$

Where:

$V_{be}$ = effective asphalt content by volume (%);

$V_a$ = percent air voids in the HMA mixture; and

$C_H$ = thickness correction term dependent on cracking type

For bottom-up or alligator cracking:

$$C_H = \frac{1}{0.000398 + \frac{0.003602}{1 + e^{(11.02 - 3.49 H_{HMA})}}}$$

For top-down or longitudinal cracking:

$$C_H = \frac{1}{0.01 + \frac{12.00}{1 + e^{(15.676 - 2.818 H_{HMA})}}}$$

Where:

$H_{HMA}$ = total HMA thickness (inches)

AASHTOWare pavement ME design calculates the incremental damage index ($\Delta DI$) by dividing the actual number of axle loads by the allowable number of axle loads within a specific time increment and axle-load interval for each axle type, a process known as Miner's hypothesis. As shown in Equation 2.4, the cumulative damage index ($DI$) is the summation of incremental damage indices over time.

$$DI = \sum(\Delta DI)_{j,m,l,p,T} = \sum(\frac{n}{N_{f\text{-}HMA}})_{j,m,l,p,T} \qquad \textbf{(2.4)}$$

Where:

$n$ = actual number of axle-load applications within a specific time period;

$j$ = axle-load interval;

$m$ = axle-load type (single, tandem, tridem, or quad);

$l$ = truck type using truck classification groups in AASHTOWare Pavement ME Design;

$p$ = month; and

$T$ = median temperature for five temperature intervals or quintiles that subdivide each month (°F).

The area of alligator cracking and length of longitudinal cracking are calculated using the total damage over time. The mathematical relationship used to predict the amount of alligator cracking is shown in Equation 2.5.

$$FC_{Bottom} = \left(\frac{1}{60}\right)\left(\frac{C_4}{1+e^{(C_1C_1^*+C_2C_2^*Log(DI_{Bottom}*100))}}\right) \quad \textbf{(2.5)}$$

Where:

$FC_{Bottom}$ = area of alligator cracking that initiates at the bottom of the HMA layers (% of total lane area);

$DI_{Bottom}$ = cumulative damage index at the bottom of the HMA layers;

$C_{1, 2, 4}$ = transfer function regression constants ($C_1$ = 1.00; $C_2$ = 1.00; and C4 = 6,000)

$C_1^* = -2C_2^*$

$C_2^* = -2.40874-39.748(1+H_{HMA})^{-2.856}$

The relationship used to predict the length of longitudinal fatigue cracking is shown in Equation 2.6.

$$FC_{\text{Top}} = 10.56\left(\frac{C_4}{1+e^{(C_1-C_2Log(DI_{\text{Top}}))}}\right) \quad \textbf{(2.6)}$$

$FC_{\text{Top}}$ = length of longitudinal cracks that initiate at the top of the HMA layer (ft/mile);

$DI_{\text{Top}}$ = cumulative damage index near the top of the HMA surface; and

$C_{1, 2, 4}$ = transfer function regression constants ($C_1$ = 7.00; $C_2$ = 3.5; and $C_2$ = 1,000).

### 2.3.1.3 Non-Load Related Cracking

The AASHTOWare MEPDG thermal cracking model is

$$\Delta C = A\,(\Delta K)^n \quad \textbf{(2.7)}$$

Where:

$\Delta C$ = change in crack depth due to a cooling cycle;

$\Delta K$ = change in the stress intensity factor due to a cooling cycle; and

$A.n$ = fracture parameters for the HMA mixture.

Reasonable estimates of $A$ and $n$ can be derived from the indirect tensile creep-compliance and strength of the HMA in accordance with the following two mathematical formulas:

$$A = K_t \beta_t 10^{[4.389 - 2.52 \log(E_{HMA} \sigma_m n)]}$$

$$\eta = 0.8 \left[ 1 + \frac{1}{m} \right]$$

Where:

$K_t$ = coefficient determined by global calibration for each input level (Level 1 = 1.5; Level 2 = 0.5; and Level 3 = 1.5);

$E_{HMA}$ = HMA indirect tensile modulus (psi);

$\sigma_m$ = mixture tensile strength (psi);

$m$ = the $m$-value derived from the indirect tensile creep compliance curve measured in the laboratory; and

$\beta_t$ = local or mixture calibration factor.

Theoretical finite element studies have developed stress intensity factor $K$ as

$$K = \sigma_{tip} \left[ 0.45 + 1.99 (C_0)^{0.56} \right]$$

Where:

$\sigma_{tip}$ = far-field stress from pavement response model at depth of crack tip (psi); and

$C_0$ = current crack length (ft).

AASHTOWare pavement ME design assumes a relationship between the probability distribution of the log of the crack depth to HMA-layer thickness ratio and the percent of cracking. The degree of cracking is predicted by Equation 2.8.

$$TC = \beta_{t1} N \left[ \frac{1}{\sigma_d} Log \left( \frac{C_d}{H_{HMA}} \right) \right] \qquad \textbf{(2.8)}$$

Where:

$TC$ = observed amount of thermal cracking (ft/mile);

$\beta_{t1}$ = regression coefficient determined by global calibration (400);

$N[z]$ = standard normal distribution evaluated at $[z]$;

$\sigma_d$ = Standard deviation of the log of the depth of cracks in the pavement (0.769), in.,

$C_d$ = crack depth (inches); and

$H_{HMA}$ = thickness of HMA layers (inches).

### 2.3.1.4 Smoothness Degradation

When predicting smoothness degradation, AASHTOWare pavement ME design assumes that surface distress results in increased roughness, or reduced smoothness. Equation 2.9, which was developed from data collected from the Long-Term Pavement Performance (LTPP) program, is implemented into AASHTOWare pavement ME design to estimate the international roughness index (IRI) over time for HMA-surfaced pavements.

$$IRI = IRI_0 + C_1(RD) + C_2(FC_{\text{Total}}) + C_3(TC) + C_4(SF) \quad \textbf{(2.9)}$$

Where:

$IRI_0$ = initial IRI after construction (inches/mile);

$SF$ = site factor;

$FC_{\text{Total}}$ = area of fatigue cracking (combined alligator, longitudinal, and reflection cracking in the wheel path) (percent of total lane area). All load-related cracks are combined based on area, and crack length is multiplied by 1 ft to convert length into area;

$TC$ = length of transverse cracking (including the reflection of transverse cracks in existing HMA pavements) (ft/mile);

$RD$ = average rut depth (inches); and

$C_{1,2,3,4}$ = calibration factors ($C_1$ = 40.0, $C_2$ = 0.400, $C_3$ = 0.008, $C_4$ = 0.015).

The site factor (SF) is calculated according to the following equation:

$$SF = Age^{1.5}\{\ln[recip + 1)(FI + 1)_{P02}]\} + \{\ln[(precip + 1)(PI + 1)_{P200}]\}$$

Where:

$Age$ = pavement age (year);

$PI$ = percent plasticity index of the soil;

$FI$ = average annual freezing index (°F-days);

$precip$ = average annual precipitation (inches);

$P_{02}$ = percent passing the 0.02 mm sieve; and

$P_{200}$ = percent passing the 0.075 mm sieve.

### 2.3.2 Performance Prediction Models for New Rigid Pavements

This section describes performance models used to calculate transverse slab cracking, mean transverse joint faulting, and smoothness degradation of jointed-plane concrete pavement (JPCP).

#### 2.3.2.1 Transverse Slab Cracking

Bottom-up and top-down modes of cracking are considered in JPCP pavements; slabs may crack from top-down or bottom-up but not from both directions. Therefore, AASHTOWare pavement ME design reports combined cracking, excluding the possibility of both modes of cracking occurring on the same slab.

MEPDG measures transverse cracking by considering the percentage of slabs with transverse cracks (all severities) in a given traffic lane and predicts distress using Equation 2.10 for bottom-up and top-down cracking.

$$CRK = \frac{100}{1+C_4(DI_F)^{C5}} \qquad \textbf{(2.10)}$$

Where:

$CRK$ = predicted amount of bottom-up or top-down cracking (fraction);

$DI_F$ = fatigue damage; and

$C_{4,5}$ = calibration coefficients ($C_4$ = 1.0, $C_5$ = -1.98).

Fatigue damage accumulations considering all critical factors for JPCP transverse cracking is presented in the general expression below, known as Miners's hypothesis:

$$DI_F = \sum \frac{n_{i,j,k,l,m,n,o}}{N_{i,j,k,l,m,n,o}}$$

Where:

$DI_F$ = total fatigue damage (top-down or bottom-up);

$ni,j,k...$ = applied number of load applications at condition $i,j,k,l,m,n;$

$Ni,j,k...$ = allowable number of load applications at condition $i,j,k,l,m,n;$

$i$ = age (including change in PCC modulus of rupture and elasticity, slab/base contact friction, deterioration of shoulder LTE);

*j* = month (including change in base elastic modulus and effective dynamic modulus of subgrade reaction);

*k* = axle type (single, tandem, and tridem for bottom-up cracking; short, medium, and long wheelbase for top-down cracking);

*l* = load level (incremental load for each axle type);

*m* = equivalent temperature difference between top and bottom PCC surfaces;

*n* = traffic offset path; and

*o* = hourly truck traffic fraction.

The allowable number of load applications is determined using the following PCC fatigue equation:

$$\log(N_{\mathrm{i,j,k,l,m,n}}) = C_1.\left(\frac{MR_{\mathrm{i}}}{\sigma_{\mathrm{i,j,k,l,m,n}}}\right)^{C2}$$

Where:

$N_{i,j,k...}$ = allowable number of load applications at condition *i,j,k,l,m,n;*

$MR_i$ = PCC modulus of rupture at age *i* (psi);

$\sigma_{i,j,k..}$ = applied stress at condition *i,j,k,l,m,n;*

$C_1$ = calibration constant (2.0); and

$C_2$ = calibration constant (1.22).

After estimating top-down and bottom-up damages, corresponding cracking is computed using Equation 2.10 and the total combined cracking is determined using Equation 2.11.

$$TCRACK = (CRK_{\text{Bottom-up}} + CRK_{\text{top-down}} - CRK_{\text{Bottom-up}}.CRK_{\text{top-down}}).100\% \qquad (2.11)$$

Where:

*TCRACK* = total transverse cracking (%, all severities);

$CRK_{Bottom\text{-}up}$ = predicted amount of bottom-up transverse cracking (fraction); and

$CRK_{Top\text{-}down}$ = predicted amount of top-down transverse cracking (fraction).

#### 2.3.2.2 JPCP Mean Transverse Joint Faulting

AASHTOWare pavement ME design uses an incremental approach to predict mean transverse joint faulting on a monthly basis; the magnitude of faulting increment is estimated based on the current faulting level. The faulting each month is a sum of faulting increments from all previous months in the pavement life beginning from the traffic opening date. Mathematically it is determined using Equations 2.12 to 2.15.

$$Fault_{\text{m}} = \sum_{i=1}^{m} \Delta Fault_{\text{i}} \quad \textbf{(2.12)}$$

$$\Delta Fault_{\text{i}} = C_{34} * (FAULTMAX_{\text{i-1}} - Fault_{\text{i-1}})^2 * \text{DE}_{\text{i}} \quad \textbf{(2.13)}$$

$$FAULTMAX_{\text{i}} = FAULTMAX_0 + C_7 * \sum_{j=1}^{m} DE_{\text{j}} * Log(1 + C_5 * 5^{EROD})^{C6} \quad \textbf{(2.14)}$$

$$FAULTMAX_0 = C_{12} * \delta_{\text{curling}} * [Log(1 + C_5 * 5.0^{EROD}) * Log(\frac{P_{200} * WetDays}{P_s})]^{C6} \quad \textbf{(2.15)}$$

Where:

$Fault_{\text{m}}$ = mean joint faulting at the end of month (m, inches);

$\Delta Fault_{\text{i}}$ = incremental change (monthly) in mean transverse joint faulting during month *i* (inches);

$FAULTMAX_{\text{i}}$ = maximum mean transverse joint faulting for month *i* (inches);

$FAULTMAX_0$ = initial maximum mean transverse joint faulting (inches);

*EROD* = base/subbase erodibility factor;

$DE_i$ = differential density of energy of subgrade deformation accumulated during month *I*;

$\delta_{curling}$ = maximum mean monthly slab corner upward deflection PCC due to temperature curling and moisture warping;

$P_s$ = overburden on subgrade (lb);

$P_{200}$ = percent subgrade material passing #200 sieve;

*WetDays* = average annual number of wet days (greater than 0.1 inches rainfall); and

$C_{1,2,3,4,5,6,7,12,34}$ = global calibration constants ($C_1$ = 1.0184; $C_2$ = 0.91656; $C_3$ = 0.0021848; $C_4$ = 0.0008837; $C_5$ = 250; $C_6$ =0.4; $C_7$ = 1.83312).

$C_{12} = C_1 + C_2 * FR^{0.25}$

$C_{34} = C_3 + C_4 * FR^{0.25}$

*FR* = Base freezing index defined as percentage of time the top base temperature is below freezing (32 ˚F) temperature .

#### 2.3.2.3 Smoothness Degradation of JPCP

AASHTOWare pavement ME design predicts smoothness as a function of the initial as-constructed profile of the pavement and any change in the longitudinal profile over time and traffic due to distresses and foundation movements (AASHTO, 2015). The IRI model was calibrated and validated using LTPP field data to ensure that it would generate realistic results under a variety of climatic and field conditions. Equation 2.16 is the final calibrated model.

$$IRI = IRI_1 + C1 * CRK + C2 * SPALL + C3 * TFAULT + C4 * SF \quad \textbf{(2.16)}$$

Where:

*IRI* = predicted IRI (inches/mile);

$IRI_1$ = initial smoothness measured as IRI (inches/mile);

*CRK* = percent slabs with transverse cracks (all severities);

*SPALL* = percent of joints with spalling (medium and high severities);

*TFAULT* = total joint faulting cumulated per mile (inches);

*C1* = 0.8203;

*C2* = 0.4417;

*C3* = 1.4929;

*C4* = 25.24; and

*SF* = site factor

$$SF = AGE\ (1 + 0.5556 * FI)(1 + P_{200}) * 10^{-6}$$

Where:

*AGE* = pavement age (year);

*FI* = freezing index (˚F-days); and

$P_{200}$ = percent subgrade material passing No. 200 sieve.

Transverse cracking and faulting were computed using the prediction models described earlier. Transverse joint spalling is determined using Equation 2.17.

$$SPALL = \left[\frac{AGE}{AGE+0.01}\right]\left[\frac{100}{1+1.005^{(-12*AGE+SCF)}}\right] \quad \textbf{(2.17)}$$

Where:

*SPALL* = percentage joints spalled (medium and high severities);

*AGE* = pavement age since construction (year); and

*SCF* = scaling factor based on site condition, design, and climate

$$SCF = -1400 + 350.AC_{\text{PCC}}.(0.5 + PREFORM) + 43.4\, f'c^{0.4} - 0.2\,(FT_{\text{cycle}}.AGE) + 43H_{\text{pcc}} - 536\, WC_{\text{pcc}}$$

Where:

$AC_{pcc}$ = PCC air content (%);

*AGE* = time since construction (yr);

*PREFORM* = 1 if preformed sealant is present; 0 if not;

$f'c$ = PCC compressive strength (psi);

$FT_{cycle}$ = average annual number of freeze-thaw cycles;

$H_{PCC}$ = PCC slab thickness (inches); and

$WC_{PCC}$ = PCC water/cement ratio.

## 2.4 AASHTOWare Pavement ME Design Input

AASHTOWare pavement ME design has three hierarchical input levels based on the designer's knowledge of the input parameters. Inputs of a new pavement design in the software can be classified as traffic, climate, and material properties. Each category contains a number of subcategories that allow a designer to modify any design inputs in order attain desired predicted distresses and reliability (Kasperick, 2013). The three hierarchical levels of input suitable for assigning material and traffic input parameter values are briefly described below:

- **Input Level 1** - Input parameters are directly measured. Site-specific or project-specific data is required for traffic inputs such as average annual daily truck traffic (AADTT), truck lane usage, percentage of trucks, axle-load distribution and truck classification. Laboratory or field testing data such as dynamic modulus (E*) testing of HMA concrete, coefficient of thermal expansion (CTE) of concrete, or falling weight deflectometer (FWD) deflection testing are required for material input. Level 1 input requires more resources and time than other levels in order to handle the huge testing and data collection

effort. This level is used primarily for designing pavements with heavy traffic or unusual site features.

- **Input Level 2 -** Input parameters are user-selected and can be estimated from a limited testing program or derived from correlations or regression equations. Examples of Level 2 inputs include estimating HMA dynamic modulus (E*) from binder, aggregate, and mix properties; estimating PCC elastic moduli from compressive strength tests; or using regional traffic classification data based on functional class of highway in the state (Darter, 2014). This level is utilized when a scope of testing or resource is not available.
- **Input Level 3**- Input parameters are user-selected, typical average values for the region or best-estimated default values, such as unbound materials' default resilient modulus values or default PCC CTE for a given coarse aggregate type. Because this input level has the least knowledge about specific project-related data, it is typically used to design low-volume roads.

The designer provides inputs to the software. The main screen that appears after starting a new flexible pavement trial design is shown in Figure 2.4.

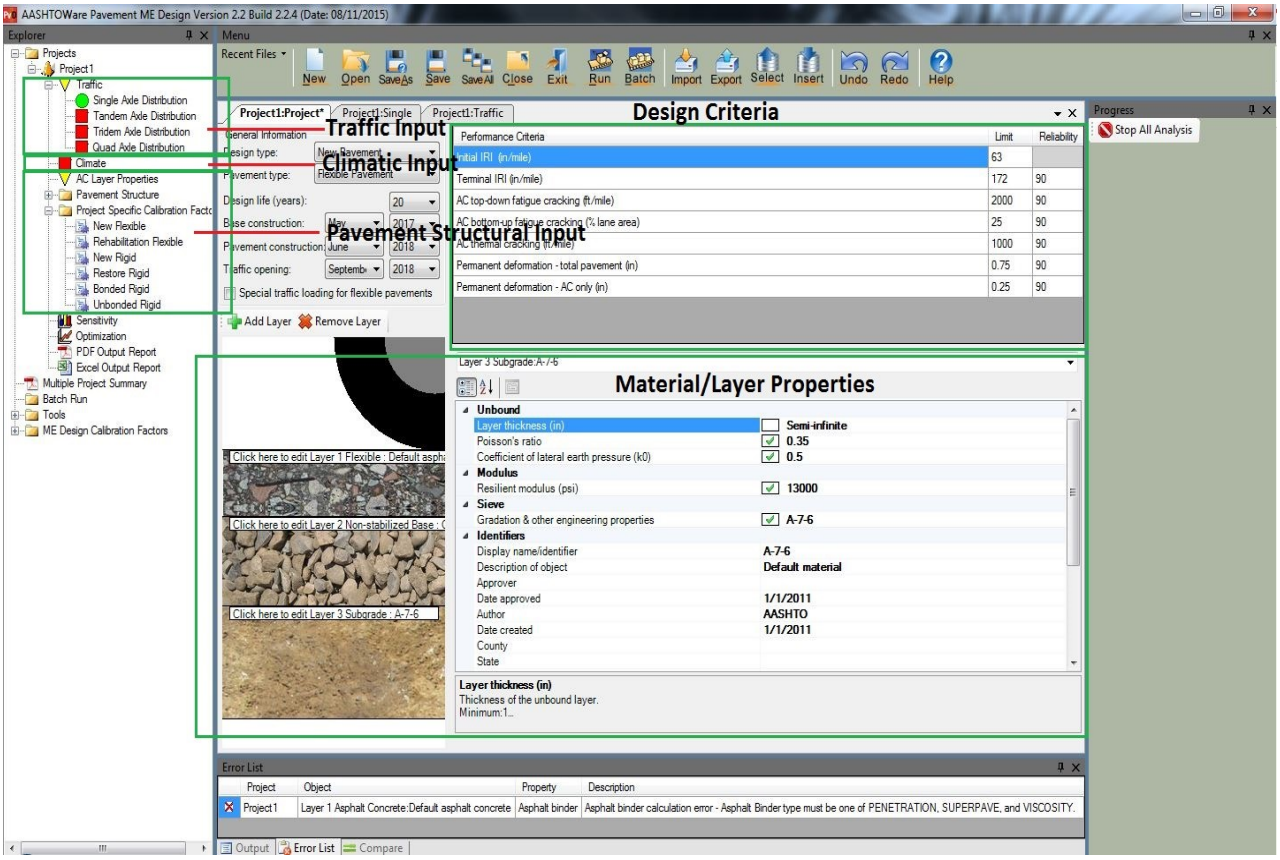


**Figure 2-4: AASHTOWare pavement ME design main screen**

### 2.4.1 Traffic Inputs

Traffic inputs in AASHTOWare pavement ME design primarily deal with truck traffic characteristics. These are the key inputs in the structural design and analysis of the pavement structure. Traffic inputs necessary to complete analysis in ME design are briefly described below:

- **Base Year Truck Volume and Speed:** This section of input requires base year two-way AADTT, number of lanes in the design direction, percentage of trucks in the design direction, percentage of trucks in the design lane, and operational speed (kph).
- **Traffic Capacity Cap:** This control allows a designer to impose a cap on estimated traffic volumes used in the design process so that expected highway capacity is not exceeded (AASHTO, 2014). Needed inputs include AADT excluding trucks, non-truck linear traffic growth rate, highway facility type, traffic signal, highway terrain type, rural or urban highway environment, capacity limit, and enforced highway capacity limit.

- **Axle Configuration:** Sets of required inputs include average axle width (m), dual tire spacing (mm), tire pressure (kPa), tandem-axle spacing (m), tridem-axle spacing (m), and quad-axle spacing (m).
- **Lateral Wander:** Choices of inputs are mean wheel location (mm), traffic wander standard deviation (mm), and design lane width (m).
- **Wheelbase:** Input options include average spacing of short axles (m), average spacing of medium axles (m), average spacing of long axles (m), percentage of trucks with short axles, percentage of trucks with medium axles, and percentage of trucks with long axles.
- **Vehicle Class Distribution and Growth:** Represents normalized distribution of various truck classes within the traffic stream. Cumulative sum of all incremental values for all truck classes should equal 100 %.
- **Monthly Distribution Factors:** The distribution of monthly truck volumes in a typical year is expressed by this value. The sum of all monthly distribution factors for a specific truck class must be 12.
- **Hourly Distribution Factors:** This input is only required for rigid pavement design. This value defines the percentage of trucks using a road facility each hour of the day. The sum of total hourly distribution factors must be 100 %.
- **Axle Load Spectra:** A histogram or distribution of axle loads for a specific axle type (single, tandem, tridem, or quad) and vehicle class (class 4 to class 13) is known as axle load spectra.

### 2.4.2 Climatic Inputs

The performance of flexible and rigid pavements is significantly affected by environmental conditions such as precipitation, temperature, freeze-thaw cycles, and depth of water table. These factors affect temperature and moisture contents of unbound materials, which consequently affect the load-carrying capacity of the pavement. Temperature levels and temperature gradients also directly impact the stiffness of asphaltic materials and stress and deformations for the PCC layer, respectively (AASHTO, 2014). In order to accurately predict the factor outcomes on pavement performance, AASHTOWare pavement ME design requires these inputs to be locally calibrated,

which is achieved using a modeling tool known as the enhanced integrated climate (EICM) model that is embedded in the software.

AASHTOWare pavement ME design uses climate data from weather stations throughout the United States to utilize the EICM model. These weather stations are typically located in airports/airfields. Inputs taken from these weather stations include:

- **Latitude**: specific latitude of a place in decimal degrees
- **Longitude**: specific longitude of a place in decimal degrees
- **Elevation**: specific elevation of a project site in order to determine the lapse rate that temperature change due to elevation change
- **Depth of water table**: average depth of groundwater table on an annual or seasonal basis, usually defined from the top surface of subgrade to the groundwater table
- **Climate station**: specific weather station for a project site, including a single weather station or a virtual weather station using several weather stations in proximity to the project site

### 2.4.3 Material Inputs

This section describes material inputs of AASHTOWare pavement ME design for new flexible and JPCP pavement.

#### 2.4.3.1 Material Inputs for Flexible Pavements

The AASHTOWare pavement ME design classifies all flexible pavement materials according to the following categories:

- HMA
- Dense-graded asphalt
- Open-graded asphalt
- Asphalt-stabilized base mixes
- Sand-asphalt mixtures
- Stone-matrix asphalt (SMA)
- Cold-mix asphalt
- Central-plant processed

- Cold in-place recycling

Fundamental material inputs required for asphalt concrete layers are presented in Table 2-2.

**Table 2-2: Material inputs for asphalt layer**

| Asphalt Layer | Mixture Volumetrics | Mechanical Properties | Thermal Properties |
|---|---|---|---|
| Thickness | Unit weight | Dynamic modulus input level (1,2 or 3) | Thermal conductivity |
| | Effective binder content | HMA Estar predictive model | Heat capacity |
| | Air Voids | Reference temperature | Thermal contraction |
| | Poisson's ratio | Asphalt binder (Superpave performance grade, viscosity grade or penetration grade) | |
| | | Indirect tensile strength | |
| | | Creep compliance (Level 1, 2 or 3) | |

Other layers must be placed beneath the asphalt concrete layer in order to constitute a flexible pavement. The following sections introduce those layers for ME design.

***Chemically Stabilized Layer***

A chemically stabilized layer includes lean concrete, cement stabilized, open-graded cement stabilized, soil cement, lime-cement-flyash, or lime-treated materials (AASHTO, 2014). Essential inputs for a chemically stabilized layer can be classified as general, strength, and thermal properties.

- General
  - Layer thickness
  - Unit weight
  - Poisson's ratio
- Strength
  - Elastic/resilient modulus
  - Minimum elastic/resilient modulus
  - Modulus of rupture
- Thermal
  - Thermal conductivity

- Heat capacity

***Non-Stabilize Layer***

A non-stabilized layer includes AASHTO soil classes A-1 through A-3 and other commonly practiced materials, such as crushed stone, crushed gravel, river gravel, permeable aggregate, and cold-recycled asphalt material. Input parameters are listed below.

- General
  - Layer thickness
  - Poisson's ratio
  - Coefficient of lateral earth pressure
- Modulus
  - Resilient modulus (Level 2 or 3)
- Sieve (Gradation & other engineering properties)
  - Sieve size table (percent passing)
  - Liquid limit
  - Plasticity Index
  - Layer compacted or not
  - Maximum dry unit weight
  - Saturated hydraulic conductivity
  - Specific gravity of solids
  - Optimum gravimetric water content
  - User-defined soil water characteristic curve

***Subgrade***

Subgrade is the bottommost layer of a flexible pavement. According to the AASHTO soil classification system, soil classes A-1 through A-7-6 can be defined as subgrade materials. Key input parameters are:

- General
  - Layer thickness
  - Poisson's ratio

- Coefficient of lateral earth pressure
- Modulus
  - Resilient Modulus (Level 2 or 3)
- Sieve (Gradation & other engineering properties)
  - Sieve size table (percent passing)
  - Liquid limit
  - Plasticity index
  - Layer compacted or not
  - Maximum dry unit weight
  - Saturated hydraulic conductivity
  - Specific gravity of solids
  - Optimum gravimetric water content
  - User-defined soil water characteristic curve

***Bedrock***

A bedrock layer is not usually present in a flexible pavement alignment. If it is present, however, it must be fully accounted for in the pavement design since bedrock can significantly impact the pavement's mechanistic responses (AASHTO 2014). Main inputs are layer thickness, unit weight, Poisson's ratio, and elastic modulus of bedrock material.

#### 2.4.3.2 Material Inputs for Rigid Pavements

In this study newly constructed JPCP pavements represented rigid pavements consisting of Portland cement, water, and fine and coarse aggregates. Therefore, PCC properties such as early and long-term strength, elastic modulus, shrinkage, thermal expansion, and durability largely depend on the quantities and qualities of these construction materials. Primary PCC material inputs required by AASHTOWare ME design include flexural strength, elastic modulus, CTE, ultimate shrinkage, and concrete mix properties such as cement type, cement content, and aggregate type. Key inputs are listed in Table 2-3.

**Table 2-3: Material Inputs for PCC**

| PCC Inputs | Thermal Properties | Mix Properties | Strength |
|---|---|---|---|
| Thickness | PCC coefficient of thermal expansion | Cement type (Type I, II or III) | PCC strength and modulus of rupture |
| Unit weight | PCC thermal conductivity | Cementitious material content | |
| Poisson's ratio | PCC heat capacity | Water to cement ratio | |
| | | Aggregate type (Quartzite, Limestone, Granite etc.) | |
| | | PCC set temperature | |
| | | Ultimate shrinkage | |
| | | Reversible Shrinkage | |
| | | Time to develop 50% of ultimate shrinkage | |
| | | Curing method | |

Other JPCP layers beneath the PCC slab may include an asphalt concrete base layer, a chemically stabilized layer, a non-stabilized layer, subgrade, and bedrock. Inputs of these layers are identical to flexible pavement input described in section 2.3.3.1.

***JPCP Design Properties***

Certain design features and construction practices influence the long-term performance of JPCP (AASHTO 2014). These are incorporated into the ME design in the form of following inputs:

- Widened PCC slabs
- Joint spacing
- Shoulder type (tied vs untied PCC or asphalt concrete)
- Presence and size of dowel bars
- Dowel bar spacing
- Base type and erodibility
- PCC curing method (curing compound versus. wet curing)
- Permanent curl/warp effective temperature difference in the PCC

- PCC/base layer friction loss age
- Initial smoothness
- Sealant type

## 2.5 Effort of Local Calibration of the Mechanistic-Empirical Pavement Design Guide

Following the release of MEPDG in 2004 (NCHRP 1-37 A), a number of national research studies supported by NCHRP and FHWA were conducted to ensure proper implementation of the method. In addition, a large number of state highway agencies attempted local calibration of MEPDG as a first step for implementation of this pavement design method. Most highway agencies followed AASHTO's local calibration guide, released in 2010. Although a majority of local calibration in MEPDG was executed only for flexible pavements, a few studies also focused on JPCP. This section describes local calibration approaches of state highway agencies, with emphasis on their methodologies and outcomes.

### 2.5.1 Calibration and Implementation of MEPDG in Arizona

The Arizona Department of Transportation (ADOT) attempted local calibration of AASHTO DARWin-ME pavement design guide and proposed a practical user guide for obtaining inputs, conducting design, and establishing the recommended pavement design (Darter, 2014). ADOT had selected four pavement types:

- HMA pavements
- Composite pavements, which is a thin asphalt rubber friction course over JPCP and continuously reinforced concrete pavement (CRCP)
- JPCP and CRCP
- HMA overlay on flexible pavements

A total of 180 pavement sections were obtained from the LTPP experiment, previous field research studies and other projects in the pavement management database. The principal objectives of this study were to ensure that all design inputs are appropriate to Arizona conditions and

resources, to guarantee that the distress and IRI prediction models are unbiased in order to reduce the prediction error of these models, and to provide a user guide and training for ADOT designers and consultants.

Using Microsoft Excel, researchers created a huge ADOT - specific pavement database that constituted input data of 180 pavement sections. Key inputs of that database were design, material and construction inputs for each section, previous traffic loading information, and measured performance data over the design life of the pavement. These data were collected from the LTPP database, ADOT files and videos, and field surveys conducted by the research team.

The researchers identified several crucial inputs based on their relative importance and sensitivity, and they worked vigorously to more accurately define these inputs and establish Arizona default inputs, as listed below.

- Arizona-specific default values of design, traffic, materials, and construction inputs
- Arizona-specific subgrade soil resilient modulus
- Time of full slab and base friction for various base courses
- Performance criteria and design reliability levels for all classes of highways
- ADOT project-specific traffic inputs
- Corrected weather station data

The calibration process began as soon as the input database was established. The researchers had undertaken a formal verification, calibration, and validation process for the local calibration of the distress and IRI models in ME design. In the verification stage model predictions were tested using global coefficients compared to Arizona performance data. If the model demonstrated any type of bias (over or underprediction), it was considered for recalibration. The recalibration process included identifying new local coefficients for each model using Arizona performance data. If the new coefficients sufficiently removed the bias and reduced the prediction error, then the model was confirmed to be locally calibrated. The validation process included an independent check of the model using 10 % of the data withheld from recalibration, removal of bias, and improvements of model prediction accuracy, resulting in successful calibration of most of the distress and IRI models. Notable improvement of the distress and IRI models indicated that the Arizona-calibrated models provide much more reliable and cost-effective designs than models using global calibration coefficients.

### 2.5.2 Calibration and Implementation of MEPDG for Colorado

The main objective of this study (Mallela, 2013) was to incorporate the MEPDG guide and its accompanying software, AASHTOWare pavement ME design, into the daily pavement design, evaluation, rehabilitation, management, and forensic analysis practices and operations of the Colorado Department of Transportation (CDOT). The entire study was consisted of following major tasks:

- Verification, calibration, and validation of MEPDG global performance prediction models in accordance with Colorado pavement projects
- Design comparisons and sensitivity analysis studies to establish a certain confidence limit in the pavement design procedure
- Development of a Colorado MEPDG pavement design guide so that CDOT personnel can effectively obtain proper inputs, run the ME design, and interpret results

The researchers worked extensively to identify and characterize default inputs of MEPDG by reviewing traffic, climate, and other data records; by laboratory testing strength, modulus and other properties and field surveys; and by conducting destructive and non-destructive tests of various in-service pavements in Colorado. The outcome of this effort was a Colorado-specific project database with all key inputs required for the design and analysis of new and rehabilitated flexible and rigid pavements. Details of 126 new HMA, new JPCP, HMA overlay over JPCP, and unbonded JPCP over JPCP-rehabilitated pavement projects throughout Colorado were used to formulate the database, which was then used to develop Colorado-specific MEPDG traffic, material, climate, and design inputs. Verification and calibration of the distress and smoothness prediction models were also based on that data. For flexible pavement, four performance prediction models (alligator cracking, rutting, transverse cracking, and smoothness (IRI)) were recalibrated for local Colorado conditions; the recalibrated models demonstrated convincing improvement in terms of goodness of fit and bias. For JPCP, the three performance models (transverse cracking, transverse joint faulting, and smoothness (IRI)) were found to be sufficient, so no further calibration was required for local Colorado conditions.

A comprehensive sensitivity analysis of the performance models and design comparisons was performed to integrate local Colorado models into the MEPDG design procedure. Using local calibration results, the research team also updated the CDOT pavement design manual. Local

calibration results proved that use of ME design in the pavement design procedure in Colorado will reliably assist pavement design at optimum cost.

### 2.5.3 Local Calibration of MEPDG Performance Prediction Models in Iowa

The primary objective of this project was to improve the accuracy of MEPDG-predicted pavement performance of the Iowa pavement system by locally calibrating performance prediction models (Ceylan, 2013). A total of 35 HMA sections, 35 JPCP sections, and 60 HMA over JPCP sections were chosen for this study, and MEPDG inputs of selected sections were collected mainly from Iowa DOT pavement management information system (PMIS), previous records of material testing, and project reports relevant to MEPDG implementation in Iowa. Measured performance data of selected pavement sections were extracted from Iowa DOT PMIS.

After gathering all input data, performance of the nationally calibrated MEPDG models was evaluated for Iowa conditions. For local calibration, linear and nonlinear optimization techniques were used to improve the accuracy of performance prediction models. Principal outcomes of the calibration approach are listed below.

- For Iowa JPCP sections, locally calibrated joint faulting, transverse cracking, and IRI models showed improved predictions compared to their nationally calibrated counterparts.
- Locally calibrated factors efficiently increased the accuracy of rutting predictions and somewhat increased the accuracy of top-down cracking predictions for Iowa HMA and Iowa HMA over JPCP sections.
- For new HMA pavement sections in Iowa, the nationally calibrated alligator (bottom-up) cracking model proved to be sufficient.
- Nationally and locally calibrated alligator (bottom-up) cracking models provided acceptable predictions for Iowa HMA over JPCP.
- Use of proper binder grade in Iowa climatic conditions failed to predict or predicted minimal thermal cracking. Without proper design considerations, however, significant thermal cracking was observed in Iowa HMA and HMA over JPCP.
- The IRI model with nationally-calibrated distress inputs with nationally-calibrated coefficients and IRI model of locally-calibrated distress inputs with nationally-

calibrated coefficients showed good agreement for Iowa HMA pavement and HMA over JPCP sections.

Because of significant differences between predictions of the two software versions (MEPDG version 1.1 and DARWin-ME), the Iowa study highly recommended that a local calibration study be repeated while design procedure will shift from DARWin-ME solution to AASHTOWare Pavement ME Design version 1.3.

### 2.5.4 Calibration of MEPDG for Nevada

The primary objective of this study was to locally calibrate bottom-up fatigue cracking and the rutting model in order to properly adapt Nevada's local conditions for materials, traffic, and climate (Nabhan, 2015). Input data were collected from the Nevada Department of Transportation (NDOT) Pavement Management Systems (PMS) database and then transformed to match MEPDG model requirements. In addition, field-produced mixtures were sampled from 45 paving projects from three districts in Nevada in order to develop a material database. Dynamic modulus, binder properties, rutting, and fatigue properties were tested using those mixtures in order to characterize polymer-modified asphalt binder mixture technologies in Nevada, which is essential for local calibration since nationally calibrated models use unmodified binders.

Local calibration was performed by optimizing local calibration factors to reduce the sum of error squared between predicted and measured distresses data. Calibration was performed for new and rehabilitated sections. The study recommended that additional performance monitoring of the polymer-modified paved sections is necessary since the calibration was validated using only 10 years of performance data.

### 2.5.5 Local Calibration of the MEPDG for Flexible Pavement Design in North Carolina

The primary objective of this local calibration study was to calibrate MEPDG performance prediction models for North Carolina materials and conditions using data gathered from the research projects (Kim, 2011).

The scope of this study was broadly divided into the following tasks:

- Development of a geographic information system (GIS)-based local subgrade soil database

- Characterization of 12 commonly used asphalt mixtures in North Carolina based on rutting and fatigue cracking performance
- Characterization of local North Carolina traffic
- Local calibration of MEPDG flexible pavement distress prediction models to reflect local materials and conditions

A total of 46 pavement sections was chosen for this study: 22 were LTPP sites and 24 were non-LTPP sites. LTPP sites were used for calibration because they contained more detailed distress and materials information, and the non-LTPP sections were used for validation.

North Carolina-specific inputs such as subgrade soil and traffic database were built using a GIS-based methodology. The triaxial repeated load permanent deformation (TRLPD) test and the direct tension cyclic test were conducted in the laboratory to develop material-specific HMA rutting and fatigue cracking model coefficients. A multidimensional clustering methodology and a pavement damage-based approach was applied to characterize local traffic and to develop traffic catalogs for traffic parameters required as inputs in the MEPDG.

Primary MEPDG runs made with default calibration values showed that the rut depth and fatigue-cracking predictions differed significantly from the measured values. Two strategies were used to locally calibrate the rutting and fatigue cracking models: the generalized reduced gradient (GRG) method and the genetic algorithm (GA) optimization technique. The GA-based approach was statistically better for total rut depth and alligator-cracking predictions than the GRG method. Although local calibration reduced bias and standard error between the predicted and measured rut depth and fatigue cracking percentage values, the improvement was not significant enough to accept the null hypothesis that the measured data are equal to the predicted data at the 95% confidence interval. Final study results included a set of local calibration factors for the permanent deformation and fatigue-cracking performance prediction models in the MEPDG for North Carolina and the North Carolina MEPDG user reference guide.

### 2.5.6 Local Calibration of MEPDG for Northeastern United States

The key objective of this study was to calibrate the MEPDG flexible pavement performance models in order to meet local condition requirements of the northeastern region of the United States, including Connecticut, Maine, Massachusetts, New Jersey, Pennsylvania, Vermont, New Hampshire, and New York (Momin, 2011). Seventeen pavement sections were

selected for the study, and input data was obtained from the LTPP database of the general pavement studies (GPS) sections of these states. Predicted distresses of rutting, fatigue cracking (alligator and longitudinal), thermal cracking, and IRI derived from MEPDG software (Version 1.1) simulation runs using nationally calibrated coefficients were compared to LTPP measured distress data. Although quite a fair amount of agreement was observed between the predicted and measured distress, a significant amount of bias remained. An attempt was made to minimize the bias by recalibrating MEPDG distress prediction models.

In order to calibrate permanent deformation models of each layer of a flexible pavement, a simple linear regression with no intercept was performed, and a new set of model coefficients ($\beta r1$, $\beta_{GB}$, and $\beta_{SG}$) were proposed for asphalt concrete, granular base, and subgrade layer models. Appropriate model coefficients ($C_1$, $C_2$, and $C_4$) were derived from the fatigue damage output of MEPDG software in order to calibrate the alligator (bottom-up fatigue cracking) and longitudinal (top-down fatigue cracking) cracking models. The thermal-cracking model could not be calibrated because the measured transverse cracking data in the LTPP database did not increase with time as expected. Finally, the IRI model was calibrated by conducting a simple linear regression to estimate the model coefficients ($C_1$, $C_2$, $C_3$, and $C_4$) based on other distresses (rutting, total fatigue cracking, and transverse cracking).

### 2.5.7 Calibration of MEPDG for Local Paved Roads in Wyoming

This study was done to develop traffic characteristic inputs and locally calibrate MEPDG performance prediction models coefficients so that local paved road design could become more representative (Kasperick, 2013). Since local roads were experiencing heavy truck traffic associated with the oil and gas industry, Wyoming-specific traffic inputs were essential.

Predicted distresses calculated from DARWIN-ME using global calibration coefficients differed significantly from measured distresses on local paved roadways, particularly for IRI, rutting, alligator cracking, transverse cracking, and longitudinal cracking. Measured distresses were estimated using Pathway Services Inc. and associated surface imaging. Input data were collected from local county road maintenance superintendents, the Wyoming Department of Transportation (WYDOT), and previous research regarding climatic data in Wyoming. Weigh-in motion (WIM) data collected from non-interstate roadways across Wyoming were used as localized traffic inputs.

A significant amount of error and bias were found between predicted and measured distresses, so calibration coefficients for IRI, alligator cracking, rutting, and longitudinal cracking were adjusted to reduce bias and sum of squared errors. Coefficients that significantly reduced the sum of squared errors and bias were considered as final calibration coefficients. A sensitivity analysis was also performed to determine the effect of layer thicknesses on the prediction capabilities of the AASHTOWare ME software.

### 2.5.8 MEPDG Calibration for Pavement Rehabilitation in Oregon

A majority of pavement work conducted by the Oregon Department of Transportation (ODOT) involves the rehabilitation of existing pavements. Although HMA overlays are typically preferred for rigid and flexible pavements, HMA overlays are susceptible to fatigue cracking (alligator and longitudinal cracking), rutting, and thermal cracking. Therefore, the main objective of this study was to calibrate the design process for rehabilitation of existing pavement structures in Oregon (Williams, 2013). Forty-four pavement sections throughout the state were chosen for the study, and MEPDG software (Version 1.1) was used with nationally calibrated coefficients to make a detailed comparison of predictive and measured distresses. Results showed that software-predicted distresses did not accurately comply with measured distresses, thereby requiring local calibration of the performance prediction models.

Among various types of distresses, AASHTOWare ME overpredicted total rutting compared to measured total rutting and, compared to field-measured data, considerably underestimated the amount of cracking for alligator (bottom-up) and thermal cracking. A significant amount of variability between predicted and measured values was also observed for longitudinal (top-down) cracking.

Performance prediction models for rutting, alligator, longitudinal, and thermal cracking of HMA overlays were locally calibrated for Oregon conditions. After calibration, the locally calibrated models for rutting, alligator, and longitudinal cracking showed improved predictions with lower bias and standard error than the nationally calibrated models, However, some inconstancy was observed between predicted and measured distresses, even after the calibration, for longitudinal and transverse cracking, potentially due to the presence of a significant lack-of-fit modeling error for the occurrence of longitudinal cracks in AASHTOWare ME design.

## 2.6 Summary

MEPDG has brought some evolutionary changes in the design and performance evaluation of flexible pavements and JPCP. Distress prediction models of these pavements are becoming a reliable way to assess the design strategy so that the distresses can be minimized in the design life. A number of state highway agencies has locally calibrated the AASHTOWare ME design to adopt with their local conditions. Local calibration of the performance prediction model coefficients for Kansas may be helpful in the paradigm shift of current AASHTO design guide (1993) to MEPDG in the pavement design policy of the state.

# Chapter 3 - Methodology

This chapter describes the procedure for the local calibration of performance prediction models of AASHTOWare Pavement ME Design software version 2.2. The calibration process is based on guidelines for local calibration in the MEPDG guide (AASHTO, 2010) developed under NCHRP Research Project 1-40B. The 10-step procedure for local calibration followed in this study is listed below.

1. Select hierarchical level of input for each parameter.
2. Develop local experimental plan and sampling technique.
3. Estimate sample size for various distress prediction models.
4. Select roadway segments.
5. Extract and evaluate distress and project data.
6. Conduct field and forensic investigations.
7. Assess local bias by validating globally calibrated values to local conditions, policies, and materials.
8. Eliminate local bias of distress and IRI prediction models.
9. Assess the standard error of estimate (Se).
10. Reduce the standard error of estimate (Se).

The following sections describe the local calibration methodology by briefly discussing these 10 steps.

## 3.1 Select Hierarchical Input Level

The selection of the hierarchical input level is one of the most important steps in local calibration. Because this selection is primarily an agency decision, KDOT-provided inputs were mostly used in this study; therefore, the inputs were coherent with KDOT's current field and laboratory testing capabilities, material and construction specifications, and traffic data collection procedures and equipment. The input selection procedure can be broadly divided into three categories: traffic, climate, and materials.

### 3.1.1 Traffic Input

The AASHTOWare pavement ME design software allows a designer to input traffic parameters at three levels. Level 1 is project-specific with extensive traffic volume and load data, Level 2 is regional input parameters derived from weigh-in motion (WIM) and automatic vehicle classifier (AVC) stations across the state, and Level 3 is based on global default values already included in the software.

This study used site-specific traffic inputs such as AADTT data, operational speed, number of lanes, and the percentage of trucks in a design direction or lane. Details of site-specific inputs are shown in Table 3-1. General information regarding the sections and growth factor was used as per KDOT suggestions. Additional input parameters, such as vehicle class factor (VCF), monthly adjustment factors (MAFs), hourly distribution factors (HDFs), axles per truck, and axle load spectrum, were generated from 11 AVC stations and 10 WIM stations in Kansas. Therefore, these derived traffic parameters were considered to be statewide Level 2 traffic input for the state of Kansas.

**Table 3-1 : General traffic inputs**

| Input Parameters | | Source | Value used | Input Level |
|---|---|---|---|---|
| (AADTT) | Two-way AADTT | Actual Project Data (APD) | As in APD | 1 |
| | Number of lanes | APD | As in APD | 1 |
| | Percent trucks in design direction | Default | 50 | 3 |
| | Percent trucks in design lane | KDOT suggested | 95 or 100 (for 2 lanes) | 3 |
| | Operational speed (mph) | APD | As in APD | 1 |
| Axle Configuration | Average axle width (ft) | Default | 8.5 | 3 |
| | Dual tire spacing (in.) | Default | 12 | 3 |
| | Tire pressure (psi) | Default | 120 | 3 |
| | Tandem axle spacing (in.) | Default | 51.6 | 3 |
| | Tridem axle spacing (in.) | Default | 49.2 | 3 |
| | Quad axle spacing (in.) | Default | 49.2 | 3 |
| Lateral Wander | Mean wheel location (in.) | Default | 18 | 3 |
| | Traffic wander standard deviation (in.) | Default | 10 | 3 |
| | Design lane width (ft) | Default | 12 | 3 |

| Input Parameters | | Source | Value used | Input Level |
|---|---|---|---|---|
| Wheelbase | Average spacing of short axles (ft) | Default | 12 | 3 |
| | Average spacing of medium axles (ft) | Default | 15 | 3 |
| | Average spacing of long axles (ft) | Default | 18 | 3 |
| | Percent trucks with short axles | KDOT suggested | 50 | 3 |
| | Percent trucks with medium axles | KDOT suggested | 25 | 3 |
| | Percent trucks with long axles | KDOT suggested | 25 | 3 |
| Growth factor (%) | | KDOT suggested | Rural – 2%<br>Urban – 3% | 3 |

This study also included extensive work to produce Level 2 regional traffic inputs for Kansas. Input parameters were derived from data gathered from 11 AVC stations and 10 WIM stations throughout the state. Lists of these WIM and AVC stations are presented in Table 3-2 and 3-3, respectively.

**Table 3-2: WIM stations**

| WIM Station | County | Route | Functional Classification |
|---|---|---|---|
| 2WOA86 | Seward | US-54 | Rural Principle Arterial |
| 3MXC22 | Meade | US-54 | Rural Principle Arterial |
| 4LGSU3 | Thomas | I-70 | Rural Interstate |
| 9M4PS3 | Saline | I-70 | Rural Interstate |
| 9ORQP1 | Sedgwick | I-135 | Urban Interstate |
| 9Q9OK1 | Sedgwick | I-135 | Urban Interstate |
| BWGAA6 | Lyon | I-35 | Urban Interstate |
| DVMSP3 | Douglas | I-70 | Urban Interstate |
| F07WC7 | Wyandotte | I-70 | Urban Interstate |
| 2OPUF5 | Logan | US-83 | Rural Principle Arterial |

**Table 3-3: AVC stations**

| AVC Station | County | Route | Functional Classification |
|---|---|---|---|
| 7HOM63 | Russel | I-70 | Urban Principle Arterial |
| 7XRME7 | Kingman | US-54 | Rural Principle Arterial |
| 9LON61 | Sedgwick | I-235 | Urban Principle Arterial |
| 9Q9OK1 | Sedgwick | I-135 | Urban Principle Arterial |
| 61ILI3 | Kiowa | US-54 | Rural Principle Arterial |
| 91TFY5 | Republic | US-81 | Rural Principle Arterial |
| AW9N83 | Butler | US-400 | Rural Principle Arterial |
| CTQ1D1 | Brown | US-36 | Rural Principle Arterial |
| CV64B3 | Montgomery | I-166 | Rural Principle Arterial |
| F10VD5 | Bourbon | US-69 | Rural Principle Arterial |
| 0DT453 | Sherman | I-70 | Rural Principle Arterial |

Input parameters derived from these WIM and AVC stations are described below.

#### 3.1.1.1 Vehicle Class Factor

VCFs determine the frequency of trucks in each vehicle class from FHWA vehicle Class 4 to Class 13. FHWA vehicle category classification is shown in Figure 3-1. Level 3 VCFs in the AASHTOWare pavement ME design software are based on roadway function, classification, and truck traffic classification (TTC) groups for a particular roadway. In this study VCFs were generated from AVC data of eight stations located on rural principal arterials in Kansas.

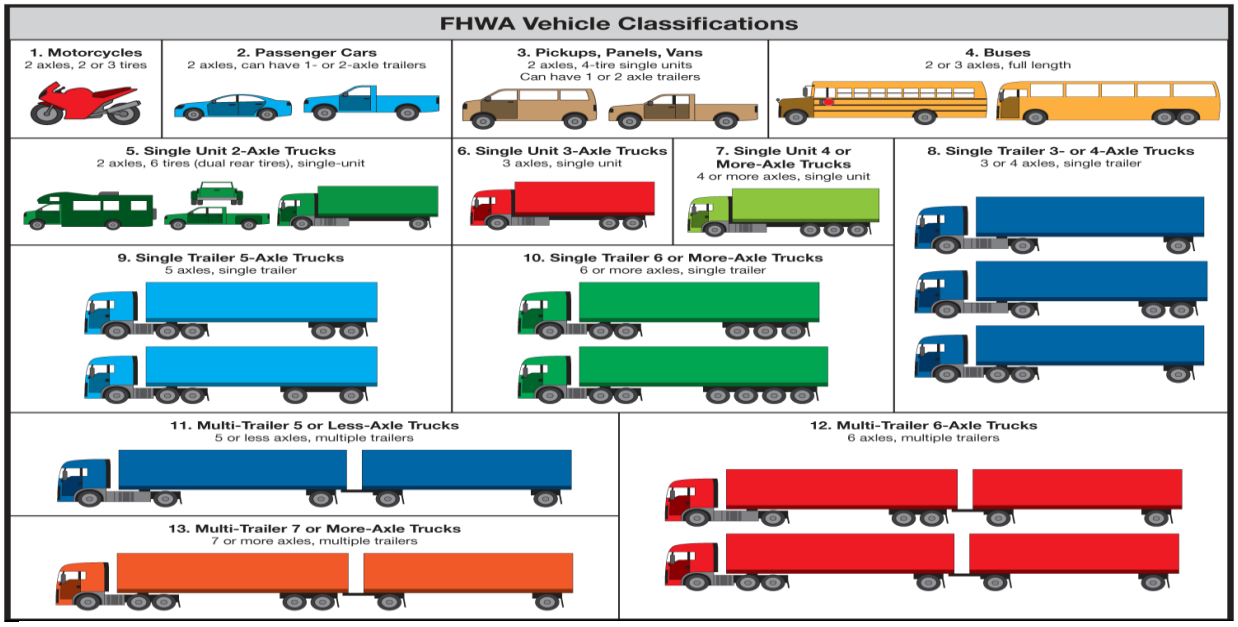


**Figure 3-1: FHWA vehicle classification (Source: TxDOT)**

The weighted average values of VCF were obtained based on the number of trucks in each class, as shown in Table 3-4. VCF values of individual AVC stations are presented in the appendix (Table A-1).

**Table 3-4: Vehicle class distribution**

| Vehicle Class | Vehicle Class Factor |
|---|---|
| Class 4 | 29.47 |
| Class 5 | 6.87 |
| Class 6 | 5.24 |
| Class 7 | 1.59 |
| Class 8 | 5.32 |
| Class 9 | 45.56 |
| Class 10 | 2.07 |
| Class 11 | 2.89 |
| Class 12 | 0.81 |
| Class 13 | 0.17 |

#### 3.1.1.2 Monthly Adjustment Factors

Truck traffic MAFs are defined as the proportion of annual truck traffic for a particular truck class for a specific month (NCHRP, 2004). These factors are used to determine monthly variation in truck traffic within a base year. MAFs are influenced by factors such as adjacent lane use, location of industries, and roadway location (Khanum, 2005). This study conducted a two-dimensional clustering analysis with MAF values derived from the 11 AVC stations throughout Kansas. Class 9 was found to be the prevalent vehicle class in Kansas. Average MAFs were calculated from all the stations, as shown in Table 3-5. MAFs of individual stations are provided in the appendix tables A-2 to A-12.

#### 3.1.1.3 Hourly Distribution Factors

HDFs, which are required only for rigid pavements, are derived from the percentage of AADTT at each hour of the day (NCHRP, 2004). The hourly distribution of truck traffic is required to compute incremental damage of the pavement structure for various thermal gradients during a 24-hour period (Khanum, 2005). In this study HDF values that were generated from 11 AVC stations located along urban and rural principal arterials in Kansas were classified based on the functional class of the roadway. Average HDFs were calculated from the 11 AVC stations, as shown in Table 3-6. HDFs of individual stations are provided in the appendix (Table A-13).

**Table 3-5: Monthly adjustment factor**

| Month | Class 4 | Class 5 | Class 6 | Class 7 | Class 8 | Class 9 | Class 10 | Class 11 | Class 12 | Class 13 |
|---|---|---|---|---|---|---|---|---|---|---|
| Jan | 1.07 | 0.90 | 0.90 | 0.65 | 0.76 | 0.94 | 1.19 | 1.11 | 1.23 | 0.86 |
| Feb | 1.14 | 0.88 | 0.90 | 0.55 | 0.79 | 0.97 | 0.95 | 1.14 | 1.16 | 0.85 |
| Mar | 1.30 | 1.03 | 1.00 | 0.86 | 0.87 | 1.04 | 1.12 | 1.14 | 1.07 | 0.91 |
| Apr | 1.03 | 1.28 | 1.22 | 1.19 | 1.15 | 1.17 | 1.26 | 1.10 | 1.22 | 1.24 |
| May | 1.04 | 1.22 | 1.07 | 0.95 | 1.12 | 1.05 | 1.15 | 0.97 | 1.10 | 1.08 |
| Jun | 1.00 | 1.11 | 1.09 | 1.07 | 1.05 | 1.06 | 0.99 | 0.91 | 0.87 | 1.19 |
| Jul | 0.94 | 1.09 | 1.06 | 1.18 | 1.08 | 1.05 | 0.96 | 0.94 | 0.83 | 1.11 |
| Aug | 0.83 | 1.01 | 1.08 | 1.07 | 1.07 | 1.04 | 1.02 | 0.94 | 0.81 | 1.14 |
| Sep | 0.87 | 0.92 | 0.94 | 1.01 | 0.97 | 0.90 | 0.86 | 0.79 | 0.68 | 0.91 |
| Oct | 1.04 | 1.03 | 1.00 | 0.90 | 1.08 | 1.00 | 0.87 | 0.97 | 0.83 | 0.97 |
| Nov | 0.96 | 0.76 | 0.83 | 1.91 | 1.34 | 0.79 | 0.78 | 0.95 | 1.16 | 0.86 |
| Dec | 0.77 | 0.75 | 0.91 | 0.67 | 0.73 | 0.99 | 0.85 | 1.03 | 1.04 | 0.89 |

**Table 3-6: Hourly distribution factors**

| Hour | Hourly Truck Distribution (%) |
|---|---|
| Midnight | 1.64 |
| 1 | 1.37 |
| 2 | 1.38 |
| 3 | 1.51 |
| 4 | 1.82 |
| 5 | 2.27 |
| 6 | 3.16 |
| 7 | 4.29 |
| 8 | 5.44 |
| 9 | 6.21 |
| 10 | 6.51 |
| 11 | 6.62 |
| Noon | 6.63 |
| 13 | 6.66 |
| 14 | 6.53 |
| 15 | 6.31 |
| 16 | 6.14 |
| 17 | 5.61 |
| 18 | 4.83 |
| 19 | 4.08 |
| 20 | 3.52 |
| 21 | 2.99 |
| 22 | 2.45 |
| 23 | 2.05 |

### 3.1.1.4 Axle Group per Vehicle

AASHTOWare pavement ME design software requires average number of axle group per vehicle (AGPV) and axle load spectra in order to compute average damage imposed on the pavement structure by truck traffic in each vehicle class (Romanoschi et al., 2011). AGPV is obtained for each vehicle class by dividing the total number of axles (single/tandem/tridem/quad) by the number of trucks. In this study WIM data (Table 3-2) was used to compute average AGPV values for rural and urban roadways in Kansas, as presented in Table 3-7. AGPV of individual WIM stations are presented in the appendix (Table A-14 to A-23).

**Table 3-7: Axle group per vehicle for rural and urban roadways for Kansas**

| Vehicle Class | Kansas Rural | | | | Kansas Urban | | | |
|---|---|---|---|---|---|---|---|---|
| | Single | Tandem | Tridem | Quad | Single | Tandem | Tridem | Quad |
| 4 | 1.8976 | 0.2842 | 0 | 0 | 2.2106 | 0.5738 | 0.002 | 0 |
| 5 | 2.1562 | 0.68 | 0.775 | 0 | 2.0794 | 0.5026 | 0.642 | 0 |
| 6 | 1.3214 | 1.695 | 0 | 0 | 1.3536 | 1.647 | 0 | 0 |
| 7 | 2.2 | 0.8 | 0.1 | 0.134 | 1.8664 | 0.9592 | 0.922 | 0.4494 |
| 8 | 2.1906 | 1.5198 | 0 | 0 | 2.3046 | 1.4924 | 0 | 0 |
| 9 | 1.5398 | 3.4524 | 0.0068 | 0 | 1.531 | 3.457 | 0.0164 | 0 |
| 10 | 2.6446 | 2.0014 | 1.2256 | 0.008 | 2.2142 | 2.062 | 1.5888 | 0.2864 |
| 11 | 4 | 0 | 0 | 0 | 5 | 0 | 0 | 0 |
| 12 | 3.843 | 1.7544 | 0 | 0 | 3.9932 | 2.007 | 0 | 0 |
| 13 | 2.525 | 0.816 | 0.55 | 0 | 3.6968 | 1.067 | 0 | 0 |

### 3.1.1.5 Axle Load Spectra

AASHTOWare pavement ME design software requires the frequency of total axle load applications within each load class interval for a specific axle type (single, tandem, tridem, and quad) and vehicle class (Classes 4 through 13) for each month of the year. For single axles, load distribution ranges from 3,000 to 40,000 lbs at 1,000-lb intervals; for tandem axle, distribution ranges from 6,000 to 80,000 lbs at 2,000-lb intervals; and for tridem and quad axles, distribution ranges from 12,000 to 102,000 lbs at 3,000-lb intervals.

In this study axle load spectra were derived manually using KDOT-provided WIM data. For all WIM stations “W” card data were processed for 48 hours of data. Although AASHTOWare ME requires normalized axle load distribution for each month of the year, truck weight data were not available at any site for all months of the year. However, previous researchers have suggested

that variations in axle load spectra across the months within a year and across the years are not significant (Tam & Von Quintus, 2004; Khanum, 2005). Therefore, this study used axle load spectra derived from 48 hours of WIM data for each month of the year.

Axle load spectra were developed for 10 WIM stations: five on rural roadways and five on urban roadways. Statewide distribution of axle loads for rural and urban roadways was developed by taking averages across respective WIM sites.

### 3.1.2 Climatic Inputs

Among all climatic inputs, the geo coordinates (latitude and longitude) and elevations for all pavement sections were given input as site-specific values, or Level 1 inputs. Depth of the water table for all segments was set at 50 ft because this value does not affect performance predicted by MEPDG. Climatic stations used in this study were chosen from the default locations in the software or a virtual weather station created to more accurately depict the effect of climate on pavement structure. Brief descriptions of the climatic stations, as well as other inputs used in this study for flexible and JPCP pavements, are presented in Table 3-8 and Table 3-9, respectively.

**Table 3-8: Site-specific climatic inputs for flexible pavement sections**

| Project Name | Climate Station | Latitude (deg) | Longitude (deg) | Elevation (ft) |
|---|---|---|---|---|
| 003U0007300-NB | Topeka, KS/ Kansas City, MO | 39.008 | -95.212 | 827 |
| 007U0007500-NB | Topeka, KS/ Kansas City, MO | 39.008 | -95.212 | 827 |
| 008U0007700-NB-1 | Wichita, KS | 37.647 | -97.429 | 1320 |
| 008U0007700-NB-2 | Wichita, KS/ Emporia, KS | 37.647 | -97.429 | 1320 |
| 008U0007700-NB-3 | Wichita, KS/ Emporia, KS | 37.647 | -97.429 | 1320 |
| 008U0005400-EB | Wichita, KS | 37.647 | -97.429 | 1320 |
| 011U0006900-NB | Parsons, KS/ Joplin, MO | 39.008 | -95.212 | 827 |
| 019K0000700-NB-1 | Parsons, KS/ Joplin, MO | 37.647 | -97.429 | 1320 |
| 019K0000700-NB-2 | Parsons, KS/ Joplin, MO | 37.647 | -97.429 | 1320 |
| 019U0016000-EB | Parsons, KS | 37.328 | -95.504 | 869 |
| 022K0000700-NB | St. Joseph, MO | 39.008 | -95.212 | 827 |
| 023U0004000-EB | Lawrence, KS | 39.008 | -95.212 | 827 |
| 025K0009900-NB | Parsons, KS/ Coffeyville, KS | 39.008 | -95.212 | 827 |
| 027K0015600-EB | Manhattan, KS/ Wichita, KS | 39.008 | -95.212 | 827 |
| 028U0005000-EB | Garden City, KS | 37.927 | -100.725 | 2878 |
| 031K0001800-WB | Manhattan, KS | 39.134 | -96.679 | 1048 |
| 033U0028300-NB | Kansas City, MO/ Hill City, KS | 39.008 | -95.212 | 827 |
| 052U0007300-NB | Topeka, KS/ Kansas City, MO | 39.008 | -95.212 | 827 |
| 065K0002700-NB | Garden City, KS/ Guymon, OK | 37.927 | -100.725 | 2878 |
| 065U0005600-EB | Garden City, KS/ Guymon, OK | 37.927 | -100.725 | 2878 |
| 069U0028300-NB | Concordia, KS/ Hill City, KS | 39.549 | -97.652 | 1469 |
| 082U0018300-NB | Russell, KS/ Hill City, KS | 39.549 | -97.652 | 1469 |
| 088U0005400-WB | Garden City, KS/ Guymon, OK | 37.927 | -100.725 | 2878 |
| 091K0002700-NB | Goodland, KS | 39.368 | -101.693 | 3647 |
| 095U0005600-EB | Garden City, KS/ Guymon, OK | 37.927 | -100.725 | 2878 |
| 098U0028300-NB | Russell, KS/ Hill City, KS | 38.872 | -98.828 | 1864 |
| 103K0003900-NB | Coffeyville, KS/ Chanute, KS | 37.091 | -95.566 | 749 |

**Table 3-9:Site-specific climatic inputs for JPCP sections**

| Project Name | Climate Station | Latitude (deg) | Longitude (deg) | Elevation (ft) |
|---|---|---|---|---|
| 018U0007700-NB | Winfield/Arkansas City, KS | 37.0706233 | -97.0240309 | 1065 |
| 018K0036000-EB | Winfield/Arkansas City, KS | 37.225067 | -96.9781722 | 1117 |
| 031I0007000-EB | Manhattan, KS | 39.0449709 | -96.7501042 | 1150 |
| 040I0013500-NB-1 | Hutchinson, KS | 38.068 | -97.861 | 1523 |
| 040I0013500-NB-2 | Hutchinson, KS | 38.068 | -97.861 | 1523 |
| 043U0007500-NB | Topeka, KS / Manhattan, KS | 39.2600283 | -95.7196306 | 1104 |
| 043U0007500-NB2 | Topeka, KS / Manhattan, KS | 39.3727421 | -95.7390952 | 1146 |
| 046K0000700-SB | Olathe, KS | 38.90533 | -94.8529777 | 960 |
| 055U0004000-EB | Goodland, KS | 39.368 | -101.693 | 3647 |
| 056I0003500-SB-1 | Emporia, KS | 38.4258742 | -96.2098737 | 1140 |
| 056U0005000-EB | Emporia, KS | 38.406537 | -96.2994248 | 1127 |
| 059I0013500-NB | Hutchinson, KS/Salina, KS | 38.2773303 | -97.5862339 | 1489 |
| 061I0003500-NB | Olathe, KS | 38.7112102 | -95.0425239 | 990 |
| 063U0040000-EB | Parsons, KS | 37.328 | -95.504 | 869 |
| 067U0016900-NB | Chanute, KS | 37.509554 | -95.4712541 | 1016 |
| 079U0008100-NB | Concordia, KS | 39.8509181 | -97.6153008 | 1552 |
| 085I0007000-EB | Salina, KS | 38.8806726 | -97.5810515 | 1219 |
| 103U0040000-EB | Chanute, KS | 37.5711968 | -95.8515186 | 1127 |

### 3.1.3 Materials Input

This study utilized site-specific inputs such as volumetric data of the asphalt concrete mixture and physical properties of Portland cement concrete. KDOT-suggested values and MEPDG default values were also provided as material inputs in the ME design software.

#### 3.1.3.1 Asphalt Concrete Properties

AASHTOWare pavement ME design software requires dynamic modulus (E*), creep compliance, and indirect tensile strength of the asphalt mix for Level 1 input. Dynamic shear modulus (G*) and phase angle (δ) values of the asphalt binder are also required to generate dynamic modulus master curves for asphalt mixes. Since these data were not available for the selected projects, Level 3 input values (aggregate gradation, binder grade, mix volumetric properties) were extracted from the KDOT website for surface layer, intermediate layer, and base

layer. However, because even Level 3 inputs were not available for Project 065K0002700-NB, KDOT suggested that the aggregate gradation be the midpoint value of the BM-1T mix for surface course and BM-2C mix (KDOT 1990 specification) for binder and base courses. Both mixes contained an AC-10 asphalt cement equivalent to a PG 58-28 binder. Level 3 inputs for all projects are listed in the appendix B. Brief descriptions of all other AC property inputs are given in Table 3-10.

**Table 3-10: Inputs of AC properties**

| Input Parameters | | Source | Value Used | Input Level |
|---|---|---|---|---|
| Mixture Volumetrics | Thickness (in.) | APD | As in APD | 1 |
| | Unit weight (pcf) | Default | 140 | 3 |
| | Poisson's ratio | Default | 0.35 | 3 |
| | Air voids (%) | Default | 7 | 3 |
| | Effective binder content (%) | KDOT suggested | As KDOT suggestion | 3 |
| Mechanical Properties | Preference temperature (˚ F) | Default | 70 | 3 |
| | Indirect tensile strength at 14 ˚F (psi) | Default | Default value | 3 |
| | Creep compliance (1/psi) | Default | Default value | 3 |
| Thermal | Thermal conductivity (BTU/hr-ft-˚ F) | Default | 0.67 | 3 |
| | Heat capacity (BTU/lb-˚F) | Default | 0.23 | 3 |
| | Thermal contraction | Default | 1.30E-05 | 3 |
| AC Layer Properties | AC surface shortwave absorptivity | Default | 0.85 | 3 |
| | Is endurance limit applied? | Default | No | 3 |
| | Endurance limit (Microstrain) | Default | 100 | 3 |
| | Layer interface | Default | Full friction interface | 3 |

### 3.1.3.2 JPCP properties

Inputs were given at different levels for JPCP properties. Brief descriptions of all JPCP property inputs are listed in Table 3-11.

**Table 3-11: Inputs of JPCP properties**

| Input Parameters | | Source | Value Used | Input Level |
|---|---|---|---|---|
| Slab thickness | | APD | As in APD | 1 |
| Unit weight | | KDOT suggested | 140 pcf | 3 |
| Poisson's ratio | | Default | 0.2 | 3 |
| Coefficient of thermal expansion | Limestone | KDOT suggested | $5.5 \times 10^{-6}$ in/in/°F | 3 |
| | Non-Limestone | KDOT suggested | $6 \times 10^{-6}$ in/in/°F | 3 |
| Thermal conductivity | | Default | 1.25 | 3 |
| PCC heat capacity | | Default | 0.25 | 3 |
| Cement type | | APD | As in APD | 1 |
| Cementitious content | | APD | As in APD | 1 |
| Water to cement ratio | | APD | As in APD | 1 |
| Aggregate type | | APD | As in APD | 1 |
| Reversible shrinkage | | KDOT suggested | 35 | 3 |
| 50% of ultimate shrink | | Default | 35 | 3 |
| Curing method | | APD/Default | As in APD/ Curing compound | 1/3 |
| Compressive strength | | APD/KDOT suggested | As in APD | 1/3 |
| Joint spacing | | APD | As in APD | 1 |
| Sealant type | | APD | As in APD | 1 |
| Dowel spacing | | APD | As in APD | 1 |
| Dowel diameter | | KDOT suggested | 6″<Pavement Depth<9″, use 1″ diameter | 3 |
| | | | 9″≤Pavement Depth<11″, use 1.25″ diameter | |
| | | | Pavement Depth≥11″, use 1″ diameter | |
| Widened slab | | APD | As in APD | 1 |
| Tied shoulders | | APD | As in APD | 1 |
| Erodibility index | | KDOT suggested | 2 | 3 |

### 3.1.3.3 Base Course Material Inputs

Pavement sections used in this study were constructed with either cement or asphalt-treated base, granular base, or lime-treated subgrade (LTSG). Brief descriptions of all base course property inputs are given in Table 3-12.

**Table 3-12: Inputs of base course materials**

| Input Parameters | | Source | Value Used | Input Level |
|---|---|---|---|---|
| Cement/ Asphalt treated base | Thickness | APD | As in APD | 1 |
| | Poisson's ratio | Default | 0.2 | 3 |
| | Elastic/resilient modulus | KDOT suggested | 1,000,000 psi | 3 |
| Granular/ aggregate base | Thickness | APD | As in APD | 1 |
| | Poisson's ratio | Default | 0.35 | 3 |
| | Elastic/resilient modulus | KDOT suggested | 31,000 psi | 3 |
| Bound drainable base | Thickness | APD | As in APD | 1 |
| | Poisson's ratio | KDOT suggested | 0.35 | 3 |
| | Elastic/resilient modulus | KDOT suggested equation | LTSG Mr = (2.03 × untreated subgrade Mr) + 225 | 3 |
| | Gradation | Default | Default values | 3 |

### 3.1.3.4 Subgrade Soil Inputs

The subgrade soil of almost all pavement sections was classified as A-7-6. Beneath the LTSG layer a 12-inch compacted subgrade layer was assumed for all projects. KDOT provided a list of average county-wide soil-resilient modulus values used in the calibration. These values are shown in Table 3-13. Subgrade soil gradation values for each county were obtained from soil survey reports from the Soil Conservation Service. Extracted engineering properties of subgrade soils of flexible and concrete pavements are shown in Table 3-14 and 3-15, respectively.

**Table 3-13: Resilient modulus of soil by county**

| County | Resilient Modulus (Mr) (psi) |
|---|---|
| Atchison | 2600 |
| Brown | 2600 |
| Butler | 2600 |
| Cherokee | 3900 |
| Crawford | 2900 |
| Doniphan | 2600 |
| Douglas | 2700 |
| Edwards | 4000 |
| Elk | 2600 |
| Ellsworth | 4600 |
| Finney | 3200 |
| Geary | 2800 |
| Gove | 4900 |
| Graham | 3900 |
| Gray | 4100 |
| Haskell | 2900 |
| Johnson | 2600 |
| Kiowa | 4500 |
| Leavenworth | 3100 |
| McPherson | 2600 |
| Miami | 3600 |
| Montgomery | 3500 |
| Morton | 4400 |
| Norton | 3600 |
| Osage | 2600 |
| Republic | 2700 |
| Riley | 3100 |
| Rooks | 3500 |
| Russell | 2600 |
| Sedgwick | 4100 |
| Seward | 4700 |
| Shawnee | 3100 |
| Sheridan | 3700 |
| Sherman | 4100 |
| Stevens | 4500 |
| Thomas | 5000 |
| Trego | 3500 |
| Wyandotte | 3300 |

## Table 3-14: Engineering properties of subgrade soil of flexible pavement

| Project No. | County | Soil Type | Gradation (% Passing) | | | | Atterberg Limits | |
|---|---|---|---|---|---|---|---|---|
| | | | #4 Sieve | #10 Sieve | #40 Sieve | #200 Sieve | Liquid Limit | Plasticity Index |
| 003U0007300-NB | Atchison | Sharpsburg Silty Clay Loam | 100 | 100 | 100 | 95-100 | 40-60 | 20-35 |
| 007U0007500-NB | Brown | Judson Silt Loam | 100 | 100 | 100 | 95-100 | 30-50 | 15-25 |
| 008U0007700-NB-1 | Butler | Ladysmith Silt Clay Loam | 100 | 100 | 95-100 | 95-100 | 47 | 27 |
| 008U0007700-NB-2 | Butler | Vedigris Silt Loam | 100 | 100 | 95-100 | 95-100 | 47 | 27 |
| 008U0007700-NB-3 | Butler | Labette-Dwight complex Silt Loam | 100 | 100 | 95-100 | 95-100 | 47 | 27 |
| 008U0005400-EB | Butler | Vedigris Silt Loam | 100 | 100 | 95-100 | 90-100 | 52 | 29 |
| 011U0006900-NB | Cherokee | Labette-Dwight complex Silt Loam | 100 | 100 | 95-100 | 90-100 | 47 | 27 |
| 019K0000700-NB-1 | Crawford | Parsons Silt Loam | 100 | 100 | 95-100 | 85-95 | 49 | 30 |
| 019K0000700-NB-2 | Crawford | Lula Silt Loam | 100 | 100 | 98 | 91 | 57 | 32 |
| 019U0016000-EB | Crawford | Lula-Clareson complex | 100 | 100 | 98 | 91 | 57 | 32 |
| 022K0000700-NB | Doniphan | Monona silt loam | 100 | 100 | 95-100 | 95-100 | 30-45 | 10-20 |
| 023U0004000-EB | Douglas | Martin silt clay loam | 100 | 100 | 95-100 | 80-98 | 41-70 | 25-40 |
| 025K0009900-NB | Elk | Kenoma silt loam | 85-100 | 85-100 | 75-100 | 75-95 | 45-65 | 25-44 |
| 027K0015600-EB | Ellsworth | Crete silt loam | 100 | 100 | 100 | 95-100 | 30-55 | 10-35 |
| 028U0005000-EB | Finney | Ulysses silt loam | 100 | 100 | 100 | 90-100 | 30-55 | 10-35 |
| 031K0001800-WB | Geary | Muir silt clay loam | 100 | 100 | 95-100 | 90-100 | - | - |
| 033U0028300-NB | Graham | Holdrege silt loam | 100 | 100 | 95-100 | 95-100 | 25-40 | 9-17 |
| 052U0007300-NB | Leavenworth | Marshall silt loam | 100 | 100 | 90-100 | 95-100 | 44 | 23 |
| 065K0002700-NB | Morton | Dalhart loamy fine sand | 92 | 64 | 20 | 9 | 16 | 2 |
| 065U0005600-EB | Morton | Dalhart loamy fine sand | 92 | 64 | 20 | 9 | 16 | 2 |
| 069U0028300-NB | Norton | Holdrege silt loam | 100 | 100 | 98-100 | 95-100 | 30-45 | 5-20 |
| 082U0018300-NB | Rooks | Harney silt loam | 100 | 100 | 95-100 | 85-100 | 30-40 | 10-20 |
| 084U0028100-NB | Russell | Nibson silt loam | 85-95 | 80-95 | 60-90 | 55-90 | 30-45 | 10-25 |
| 088U0005400-WB | Seward | Richfield silt loam | 100 | 100 | 100 | 90-100 | 30-45 | 30-45 |
| 091K0002700-NB | Sherman | Keith silt loam | 100 | 100 | 100 | 85-100 | 30-45 | 10-25 |
| 095U0005600-EB | Stevens | Ulysses silt loam | 100 | 100 | 100 | 90-100 | 30-55 | 10-35 |
| 098U0028300-NB | Trego | Hord silt loam | 100 | 100 | 100 | 85-100 | 25-40 | 6-21 |
| 103K0003900-NB | Wilson | Hord silt loam | 100 | 100 | 100 | 85-100 | 25-40 | 6-21 |

**Table 3-15: Engineering properties of subgrade soil of rigid pavement**

| Project No. | County | Soil Type | Gradation (% Passing) | | | | Atterberg Limits | |
|---|---|---|---|---|---|---|---|---|
| | | | #4 Sieve | #10 Sieve | #40 Sieve | #200 Sieve | Liquid Limit | Plasticity Index |
| 018K0036000-EB | Cowley | Labette silt clay loam | 60-100 | 60-100 | 60-95 | 60-95 | 40-60 | 20-35 |
| 018U0007700-NB | Cowley | Labette silt clay loam | 60-100 | 60-100 | 60-95 | 60-95 | 40-60 | 20-35 |
| 031I0007000 | Geary | Chase silty clay loam | 100 | 100 | 95-100 | 90-100 | -* | -* |
| 040I0013500-NB-1 | Harvey | Ladysmith silty clay loam | - | 100 | 95-100 | 90-100 | -* | -* |
| 040I0013500-NB-2 | Harvey | Ladysmith silty clay loam | - | 100 | 95-100 | 90-100 | -* | -* |
| 043U0007500-NB-1 | Jackson | Pawnee clay loam | 95-100 | 95-100 | 85-100 | 70-85 | 50-70 | 25-45 |
| 043U0007500-NB-2 | Jackson | Pawnee clay loam | 95-100 | 95-100 | 85-100 | 70-85 | 50-70 | 25-45 |
| 046K0000700-SB | Johnson | Grundy silty clay loam | 100 | 100 | 95-100 | 95-100 | 45-55 | 30-40 |
| 055U0004000-WB | Logan | Keith silt clay loam | 100 | 100 | - | 90-100 | -* | -* |
| 085I0007000-EB | Saline | Detroit Silty Clay Loam | 95-100 | 95-100 | 85-100 | 70-85 | 50-70 | 25-45 |
| 056I0003500-SB-1 | Lyon | Kenoma Silt Loam | 85-100 | 85-100 | 85-100 | 85-100 | 50-65 | 30-45 |
| 056U0005000-EB-1 | Lyon | Osage Silty Clay | 100 | 100 | 100 | 95-100 | 50-80 | 30-55 |
| 059I0013500-NB | Mcpherson | Crete Silty Clay Loam | 100 | 100 | 100 | 95-100 | 50-65 | 25-38 |
| 061I0003500-NB | Miami | Woodson Silty Clay Loam | 100 | 95-100 | 95-100 | 90-100 | 50-65 | 30-45 |
| 063U0040000-EB | Montgomery | Dennis Silty Clay Loam | 98-100 | 98-100 | 94-100 | 75-98 | 33-48 | 13-25 |
| 067U0016900-NB | Neosho | Kenoma Silty Clay Loam | 85-100 | 85-100 | 85-100 | 85-100 | 50-75 | 30-48 |
| 079U0008100-NB | Republic | Crete Silty Clay Loam | 100 | 100 | - | 90-100 | 50-75 | 30-48 |
| 030I0003500-NB-3 | Franklin | Kenoma Silt Loam | 85-100 | 85-100 | 85-100 | 85-100 | 50-75 | 30-48 |
| 099I0007000-EB-2 | Wabaunsee | Martin Silt clay Loam | 100 | 100 | 95-100 | 80-100 | 40-70 | 25-40 |
| 103U0040000-EB | Wilson | | 98-100 | 98-100 | 96-100 | 65-98 | 40-60 | 24-34 |

## 3.2 Develop Local Experimental Plan and Sampling Technique

A sampling template usually is created in order to select projects that representatively reflect current and future agency practices for the design and construction of pavements. However, since the projects in this study were selected and supplied directly from KDOT, no specific sampling technique was used for this study.

## 3.3 Estimate Sample Size

Sample size estimation approximates the minimum sample size or the minimum number of pavement projects needed for local calibration and validation of MEPDG distress prediction models depending on the model error or standard error of estimate (SEE), the confidence level for statistical analysis, and the threshold value of performance indicators at an agency's design reliability level. The required number of pavement projects for local calibration and validation of MEPDG models as recommended byAASHTO (2008) are presented in Table 3-16.

**Table 3-16: Estimated number of pavement projects required for the local calibration and validation**

| Pavement Type | Performance Indicator | Performance Indicator Threshold (at 90% Reliability) | Standard Error of Estimate (SEE) | Minimum Number of Projects Required for Local Calibration and Validation | Minimum Number of Projects Required for Each Pavement Type |
|---|---|---|---|---|---|
| New HMA | Alligator cracking | 20% lane area | 5.01% | 16 | 18 |
| | Transverse thermal cracking | Crack spacing >100 ft of 630 ft/mi | N/A | 18 | |
| | Rutting | 0.4 inches | 0.107 inches | 14 | |
| | IRI | 169 inches/mi | 18.9 inches/mi | 80 | |
| New JPCP | Faulting | < 0.15 inches | 0.033 inches | 21 | 21 |
| | Transverse cracking | < 10% slabs | 4.52% | 5 | |
| | IRI | 169 inches/mi | 17.1 inches/mi | 98 | |

Source: AASHTO, 2010

With the exception of the IRI model, the sample size, or number of pavement projects, was higher than the minimum recommended number of projects. However, since accuracy of the IRI model depends on the accuracy of other distress prediction models of MEPDG, a large number of

projects do not need to be adopted in order to calibrate and validate IRI models if other models are accurately calibrated and reliable.

## 3.4 Select Pavement Projects

KDOT selected 27 flexible pavement projects and 22 JPCP projects for this study. A total of 21 pavement projects were taken for flexible pavement distress model calibration and six projects were selected for validation. Table 3-17 provides a general description of the projects used for local calibration.

**Table 3-17: Selected projects for local calibration of new flexible pavement**

| No. | Project Name | Route | County | Begin milepost | End milepost | Length (mile) |
|---|---|---|---|---|---|---|
| 1 | 007U0007500-NB | US-75 | Brown | 13.05 | 19.68 | 6.63 |
| 2 | 008U0005400-EB | US-54 | Butler | 17.47 | 25.69 | 8.22 |
| 3 | 008U0007700-NB-1 | US-77 | Butler | 0.00 | 12.71 | 12.71 |
| 4 | 008U0007700-NB-2 | US-77 | Butler | 33.88 | 43.44 | 9.56 |
| 5 | 008U0007700-NB-3 | US-77 | Butler | 43.44 | 50.67 | 7.23 |
| 6 | 011U0006900-NB | US-69 | Cherokee | 8.45 | 11.44 | 2.99 |
| 7 | 019K0000700-NB-1 | K-7 | Crawford | 0.00 | 4.97 | 4.97 |
| 8 | 019K0000700-NB-2 | K-7 | Crawford | 4.97 | 10.99 | 6.02 |
| 9 | 019U0016000-EB | US-160 | Crawford | 9.69 | 14.54 | 4.85 |
| 10 | 023U0004000-EB | US-40 | Douglas | 11.24 | 12.44 | 1.20 |
| 11 | 025K0009900-NB | K-99 | Elk | 12.92 | 21.72 | 8.80 |
| 12 | 027K0015600-EB | K-156 | Ellsworth | 5.63 | 18.40 | 12.77 |
| 13 | 028U0005000-EB | US-50 | Finney | 19.88 | 29.37 | 9.48 |
| 14 | 031K0001800-WB | K-18 | Geary | 15.55 | 17.55 | 2.00 |
| 15 | 033U0028300-NB | US-283 | Graham | 16.96 | 30.36 | 13.40 |
| 16 | 052U0007300-NB | US-73 | Leavenworth | 18.45 | 20.92 | 2.47 |
| 17 | 065K0002700-NB | K-27 | Morton | 0.00 | 2.67 | 2.67 |
| 18 | 065U0005600-EB | US-56 | Morton | 19.76 | 21.87 | 2.12 |
| 19 | 069U0028300-NB | US-283 | Norton | 21.55 | 32.05 | 10.50 |
| 20 | 082U0018300-NB | US-183 | Rooks | 0.00 | 5.92 | 5.92 |
| 21 | 095U0005600-EB | US-56 | Stevens | 8.57 | 11.12 | 2.55 |

Projects used to validate locally calibrated models are listed in Table 3-18.

**Table 3-18: Selected projects for validation of locally calibrated flexible pavement models**

| No. | Project Name | Route | County | Begin milepost | End milepost | Length (mile) |
|---|---|---|---|---|---|---|
| 1 | 003U0007300-NB | US-73 | Atchison | 0.00 | 4.14 | 4.14 |
| 2 | 022K0000700-NB | K-7 | Doniphan | 5.92 | 11.71 | 5.79 |
| 3 | 088U0005400-WB | US-54 | Seward | 0.00 | 3.87 | 3.87 |
| 4 | 091K0002700-NB | K-27 | Sherman | 0.00 | 4.19 | 4.19 |
| 5 | 098U0028300-NB | US-283 | Trego | 10.03 | 21.49 | 11.46 |
| 6 | 103K0003900-NB | K-39 | Wilson | 14.47 | 16.43 | 1.96 |

Locations of selected flexible projects are shown in Figures 3-2.

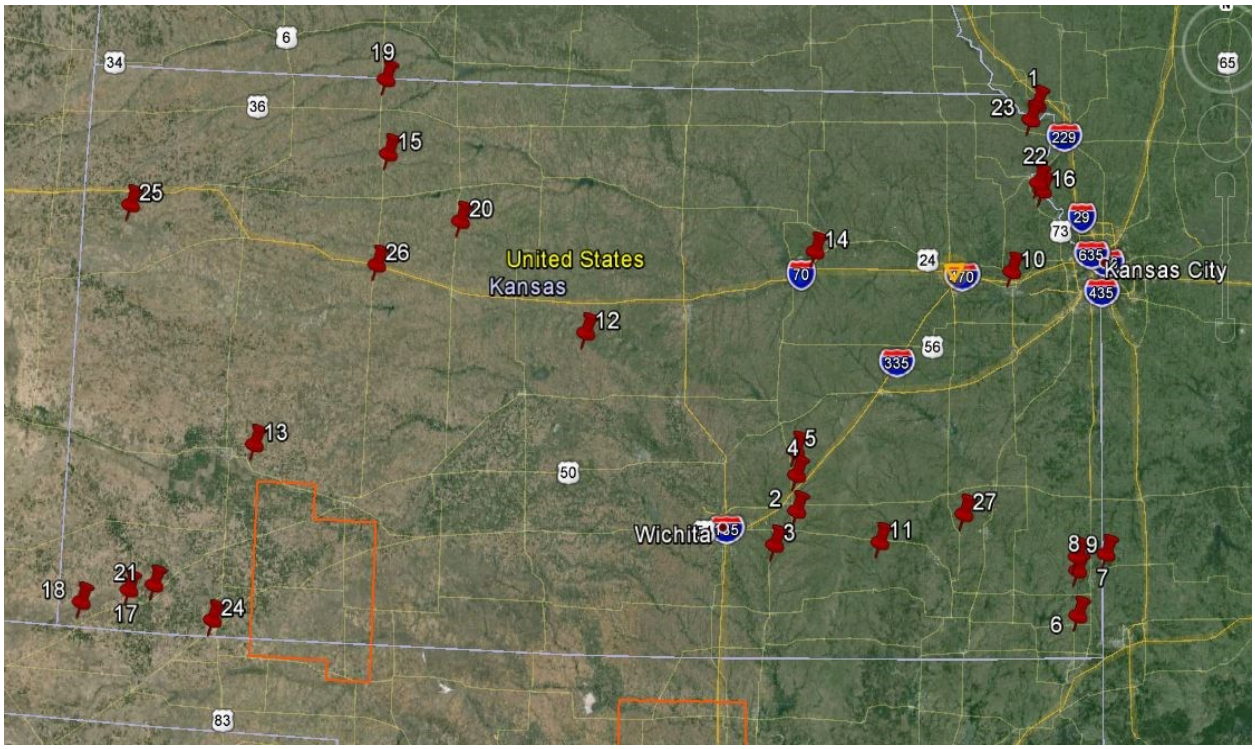


**Figure 3-2: Locations of the selected new flexible pavement projects in Kansas (Google Earth, 2016)**

Out of the 22 JPCP projects, 17 pavement projects were selected for JPCP distress model calibration and five projects were selected for validation. Table 3-19 provides a general description of projects used for local calibration of JPCP models.

**Table 3-19: Selected JPCP projects for local calibration**

| No. | Project Name | Route | County | Begin milepost | End milepost | Length (mile) |
|---|---|---|---|---|---|---|
| 1 | 018K0036000-EB | K-360 | Cowley | 0.00 | 2.95 | 2.95 |
| 2 | 018U0007700-NB | US-77 | Cowley | 4.62 | 8.51 | 3.89 |
| 3 | 031I0007000-EB | I-70 | Geary | 18.82 | 26.53 | 7.71 |
| 4 | 040I0013500-NB-1 | I-135 | Harvey | 7.47 | 13.39 | 5.92 |
| 5 | 040I0013500-NB-2 | I-135 | Harvey | 13.39 | 20.83 | 7.44 |
| 6 | 043U0007500-NB-1 | US-75 | Jackson | 0.00 | 8.02 | 8.02 |
| 7 | 043U0007500-NB-2 | US-75 | Jackson | 8.02 | 17.33 | 9.31 |
| 8 | 046K0000700-SB | K-7 | Johnson | 12.47 | 15.14 | 2.67 |
| 9 | 056I0003500-SB-1 | I-35 | Lyon | 11.51 | 16.60 | 5.09 |
| 10 | 056U0005000-EB-1 | US-50 | Lyon | 0.00 | 4.89 | 4.89 |
| 11 | 059I0013500-NB | I-135 | McPherson | 6.29 | 14.30 | 8.01 |
| 12 | 061I0003500-NB | I-35 | Miami | 0.00 | 2.56 | 2.56 |
| 13 | 063U0040000-EB | US-400 | Montgomery | 2.06 | 11.86 | 9.80 |
| 14 | 067U0016900-NB | US-169 | Neosho | 7.14 | 13.31 | 6.17 |
| 15 | 079U0008100-NB | US-81 | Republic | 13.29 | 17.46 | 4.17 |
| 16 | 085I0007000-EB | I-70 | Saline | 14.72 | 24.02 | 9.30 |
| 17 | 103U0040000-EB | US-400 | Wilson | 3.56 | 11.75 | 8.19 |

Projects used to validate locally calibrated models are listed in Table 3-20.

**Table 3-20: Selected projects for validation of locally calibrated new JPCP models**

| No. | Project Name | Route | County | Begin milepost | End milepost | Length (mile) |
|---|---|---|---|---|---|---|
| 1 | 019U0006900-NB | US-69 | Crawford | 15.71 | 23.90 | 8.19 |
| 2 | 029U0005600-EB | US-56 | Ford | 12.17 | 15.60 | 3.43 |
| 3 | 030I0003500-NB-3 | I-35 | Franklin | 19.87 | 26.85 | 6.97 |
| 4 | 055U0004000-WB | US-40 | Logan | 35.69 | 38.65 | 2.96 |
| 5 | 099I0007000-EB-2 | I-70 | Wabaunsee | 5.19 | 8.02 | 2.83 |

Locations of selected JPCP projects are shown in Figures 3-3.

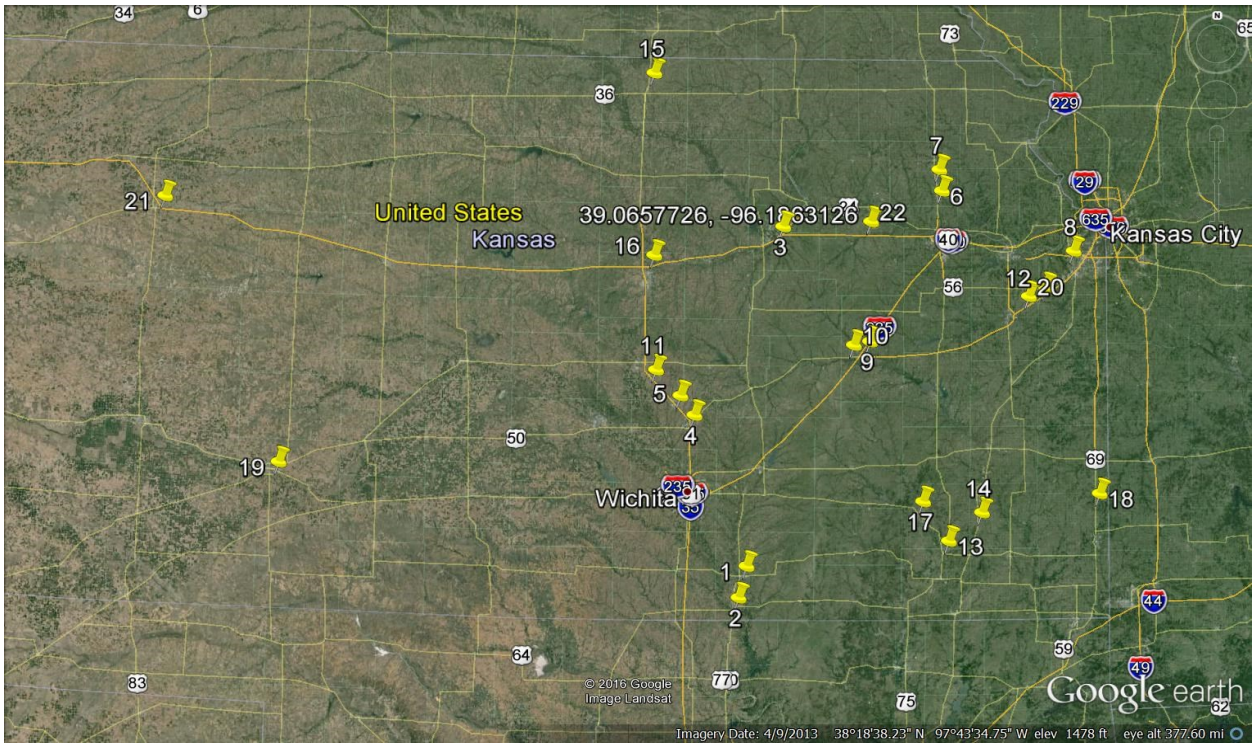


**Figure 3-3: Locations of selected New JPCP projects in Kansas (Google Earth, 2016)**

## 3.5 Extract and Evaluate Measured Distress and Project Data

Extraction and evaluation of measured distress and project data requires four activities, as described in the following sections (AASHTO, 2010).

### 3.5.1 Extract and Convert Measured Data

Measured distress data must first be extracted, reviewed, and, if necessary, converted into values predicted by the MEPDG. AASHTO suggests that a consistent definition and a measurement protocol of surface distress should be used throughout the calibration and validation process. Agencies can use LTPP-measured distress data or their own PMS database for local calibration. When using PMS data, a minimum of three observations per project should be taken to use it for calibration or using the PMS condition survey data from the established PMS segments is recommended. In this study measured pavement distress and IRI data were collected from the KDOT PMIS database.

### 3.5.2 Comparison of Distress Values

Comparison of distress values includes comparison of maximum measured distress values with trigger values or design criteria specified by an agency. According to AASHTO, the average maximum measured distress values from samples should exceed 50% of the design criteria as a minimum because if maximum distress values are significantly lower than the agency's design criteria for that distress (less than 50% of the design criteria), the accuracy and bias of the transfer function may not be well-defined at the values that trigger major rehabilitation (AASHTO, 2010). Limiting values for distress types and their corresponding maximum measured distresses for flexible and JPCP pavements are presented in Table 3-21 and 3-22, respectively.

**Table 3-21: KDOT specified threshold value and maximum measured distress for flexible pavement**

| Performance Criteria | KDOT Limit | Average Maximum Measured Distress Value |
|---|---|---|
| Initial IRI (inches/mile) | 60 | - |
| Terminal IRI (inches/mile) | 164 | 105 |
| AC top-down fatigue cracking (ft/mile) | 500 | 12965 |
| AC bottom-up fatigue cracking (% lane area) | 10 | 0 |
| AC thermal cracking (ft/mile) | 700 | 1109 |
| Permanent deformation - total pavement (inches) | 0.5 | 0.31 |
| Permanent deformation - AC only (inches) | 0.5 | - |

**Table 3-22: KDOT - specified threshold value and maximum measured distress for JPCP**

| Performance Criteria | KDOT Limit | Average Maximum Measured Distress Value |
|---|---|---|
| Terminal IRI (inches/mile) | 164 | 143 |
| JPCP transverse cracking (% slabs) | 5 | N/A |
| Mean joint faulting (inches) | 0.12 | 0.009 |

Results in Table 3-21 and 3-22 show that, the IRI of flexible and concrete pavement and rut depth of flexible pavement were within the limits of design thresholds. However, the maximum values of AC top-down cracking and thermal cracking were much higher than the KDOT-specified values, but measured values of mean joint faulting of JPCP were much lower than the KDOT threshold value.

### 3.5.3 Checking Anomalies and Outliers

Measured distress data of all pavement sections should be evaluated and checked for outliers and anomalies using a thorough visual inspection of data with time to ensure reasonability of the distress data or using a detailed statistical comparison of measured performance data. In this study statistical analysis was performed to find the outliers and some explicit outliers and anomalies were excluded from the measured data set.

### 3.5.4 Determination of All MEPDG Inputs

In this stage all MEPDG inputs, including site-specific values, KDOT-suggested input values and default values are determined. Details of all inputs were discussed in Section 3.1.

## 3.6 Conduct Field and Forensic Investigations

For this local calibration study inputs were collected from various sources, including actual project data, KDOT-suggested input values, and MEPDG default values. Although no field or forensic investigations were conducted in the study, these evaluations are necessary when any data element is missing or key inputs must be validated. Field or forensic investigations are recommended because they improve the reliability of the calibrated models.

## 3.7 Assess Local Bias from Global Calibration Factors

In this step global calibration values of MEPDG were used to calculate the performance indicator for each roadway section. The predicted values were then compared to the measured values to determine the bias and SEE to validate each distress prediction model for local conditions, policies, specifications, and materials (AASHTO, 2010). Bias is the difference between MEPDG-predicted output values and field-observed distresses. If the software-predicted distress is systemically different from the field-measured distress, then statistical bias exists in the model and it must be calibrated, requiring the standard error of sampling distribution which is also known as SEE. AASHTO defines the SEE as the standard deviation of residual errors for pavement sections included in the calibration data set for each prediction model (AASHTO, 2010). AASHTOWare Pavement ME Design (version 2.2) was executed with global calibration factors

to predict performance indicators for selected pavement projects. A reliability of 50% was used to predict average pavement performance in this study.

In addition to bias and SEE, an attempt was made to quantify utility of the global and calibrated performance models using the coefficient of determination ($R^2$) parameter. The purpose of this parameter is to represent the proportion of the sum of squares of deviations of AASHTOWare predicted values about their mean that can be attributed to a linear relationship between predicted and field measured data (Mendenhall, 2012).

The null hypothesis for the sampling template had to be evaluated in order to determine bias, and a paired t-test had to determine initial bias between actual distress and AASHTOWare-predicted data (with globally calibrated coefficients). Paired t-test analysis typically determines whether the mean of the differences between two paired samples differs from zero or a target value (Minitab, 2016). In this case, the paired t-test calculated the difference within each predicted and measured pair dataset, determined the mean of these changes, and reported whether the mean of the difference was statistically significant. This study conducted a paired t-test at 95% confidence level. The null hypothesis was

$$\text{Hypothesis, } H_0 : \sum(\text{Measured-Predicted}) = 0 \qquad (3.1)$$

Acceptance or rejection of the null hypothesis was based on the observed significance level or p-value. At 95% confidence level the p-value (probability of occurrence of a given event) generated from the paired t-test was expected to be greater than or equal to 0.05 in order for the null hypothesis to be accepted. If the null hypothesis was rejected, the distress model in the AASHTOWare Pavement ME Design software had to be calibrated to eliminate local bias.

## 3.8 Eliminate Local Bias

If bias is found to be significant from global calibration coefficients, it must be eliminated by local calibration. The calibration process usually depends on the cause of bias and accuracy desired by the agency. The following three approaches generally are followed in order to eliminate bias (AASHTO, 2010):

- If residuals errors are always positive or negative with a low SEE compared to the limiting value and the slope of residual errors versus predicted values is relatively

constant and close to zero, then the precision of the prediction model is reasonable but the accuracy is poor. This situation generally requires the least level of effort, and most of the time a few number of runs or iterations is enough to reduce the bias.

- If the bias is low and relatively constant with time but the residual errors have wide variation from positive to negative values, then the accuracy of the model is reasonable but the precision is poor. The coefficients of the prediction equation can be used to reduce the bias, but the value of the local calibration coefficients may be dependent on site features, material properties, or design features in the sampling template. This condition usually requires an increased number of MEPDG runs and higher effort to reduce the bias.
- If the residual error versus the predicted values show a significant and variable slope that appears to be dependent on the predicted value, then the correlation between the predicted and measured values is very poor and the precision of the prediction model is also poor. This is the most complex condition for local calibration because the exponents of the number of loading cycles must be considered. This condition also requires the highest level of effort and much more MEPDG runs to reduce the bias.

If the null hypothesis is rejected in Equation 3.1, the distress model in AASHTOWare pavement ME design software must be calibrated to eliminate local bias. In this study the methods used to eliminate local bias included iterative runs of AASHTOWare ME design with adjusted calibration coefficients and linear optimization of the calibration coefficients. Detail procedures are described in Chapters 4 and 5.

## 3.9 Assess the Standard Error of Estimate

In this step SEE derived from locally calibrated models is compared to the SEE of the nationally calibrated distress prediction models of MEPDG, and the reasonability is checked. Reasonable values of the SEE of nationally calibrated models are provided in Table 3-16.

The null hypothesis is initially evaluated for the sampling template with respect to the standard error. The null hypothesis for this primary assessment is that no significant difference exists between the standard error of global and local calibration attempts at the selected level of

confidence (AASHTO, 2010). Based on acceptance or rejection of the null hypothesis, the following approaches can be taken:

- If the null hypothesis is rejected and the local calibration has a higher standard error term, then that distress model must be recalibrated in order to lower the standard error.
- If the null hypothesis is rejected and the local calibration has a lower standard error term, then local calibration coefficients are recommended.
- If the null hypothesis is accepted, then the local and global standard errors are considered to be identical, and locally calibrated coefficients should be used.

Detailed procedure of the estimation of SEE is described in Chapters 4 and 5.

## 3.10 Reduce the Standard Error of Estimate

If the user agency determines that the standard error is too large, resulting in overly conservative design in higher reliability levels, then local calibration values of the transfer function or statistical model may need to be revised. An agency must decide about that, however, because the process can be very complicated and potentially require external revisions to local calibration parameters or agency-specific input values in order to improve precision of the prediction model (AASHTO, 2010).

Two types of errors commonly constitute the standard error: lack-of-fit, or model error and measurement error. Local calibration can reduce only lack-of-fit portion of the standard error. The measurement error is the larger of the error components, and changes only to values of local calibration coefficients will not change the magnitude of this error. Therefore, the agency must decide whether or not to spend additional money and effort on reducing measurement errors. If the determination is made that the extra effort will significantly reduce the SEE of the specific distress or IRI prediction models, they can revise the local calibration process.

The standard error of each cell of the matrix must be determined in order to establish whether the local standard error term is dependent on any primary or secondary input parameter of the sampling matrix. The local standard error results can be used to make necessary revisions to specific local calibration parameters. After the revisions are complete, the local calibration values are adjusted to reduce the standard error of the recalibrated data set. Based on goodness-of-

fit criteria, a fitting process of the model constants are evaluated on the best set of values for the coefficients of the model. The analytical approaches used are based on least squares using multiple regression analysis, stepwise regression analysis, principal components analysis, or principal components regression analysis. This study used least square regression analysis to test the goodness-of-fit of the recalibrated models, as described in Chapters 4 and 5.

# Chapter 4 - Local Calibration and Validation of Flexible Pavement MEPDG Models

This chapter describes local calibration and validation of nationally calibrated MEPDG distress prediction models of newly constructed asphalt concrete pavement in Kansas. Calibrated performance prediction models include the permanent deformation or rutting model, the top-down fatigue (longitudinal) cracking model, the bottom-up (alligator) cracking model, the thermal (transverse) cracking model, and the IRI model. All statistical analysis was performed using Microsoft Excel statistical toolbox. The hypothesis presented in Equation 3.1 was examined throughout all statistical analyses. A paired t-test was performed at 95% confidence level to identify any significant difference between measured and predicted data. The probability of attaining a predicted value equal to the measured value was denoted as the *P* value. If the *P* value was equal to or greater than 0.05, then the null hypothesis was accepted.

## 4.1 Calibration of Permanent Deformation or Rutting Model

MEPDG computes rut depths within HMA, unbound aggregate layers, and subgrade foundation. Unless otherwise specified by the agency, local calibration for this model typically should be conducted in context of total predicted rut depth (AASHTO, 2010). This study found that subgrade rutting significantly contributes to total rut depth, so calibration was performed for AC rutting and subgrade rutting.

### 4.1.1 Assessment of Local Bias and Standard Error of the Estimate from Global Calibration Factors

Local bias was determined by conducting hypothesis testing for the total permanent deformation model with globally calibrated coefficients. Measured data was compared to predicted data; the globally calibrated model showed significant bias in the paired t-test, and the null hypothesis was rejected at 95% confidence interval. Results are presented in Table 4-1.

**Table 4-1: Statistical analysis summary for globally calibrated factors for the rutting model**

| Bias | Se | Se/Sy | $R^2$ | P-value | Hypothesis, $H_0$ : ∑(Meas.-Pred.) = 0 |
|---|---|---|---|---|---|
| -17.86 | 0.06 | 1.20 | 0.25 | <0.0001 | Rejected |

Measured versus predicted total rutting for global calibration factors is shown in Figure 4-1, demonstrating that these values are quite apart from one another for all projects.

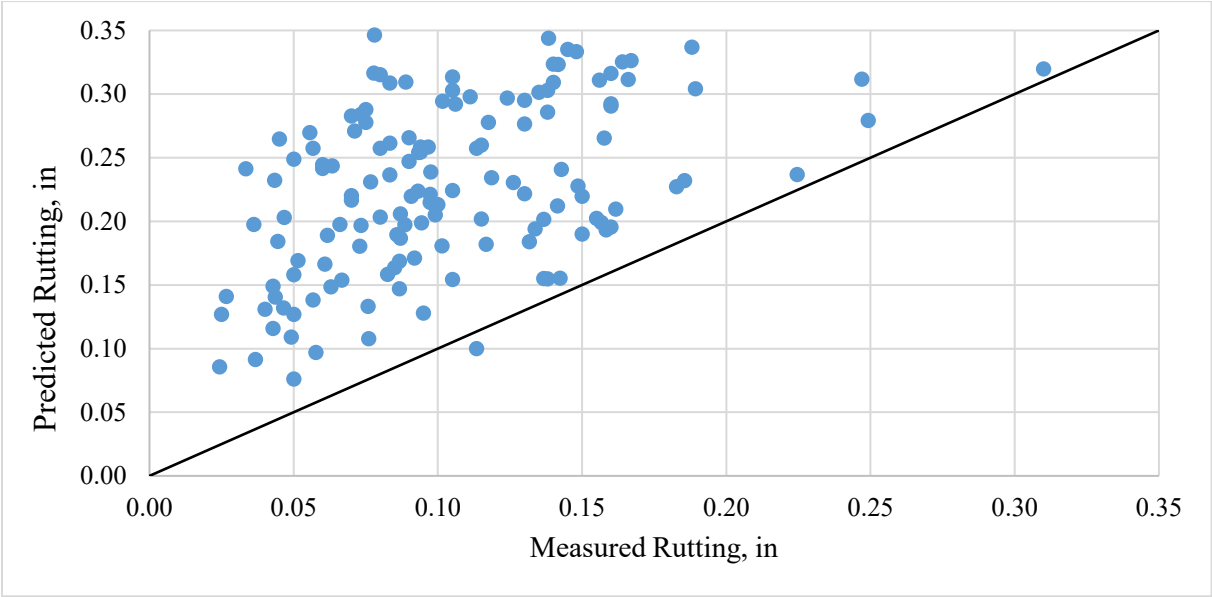


**Figure 4-1: Predicted versus measured total rut depth with globally calibrated factors**

Figure 4-1 shows a significant amount of bias, proving that AASHTOWare Pavement ME design overestimated the rutting of newly constructed flexible pavements in Kansas.

### 4.1.2 Elimination of Local Bias for the Rutting Model

Equations 2.1 and 2.2 showed that the calibration parameter $\beta_{1r}$, $\beta_{s1}$ can be optimized outside of the AASHTOWare software to reduce bias and standard error. The generalized reduced gradient (GRG) nonlinear optimization technique was performed using a Microsoft Excel Solver to optimize $\beta_{1r}$ and $\beta_{s1}$. However, $\beta_{2r}$ and $\beta_{3r}$ are not direct multipliers and cannot be optimized outside of the AASHTOWare software. These two calibration coefficients denote the effect of temperature and the number of loading cycles on the HMA layers, respectively (Kim et al. 2011).

AASHTOWare Pavement ME Design software was executed numerous times using a large factorial of $\beta_{2r}$ and $\beta_{3r}$, as shown in Table 4-2. The combination that resulted in the smallest sum of square of error (SSE) was selected for $\beta_{2r}$ and $\beta_{3r}$.

**Table 4-2: Factorial of $\beta_{2r}$ and $\beta_{3r}$ for trial ME design run**

| No. | $\beta_{2r}$ | $\beta_{3r}$ |
|---|---|---|
| 1 | 0.5 | 0.5 |
| 2 | 0.5 | 0.75 |
| 3 | 0.5 | 1 |
| 4 | 0.5 | 1.25 |
| 5 | 0.5 | 1.5 |
| 6 | 0.75 | 0.5 |
| 7 | 0.75 | 0.75 |
| 8 | 0.75 | 1 |
| 9 | 0.75 | 1.25 |
| 10 | 0.75 | 1.5 |
| 11 | 1 | 0.5 |
| 12 | 1 | 0.75 |
| 13 | 1 | 1 |
| 14 | 1 | 1.25 |
| 15 | 1 | 1.5 |
| 16 | 1.25 | 0.5 |
| 17 | 1.25 | 0.75 |
| 18 | 1.25 | 1 |
| 19 | 1.25 | 1.25 |
| 20 | 1.25 | 1.5 |
| 21 | 1.5 | 0.5 |
| 22 | 1.5 | 0.75 |
| 23 | 1.5 | 1 |
| 24 | 1.5 | 1.25 |
| 25 | 1.5 | 1.5 |
| 26 | 1.1 | 0.95 |
| 27 | 1.15 | 0.7 |
| 28 | 1.15 | 0.85 |
| 29 | 1.3 | 0.85 |

The adjusted coefficients were used as locally calibrated coefficients in the permanent deformation model in the AASHTOWare Pavement ME Design software, and a paired t-test was conducted between the measured data and the predicted data. Results of the paired t-test after local

calibration showed that the bias was significantly reduced, leading to acceptance of the null hypothesis (Table 4-3).

**Table 4-3: Statistical analysis summary for locally calibrated factors for the rutting model**

| Bias | Se | Se/Sy | $R^2$ | p-value | Hypothesis, $H_0$ : ∑(Meas.-Pred.) = 0 |
|---|---|---|---|---|---|
| -0.81 | 0.05 | 1.00 | 0.37 | 0.134 | Accepted |

As shown in Figure 4-2, measured versus predicted total rutting values for local calibration factors wrapped nicely around the 45˚ line as expected.

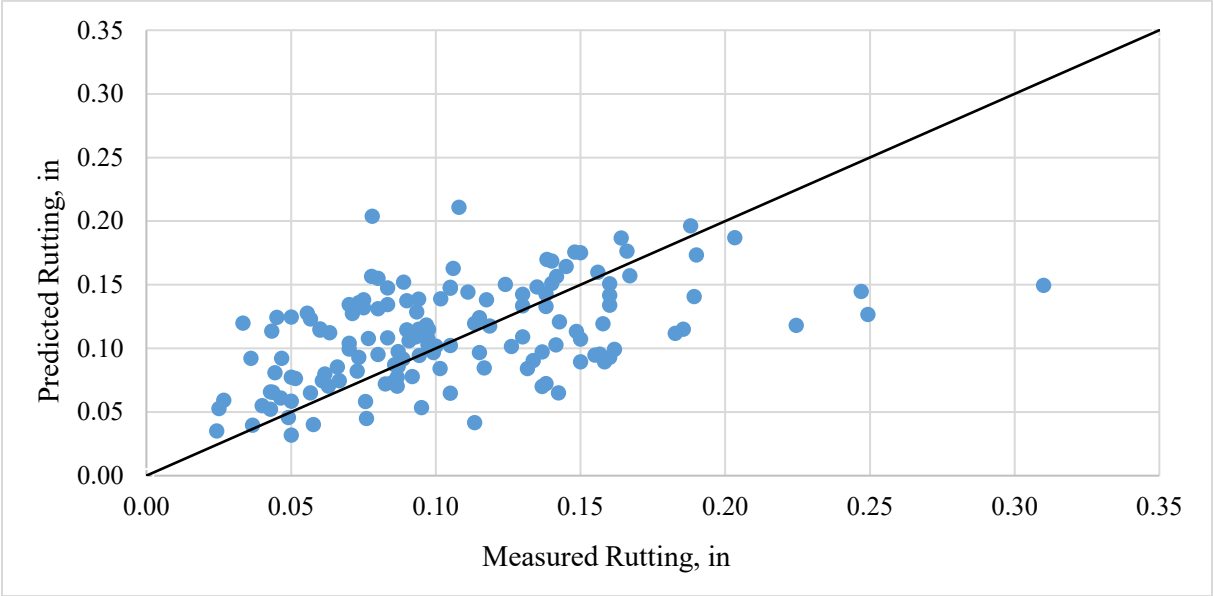


**Figure 4-2: Measured versus predicted rutting with locally calibrated coefficients**

Results in Table 4-3 show that the standard error of estimate (Se) decreased slightly after calibration (0.05 in.). The local calibration guide for AASHTOWare software recommends that the Se of the permanent deformation model be within 0.10 in., so the calibration criteria was satisfied.

### 4.1.3 Validation of the Model

Following local calibration, validation is a systematic process that re-examines the recalibrated model to determine if desired accuracy has been achieved between the calibrated

model and an independent set of observed data. Validation of the rutting model was performed with six randomly selected pavement sections around Kansas. Statistical analysis results for the permanent deformation model after validation are shown in Table 4-4. The bias and standard error were low with locally calibrated factors.

**Table 4-4: Summary of statistical analysis for rutting model for validation of local coefficients**

| Bias | Se | Se/Sy | $R^2$ | p-value | Hypothesis, $H_0 : \sum$(Meas.-Pred.) = 0 |
|---|---|---|---|---|---|
| -0.47 | 0.049 | 0.865 | 0.24 | 0.063 | Accepted |

### 4.1.4 Calibration Results

Upon completion of local calibration and validation, the coefficients shown in Tables 4-5 and 4-6 were selected for the asphalt concrete and subgrade permanent deformation models. Adjusted coefficients are shown in bold font.

**Table 4-5: Calibrated AC rutting model coefficients**

| **$Br_1$** | $Br_2$ | **$Br_3$** |
|---|---|---|
| **0.75** | 1.0 | **0.85** |

**Table 4-6: Calibrated Subgrade rutting model coefficients**

| **$Bs_1$ (fine)** | $Bs_1$ (granular) |
|---|---|
| **0.4** | 1.0 |

## 4.2 Calibration of the Load-Related Cracking Model

AASHTOWare Pavement ME Design software predicts two types of fatigue or load-related cracking: bottom-up (alligator) cracking and top-down (longitudinal) cracking. Local calibration attempts of these models are described in this section.

### 4.2.1 Calibration of the Top-down Fatigue Cracking Model

Longitudinal, or top-down, fatigue cracking initiates at the surface of the HMA pavement, and cracks connect longitudinally with continued traffic loading. Although the MEPDG does not

predict severity of longitudinal cracks, the magnitude of cracks are expressed by low, medium, or high terms. Local calibration of load-related cracking should be performed as total cracking that incorporates both alligator and longitudinal cracking unless an agency cuts cores or trenches and confirms where cracks initiate (AASHTO, 2010). Since only limited bottom-up cracking occurs in HMA pavements in Kansas and the PMIS database does not contain any bottom-up cracking data, calibration was performed only for top-down cracking in this study.

#### 4.2.1.1 Assessment of Local Bias and Standard Error of the Estimate from Global Calibration Factors

Local bias was determined by conducting hypothesis testing for the top-down cracking model with globally calibrated coefficients. The globally calibrated model showed significant bias in the paired t-test, and the null hypothesis was rejected at 95% confidence interval. Statistical results are shown in Table 4-7.

**Table 4-7: Statistical analysis summary for locally calibrated factors for the top-down cracking model**

| Bias | Se | $R^2$ | p-value | Hypothesis, $H_0$ : $\sum$(Meas.-Pred.) = 0 |
|---|---|---|---|---|
| 174395 | 2899 | N/A | <0.0001 | Rejected |

Figure 4-3 shows measured versus predicted top-down cracking for global calibration factors, demonstrating that AASHTOWare ME design severely under predicted top-down fatigue cracking for HMA pavements in Kansas. Therefore, local calibration of the top-down cracking model is essential.

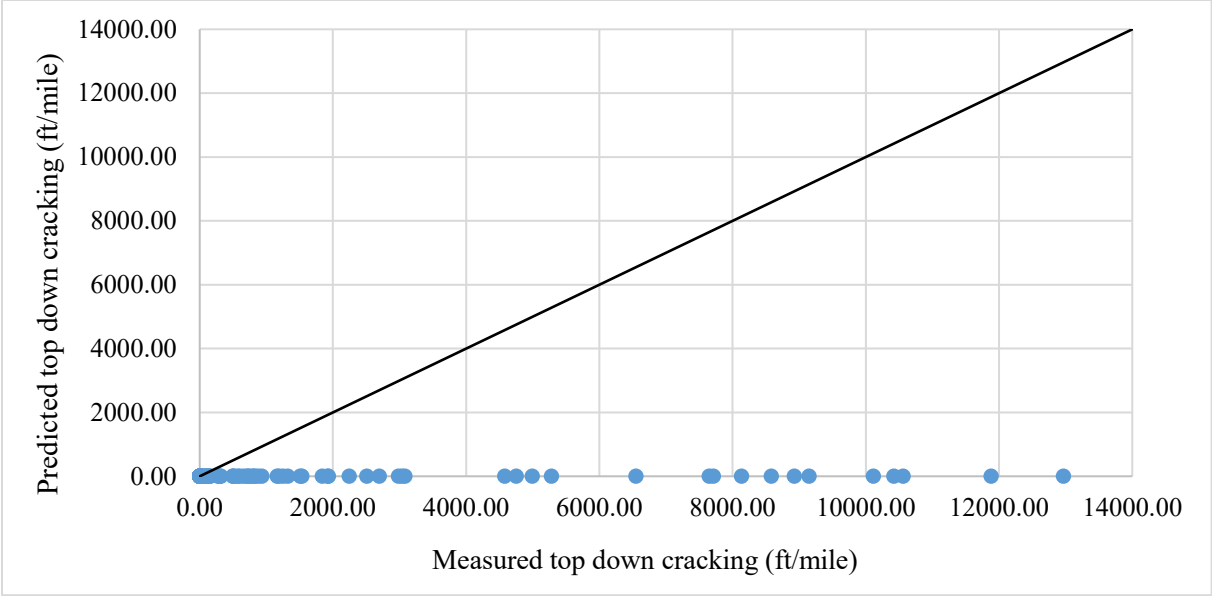


**Figure 4-3: Measured versus predicted top-down cracking with global factors**

#### 4.2.1.2 The Variability in Measured Data

Extracted top-down cracking data from the PMIS database showed a high degree of variability. Average top-down cracking on the selected projects varied from 13,000 ft/mile to 0 ft/mile, as shown in Figure 4-4.

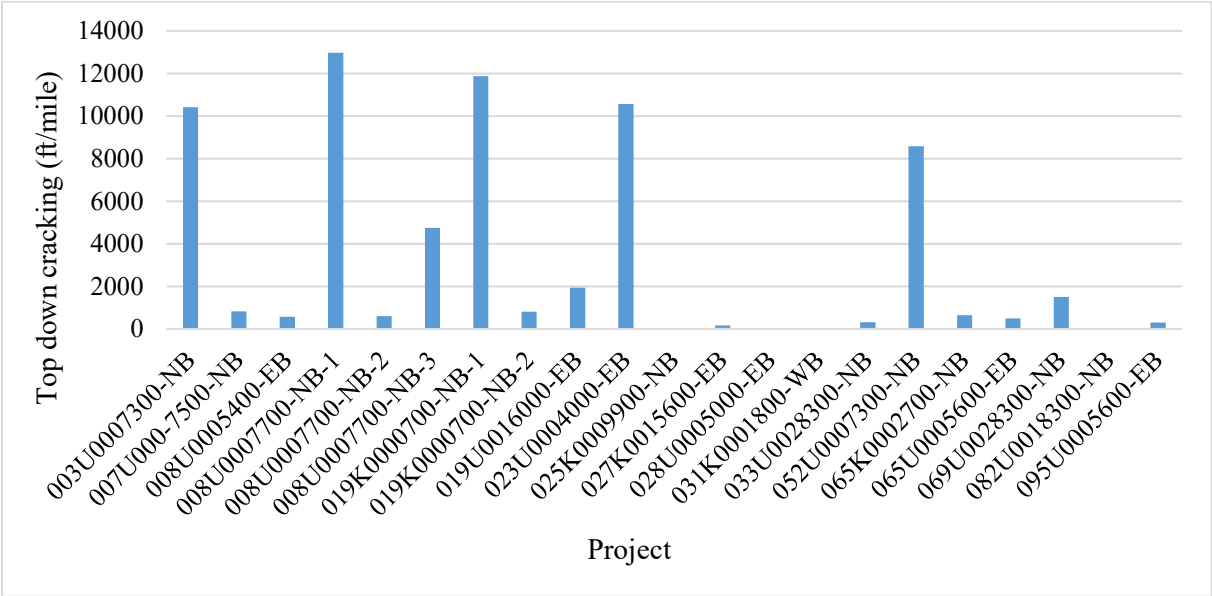


**Figure 4-4: Variability in KDOT measured top-down cracking data**

In order to reduce this variability, the top-down cracking model was calibrated without including projects with "zero" measured value.

#### 4.2.1.3 Elimination of Local Bias for the Top-Down Cracking Model

The following steps were used to eliminate local bias in the top-down cracking model:

- Locally calibrate the $N_f$-HMA model (Equation 2.3) and the transfer function of the top-down cracking model.
- Optimize calibration parameter $\beta_{f1}$, C1, C2 outside of the AASHTOWare ME software environment using Microsoft Excel Solver.
- Optimize calibration parameter $\beta_{f2}$ and $\beta_{f3}$ by repeatedly running AASHTOWare Pavement ME Design software for a large factorial of $\beta_{f2}$ and $\beta_{f3}$.

Calibration of the top-down cracking model according to these steps reduced the bias from 174,395 in/mile to 59,986 in/mile, but the calibrated model still showed a very high standard error of 2,750 in/mile. Although the local calibration guide for AASHTOWare software recommends that the Se of the top-down cracking model be within 600 in/mile. The null hypothesis in the t-test was accepted. Summary statistics are shown in Table 4-8.

**Table 4-8: Statistical analysis summary for locally calibrated factors for the top-down cracking model**

| Bias | Se | $R^2$ | P-value | Hypothesis, $H_0$ : $\sum$(Meas.-Pred.) = 0 |
|---|---|---|---|---|
| 59,986 | 2,750 | N/A | 0.051 | Accepted |

#### 4.2.1.4 Validation of the Model

Since all projects without "zero" measured top-down cracking value were used for calibration, the top-down cracking model was not validated further. However, the resulting calibrated model yielded high top-down cracking for all projects and exceeded the KDOT-recommended trigger value of 500 ft/mile for a 10-year design life.

#### 4.2.1.5 Calibration Results

After completion of local calibration of the top-down cracking model, the coefficients shown in Tables 4-9 and 4-10 were selected as calibrated coefficients. Adjusted coefficients are shown in bold font.

**Table 4-9: Calibrated AC fatigue model coefficients**

| $B_{f1}$ | $B_{f2}$ | **$B_{f3}$** |
|---|---|---|
| 1 | 1 | **1.60** |

**Table 4-10: Calibrated AC top-down fatigue cracking model coefficients**

| **C1** | **C2** | C3 | C4 |
|---|---|---|---|
| **0.90** | **0.45** | 0 | 1000 |

### 4.2.2 Calibration of the Bottom-Up Fatigue Cracking Model

Bottom-up cracks initiate at the bottom of the HMA layer, with initial indications of multiple short, longitudinal, or transverse cracks in the wheel path that become interconnected laterally with continued traffic loading. Cracks in the connected state create a chicken wire or alligator pattern. So bottom-up cracking is also known as alligator cracking. MEPDG calculates alligator cracking as a percent of total lane area. Although MEPDG does not predict severity of alligator cracks, the magnitude of cracks are expressed in low, medium, or high terms.

As mentioned, the KDOT PMIS database does not include any bottom-up cracks for projects considered for calibration and validation. Moreover, KDOT recognizes all load-related cracking as top-down cracking. Since measured data for bottom-up fatigue cracking model were not available, the bottom-up fatigue cracking model was not calibrated.

## 4.3 Calibration of AC Thermal Cracking Model

Thermal cracking, or transverse cracking, is non-wheel-load-related cracking that is predominant in areas perpendicular to the pavement centerline. These cracks are caused by low temperatures or thermal cycling. MEPDG estimates transverse cracking in feet per mile (meters per kilometer) or spacing of transverse cracks in feet (AASHTO, 2010). MEPDG does not predict severity of transverse cracks, but crack magnitude is expressed in low, medium, or high terms.

### 4.3.1 Assessment of Local Bias and Standard Error of the Estimate from Global Calibration Factors

Local bias was determined by conducting hypothesis testing for the AC thermal cracking model with globally calibrated coefficients. Paired t-test at 95% confidence level resulted in p-value lower than 0.05, indicating significant bias in the thermal fracture model. Statistical analysis results are shown in Table 4-11.

**Table 4-11: Statistical analysis summary for globally calibrated factors for the thermal cracking model**

| Bias | Se | Se/Sy | $R^2$ | P-value | Hypothesis, $H_0$ : ∑(Meas.-Pred.) = 0 |
|---|---|---|---|---|---|
| 2,724 | 98.6 | 1.00 | N/A | <0.0001 | Rejected |

Measured versus predicted thermal cracking is shown in Figure 4-5.

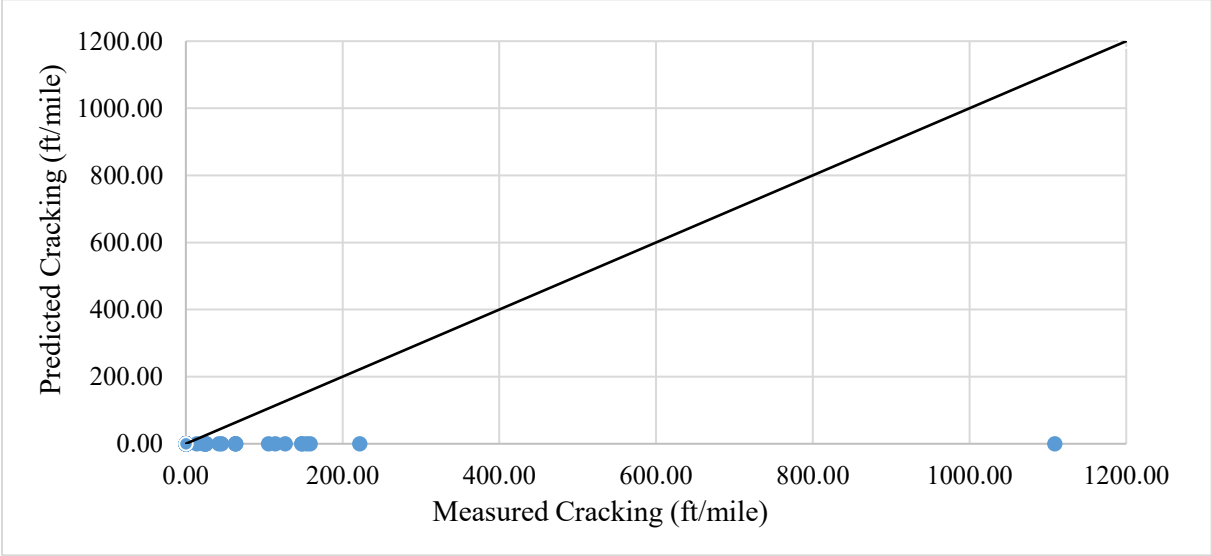


**Figure 4-5: Predicted versus measured transverse cracking with globally-calibrated factors**

Table 4-11 shows a significant difference between measured and predicted transverse cracking at 95% confidence level. The Se was found to be 98.6 ft/mile; AASHTO recommends that the Se be within 250 ft/mile. According to Figure 4-5, MEPDG underpredicted thermal cracking for all selected pavement projects, necessitating local calibration.

### 4.3.2 Elimination of Local Bias for the Thermal Cracking Model

The AC thermal cracking model has only one calibration coefficient. The globally adjusted value derived from LTPP sites are

Level 1 = 1.5

Level 2 = 0.5

Level 3 = 1.5

Only 13 out of 27 projects in this study showed transverse cracking. Level 1 input (creep compliance and indirect tensile strength) data for this study was not available, so an initial attempt was made to calibrate the AC thermal cracking model for Level 3 inputs. Since the AASHTOWare software did not predict transverse cracking for any project with global values, calibration of the model to force the predicted data to match with the measured data yielded a model that generated high AC thermal cracking for all projects. Therefore, KDOT should calibrate the AC thermal cracking model based on the districts, and only districts showing AC transverse cracking should be calibrated in the future. Further attempts to calibrate the transverse cracking model were not carried out in this study.

## 4.4 Calibration of IRI Model

In AASHTOWare Pavement ME Design IRI is the measure of functional adequacy quantified by pavement smoothness. IRI is predicted empirically as a function of pavement distresses, such as length of longitudinal cracking, area of transverse fatigue cracking, average rut depth, site factors that represent foundation shrink/swell and frost heave capabilities, and estimated IRI at the time of construction (Initial IRI). Unit of smoothness calculated by ME design is inches per mile.

### 4.4.1 Assessment of Local Bias and Standard Error of the Estimate from Global Calibration Factors

Local bias was determined using globally calibrated factors for the IRI model. The globally calibrated model showed significant bias in the paired t-test, and the null hypothesis was rejected at 95% confidence interval. Results are presented in Table 4-12.

**Table 4-12: Statistical analysis summary for globally calibrated factors for the IRI model**

| Bias | Se | Se/Sy | $R^2$ | P-value | Hypothesis, $H_0$ : ∑(Meas.-Pred.) = 0 |
|---|---|---|---|---|---|
| -1487.6 | 9.72 | 0.871 | 0.24 | 0.053 | Rejected |

Measured versus predicted IRI (globally calibrated) relationship is shown in Figure 4-6.

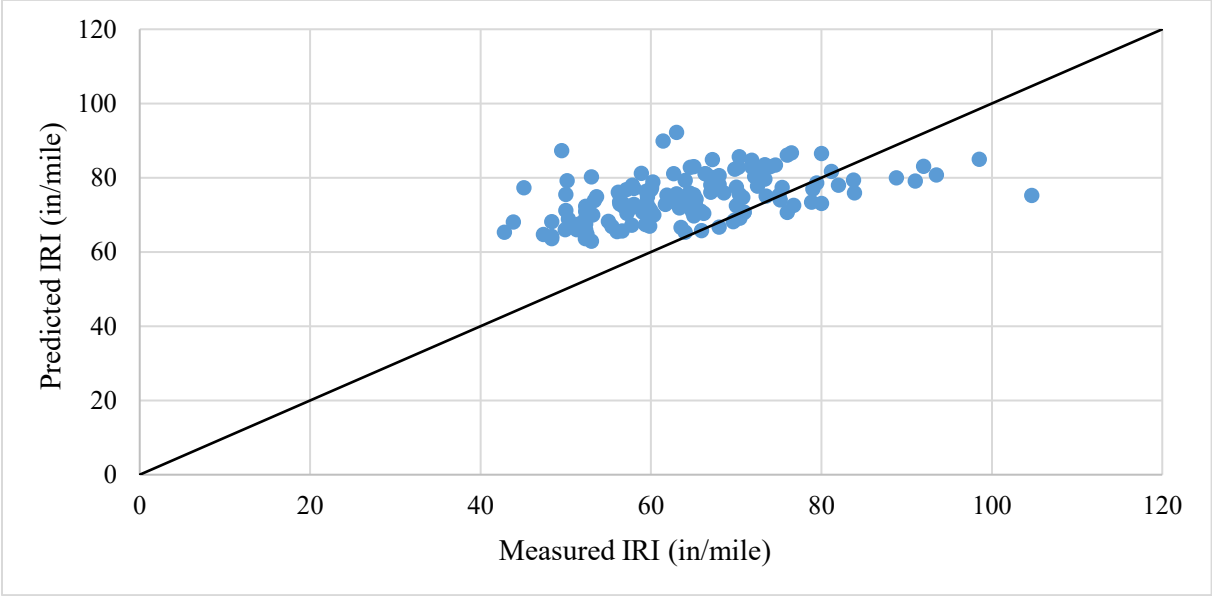


**Figure 4-6: Predicted versus measured IRI with globally-calibrated factors**

Figure 4-6 shows that ME design slightly overpredicted the IRI value, thereby necessitating local calibration.

### 4.4.2 Elimination of Local Bias for the IRI Model

Equation 2.9 showed that data for subgrade soil percent passing the 0.02 mm sieve was required in order to calculate the site factor parameter. Since this data was not available, optimization could not be performed to adjust the calibration coefficients. AASHTOWare software was run multiple times using a large factorial of C1, C2, and C4 to eliminate bias between the measured and predicted data. Coefficient C3 remained at the global value. Summary parameters of the statistical analysis after local calibration are listed in Table 4-13. Bias and standard error were reduced significantly.

**Table 4-13: Statistical analysis summary for locally calibrated factors for the IRI model**

| Bias | Se | Se/Sy | $R^2$ | P-value | Hypothesis, $H_0$ : ∑(Meas.-Pred.) = 0 |
|---|---|---|---|---|---|
| -215.8 | 10.13 | 0.908 | 0.22 | 0.077 | Accepted |

Figure 4-7 shows measured versus predicted IRI after local calibration.

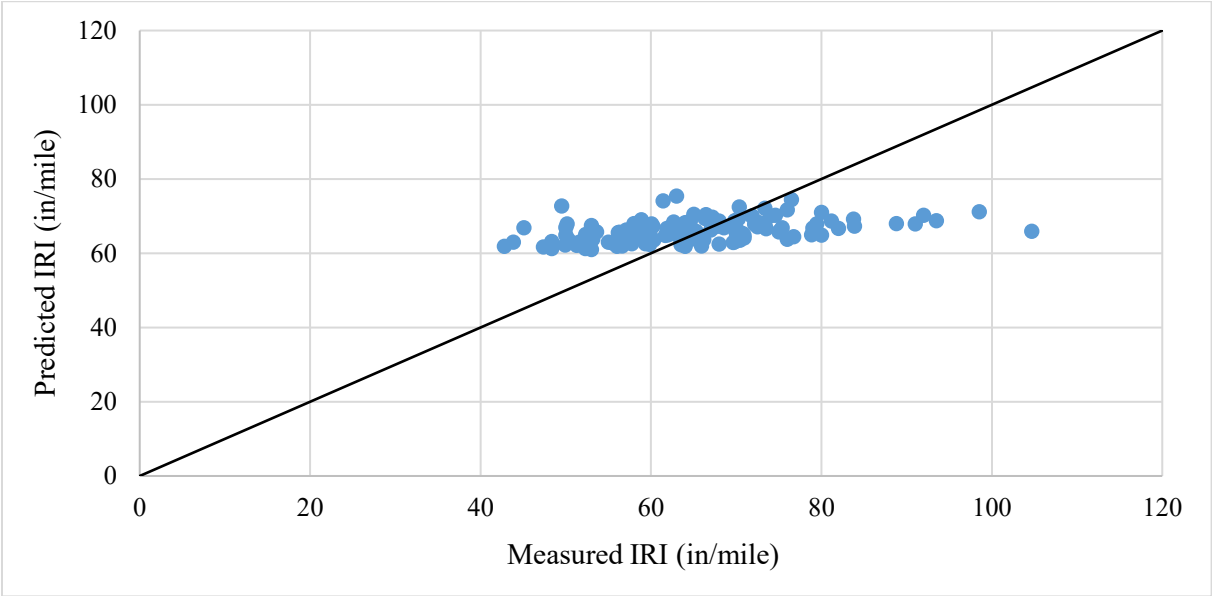


**Figure 4-7: Predicted vs measured IRI with local calibration factors**

### 4.4.3 Validation of the Model

Statistical analysis results for the IRI model after validation are shown in Table 4-14.

**Table 4-14: Summary of statistical analysis for IRI model for validation of local coefficients**

| Bias | Se | Se/Sy | $R^2$ | P-value | Hypothesis, $H_0$ : ∑(Meas.-Pred.) = 0 |
|---|---|---|---|---|---|
| -8.65 | 14.7 | 0.911 | 0.30 | 0.93 | Accepted |

Although the bias and standard error were low with locally calibrated factors, Table 4-14 shows that the Se increased slightly after calibration. The standard error is usually obtained by

taking the positive square root of the variance of the statistic. The local calibration guide for AASHTOWare ME (AASHTO, 2010) lists four components of the Se. The first component is related to measurement errors associated with distress or smoothness measurements in the field. The second source of error is an input error that is related to the underestimation or overestimation of certain input parameters required by the MEPDG. The third source of error is related to deficiencies in the transfer functions within the AASHTOWare pavement ME design software. The fourth source of error is defined as pure error, which is dependent on input level, distress type, and prediction equation.

The distress/IRI measurement error is a major contributor to the error components. KDOT must decide whether to employ additional cost and effort to reduce total standard error. Nonetheless, the design guide recommends that the Se of the IRI model should be within 17 in/mile.

### 4.4.4 Calibration Results

After completion of local calibration, coefficients of the IRI model for new flexible pavements in Kansas were obtained, as shown in Table 4-15. Adjusted coefficients are shown in bold font.

**Table 4-15: Calibration coefficients of the flexible pavement IRI model**

| **C1** | C2 | C3 | **C4** |
|---|---|---|---|
| **33** | 0.4 | 0.008 | **0.01** |

# Chapter 5 - Local Calibration and Validation of Jointed Plain Concrete Pavement MEPDG Models

This chapter describes local calibration and validation of nationally calibrated MEPDG distress prediction models of newly constructed JPCPs in Kansas. Performance prediction models for attempted calibration included transverse joint faulting model and IRI model. The transverse slab cracking model could not be calibrated due to lack of measured performance data. Statistical procedures for local calibration were identical to the procedures described in Chapter 4 for flexible pavements.

## 5.1 Calibration of Transverse Joint Faulting Model

Because joint faulting of a JPCP varies widely from joint to joint, AASHTOWare Pavement ME Design considers the mean faulting of all transverse joints in a pavement to be the predicted faulting. The unit of faulting calculated by ME design is inches. Joint faulting is one of the most important deterioration mechanisms of JPCP due to its significant impact on ride quality.

### 5.1.1 Assessment of Local Bias and Standard Error of the Estimate from Global Calibration Factors

Local bias was determined by conducting hypothesis testing for the transverse joint faulting model with globally-calibrated coefficients. Paired t-test at 95% confidence level resulted in p-value less than 0.05, indicating significant bias in the transverse joint faulting model. Statistical analysis results are shown in Table 5-1.

**Table 5-1: Statistical analysis summary for globally calibrated factors for the joint faulting model**

| Bias | Se | Se/Sy | $R^2$ | P-value | Hypothesis, $H_0$ : $\sum$(Meas.-Pred.) = 0 |
|---|---|---|---|---|---|
| 0.7748 | 0.0115 | 6.43 | poor | <0.0001 | Rejected |

Table 5-1 shows a significant difference between predicted and measured faulting at 95% confidence level. The Se was found to be 0.0115 in.; AASHTO recommends that the Se be within 0.05 in. Predicted versus measured faulting is shown in Figure 5-1.

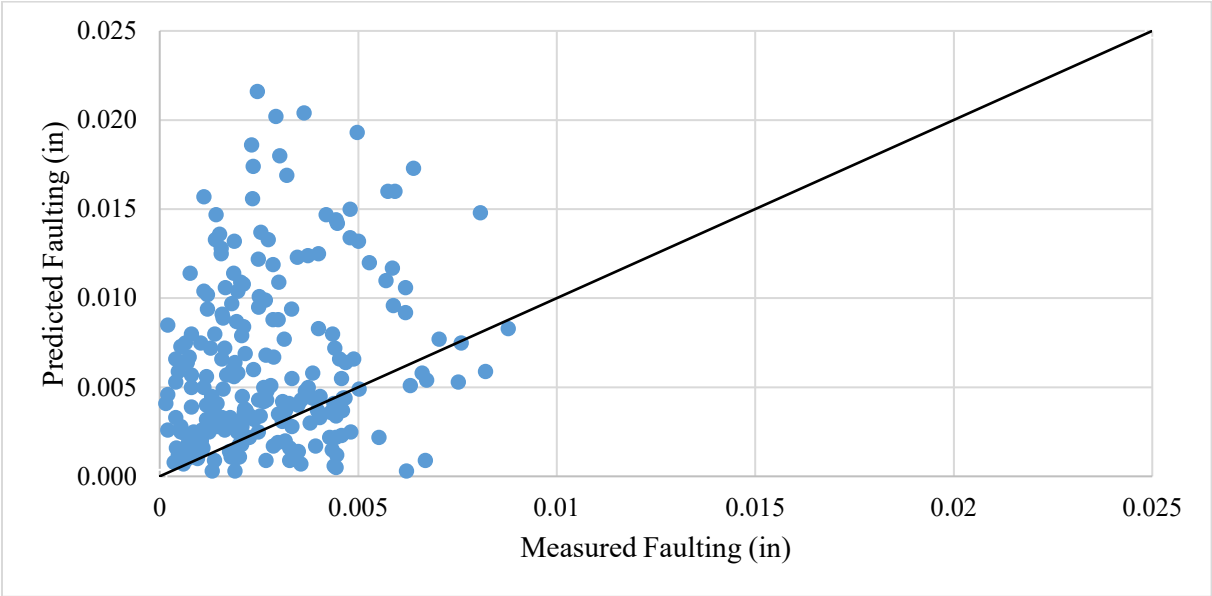


**Figure 5-1: Predicted versus measured faulting with nationally-calibrated factors**

Figure 5-1 shows that ME design significantly overpredicted faulting for selected JPCP projects in Kansas, thereby necessitating local calibration of the transverse joint faulting model.

### 5.1.2 Elimination of Local Bias for the Faulting Model

In order to calibrate the faulting model, initial sensitivity analysis was performed with two randomly selected projects (031I0007000-EB and 019U0006900-NB). Since the faulting model contained eight calibration factors, the most sensitive coefficients had to be identified. Sensitivity analysis was done by determining the least square sum of error (LSSE) from the regression model of measured and actual distress data by varying only one calibration factor at a time while keeping all other input parameters constant. Table 5-2 and Table 5-3 show SSE values for varying faulting model coefficients for projects 031I0007000-EB and 019U0006900-NB, respectively.

**Table 5-2: Sensitivity analysis for faulting model coefficients for project 031I0007000-EB**

| Coefficient | SSE for Global Coefficient | SSE after increasing global coefficient by | | | | SSE after decreasing global coefficient by | | | |
|---|---|---|---|---|---|---|---|---|---|
| | | 5% | 10% | 20% | 50% | 5% | 10% | 20% | 50% |
| C1 | 6.90E-05 | 7.60E-05 | 8.10E-05 | 9.50E-05 | 1.50E-04 | 6.30E-05 | 5.90E-05 | 4.90E-05 | 2.70E-05 |
| C2 | 6.90E-05 | 7.60E-05 | 8.60E-05 | 1.10E-04 | 1.80E-04 | 6.20E-05 | 5.50E-05 | 4.40E-05 | 1.90E-05 |
| C3 | 6.90E-05 | 7.30E-05 | 7.50E-05 | 8.20E-05 | 1.00E-04 | 6.60E-05 | 6.30E-05 | 5.70E-05 | 4.00E-05 |
| C4 | 6.90E-05 | 7.30E-05 | 7.60E-05 | 8.20E-05 | 1.00E-04 | 6.60E-05 | 6.30E-05 | 5.60E-05 | 4.20E-05 |
| C5 | 6.90E-05 | 7.00E-05 | 7.00E-05 | 7.20E-05 | 7.60E-05 | 6.80E-05 | 6.70E-05 | 6.60E-05 | 6.00E-05 |
| C6 | 6.90E-05 | 8.20E-05 | 9.80E-05 | 1.40E-04 | 3.90E-04 | 5.80E-05 | 4.80E-05 | 3.40E-05 | 1.20E-05 |
| C7 | 6.90E-05 | 6.90E-05 | 6.90E-05 | 6.90E-05 | 6.90E-05 | 6.90E-05 | 6.90E-05 | 6.90E-05 | 6.90E-05 |

**Table 5-3: Sensitivity analysis for faulting model coefficients for project 019U0006900-NB**

| Coefficient | SSE for Global Coefficient | SSE after increasing global coefficient by | | | | SSE after decreasing global coefficient by | | | |
|---|---|---|---|---|---|---|---|---|---|
| | | 5% | 10% | 20% | 50% | 5% | 10% | 20% | 50% |
| C1 | 9.60E-06 | 1.10E-05 | 1.20E-05 | 1.30E-05 | 2.20E-05 | 8.40E-06 | 7.80E-06 | 6.40E-06 | 3.20E-06 |
| C2 | 9.60E-06 | 1.10E-05 | 1.10E-05 | 1.40E-05 | 2.30E-05 | 8.20E-06 | 7.60E-06 | 6.30E-06 | 2.80E-06 |
| C3 | 9.60E-06 | 1.00E-05 | 1.10E-05 | 1.20E-05 | 1.50E-05 | 8.80E-06 | 8.30E-06 | 7.80E-06 | 5.00E-06 |
| C4 | 9.60E-06 | 1.00E-06 | 1.00E-05 | 1.10E-05 | 1.40E-05 | 9.10E-06 | 8.60E-06 | 8.00E-06 | 5.90E-06 |
| C5 | 9.60E-06 | 9.60E-06 | 9.80E-06 | 1.00E-06 | 1.00E-05 | 9.10E-06 | 9.10E-06 | 9.10E-06 | 7.70E-06 |
| C6 | 9.60E-06 | 1.10E-05 | 1.40E-05 | 1.20E-05 | 6.10E-05 | 8.00E-06 | 6.40E-06 | 4.50E-06 | 1.50E-06 |
| C7 | 9.60E-06 | 9.60E-06 | 9.60E-06 | 9.60E-06 | 9.60E-06 | 9.60E-06 | 9.60E-06 | 9.60E-06 | 9.60E-06 |

Table 5-2 and Table 5-3 show that coefficient C6 was most sensitive; LSSE decreased by 83% when C6 was 50% lower than the global value. coefficient C6 is correlated with the influence of overburden on subgrade, percent subgrade material passing No. 200 sieve, and average annual number of wet days with faulting potential (MEPDG guide, 2003).

Sensitivity analysis showed that C1, C2, C3, and C4 were somewhat sensitive. The local calibration guide suggested adjusting coefficients C1 and C2 to influence the magnitude of mid-range and long-range faulting, whereas coefficients C3 and C4 should be adjusted to account for initial faulting. However, sensitivity analysis showed that coefficients C5 and C7 were not sensitive at all. Coefficient C5 correlated to change in erodibility with the change in rate of predicted faulting, and coefficient C7 represented the increased rate of long-term faulting.

Based on faulting data collected from the PMIS database and the AASHTOWare Pavement ME analysis with globally-calibrated coefficients, initial measured faulting was less than predicted initial faulting. The measured faulting for all projects used in calibration and validation is shown in Appendix C. Because AASHTOWare Pavement ME Design software over predicted mid-range

faulting, coefficient C1 was decreased to lower initial predicted faulting and coefficient C3 value was reduced to decrease predicted faulting in the mid-range. Coefficient C6 was also reduced to eliminate bias because it was the most sensitive coefficient.

In order to calibrate the faulting model, AASHTOWare Pavement ME analysis was executed numerous times using a large factorial of C1, C3, and C6 to eliminate bias between the measured data and predicted data. Summary parameters of the statistical analysis after local calibration are listed in Table 5-4. The bias and standard error were significantly reduced.

**Table 5-4: Statistical analysis summary for locally calibrated factors for the joint faulting model**

| Bias | Se | Se/Sy | $R^2$ | P-value | Hypothesis, $H_0$ : ∑(Meas.-Pred.) = 0 |
|---|---|---|---|---|---|
| 0.0257 | 0.0024 | 1.34 | poor | 0.4683 | Accepted |

Figure 5-2 shows predicted versus measured faulting after local calibration**.**

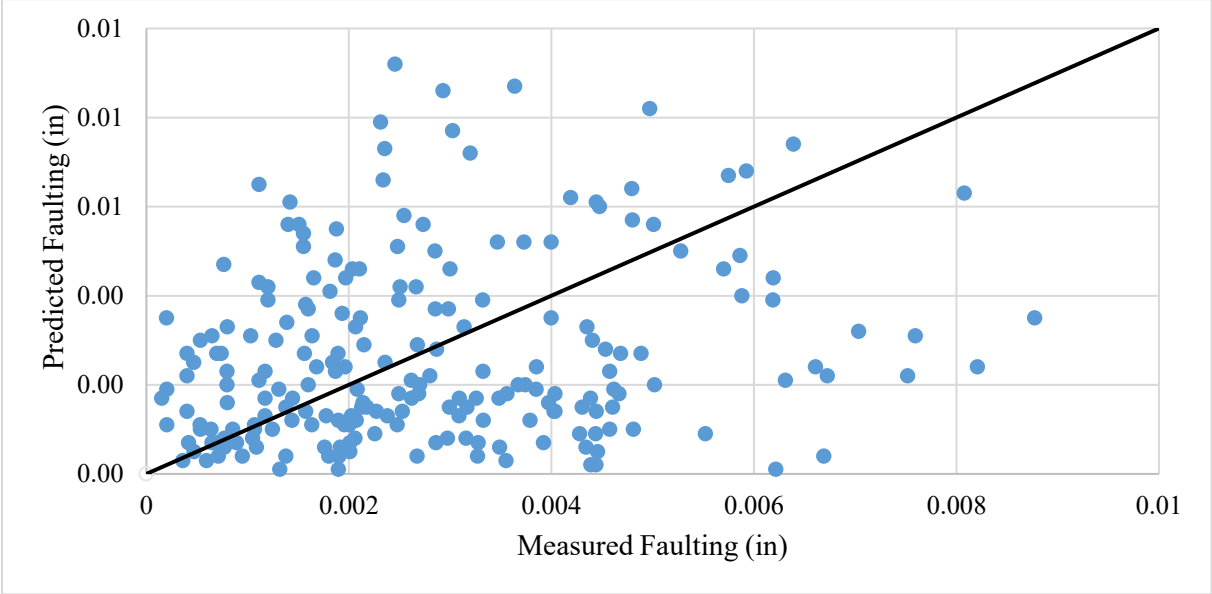


**Figure 5-2: Predicted versus measured faulting with local calibration factors**

### 5.1.3 Validation of Transverse Joint Faulting Model

Five projects were used for validation in this study. All projects considered for local calibration were pavement sections with Portland cement-treated base (PCTB). For validation, however, four out of five selected projects contained bound drainable bases (BDBs). Since KDOT

no longer designs PCCPs with BDB and consequently did not include projects with BDBs for calibration, four projects with BDBs with minimal IRI increase over time were carefully selected for validation.

Statistical analysis for the transverse joint faulting model after validation is shown in Table 5-5. The bias and standard error were low with locally calibrated coefficients.

**Table 5-5: Summary of statistical analysis for joint faulting model for validation of local coefficients**

| Bias | Se | Se/Sy | $R^2$ | P-value | Hypothesis, $H_0$ : ∑(Meas.-Pred.) = 0 |
|---|---|---|---|---|---|
| 0.0198 | 0.00195 | 0.96 | poor | 0.2015 | Accepted |

### 5.1.4 Calibration Results

The coefficients shown in Table 5-6 were selected after local calibration was completed. Adjusted coefficients are shown in bold font.

**Table 5-6: Calibration coefficients for the transverse joint faulting model**

| **C1** | C2 | **C3** | C4 | C5 | **C6** | C7 | C8 |
|---|---|---|---|---|---|---|---|
| **0.565** | 1.636 | **0.00235** | 0.00444 | 250 | **0.2444** | 7.3 | 400 |

## 5.2 Calibration of the Transverse Slab Cracking Model

Since measured cracking data for JPCPs were not available, the cracking model could not be calibrated; the global calibration values shown in Table 5-7 were taken as local values.

**Table 5-7: Coefficients for the PCC cracking model**

| C1 | C2 | C3 | C4 |
|---|---|---|---|
| 2 | 1.22 | 0.52 | -2.17 |

## 5.3 Calibration of the IRI Model

IRI is predicted empirically in the AASHTOWare Pavement ME Design as a function of pavement distresses for JPCP sections, such as percent of transverse cracking, percentage of joints with spalling, total joint faulting, site factors that represent pavement age, freezing index, size

distribution of subgrade material, and estimated IRI at the time of construction (initial IRI). Unit of smoothness calculated by ME design is inches per mile.

### 5.3.1 Assessment of Local Bias and Standard Error of the Estimate from Global Calibration Factors

Local bias was determined using globally calibrated factors for the IRI model. The globally calibrated model showed significant bias in the paired t-test, and the null hypothesis was rejected at 95% confidence interval. Results are presented in Table 5-8.

**Table 5-8: Statistical analysis summary for globally calibrated factors for the IRI model**

| Bias | Se | Se/Sy | $R^2$ | P-value | Hypothesis, $H_0$ : ∑(Meas.-Pred.) = 0 |
|---|---|---|---|---|---|
| 504.155 | 13.003 | 0.919 | 0.209 | 0.010 | Rejected |

The predicted versus measured IRI (globally calibrated) relationship is shown in Figure 5-3.

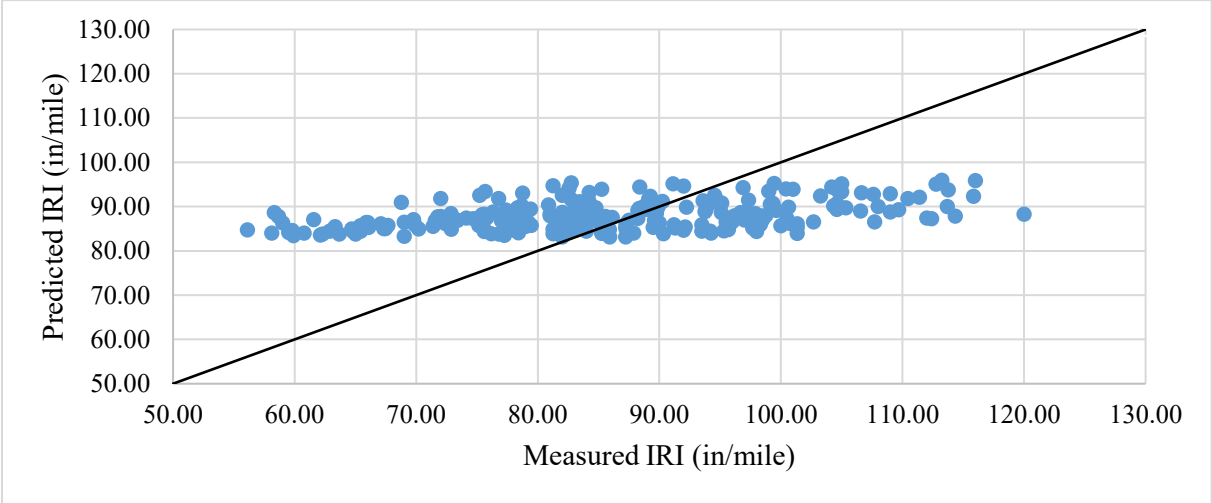


**Figure 5-3: Predicted versus measured IRI with globally-calibrated factors**

As shown in Figure 5-3, the ME design underpredicted IRI values for JPCP sections in Kansas, thereby necessitating local calibration to improve model accuracy.

### 5.3.2 Elimination of Local Bias for the IRI Model

In order to eliminate local bias in the IRI model, the generalized reduced gradient (GRG) nonlinear optimization technique was performed using Microsoft Excel Solver in following steps:

1) Equation 2.16 was defined in the Excel spreadsheet as a summation of cracking, spalling, faulting, and site factor multiplied by coefficients C1, C2, C3, and C4, respectively.
2) Residual errors for the full set of data were obtained as the difference between measured and predicted IRI.
3) The SSE was obtained from the residuals, and the sum of SSE was computed.
4) Microsoft Solver was used to adjust the coefficients to minimize SSE for the entire data set.
5) The adjusted coefficients were used as calibrated coefficients of the IRI model in the AASHTOWare Pavement ME Design software, and a paired t-test was conducted between the measured data and predicted data.

#### 5.3.2.1 Influence of Initial IRI in Calibration

While calibrating the IRI model, the initial IRI was set to 63 in/mile based on previous studies; calibration coefficient C4 was found to be 136 (global value is 25.24). Statistical parameters were satisfactory for calibration and validation, but many KDOT projects were failing in IRI. Since AASHTOWare pavement ME design software predicted small cracking, spalling, and faulting values, key parameters in the IRI model were the site factor and initial IRI. The PMIS database did not contain initial IRI values for these projects; therefore, a value of 83 in/mile was used as initial IRI in the calibration project per KDOT recommendation.

#### 5.3.2.2 Elimination of Bias after Adjustment of Initial IRI

Results of the paired t-test after local calibration are shown in Table 5-9. Results showed that the bias was significantly reduced.

**Table 5-9: Statistical analysis summary for locally calibrated factors for the IRI model**

| Bias | Se | Se/Sy | $R^2$ | P-value | Hypothesis, $H_0$ : ∑(Meas.-Pred.) = 0 |
|---|---|---|---|---|---|
| 288.252 | 13.170 | 0.931 | 0.204 | 0.148 | Accepted |

As shown in Table 5-9, the Se increased slightly after calibration. The guide for local calibration of mechanistic-empirical design advocates recalibrating the model to reduce Se if the agency feels that the standard error is too large, resulting in an overly conservative design at higher reliability levels. As mentioned, the total standard error contained four components. According to the design guide, out of these four components, only "input error" can be reduced via calibration. The guide also states that the distress/IRI measurement error is a major contributor to the error components, requiring the agency to decide whether or not to employ additional cost and effort to reduce the total standard error. Nonetheless, the design guide recommends that the Se of the JPCP IRI model should be within 17 in/mile (AASHTO, 2010). The predicted versus measured IRI (locally calibrated) relationship is shown in Figure 5-4.

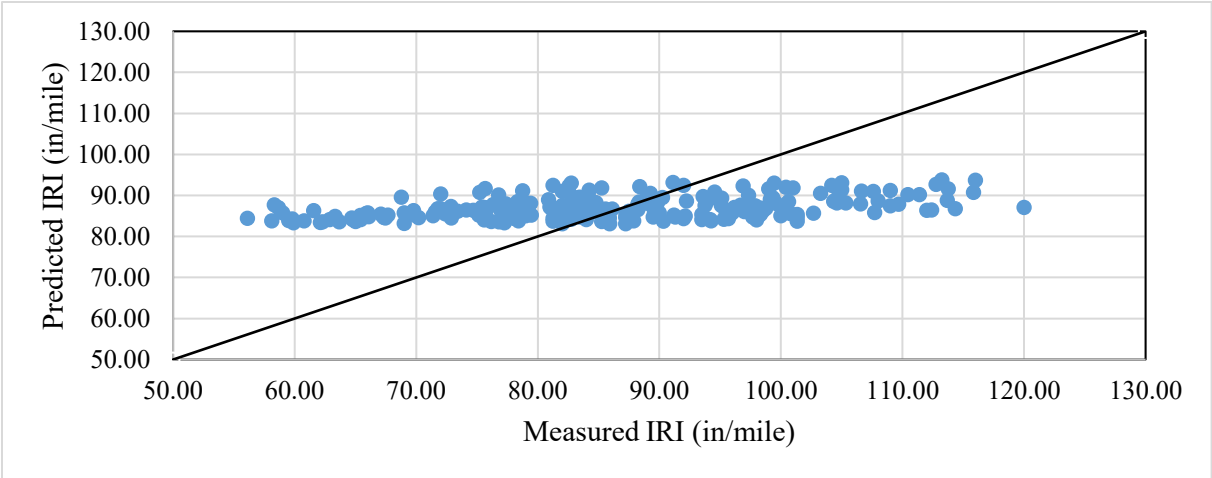


**Figure 5-4: Predicted versus measured IRI with locally-calibrated factors**

### 5.3.3 Validation of the IRI Model

Statistical analysis results for the IRI model after validation are shown in Table 5-10, demonstrating that the bias and standard error were low with locally calibrated factors.

**Table 5-10: Summary of statistical analysis for IRI model for validation of local coefficients**

| Bias | Se | Se/Sy | $R^2$ | P-value | Hypothesis, $H_0$ : ∑(Meas.-Pred.) = 0 |
|---|---|---|---|---|---|
| 356.9 | 8.67 | 0.908 | 0.245 | <0.0001 | Rejected |

As shown in Table 5-10, the p-value obtained from the paired t-test for the IRI model was very small, so the null hypothesis was rejected. It is mainly because projects considered for IRI model validation were intentionally chosen with very low IRI increase with time. Nonetheless, the bias and standard error were relatively small with locally-calibrated coefficients.

### 5.3.4 Calibration Results

Coefficients of the IRI model after local calibration for JPCP in Kansas are shown in Table 5-11. Adjusted coefficients are shown in bold font.

**Table 5-11: Calibration coefficients of the JPCP IRI model**

| C1 | C2 | C3 | C4 |
|---|---|---|---|
| 0.8203 | 0.4417 | 1.4929 | **18.75** |

# Chapter 6 - Conclusions and Recommendations

## 6.1 Conclusions

The primary objective of this study was to locally calibrate MEPDG performance prediction models to Kansas conditions. Twenty-seven flexible pavement projects and 22 JPCP projects were chosen throughout the state. Twenty-one pavement projects were selected for flexible pavement distress model calibration, and six projects were selected for validation. Performance prediction models calibrated for flexible pavements in Kansas included the permanent deformation or rutting model, the top-down fatigue (longitudinal) cracking model, the bottom-up (alligator) cracking model, the thermal (transverse) cracking model, and the IRI model. The transverse joint faulting model and the IRI model were locally calibrated for JPCP performance models. The transverse slab cracking model could not be calibrated due to lack of measured performance data. The following conclusions were based on local calibration and statistical analysis results:

1. A significant amount of bias was evident between the measured and predicted data of rutting, and AASHTOWare ME design overestimated the rutting of newly constructed flexible pavements in Kansas. Therefore, local calibration was performed by eliminating the bias and adjusting the AC and subgrade rutting model coefficients. The bias was significantly reduced after calibration, and the null hypothesis was accepted. Calibrated coefficients showed significantly better predictions of permanent deformation compared to nationally-calibrated models.
2. AASHTOWare ME design severely underpredicted top-down fatigue cracking for HMA pavements in Kansas. Local calibration was conducted by optimizing the calibration parameter using Microsoft Excel Solver and by repeatedly running AASHTOWare pavement ME design software for a large factorial of adjusted coefficients. Although the calibrated model showed very high Se after local calibration, the null hypothesis in the t-test was accepted. The calibrated model could not be validated further because all projects with measured top-down cracking values were used for calibration. The calibrated model yielded higher top-down cracking for all projects and exceeded the KDOT-recommended trigger value.

3. Because the KDOT PMIS database did not indicate any bottom-up cracks for projects considered for calibration and validation and because KDOT recognizes all load-related cracking as top-down cracking, the bottom-up fatigue cracking model was not calibrated.
4. A significant amount of bias was found, and MEPDG did not predict any thermal cracking for all selected pavement projects with global coefficients. Although local calibration was attempted, it forced the predicted data to match the measured data, yielding a model that generated high, unrealistic AC thermal cracking for all projects.
5. The globally-calibrated IRI model showed significant bias in the paired t-test, and the null hypothesis was rejected. Because ME design slightly overpredicted the IRI value, local calibration was attempted. The bias and standard error were low with locally calibrated factors, but the Se increased slightly after calibration. Nonetheless, the Se of the IRI model was within the range of the design guide; therefore, calibration of the IRI model was successful.
6. Statistical analysis results revealed significant bias in the JPCP transverse joint faulting model. ME design also significantly overpredicted faulting for the selected JPCP projects. The locally calibrated faulting model more efficiently predicted distress compared to the national model after validation, bias, and standard error had been significantly reduced.
7. With the significant bias and rejection of the null hypothesis from the paired t-test with the globally calibrated IRI factor, it was needed to be calibrated. Although the Se increased slightly after calibration, it was within the recommended range according to the design guide. The null hypothesis for validation was also rejected because the projects considered for model validation were intentionally chosen with minimal IRI increase over time. Nevertheless, the bias and standard error were relatively small with locally calibrated coefficients.
8. Measured cracking data for JPCPs were not available, so the cracking model could not be calibrated and global calibration values were taken as local values.

## 6.2 Recommendations

1. Typical HMA mixtures (virgin and with recycled materials) used in new flexible pavement in Kansas should be characterized using the dynamic modulus test and the dynamic shear rheometer (DSR) test. Complex modulus and phase angle for typical binders derived from the DSR test may be helpful for increased reliability of calibration based on Level 1 inputs.
2. Low-temperature cracking behavior of HMA mix should be investigated using creep compliance and indirect tensile strength tests.
3. KDOT should calibrate the AC thermal cracking model by district, and only projects showing AC transverse cracking should be used in calibration in the future.
4. Projects that show bottom-up fatigue cracking should be identified and the bottom-up fatigue cracking model should be locally calibrated.
5. For the rutting model, deriving field calibration parameters (K1, K2, K3) from triaxial repeated loading permanent deformation (TRLPD) tests may result in more accurate calibration.
6. Although only pavement sections with PCTB base layer was considered for calibration for JPCP, variability could occur in the design of new pavements with granular base (GB), aggregate base (AB-3), or bound drainable bases (BDBs). Four projects with the BDB base layer were used for validation in this study; however, these four projects were specifically chosen with very low increase in IRI over time. The addition of different base types could lead to more realistic calibration.
7. During JPCP calibration 217 measured data points were compared to corresponding predicted data. In many cases the maximum faulting was observed during the initial year of the design life, whereas AASHTOWare pavement ME design software predicts mean joint transverse faulting incrementally over time. Thus, several outliers should have been removed from the data for more accurate calibration.
8. A more sophisticated optimization technique, such as a genetic algorithm (GA), could potentially improve the accuracy of the calibration results.
9. This study adopted the traditional split-sample approach for calibration-validation of the MEPDG models. More advanced statistical approaches, such as jack-knife

testing and bootstrapping techniques, reportedly improve calibration precision. These approaches should be investigated in future studies.

## 6.3 Study Limitations

1. As stated, many inputs were used as level 2 and 3 in the AASHTOWare program, but time limitations of the research project did not allow exploration of all level 1 inputs. Lack of level 1 inputs may have diminished calibration accuracy.
2. No field testing or forensic investigations were performed in this study due to time and budget constraints and as per KDOT decision. Field and forensic investigations could have increased the credibility of some material inputs.
3. Measured data collected for this study were derived from the KDOT PMIS database, with the data primarily originating between the years 2000 and 2012 when distress data were collected by manual distress survey. In 2013 KDOT introduced an automated cracking data collection system known as the laser crack measurement system (LCMS). Cracking data after the year 2013 are still being processed and were not included in the PMIS database. More precise cracking data would benefit the calibration of MEPDG cracking models.

## 6.4 Scope of Future Research

KDOT is currently attempting to incorporate MEPDG in the design of flexible and rigid pavement structures, but local calibration alone will not allow full implementation of the design method—MEPDG implementation will require a sustainable and long-term effort. A level 1 traffic and materials database must be established to ensure effective design with AASHTOWare. In-service pavement test sections could be constructed in order to verify the performance of MEPDG design, providing several years of familiarity before complete adoption of the MEPDG design procedure. Implementation effort is another potential source of future research. In addition, the calibration process must be reassessed if significant changes occur in any of the performance models, thereby requiring version upgrades of AASHTOWare software.

# References


AASHTO. (1993). "AASHTO Guide for Design of Pavement Structures," American Association of State Highway and Transportation Officials, Vol. 1, AASHTO.

AASHTO. (2014). "AASHTOWare Pavement ME Design Software Help System," American Association of State Highway and Transportation Officials, Washington, D.C.

AASHTO. (2010). "Guide for the Local Calibration of the Mechanistic-Empirical Pavement Design Guide," American Association of State Highway and Transportation Officials, Washington, D.C.

AASHTO. (2015). "Mechanistic-Empirical Pavement Design Guide: A Manual of Practice," American Association of State Highway and Transportation Officials, Washington, D.C.

AASHTO. (2008). "Mechanistic-empirical pavement design guide: A manual of practice," Interim edition, American Association of State Highway and Transportation Officials, Washington, DC.

AASHTO. (2011). "Software Help System DARWin- ME Mechanistic-Empirical Pavement Design Software," American Association of State Highway and Transportation Officials, Washington, D.C.

Abdullah, A.Q. (2015). "Development Of A Simplified Flexible Pavement Design Protocol For New York State Department Of Transportation Based On AASHTO ME Pavement Design Guide," Ph.D. Dissertation, the University Of Texas at Arlington, Arlington, Texas.

Ceylan, H., Kim, S., Gopalakrishnan, K., and Ma, D. (2013). "Iowa Calibration of MEPDG Performance Prediction Models," InTrans Project 11-401, Iowa Department of Transportation, Ames, Iowa.

Darter, M. I., Titus-Glover, L., Von Quintus, H., Bhattacharya, B. B., and Mallela, J. (2014). "Calibration and Implementation of the AASHTO Mechanistic-Empirical Pavement Design Guide in Arizona," No. FHWA-AZ-14-606, Arizona Department of Transportation Research Center, Phoenix, Arizona.

Elshaer, M. (2009). "Stresses and Strains in Flexible Pavement using Computer Program."

FHWA. (2011). "Implementing Mechanistic-Empirical Pavement Design and Darwin-ME," Federal Highway Administration, Office of Pavement Technology.

FHWA. (2014). "Table HM-12 in Highway Statistics 2014," Office of Highway Policy Information, U.S. Department of Transportation, Federal Highway Administration, Washington, D.C., <http://www.fhwa.dot.gov/policyinformation/statistics/2008/hm12.cfm> (accessed on July 20, 2016).

Huang, Y. H. (1993). Pavement analysis and design.

Kasperick, T.J. (2013). "Calibration of the Mechanistic-Empirical Pavement Design Guide for Local Paved Roads in Wyoming," M.S. Thesis, University of Wyoming, Laramie, Wyoming.

Khanum, T. (2005). "Kansas Rigid Pavement Analysis Following New Mechanistic-Empirical Design Guide," Master's Thesis, Kansas State University, Manhattan, Kansas.

Kim, Y. R., Jadoun, F. M., Hou, T., and Muthadi, N. (2011). "Local calibration of the MEPDG for flexible pavement design," No. FHWA\ NC\ 2007-07, NC Department of Transportation Research and Analysis Group, North Carolina Department of Transportation, Raleigh, North Carolina.

Mallela, J., Titus-Glover, L., Sadasivam, S., Bhattacharya, B., Darter, M., and Von Quintus, H. (2013). "Implementation of the AASHTO mechanistic-empirical pavement design guide for Colorado," No. CDOT-2013-4, Colorado Department of Transportation – Research, Denver, Colorado.

Mendenhall, W. and Sincich, T. (2012). A Second Course in Statistics Regression Analysis. Prentice Hall.

Minitab Support. (2016). "Hypothesis Tests," <http://support.minitab.com/en-us/minitab/17/topic-library/basic-statistics-and-graphs/hypothesis-tests/tests-of-means/why-use-paired-t/> (accessed on September 21, 2016).

Momin, S. A. (2011). "Local Calibration of Mechanistic Empirical Pavement Design Guide for North Eastern United States," Master's Thesis, the University Of Texas at Arlington, Arlington, Texas.

Nabhan, P. (2015). "Calibration of the AASHTO MEPDG for Flexible Pavements to Fit Nevada's Conditions," Master's Thesis, University of Nevada, Reno, Nevada.

NAPA. (2016). "Engineering Overview of Asphalt Pavement," <http://www.asphaltpavement.org/index.php?option=com_content&view=article&id=14&Itemid=33> (accessed on July 21, 2016).

NCHRP. (2004). "Guide for Mechanistic-Empirical Design of New and Rehabilitated Pavement Structures," Final Report for Project 1-37A, Part 1, 2 & 3, Chapter 4, National

Cooperative Highway Research Program, Transportation Research Board, National Research Council, Washington, D.C.

NCHRP. (2003). "Guide for Mechanistic-Empirical Design of New and Rehabilitated Pavement Structures," Structural Response Models for Rigid Pavements, Appendix QQ, National Cooperative Highway Research Program, Transportation Research Board, National Research Council, Washington, D.C.

NCHRP. (2014). "Implementation of the AASHTO Mechanistic-Empirical Pavement Design Guide and Software," NCHRP Synthesis 457, A Synthesis of Highway Practice, Transportation Research Board of the National Academics, Washington, DC.

NCHRP. (2009). "Local Calibration Guidance for the Recommended Guide for Mechanistic-Empirical Design of New and Rehabilitated Pavement Structures," NCHRP 1-40B, Final Report, National Cooperative Highway Research Program, Washington, DC.

NHI. (2002). "Introduction to Mechanistic-Empirical Pavement Design of New and Rehabilitated Pavements," Course No. 131064, National Highway Institute, Federal Highway Administration, Washington, D.C.

Romanoschi, S., Momin, S., Bethu, S., and Bendana, L. (2011). "Development of traffic inputs for new mechanistic-empirical pavement design guide: Case study," Transportation Research Record: Journal of the Transportation Research Board, Issue 2256, pp. 142-150.

Tam, W. and Von Quintus, H. (2003). "Use of long-term pavement performance data to develop traffic defaults in support of mechanistic-empirical pavement design procedures," Transportation Research Record: Journal of the Transportation Research Board, Issue 1855, pp. 176-182.

Timm, D., Birgisson, B., and Newcomb, D. (1998). "Development of mechanistic-empirical pavement design in Minnesota," In Transportation Research Record: Journal of the Transportation Research Board. No.1629, Transportation Research Board of the National Academies, Washington, D.C., pp. 181-188.

TxDOT. (2011). "Pavement Design Guide," <http://onlinemanuals.txdot.gov/txdotmanuals/pdm/pavement_types.htm#i1064971> (accessed on July 20, 2016).

Williams, R. C., and Shaidur, R. (2013). "Mechanistic-Empirical Pavement Design Guide Calibration for Pavement Rehabilitation," Final Report-SPR 718, Oregon Department of Transportation Research Section, Oregon Department of Transportation, Salem, Oregon.

# Appendix A - Traffic Inputs of AASHTOWare ME

**Table A -1: Vehicle class distribution factors for individual AVC stations**

| Class | Automatic Vehicle Class Stations | | | | | | | | | | |
|---|---|---|---|---|---|---|---|---|---|---|---|
| | CTQ1D1 | 0DT453 | 7XRME7 | 61ILJ3 | 91TFY5 | AW9N83 | CV64B3 | F10VD5 | 9LON61 | 9Q9OK1 | 7HOM63 |
| 4 | 0.55 | 0.84 | 0.8 | 52.05 | 7.4 | 2.01 | 9.16 | 0.75 | 86.71 | 0.86 | 0.84 |
| 5 | 4.27 | 2.92 | 5.42 | 10.85 | 10.17 | 3.57 | 5.31 | 5.6 | 2.89 | 12.12 | 5.59 |
| 6 | 3.36 | 1.26 | 3.26 | 1.1 | 1.72 | 2.63 | 10.94 | 4.55 | 1.87 | 10.65 | 3.21 |
| 7 | 0.34 | 0.81 | 0.55 | 2.49 | 1.16 | 0.19 | 0.33 | 0.48 | 2.4 | 1.58 | 0.78 |
| 8 | 6.64 | 3.87 | 5.28 | 2.34 | 16.54 | 5.8 | 6.02 | 5.62 | 1.29 | 9.17 | 5.5 |
| 9 | 79.07 | 77.45 | 74.9 | 1.76 | 57.49 | 78.41 | 64.91 | 77.01 | 1.82 | 62.34 | 72.53 |
| 10 | 4.14 | 1 | 1.8 | 7.03 | 3.08 | 1.42 | 1.57 | 1.37 | 2.65 | 1.37 | 2.21 |
| 11 | 0.49 | 6.27 | 5.53 | 21.19 | 0.86 | 5.43 | 0.25 | 3.66 | 0.34 | 1.35 | 6.98 |
| 12 | 0.65 | 3.59 | 2.22 | 1.16 | 0.43 | 0.27 | 0.19 | 0.76 | 0.03 | 0.26 | 2.15 |
| 13 | 0.49 | 1.99 | 0.25 | 0.05 | 1.15 | 0.28 | 1.32 | 0.2 | 0.01 | 0.29 | 0.21 |

**Table A -2: Monthly adjustment factors for AVC station 0DT453**

| Month | Class 4 | Class 5 | Class 6 | Class 7 | Class 8 | Class 9 | Class 10 | Class 11 | Class 12 | Class 13 |
|---|---|---|---|---|---|---|---|---|---|---|
| Jan | 0.68 | 0.57 | 0.95 | 0.51 | 0.57 | 0.92 | 0.62 | 0.95 | 0.93 | 0.75 |
| Feb | 0.64 | 0.58 | 0.99 | 0.59 | 0.61 | 0.96 | 0.86 | 0.93 | 0.93 | 0.79 |
| Mar | 0.82 | 0.76 | 0.85 | 0.73 | 0.72 | 1.01 | 0.85 | 0.99 | 0.99 | 0.88 |
| Apr | 0.86 | 0.86 | 0.97 | 0.81 | 0.91 | 1.03 | 1.06 | 1.07 | 1.08 | 0.93 |
| May | 0.93 | 1.13 | 0.93 | 1.24 | 1.14 | 1.02 | 0.97 | 1 | 0.98 | 1.09 |
| Jun | 1.29 | 1.5 | 1 | 1.61 | 1.38 | 1.03 | 1.33 | 0.99 | 0.99 | 1.19 |
| Jul | 1.44 | 1.6 | 1.16 | 1.58 | 1.41 | 1.07 | 1.3 | 1.08 | 1.02 | 1.32 |
| Aug | 1.27 | 1.28 | 1.07 | 1.27 | 1.3 | 1.03 | 1.08 | 0.93 | 1.04 | 1.26 |
| Sep | 1.2 | 1.09 | 1.2 | 1.18 | 1.24 | 1.06 | 1.08 | 1.02 | 1.04 | 1.29 |
| Oct | 1 | 1.07 | 1.02 | 1.09 | 1.02 | 1.01 | 0.94 | 0.99 | 1.03 | 1.19 |
| Nov | 0.95 | 0.83 | 0.89 | 0.74 | 0.8 | 0.95 | 1 | 1.03 | 1.01 | 0.79 |
| Dec | 0.92 | 0.71 | 0.98 | 0.65 | 0.9 | 0.91 | 0.91 | 1.02 | 0.95 | 0.52 |

**Table A -3: Monthly adjustment factors for AVC station 7XRME7**

| Month | Class 4 | Class 5 | Class 6 | Class 7 | Class 8 | Class 9 | Class 10 | Class 11 | Class 12 | Class 13 |
|---|---|---|---|---|---|---|---|---|---|---|
| Jan | 0.99 | 0.88 | 0.94 | 0.71 | 0.81 | 1.04 | 0.98 | 1.05 | 1.07 | 0.79 |
| Feb | 1.03 | 0.82 | 0.79 | 0.62 | 1.05 | 1.03 | 0.90 | 1.06 | 1.02 | 0.66 |
| Mar | 1.18 | 0.95 | 0.94 | 0.93 | 1.04 | 1.04 | 1.04 | 1.11 | 1.15 | 0.96 |
| Apr | 1.16 | 1.15 | 1.68 | 0.96 | 0.29 | 1.15 | 1.30 | 1.11 | 1.22 | 1.13 |
| May | 1.27 | 1.16 | 1.95 | 1.19 | 1.22 | 1.05 | 1.03 | 1.07 | 1.10 | 1.18 |
| Jun | 1.03 | 1.29 | 1.21 | 1.46 | 1.39 | 1.07 | 1.12 | 1.05 | 0.99 | 1.67 |
| Jul | 1.01 | 1.19 | 1.02 | 1.50 | 1.07 | 1.05 | 0.86 | 1.11 | 0.93 | 1.22 |
| Aug | 0.86 | 1.11 | 1.03 | 1.28 | 0.99 | 1.00 | 0.94 | 1.01 | 0.87 | 0.85 |
| Sep | 0.43 | 0.53 | 0.44 | 0.63 | 0.45 | 0.43 | 0.65 | 0.28 | 0.15 | 0.58 |
| Oct | 1.12 | 1.13 | 1.01 | 1.12 | 1.09 | 1.11 | 1.02 | 1.19 | 1.32 | 1.48 |
| Nov | 0.94 | 0.92 | 0.94 | 0.88 | 0.83 | 1.02 | 1.14 | 1.01 | 1.18 | 0.67 |
| Dec | 0.99 | 0.88 | 1.05 | 0.73 | 0.77 | 1.00 | 1.02 | 0.94 | 1.01 | 0.79 |

**Table A -4: Monthly adjustment factors for AVC station 61ILJ3**

| Month | Class 4 | Class 5 | Class 6 | Class 7 | Class 8 | Class 9 | Class 10 | Class 11 | Class 12 | Class 13 |
|---|---|---|---|---|---|---|---|---|---|---|
| Jan | 0.89 | 0.93 | 0.95 | 0.79 | 0.75 | 0.86 | 1.05 | 0.99 | 1.03 | 0.65 |
| Feb | 0.84 | 0.87 | 0.94 | 0.78 | 0.72 | 0.89 | 1.04 | 1.01 | 0.91 | 0.60 |
| Mar | 1.03 | 1.00 | 1.01 | 0.96 | 0.93 | 1.11 | 0.98 | 1.03 | 1.16 | 1.62 |
| Apr | 1.06 | 1.01 | 1.03 | 1.04 | 1.03 | 1.19 | 0.92 | 1.02 | 1.14 | 1.25 |
| May | 1.06 | 1.03 | 1.04 | 1.08 | 1.06 | 0.96 | 0.88 | 1.03 | 1.11 | 0.78 |
| Jun | 1.06 | 1.05 | 1.09 | 1.11 | 1.03 | 0.95 | 0.93 | 0.96 | 0.95 | 0.98 |
| Jul | 1.10 | 1.05 | 1.07 | 1.19 | 1.07 | 0.99 | 0.99 | 0.93 | 0.91 | 1.01 |
| Aug | 0.99 | 1.00 | 1.02 | 1.09 | 1.33 | 1.05 | 0.97 | 0.96 | 0.97 | 0.81 |
| Sep | 0.96 | 1.07 | 1.10 | 1.14 | 1.19 | 1.17 | 1.25 | 1.00 | 0.95 | 1.21 |
| Oct | 1.00 | 1.05 | 1.04 | 1.08 | 1.03 | 1.11 | 1.07 | 1.01 | 1.00 | 0.79 |
| Nov | 1.00 | 1.01 | 0.92 | 0.94 | 1.10 | 0.89 | 0.96 | 1.02 | 0.97 | 1.28 |
| Dec | 1.02 | 0.96 | 0.79 | 0.82 | 0.77 | 0.82 | 0.95 | 1.02 | 0.90 | 1.02 |

**Table A -5: Monthly adjustment factors for AVC station 91TFY5**

| Month | Class 4 | Class 5 | Class 6 | Class 7 | Class 8 | Class 9 | Class 10 | Class 11 | Class 12 | Class 13 |
|---|---|---|---|---|---|---|---|---|---|---|
| Jan | 1.06 | 1.28 | 1.36 | 0.36 | 1.02 | 1.35 | 1.16 | 1.24 | 1.06 | 0.82 |
| Feb | 1.18 | 1.24 | 1.42 | 0.39 | 0.94 | 1.33 | 1.05 | 1.23 | 0.93 | 0.77 |
| Mar | 1.58 | 1.21 | 1.59 | 0.45 | 0.94 | 1.02 | 1.87 | 1.16 | 1.17 | 1.04 |
| Apr | 1.70 | 1.15 | 1.52 | 0.45 | 0.84 | 0.90 | 1.92 | 1.02 | 1.70 | 1.31 |
| May | 1.25 | 1.06 | 0.81 | 0.43 | 0.67 | 0.90 | 0.73 | 0.95 | 0.56 | 0.89 |
| Jun | 1.22 | 1.18 | 0.76 | 0.45 | 0.72 | 0.89 | 0.59 | 0.89 | 0.57 | 1.04 |
| Jul | 0.84 | 1.15 | 0.77 | 0.44 | 0.57 | 0.85 | 0.68 | 0.90 | 0.45 | 1.09 |
| Aug | 0.43 | 1.02 | 0.58 | 0.37 | 0.52 | 0.86 | 0.65 | 0.72 | 0.55 | 1.42 |
| Sep | 0.66 | 1.02 | 0.55 | 0.40 | 0.57 | 0.93 | 0.64 | 0.91 | 0.47 | 1.27 |
| Oct | 0.87 | 1.14 | 0.76 | 0.48 | 0.68 | 0.92 | 0.67 | 0.91 | 0.71 | 1.35 |
| Nov | 1.10 | 0.16 | 0.33 | 7.49 | 4.16 | 0.05 | 0.32 | 0.54 | 2.34 | 0.26 |
| Dec | 0.12 | 0.38 | 1.56 | 0.30 | 0.37 | 2.01 | 1.74 | 1.54 | 1.48 | 0.74 |

**Table A -6: Monthly adjustment factors for AVC station AW9N83**

| Month | Class 4 | Class 5 | Class 6 | Class 7 | Class 8 | Class 9 | Class 10 | Class 11 | Class 12 | Class 13 |
|---|---|---|---|---|---|---|---|---|---|---|
| Jan | 1.68 | 0.77 | 0.56 | 0.95 | 0.57 | 0.60 | 0.52 | 0.71 | 0.82 | 0.40 |
| Feb | 2.03 | 0.86 | 0.66 | 0.32 | 0.70 | 0.72 | 0.57 | 0.98 | 1.88 | 0.53 |
| Mar | 2.51 | 1.44 | 0.67 | 0.76 | 0.67 | 1.05 | 0.72 | 1.13 | 1.37 | 0.00 |
| Apr | 0.87 | 2.71 | 1.73 | 3.03 | 2.07 | 1.83 | 1.65 | 1.38 | 2.19 | 2.13 |
| May | 0.46 | 2.02 | 1.49 | 1.14 | 2.02 | 1.34 | 1.83 | 1.35 | 1.64 | 1.46 |
| Jun | 0.93 | 0.90 | 1.15 | 0.30 | 0.98 | 1.27 | 1.14 | 1.32 | 0.77 | 1.81 |
| Jul | 0.67 | 0.90 | 1.31 | 1.26 | 1.31 | 1.38 | 1.46 | 1.30 | 0.91 | 2.04 |
| Aug | 0.51 | 0.79 | 1.75 | 1.19 | 1.15 | 1.31 | 1.66 | 1.34 | 0.75 | 1.61 |
| Sep | 0.15 | 0.41 | 0.82 | 0.63 | 0.70 | 0.66 | 0.60 | 0.66 | 0.62 | 0.37 |
| Oct | 0.23 | 0.48 | 0.68 | 0.91 | 0.92 | 0.71 | 0.73 | 0.73 | 0.36 | 0.37 |
| Nov | 0.36 | 0.36 | 0.70 | 0.76 | 0.67 | 0.64 | 0.70 | 0.64 | 0.48 | 0.13 |
| Dec | 0.61 | 0.36 | 0.48 | 0.76 | 0.24 | 0.49 | 0.41 | 0.50 | 0.22 | 1.17 |

**Table A -7: Monthly adjustment factors for AVC station CTQ1D1**

| Month | Class 4 | Class 5 | Class 6 | Class 7 | Class 8 | Class 9 | Class 10 | Class 11 | Class 12 | Class 13 |
|---|---|---|---|---|---|---|---|---|---|---|
| Jan | 0.54 | 0.91 | 0.68 | 0.97 | 0.66 | 0.91 | 1.05 | 1.23 | 0.88 | 0.58 |
| Feb | 0.68 | 0.92 | 0.75 | 0.72 | 0.58 | 0.99 | 1.16 | 1.22 | 0.91 | 0.56 |
| Mar | 0.93 | 0.98 | 1.01 | 1.11 | 0.76 | 1.07 | 1.42 | 1.26 | 1.05 | 0.80 |
| Apr | 0.67 | 0.88 | 0.88 | 1.18 | 0.86 | 1.00 | 1.14 | 0.74 | 0.91 | 0.64 |
| May | 0.64 | 1.12 | 1.12 | 1.03 | 0.85 | 1.00 | 1.39 | 0.60 | 1.03 | 0.77 |
| Jun | 0.83 | 1.35 | 1.35 | 1.59 | 0.98 | 1.06 | 1.15 | 0.91 | 1.00 | 1.26 |
| Jul | 0.78 | 1.07 | 1.07 | 1.47 | 0.97 | 1.05 | 0.96 | 0.99 | 0.95 | 1.26 |
| Aug | 0.54 | 0.92 | 0.92 | 1.54 | 0.84 | 1.02 | 1.02 | 1.27 | 1.05 | 1.60 |
| Sep | 1.67 | 1.09 | 1.09 | 1.13 | 1.45 | 0.99 | 0.72 | 0.82 | 1.18 | 1.29 |
| Oct | 2.13 | 1.14 | 1.14 | 0.37 | 1.51 | 1.02 | 1.02 | 1.15 | 1.03 | 1.09 |
| Nov | 1.38 | 1.06 | 1.06 | 0.53 | 1.35 | 0.96 | 0.96 | 0.99 | 1.00 | 1.04 |
| Dec | 1.22 | 0.93 | 0.93 | 0.37 | 1.18 | 0.93 | 0.93 | 0.82 | 1.00 | 1.12 |

**Table A -8: Monthly adjustment factors for AVC station CV64B3**

| Month | Class 4 | Class 5 | Class 6 | Class 7 | Class 8 | Class 9 | Class 10 | Class 11 | Class 12 | Class 13 |
|---|---|---|---|---|---|---|---|---|---|---|
| Jan | 2.17 | 1.02 | 0.70 | 0.34 | 0.79 | 0.97 | 2.30 | 1.81 | 2.92 | 1.96 |
| Feb | 2.13 | 0.90 | 0.84 | 0.59 | 0.83 | 0.90 | 0.86 | 1.75 | 1.67 | 1.91 |
| Mar | 1.33 | 0.95 | 1.00 | 1.10 | 1.01 | 1.08 | 0.97 | 1.46 | 0.75 | 1.41 |
| Apr | 0.83 | 1.32 | 1.05 | 1.13 | 1.02 | 1.19 | 1.27 | 1.25 | 0.56 | 1.55 |
| May | 0.74 | 1.28 | 1.09 | 0.85 | 0.91 | 1.12 | 1.44 | 0.68 | 1.46 | 1.02 |
| Jun | 0.56 | 1.00 | 1.05 | 1.31 | 0.77 | 1.10 | 0.61 | 0.16 | 0.61 | 0.06 |
| Jul | 0.51 | 0.86 | 1.05 | 0.96 | 1.11 | 0.99 | 0.65 | 0.18 | 0.31 | 0.08 |
| Aug | 0.85 | 1.02 | 1.17 | 0.88 | 1.37 | 1.04 | 0.72 | 0.29 | 0.30 | 0.07 |
| Sep | 0.84 | 1.12 | 1.17 | 1.89 | 1.09 | 0.92 | 1.02 | 0.62 | 0.00 | 0.11 |
| Oct | 0.75 | 1.00 | 1.21 | 1.14 | 1.39 | 1.04 | 0.94 | 0.79 | 0.16 | 0.58 |
| Nov | 0.86 | 0.84 | 0.89 | 0.64 | 0.97 | 0.85 | 0.77 | 1.51 | 1.48 | 1.93 |
| Dec | 0.43 | 0.71 | 0.77 | 1.18 | 0.74 | 0.80 | 0.44 | 1.50 | 1.77 | 1.32 |

**Table A -9: Monthly adjustment factors for AVC station F10VD5**

| Month | Class 4 | Class 5 | Class 6 | Class 7 | Class 8 | Class 9 | Class 10 | Class 11 | Class 12 | Class 13 |
|---|---|---|---|---|---|---|---|---|---|---|
| Jan | 0.55 | 0.86 | 1.02 | 0.56 | 0.89 | 0.88 | 1.81 | 0.91 | 1.15 | 0.93 |
| Feb | 0.63 | 0.88 | 0.84 | 0.36 | 0.87 | 0.92 | 1.14 | 0.94 | 1.03 | 0.98 |
| Mar | 1.06 | 0.97 | 0.92 | 0.85 | 0.93 | 0.97 | 1.14 | 1.00 | 0.91 | 0.56 |
| Apr | 1.05 | 1.11 | 0.92 | 0.91 | 1.16 | 1.06 | 0.85 | 1.19 | 0.98 | 1.00 |
| May | 0.99 | 1.05 | 1.09 | 0.62 | 1.11 | 1.04 | 0.94 | 1.07 | 0.90 | 1.42 |
| Jun | 1.06 | 0.98 | 1.11 | 0.71 | 1.15 | 1.07 | 1.04 | 1.03 | 1.06 | 1.49 |
| Jul | 1.22 | 0.98 | 1.01 | 1.08 | 1.11 | 1.04 | 0.76 | 1.05 | 1.14 | 0.88 |
| Aug | 1.19 | 0.97 | 1.07 | 0.94 | 1.04 | 1.00 | 1.07 | 0.96 | 0.96 | 1.47 |
| Sep | 1.07 | 1.07 | 1.20 | 1.08 | 1.05 | 1.02 | 0.88 | 1.00 | 1.04 | 1.11 |
| Oct | 1.24 | 1.17 | 1.17 | 0.99 | 0.99 | 1.10 | 0.99 | 1.05 | 1.04 | 0.92 |
| Nov | 1.11 | 0.99 | 0.91 | 3.32 | 0.84 | 0.93 | 0.72 | 0.88 | 0.85 | 0.77 |
| Dec | 0.84 | 0.96 | 0.75 | 0.58 | 0.87 | 0.97 | 0.66 | 0.93 | 0.95 | 0.47 |

**Table A -10: Monthly adjustment factors for AVC station 9LON61**

| Month | Class 4 | Class 5 | Class 6 | Class 7 | Class 8 | Class 9 | Class 10 | Class 11 | Class 12 | Class 13 |
|---|---|---|---|---|---|---|---|---|---|---|
| Jan | 0.96 | 0.97 | 0.84 | 0.77 | 0.80 | 0.95 | 1.01 | 0.94 | 0.71 | 0.70 |
| Feb | 0.96 | 0.93 | 0.84 | 0.76 | 0.80 | 0.92 | 1.00 | 0.96 | 0.72 | 0.80 |
| Mar | 0.97 | 0.95 | 0.86 | 0.82 | 0.84 | 0.94 | 0.99 | 0.98 | 0.92 | 0.83 |
| Apr | 1.03 | 0.99 | 1.01 | 1.04 | 1.06 | 0.98 | 0.99 | 0.90 | 1.05 | 1.11 |
| May | 0.97 | 0.97 | 0.91 | 0.88 | 0.90 | 0.94 | 0.98 | 0.97 | 0.94 | 0.87 |
| Jun | 1.03 | 1.02 | 1.10 | 1.18 | 1.22 | 1.06 | 1.02 | 1.07 | 1.13 | 1.03 |
| Jul | 1.02 | 1.03 | 1.10 | 1.17 | 1.18 | 1.06 | 1.02 | 1.09 | 1.11 | 1.00 |
| Aug | 1.02 | 1.04 | 1.10 | 1.16 | 1.14 | 1.04 | 1.01 | 1.07 | 1.11 | 0.99 |
| Sep | 1.01 | 1.05 | 1.10 | 1.15 | 1.12 | 1.06 | 1.02 | 1.08 | 1.14 | 1.00 |
| Oct | 1.01 | 1.05 | 1.10 | 1.14 | 1.11 | 1.05 | 1.01 | 1.08 | 1.13 | 1.09 |
| Nov | 1.01 | 1.04 | 1.09 | 1.11 | 1.08 | 1.04 | 1.00 | 1.04 | 1.11 | 1.13 |
| Dec | 1.01 | 0.94 | 0.94 | 0.81 | 0.75 | 0.95 | 0.96 | 0.80 | 0.93 | 1.45 |

**Table A -11: Monthly adjustment factors for AVC station 9Q9OK1**

| Month | Class 4 | Class 5 | Class 6 | Class 7 | Class 8 | Class 9 | Class 10 | Class 11 | Class 12 | Class 13 |
|---|---|---|---|---|---|---|---|---|---|---|
| Jan | 0.99 | 1.18 | 1.01 | 0.83 | 0.91 | 1.06 | 0.92 | 0.94 | 1.02 | 1.18 |
| Feb | 1.23 | 1.39 | 1.18 | 1.03 | 1.14 | 1.32 | 1.09 | 1.21 | 1.21 | 1.22 |
| Mar | 1.41 | 1.47 | 1.41 | 1.64 | 1.35 | 1.43 | 1.33 | 1.37 | 1.40 | 1.36 |
| Apr | 1.50 | 1.75 | 1.45 | 1.41 | 1.47 | 1.43 | 1.32 | 1.42 | 1.43 | 1.54 |
| May | 1.38 | 1.68 | 1.63 | 1.55 | 1.54 | 1.44 | 1.46 | 1.58 | 1.32 | 1.33 |
| Jun | 1.63 | 1.42 | 1.76 | 1.64 | 1.75 | 1.56 | 1.72 | 1.59 | 1.66 | 1.31 |
| Jul | 1.31 | 1.08 | 1.24 | 1.25 | 1.31 | 1.21 | 1.26 | 1.25 | 1.39 | 0.93 |
| Aug | 0.60 | 0.43 | 0.51 | 0.49 | 0.57 | 0.56 | 0.70 | 0.64 | 0.56 | 0.40 |
| Sep | 0.49 | 0.46 | 0.52 | 0.57 | 0.59 | 0.57 | 0.67 | 0.59 | 0.67 | 0.38 |
| Oct | 0.54 | 0.45 | 0.55 | 0.60 | 0.55 | 0.57 | 0.59 | 0.60 | 0.48 | 0.36 |
| Nov | 0.48 | 0.37 | 0.42 | 0.42 | 0.46 | 0.46 | 0.51 | 0.47 | 0.47 | 0.70 |
| Dec | 0.42 | 0.33 | 0.31 | 0.37 | 0.37 | 0.39 | 0.42 | 0.34 | 0.40 | 1.27 |

**Table A -12: Monthly adjustment factors for AVC station 7HOM63**

| Month | Class 4 | Class 5 | Class 6 | Class 7 | Class 8 | Class 9 | Class 10 | Class 11 | Class 12 | Class 13 |
|---|---|---|---|---|---|---|---|---|---|---|
| Jan | 0.89 | 0.77 | 0.91 | 0.80 | 0.74 | 0.97 | 1.14 | 1.04 | 1.08 | 0.83 |
| Feb | 1.08 | 0.83 | 0.80 | 1.50 | 1.00 | 0.96 | 1.65 | 1.61 | 1.12 | 0.59 |
| Mar | 1.11 | 0.85 | 0.92 | 1.54 | 1.01 | 0.97 | 1.46 | 1.37 | 1.23 | 0.95 |
| Apr | 1.09 | 1.01 | 1.52 | 1.78 | 1.21 | 1.05 | 1.68 | 1.41 | 1.24 | 1.10 |
| May | 1.11 | 1.01 | 0.88 | 1.74 | 1.07 | 0.98 | 0.76 | 0.76 | 1.03 | 1.28 |
| Jun | 0.97 | 1.22 | 1.20 | 1.56 | 1.31 | 1.02 | 1.19 | 1.08 | 1.01 | 1.80 |
| Jul | 0.87 | 1.05 | 0.94 | 0.97 | 0.94 | 0.99 | 0.64 | 0.80 | 0.87 | 1.32 |
| Aug | 0.79 | 1.04 | 1.06 | 0.77 | 0.94 | 0.97 | 0.71 | 0.75 | 0.84 | 1.03 |
| Sep | 0.96 | 1.29 | 1.09 | 0.82 | 1.04 | 1.12 | 0.92 | 0.83 | 0.96 | 0.79 |
| Oct | 1.04 | 1.11 | 0.93 | 0.64 | 0.97 | 1.02 | 0.69 | 0.81 | 0.92 | 1.00 |
| Nov | 1.07 | 0.93 | 0.97 | 0.44 | 1.01 | 0.98 | 0.60 | 0.75 | 0.86 | 0.67 |
| Dec | 1.04 | 0.88 | 0.78 | 0.44 | 0.79 | 0.96 | 0.56 | 0.80 | 0.83 | 0.63 |

**Table A -13: Hourly distribution factors for individual AVC stations**

| Hour | Automatic Vehicle Class Stations | | | | | | | | | | |
|---|---|---|---|---|---|---|---|---|---|---|---|
| | 0DT453 | 7XRME7 | 61ILI3 | 91TFY5 | AW9N83 | CTQ1D1 | CV64B3 | F10VD5 | 9LON61 | 9Q9OK1 | 7HOM63 |
| Midnight | 2.25 | 2.03 | 1.17 | 1.65 | 1.69 | 1.55 | 1.47 | 1.3 | 0.79 | 1.07 | 1.94 |
| 1 | 1.97 | 1.64 | 0.88 | 1.25 | 1.66 | 1.31 | 1.12 | 1.13 | 0.52 | 0.85 | 1.6 |
| 2 | 1.88 | 1.78 | 0.81 | 1.28 | 1.78 | 1.19 | 1.06 | 1.23 | 0.46 | 0.8 | 1.56 |
| 3 | 1.95 | 1.83 | 0.84 | 1.42 | 2.17 | 1.2 | 1.04 | 1.61 | 0.57 | 0.86 | 1.67 |
| 4 | 2.09 | 2.11 | 1.11 | 1.58 | 2.95 | 1.35 | 1.17 | 2.19 | 1.24 | 1.29 | 1.83 |
| 5 | 2.35 | 2.53 | 1.69 | 1.93 | 3.55 | 2.08 | 1.46 | 2.56 | 2.51 | 2.25 | 2.25 |
| 6 | 2.63 | 3.17 | 2.72 | 2.74 | 4.27 | 3.36 | 3.02 | 3.41 | 5.29 | 4.4 | 2.93 |
| 7 | 3.37 | 3.94 | 4.5 | 3.91 | 4.99 | 4.57 | 4.25 | 4.78 | 7.3 | 7.25 | 3.82 |
| 8 | 4.37 | 5.38 | 5.32 | 5.43 | 6.09 | 5.68 | 5.48 | 5.76 | 5.48 | 6.65 | 5.08 |
| 9 | 4.88 | 6.43 | 6.11 | 6 | 7.05 | 6.47 | 5.83 | 6.92 | 4.84 | 6.02 | 6.13 |
| 10 | 5.08 | 6.44 | 6.53 | 6.26 | 7.11 | 7.02 | 6.3 | 7.35 | 4.82 | 6.12 | 6.39 |
| 11 | 5.47 | 6.24 | 6.41 | 6.45 | 6.63 | 7.08 | 7.23 | 7.43 | 5.19 | 6.4 | 6.37 |
| Noon | 5.99 | 6.36 | 6.4 | 6.3 | 6.31 | 6.87 | 7.71 | 7.1 | 5.53 | 6.65 | 6.33 |
| 13 | 6.29 | 6.22 | 6.63 | 6.52 | 6.2 | 6.82 | 7.6 | 6.96 | 5.77 | 6.71 | 6.3 |
| 14 | 6.26 | 6.07 | 6.97 | 6.6 | 5.69 | 6.71 | 7.27 | 6.66 | 6.3 | 7.1 | 6.19 |
| 15 | 6.35 | 5.87 | 7.15 | 6.55 | 5.15 | 6.52 | 6.76 | 6.11 | 7.71 | 7.08 | 6.18 |
| 16 | 6.38 | 5.58 | 7.18 | 6.4 | 4.86 | 6.01 | 7 | 5.68 | 8.55 | 6.79 | 5.98 |
| 17 | 6.18 | 5.45 | 6.81 | 5.99 | 4.47 | 5.29 | 5.77 | 4.95 | 8.38 | 6.33 | 5.82 |
| 18 | 5.63 | 4.91 | 5.63 | 5.21 | 3.89 | 4.57 | 4.63 | 4.2 | 5.69 | 4.47 | 5.26 |
| 19 | 4.85 | 4.1 | 4.61 | 4.52 | 3.26 | 3.94 | 3.87 | 3.53 | 4.07 | 3.13 | 4.4 |
| 20 | 4.28 | 3.6 | 3.69 | 4.04 | 3 | 3.24 | 3.35 | 2.92 | 3.33 | 2.56 | 3.74 |
| 21 | 3.75 | 3.08 | 2.97 | 3.22 | 2.79 | 2.87 | 2.78 | 2.48 | 2.66 | 2.12 | 3.11 |
| 22 | 3.06 | 2.7 | 2.23 | 2.63 | 2.43 | 2.42 | 2.1 | 2 | 1.79 | 1.7 | 2.73 |
| 23 | 2.69 | 2.54 | 1.66 | 2.1 | 2.05 | 1.88 | 1.72 | 1.73 | 1.22 | 1.39 | 2.41 |

**Table A -14: Axle group per vehicle for individual WIM station 2WOA86**

| WIM site: 2WOA86 | Class 4 | Class 5 | Class 6 | Class 7 | Class 8 | Class 9 | Class 10 | Class 11 | Class 12 | Class 13 |
|---|---|---|---|---|---|---|---|---|---|---|
| Single | 2 | 2.08 | 1.57 | 0 | 2.35 | 1.75 | 2.34 | 5 | 4 | 5.63 |
| Tandem | 0 | 0.46 | 1.43 | 0 | 1.47 | 3.24 | 2.47 | 0 | 2 | 2.75 |
| Tridem | 0 | 0.04 | 0 | 0 | 0 | 0.01 | 1.28 | 0 | 0 | 2.25 |
| Quad | 0 | 0 | 0 | 0 | 0 | 0 | 0 | 0 | 0 | 0 |

**Table A -15: Axle group per vehicle for individual WIM station 3MXC22**

| WIM site: 3MXC22 | Class 4 | Class 5 | Class 6 | Class 7 | Class 8 | Class 9 | Class 10 | Class 11 | Class 12 | Class 13 |
|---|---|---|---|---|---|---|---|---|---|---|
| Single | 1.095 | 2.203 | 1.154 | 2 | 2.255 | 1.566 | 3.077 | 5 | 3.113 | 0 |
| Tandem | 0.571 | 0.441 | 1.846 | 2 | 1.574 | 3.414 | 0.256 | 0 | 0.873 | 0 |
| Tridem | 0 | 0.229 | 0 | 0 | 0 | 0.02 | 1.615 | 0 | 0 | 0 |
| Quad | 0 | 0 | 0 | 0 | 0 | 0 | 0 | 0 | 0 | 0 |

**Table A -16: Axle group per vehicle for individual WIM station 4LGSU3**

| WIM site: 4LGSU3 | Class 4 | Class 5 | Class 6 | Class 7 | Class 8 | Class 9 | Class 10 | Class 11 | Class 12 | Class 13 |
|---|---|---|---|---|---|---|---|---|---|---|
| Single | 1.757 | 2.236 | 1.472 | 1.67 | 1.995 | 1.361 | 2.055 | 5 | 4.063 | 0 |
| Tandem | 0.486 | 0.968 | 1.611 | 1.33 | 1.005 | 3.333 | 2.722 | 0 | 1.938 | 0 |
| Tridem | 0 | 0.035 | 0 | 0.5 | 0 | 0.004 | 1.33 | 0 | 0 | 0 |
| Quad | 0 | 0 | 0 | 0.67 | 0 | 0 | 0 | 0 | 0 | 0 |

**Table A -17: Axle group per vehicle for individual WIM station 9M4PS3**

| WIM site: 9M4PS3 | Class 4 | Class 5 | Class 6 | Class 7 | Class 8 | Class 9 | Class 10 | Class 11 | Class 12 | Class 13 |
|---|---|---|---|---|---|---|---|---|---|---|
| Single | 1.757 | 2.211 | 1.161 | 1.67 | 1.995 | 1.361 | 2.055 | 5 | 4.063 | 0 |
| Tandem | 0.486 | 0.519 | 1.839 | 1.33 | 1.005 | 3.633 | 2.722 | 0 | 1.938 | 0 |
| Tridem | 0 | 0.083 | 0 | 0.5 | 0 | 0.004 | 1.33 | 0 | 0 | 0 |
| Quad | 0 | 0 | 0 | 0.67 | 0 | 0 | 0 | 0 | 0 | 0 |

**Table A -18: Axle group per vehicle for individual WIM station 20PUF5**

| WIM site: 20PUF5 | Class 4 | Class 5 | Class 6 | Class 7 | Class 8 | Class 9 | Class 10 | Class 11 | Class 12 | Class 13 |
|---|---|---|---|---|---|---|---|---|---|---|
| Single | 4.636 | 2.051 | 1.25 | 4 | 2.125 | 1.558 | 3.576 | 0 | 4 | 7 |
| Tandem | 0.364 | 1.013 | 1.75 | 0 | 1.833 | 3.442 | 2.217 | 0 | 2 | 1.33 |
| Tridem | 0 | 0 | 0 | 0 | 0 | 0 | 0.359 | 0 | 0 | 0.5 |
| Quad | 0 | 0 | 0 | 0 | 0 | 0 | 0.04 | 0 | 0 | 0 |

**Table A -19: Axle group per vehicle for individual WIM station 9ORQP1**

| WIM site: 9ORQP1 | Class 4 | Class 5 | Class 6 | Class 7 | Class 8 | Class 9 | Class 10 | Class 11 | Class 12 | Class 13 |
|---|---|---|---|---|---|---|---|---|---|---|
| Single | 2.075 | 2.11 | 1.289 | 1.789 | 2.294 | 1.875 | 2.33 | 5 | 4 | 0 |
| Tandem | 0.402 | 0.345 | 1.715 | 0.684 | 1.507 | 3.089 | 1.961 | 0 | 2 | 0 |
| Tridem | 0 | 0.282 | 0 | 0.632 | 0 | 0.036 | 1.589 | 0 | 0 | 0 |
| Quad | 0 | 0 | 0 | 1.263 | 0 | 0 | 0.235 | 0 | 0 | 0 |

**Table A -20: Axle group per vehicle for individual WIM station 9Q9OK1**

| WIM site: 9Q9OK1 | Class 4 | Class 5 | Class 6 | Class 7 | Class 8 | Class 9 | Class 10 | Class 11 | Class 12 | Class 13 |
|---|---|---|---|---|---|---|---|---|---|---|
| Single | 4.607 | 2.019 | 1.301 | 1.634 | 2.327 | 1.358 | 1.7 | 5 | 6 | 7 |
| Tandem | 1.607 | 0.345 | 1.699 | 0.295 | 1.436 | 3.661 | 2 | 0 | 0 | 0 |
| Tridem | 0 | 0.01 | 0 | 1.524 | 0 | 0.003 | 1.9 | 0 | 0 | 0 |
| Quad | 0 | 0 | 0 | 0.984 | 0 | 0 | 0.4 | 0 | 0 | 0 |

**Table A -21: Axle group per vehicle for individual WIM station BWGAA6**

| WIM site: BWGAA6 | Class 4 | Class 5 | Class 6 | Class 7 | Class 8 | Class 9 | Class 10 | Class 11 | Class 12 | Class 13 |
|---|---|---|---|---|---|---|---|---|---|---|
| Single | 2.494 | 2.146 | 1.455 | 2 | 2.297 | 1.708 | 2.857 | 5 | 1.588 | 0.772 |
| Tandem | 0.501 | 0.659 | 1.545 | 2 | 1.576 | 3.269 | 2 | 0 | 4.412 | 0.913 |
| Tridem | 0 | 0.016 | 0 | 0 | 0 | 0.023 | 1 | 0 | 0 | 0 |
| Quad | 0 | 0 | 0 | 0 | 0 | 0 | 0.571 | 0 | 0 | 0 |

**Table A -22: Axle group per vehicle for individual WIM station DVMSP3**

| WIM site: DVMSP3 | Class 4 | Class 5 | Class 6 | Class 7 | Class 8 | Class 9 | Class 10 | Class 11 | Class 12 | Class 13 |
|---|---|---|---|---|---|---|---|---|---|---|
| Single | 1.877 | 2.179 | 1.45 | 2.182 | 2.275 | 1.529 | 2.264 | 5 | 4.378 | 4.412 |
| Tandem | 0.359 | 0.582 | 1.549 | 1.454 | 1.543 | 3.465 | 2.189 | 0 | 1.623 | 3.422 |
| Tridem | 0.01 | 0.013 | 0 | 0.545 | 0 | 0.006 | 1.415 | 0 | 0 | 0 |
| Quad | 0 | 0 | 0 | 0 | 0 | 0 | 0.226 | 0 | 0 | 0 |

**Table A -23: Axle group per vehicle for individual WIM station F07WC7**

| WIM site: F07WC7 | Class 4 | Class 5 | Class 6 | Class 7 | Class 8 | Class 9 | Class 10 | Class 11 | Class 12 | Class 13 |
|---|---|---|---|---|---|---|---|---|---|---|
| Single | 0 | 1.943 | 1.273 | 1.727 | 2.33 | 1.185 | 1.92 | 5 | 4 | 6.3 |
| Tandem | 0 | 0.582 | 1.727 | 0.363 | 1.4 | 3.801 | 2.16 | 0 | 2 | 1 |
| Tridem | 0 | 0 | 0 | 1.909 | 0 | 0.014 | 2.04 | 0 | 0 | 0 |
| Quad | 0 | 0 | 0 | 0 | 0 | 0 | 0 | 0 | 0 | 0 |

# Appendix B - Site-specific material properties for new flexible pavements

| Project Name | Pavement Layer | Binder Grade | Binder Content (By Volume) | Gradation (% Passing) | | | |
|---|---|---|---|---|---|---|---|
| | | | | 3/4″ | 3/8″ | #4 | #200 |
| 007U0007500-NB | Surface Course | PG 70-28 | 11.6 | 100 | 98 | 78 | 3 |
| | Binder Course | PG 64-22 | 11 | 95 | 82 | 69 | 3 |
| | Base Course | PG 70-22 | 10.1 | 95 | 82 | 69 | 3 |
| Project Name | Pavement Layer | Binder Grade | Binder Content | Gradation | | | |
| | | | | 3/4″ | 3/8″ | #4 | #200 |
| 008U0007700-NB-1 | Surface Course | PG 64-28 | 12.2 | 100 | 98 | 70 | 5 |
| | Binder Course | PG 64-28 | 9.9 | 98 | 84 | 66 | 5 |
| | Base Course | PG 64-28 | 9.9 | 98 | 84 | 66 | 5 |
| Project Name | Pavement Layer | Binder Grade | Binder Content | Gradation | | | |
| | | | | 3/4″ | 3/8″ | #4 | #200 |
| 008U0007700-NB-2 | Surface Course | PG 64-28 | 12.4 | 100 | 98 | 79 | 4 |
| | Binder Course | PG 64-28 | 9.9 | 98 | 78 | 60 | 5 |
| | Base Course | PG 64-28 | 9.7 | 99 | 79 | 40 | 3 |
| Project Name | Pavement Layer | Binder Grade | Binder Content | Gradation | | | |
| | | | | 3/4″ | 3/8″ | #4 | #200 |
| 008U0007700-NB-3 | Surface Course | PG 64-28 | 11.6 | 100 | 97 | 77 | 4 |
| | Binder Course | PG 64-28 | 10.2 | 97 | 83 | 64 | 5 |
| | Base Course | PG 64-22 | 9.2 | 98 | 83 | 63 | 3 |
| Project Name | Pavement Layer | Binder Grade | Binder Content | Gradation | | | |
| | | | | 3/4″ | 3/8″ | #4 | #200 |
| 008U0005400-EB | Surface Course | PG 64-28 | 12.3 | 100 | 98 | 73 | 5 |
| | Binder Course | PG 64-28 | 10.7 | 97 | 82 | 63 | 4 |
| | Base Course | PG 64-22 | 10.1 | 97 | 83 | 66 | 4 |

| Project Name | Pavement Layer | Binder Grade | Binder Content | Gradation | | | |
|---|---|---|---|---|---|---|---|
| | | | | 3/4″ | 3/8″ | #4 | #200 |
| 011U0006900-NB | Surface Course | PG 64-28 | 12 | 100 | 98 | 70 | 5 |
| | Binder Course | PG 64-28 | 10.9 | 95 | 82 | 57 | 4 |
| | Base Course | PG 64-22 | 11.1 | 97 | 82 | 59 | 3 |
| Project Name | Pavement Layer | Binder Grade | Binder Content | Gradation | | | |
| | | | | 3/4″ | 3/8″ | #4 | #200 |
| 019K0000700-NB-1 | Surface Course | PG 64-28 | 10.3 | 100 | 96 | 74 | 4 |
| | Binder Course | PG 64-28 | 10.9 | 100 | 76 | 53 | 3 |
| | Base Course | PG64-22 | 10.9 | 100 | 79 | 50 | 2 |
| Project Name | Pavement Layer | Binder Grade | Binder Content | Gradation | | | |
| | | | | 3/4″ | 3/8″ | #4 | #200 |
| 019K0000700-NB-2 | Surface Course | PG 64-28 | 12.4 | 100 | 94 | 71 | 3 |
| | Binder Course | PG 64-28 | 11.1 | 99 | 82 | 60 | 2 |
| | Base Course | PG 64-22 | 10.5 | 100 | 78 | 60 | 3 |
| Project Name | Pavement Layer | Binder Grade | Binder Content | Gradation | | | |
| | | | | 3/4″ | 3/8″ | #4 | #200 |
| 019U0016000-EB | Surface Course | PG 64-22 | 10 | 100 | 98 | 63 | 4 |
| | Binder Course | PG 64-22 | 9.2 | 98 | 83 | 63 | 3 |
| | Base Course | PG 64-22 | 9.2 | 98 | 83 | 63 | 3 |
| Project Name | Pavement Layer | Binder Grade | Binder Content | Gradation | | | |
| | | | | 3/4″ | 3/8″ | #4 | #200 |
| 023U0004000-EB | Surface Course | PG 76-28 | 11.5 | 100 | 98 | 60 | 4 |
| | Binder Course | PG 76-28 | 9.5 | 100 | 77 | 65 | 4 |
| | Base Course | PG 64-22 | 9.1 | 100 | 77 | 65 | 4 |

| Project Name | Pavement Layer | Binder Grade | Binder Content | Gradation | | | |
|---|---|---|---|---|---|---|---|
| | | | | 3/4″ | 3/8″ | #4 | #200 |
| 027K0015600-EB | Surface Course | PG 70-28 | 11.9 | 100 | 96 | 71 | 5 |
| | Binder Course | PG 70-28 | 10.3 | 98 | 79 | 68 | 4 |
| | Base Course | PG 64-22 | 10.1 | 98 | 76 | 65 | 3 |
| Project Name | Pavement Layer | Binder Grade | Binder Content | Gradation | | | |
| | | | | 3/4″ | 3/8″ | #4 | #200 |
| 028U0005000-EB | Surface Course | PG 70-28 | 11.8 | 100 | 94 | 70 | 4 |
| | Binder Course | PG 64-22 | 11 | 98 | 83 | 72 | 3 |
| | Base Course | PG 64-22 | 11 | 99 | 82 | 66 | 4 |
| Project Name | Pavement Layer | Binder Grade | Binder Content | Gradation | | | |
| | | | | 3/4″ | 3/8″ | #4 | #200 |
| 031K0001800-WB | Surface Course | PG 70-28 | 11.8 | 100 | 99 | 72 | 5 |
| | Binder Course | PG 70-28 | 9.6 | 98 | 84 | 67 | 2 |
| | Base Course | PG 64-22 | 9.6 | 98 | 83 | 67 | 2 |
| Project Name | Pavement Layer | Binder Grade | Binder Content | Gradation | | | |
| | | | | 3/4″ | 3/8″ | #4 | #200 |
| 033U0028300-NB | Surface Course | PG 64-28 | 11.7 | 100 | 94 | 74 | 4 |
| | Binder Course | PG 64-22 | 10.3 | 98 | 67 | 56 | 2 |
| | Base Course | PG 64-22 | 10.3 | 98 | 67 | 56 | 2 |
| Project Name | Pavement Layer | Binder Grade | Binder Content | Gradation | | | |
| | | | | 3/4″ | 3/8″ | #4 | #200 |
| 052U0007300-NB | Surface Course | PG 64-28 | 10.8 | 100 | 97 | 58 | 3 |
| | Binder Course | PG 64-28 | 9.5 | 100 | 74 | 59 | 3 |
| | Base Course | PG 64-22 | 9.2 | 100 | 73 | 58 | 3 |

| Project Name | Pavement Layer | Binder Grade | Binder Content | Gradation | | | |
|---|---|---|---|---|---|---|---|
| | | | | 3/4″ | 3/8″ | #4 | #200 |
| 065K0002700-NB | Surface Course | PG 58-28 | 11.9 | 100 | 93 | 53 | 5 |
| | Binder Course | PG 58-28 | 9 | 88 | 66 | 50 | 7 |
| | Base Course | PG 58-28 | 9 | 88 | 66 | 50 | 7 |
| Project Name | Pavement Layer | Binder Grade | Binder Content | Gradation | | | |
| | | | | 3/4″ | 3/8″ | #4 | #200 |
| 065U0005600-EB | Surface Course | PG 70-28 | 11.2 | 100 | 94 | 64 | 4 |
| | Binder Course | PG 64-22 | 9.2 | 99 | 84 | 64 | 5 |
| | Base Course | PG 64-22 | 9.6 | 99 | 84 | 64 | 5 |
| Project Name | Pavement Layer | Binder Grade | Binder Content | Gradation | | | |
| | | | | 3/4″ | 3/8″ | #4 | #200 |
| 069U0028300-NB | Surface Course | PG 64-28 | 11 | 100 | 96 | 64 | 6 |
| | Binder Course | PG 64-28 | 9.1 | 100 | 83 | 65 | 6 |
| | Base Course | PG 64-28 | 9.2 | 100 | 84 | 67 | 6 |
| Project Name | Pavement Layer | Binder Grade | Binder Content | Gradation | | | |
| | | | | 3/4″ | 3/8″ | #4 | #200 |
| 082U0018300-NB | Surface Course | PG 64-28 | 12.3 | 100 | 96 | 71 | 4 |
| | Binder Course | PG 64-28 | 10.3 | 97 | 81 | 67 | 5 |
| | Base Course | PG 64-28 | 10.1 | 97 | 80 | 69 | 4 |
| Project Name | Pavement Layer | Binder Grade | Binder Content | Gradation | | | |
| | | | | 3/4″ | 3/8″ | #4 | #200 |
| 095U0005600-EB | Surface Course | PG 70-28 | 13.1 | 100 | 97 | 79 | 5 |
| | Binder Course | PG 64-22 | 10.5 | 99 | 82 | 66 | 5 |
| | Base Course | PG 70-28 | 9.9 | 98 | 81 | 65 | 5 |

| Project Name | Pavement Layer | Binder Grade | Binder Content | Gradation | | | |
|---|---|---|---|---|---|---|---|
| | | | | 3/4″ | 3/8″ | #4 | #200 |
| 022K0000700-NB | Surface Course | PG 64-28 | 11.6 | 100 | 98 | 78 | 3 |
| | Binder Course | PG 64-28 | 9.8 | 100 | 71 | 56 | 5 |
| | Base Course | PG 64-22 | 9.9 | 100 | 80 | 63 | 3 |
| Project Name | Pavement Layer | Binder Grade | Binder Content | Gradation | | | |
| | | | | 3/4″ | 3/8″ | #4 | #200 |
| 025K0009900-NB | Surface Course | PG 64-28 | 12.9 | 100 | 95 | 72 | 2 |
| | Binder Course | PG 64-22 | 10.3 | 98 | 67 | 56 | 2 |
| | Base Course | PG 64-28 | 9.8 | 97 | 69 | 56 | 3 |
| Project Name | Pavement Layer | Binder Grade | Binder Content | Gradation | | | |
| | | | | 3/4″ | 3/8″ | #4 | #200 |
| 003U0007300-NB | Surface Course | PG 64-28 | 10.9 | 100 | 97 | 61 | 4 |
| | Binder Course | PG 64-28 | 9.4 | 100 | 72 | 56 | 4 |
| | Base Course | PG 64-22 | 9.3 | 100 | 73 | 58 | 3 |
| Project Name | Pavement Layer | Binder Grade | Binder Content | Gradation | | | |
| | | | | 3/4″ | 3/8″ | #4 | #200 |
| 022K0000700-NB | Surface Course | PG 64-28 | 11.6 | 100 | 98 | 78 | 3 |
| | Binder Course | PG 64-28 | 9.8 | 100 | 71 | 56 | 5 |
| | Base Course | PG 64-22 | 9.9 | 100 | 80 | 63 | 3 |
| Project Name | Pavement Layer | Binder Grade | Binder Content | Gradation | | | |
| | | | | 3/4″ | 3/8″ | #4 | #200 |
| 088U0005400-WB | Surface Course | PG 70-28 | 10.9 | 100 | 94 | 71 | 4 |
| | Binder Course | PG 70-28 | 9.6 | 98 | 82 | 68 | 4 |
| | Base Course | PG 64-22 | 9.8 | 97 | 81 | 66 | 4 |

| Project Name | Pavement Layer | Binder Grade | Binder Content | Gradation | | | |
|---|---|---|---|---|---|---|---|
| | | | | 3/4″ | 3/8″ | #4 | #200 |
| 091K0002700-NB | Surface Course | PG 64-28 | 13.6 | 100 | 98 | 84 | 6 |
| | Binder Course | PG 64-28 | 9.7 | 98 | 76 | 59 | 5 |
| | Base Course | PG 64-22 | 9.7 | 98 | 73 | 54 | 3 |
| Project Name | Pavement Layer | Binder Grade | Binder Content | Gradation | | | |
| | | | | 3/4″ | 3/8″ | #4 | #200 |
| 098U0028300-NB | Surface Course | PG 64-28 | 11.9 | 100 | 97 | 75 | 4 |
| | Binder Course | PG 64-28 | 10.9 | 95 | 82 | 57 | 4 |
| | Base Course | PG 64-22 | 10.5 | 99 | 80 | 71 | 4 |
| Project Name | Pavement Layer | Binder Grade | Binder Content | Gradation | | | |
| | | | | 3/4″ | 3/8″ | #4 | #200 |
| 103K0003900-NB | Surface Course | PG 64-28 | 10.7 | 100 | 98 | 67 | 5 |
| | Binder Course | PG 64-28 | 8.7 | 99 | 79 | 61 | 4 |
| | Base Course | PG 64-28 | 8.7 | 99 | 79 | 61 | 5 |

# Appendix C - Measured and Predicted Performance Data for Flexible and Rigid Pavements

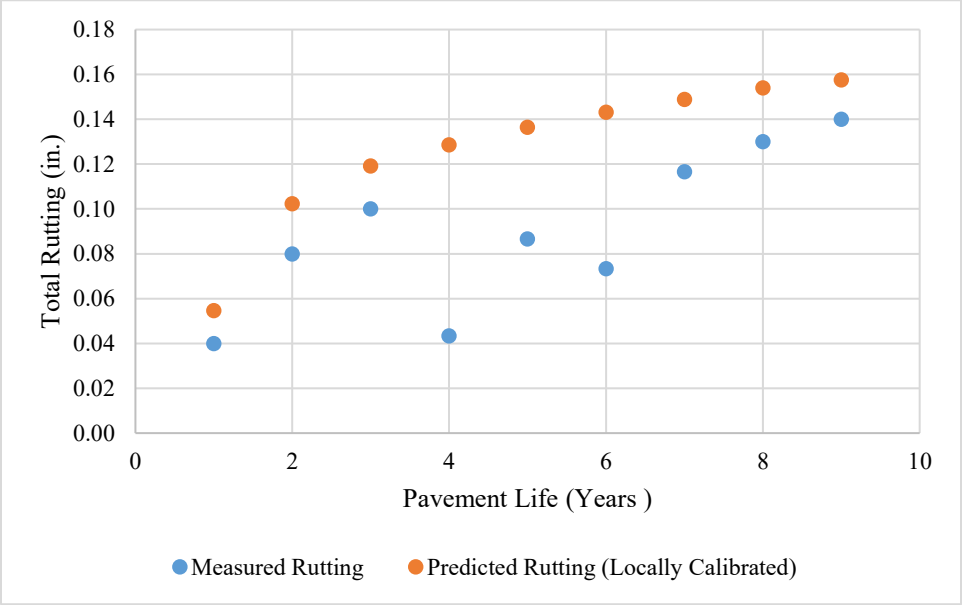


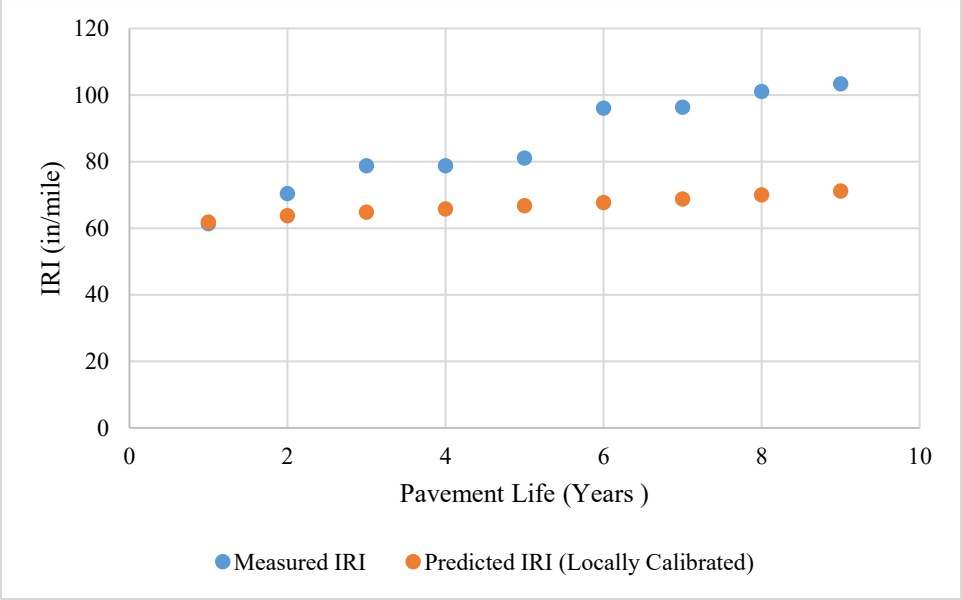


**Figure C-1: Measured and Predicted Performance Data for Project 003U0007300-NB**

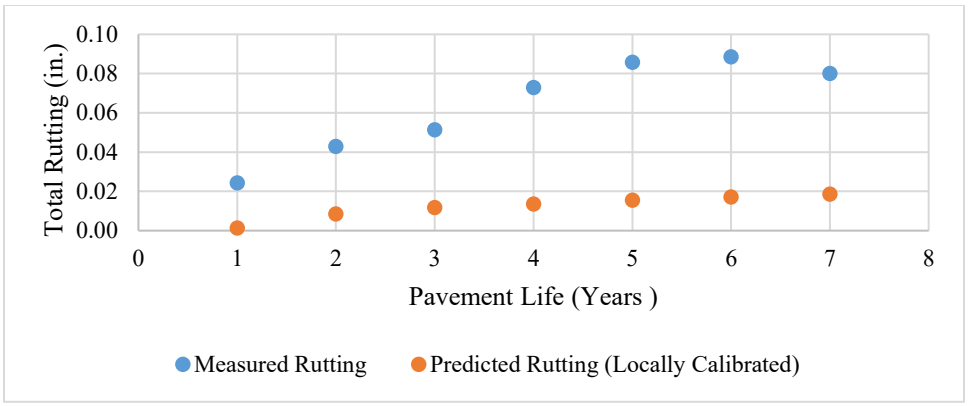



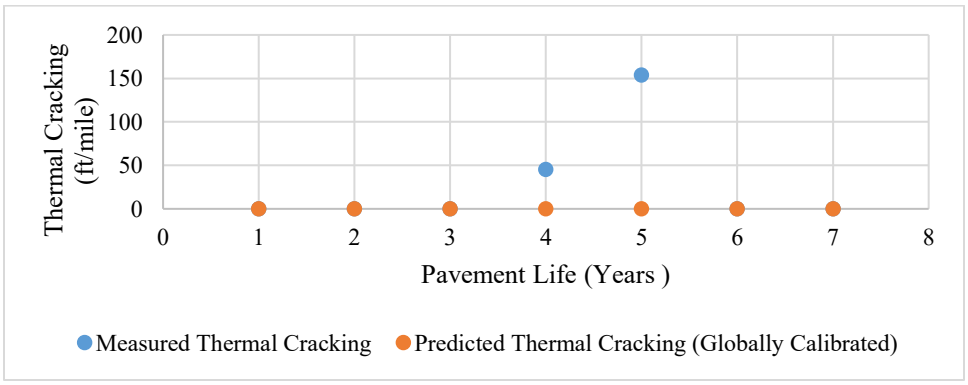


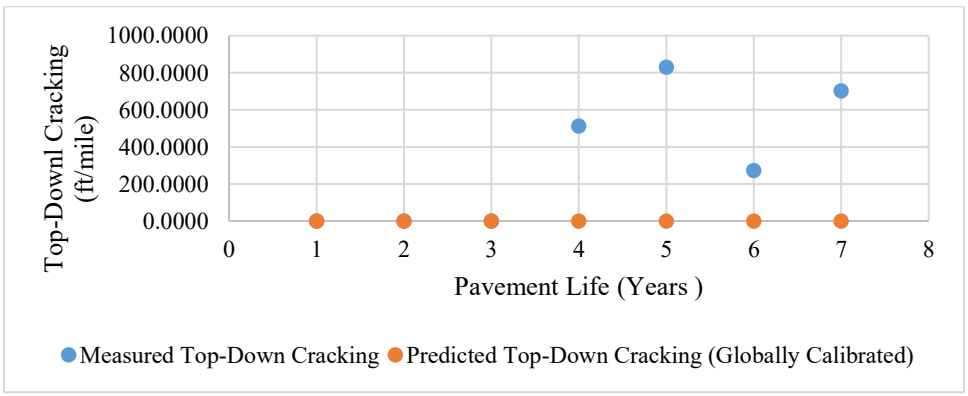


**Figure C-2: Measured and Predicted Performance Data for Project 007U0007500-NB**

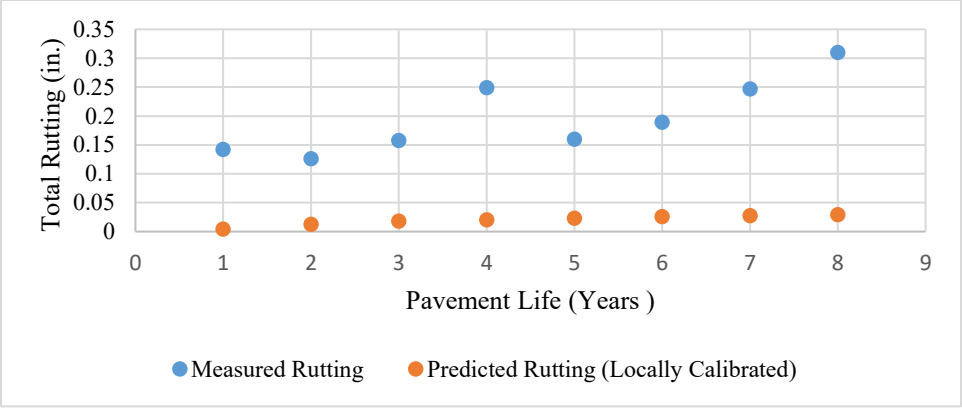


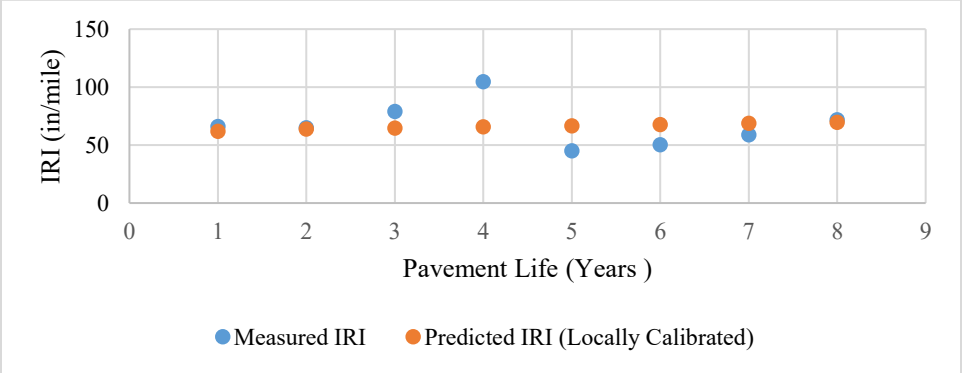


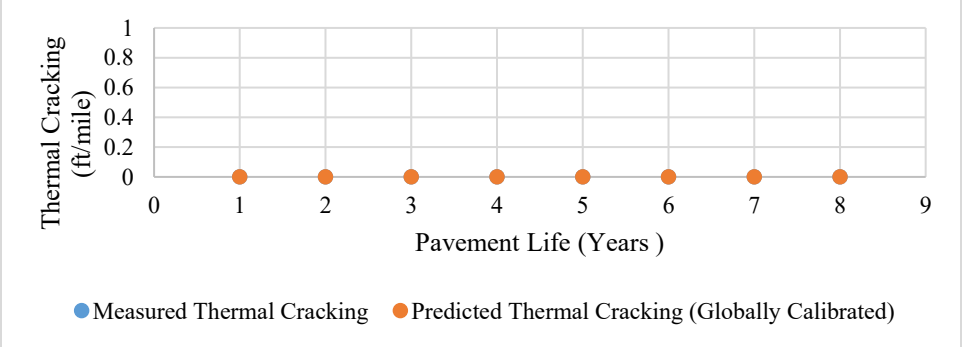


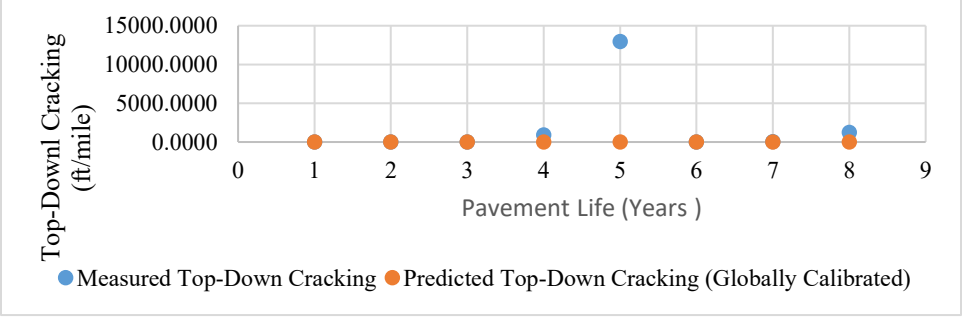


**Figure C-3: Measured and Predicted Performance Data for Project 008U0007700-NB-1**

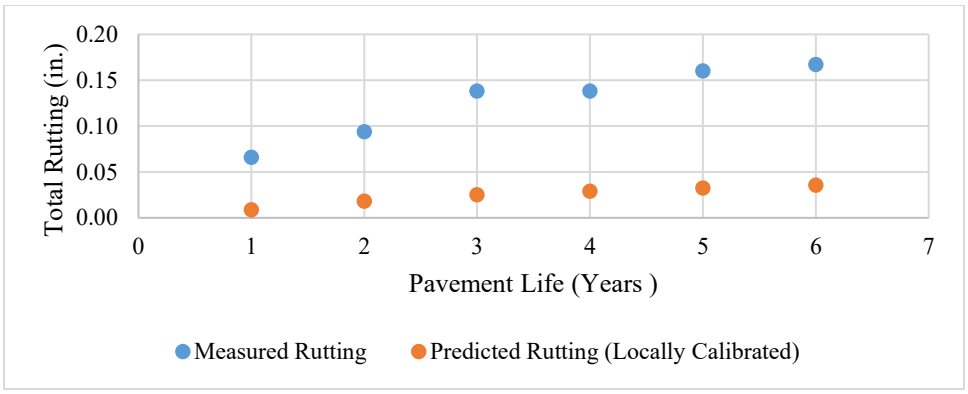


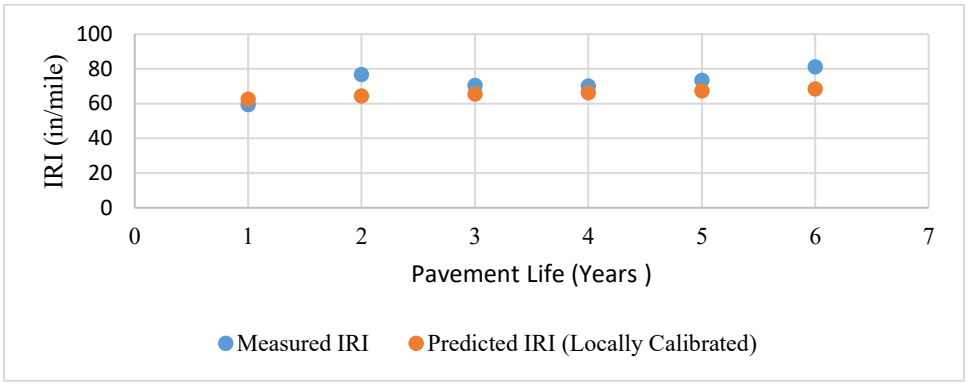


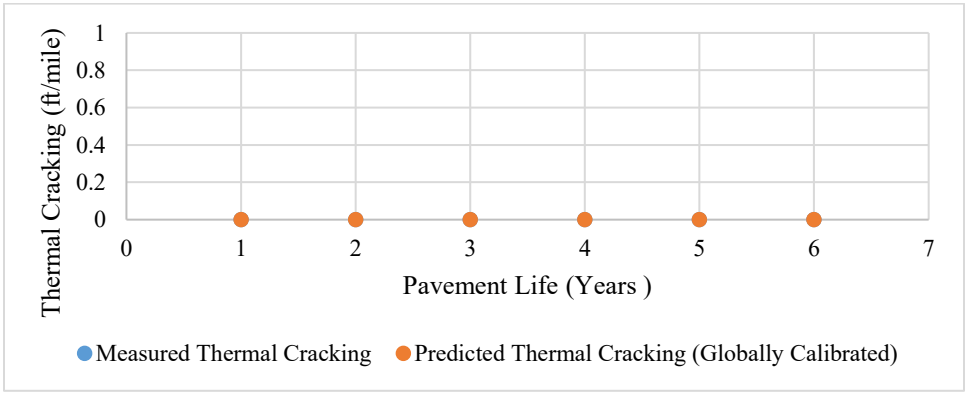


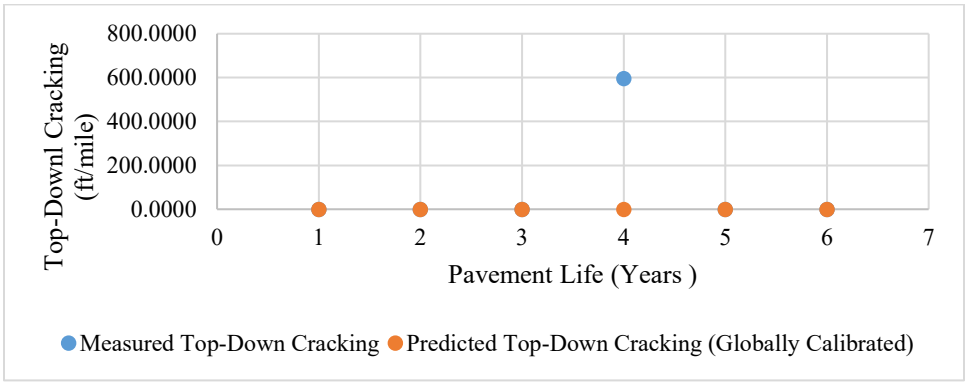


**Figure C-4: Measured and Predicted Performance Data for Project 008U0007700-NB-2**

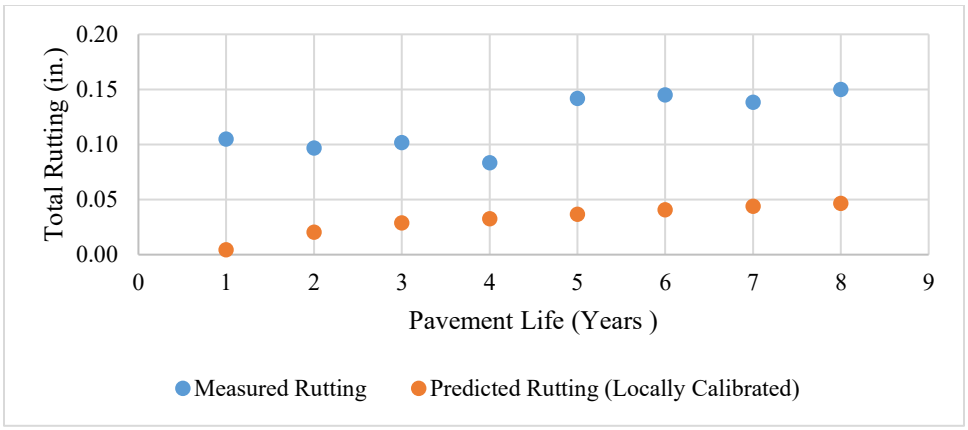


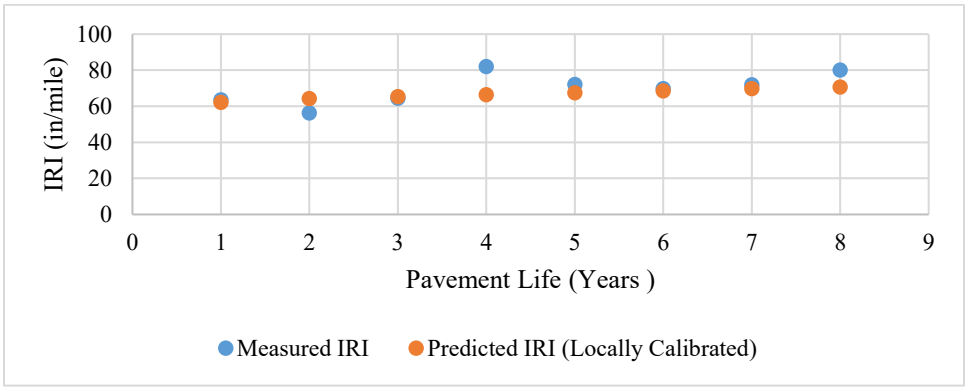


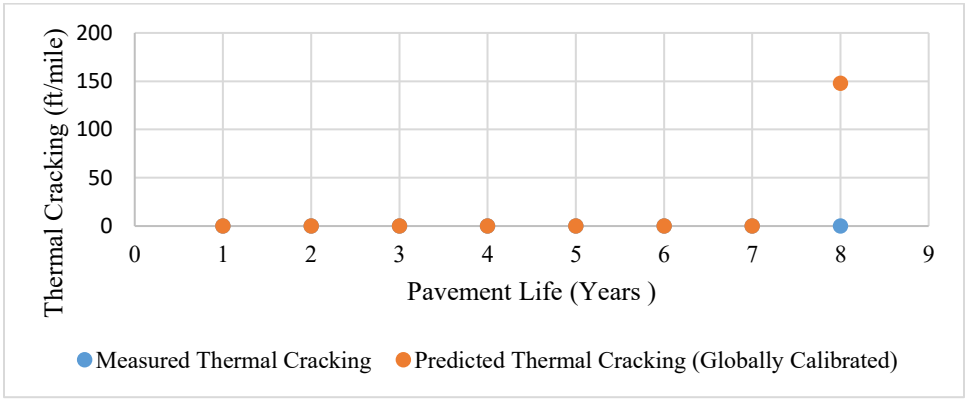


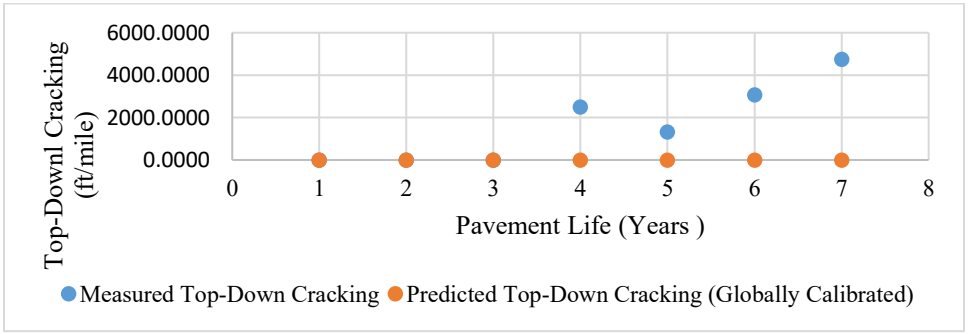


**Figure C-5: Measured and Predicted Performance Data for Project 008U0007700-NB-3**

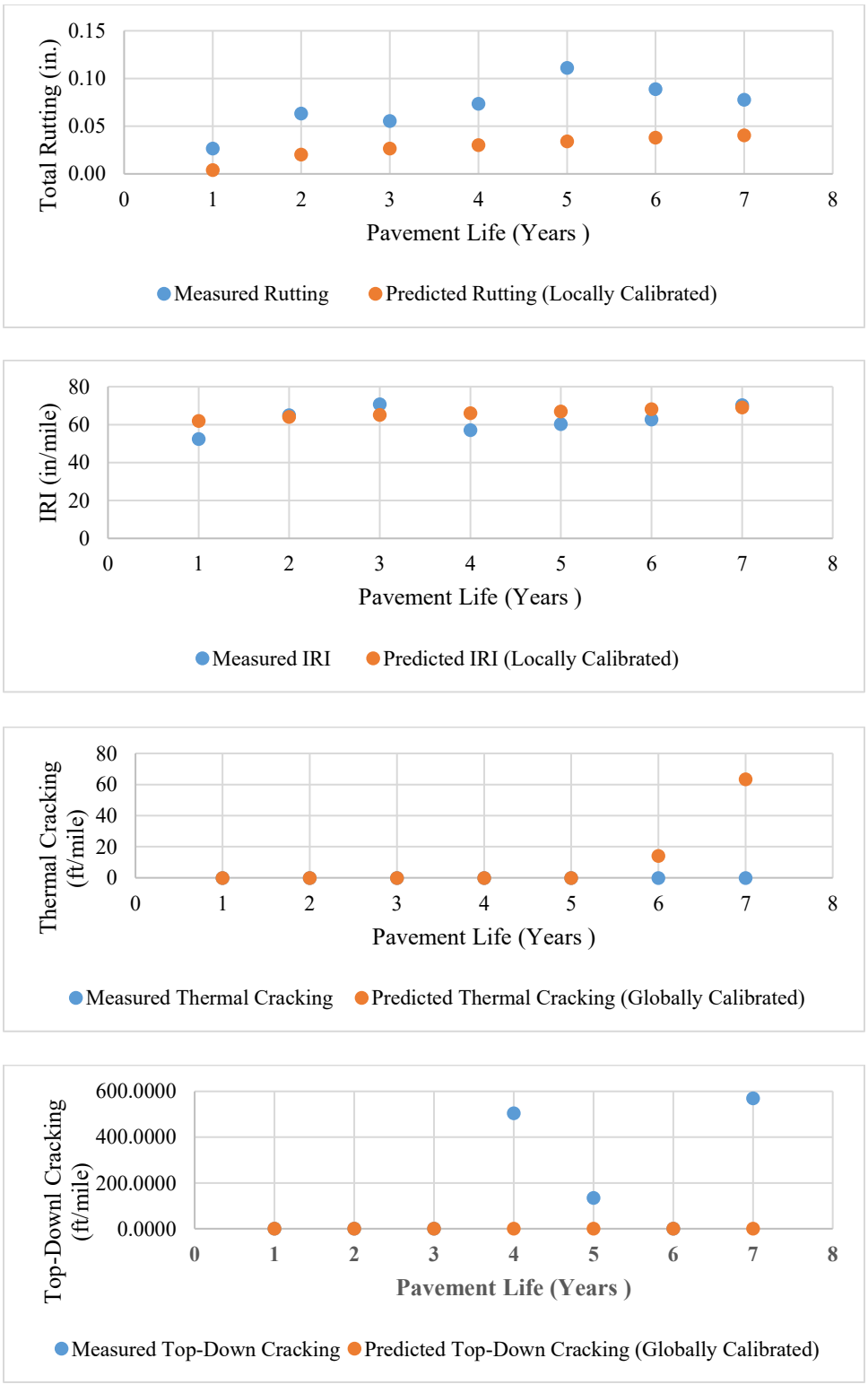


**Figure C-6: Measured and Predicted Performance Data for Project 008U0005400-EB**

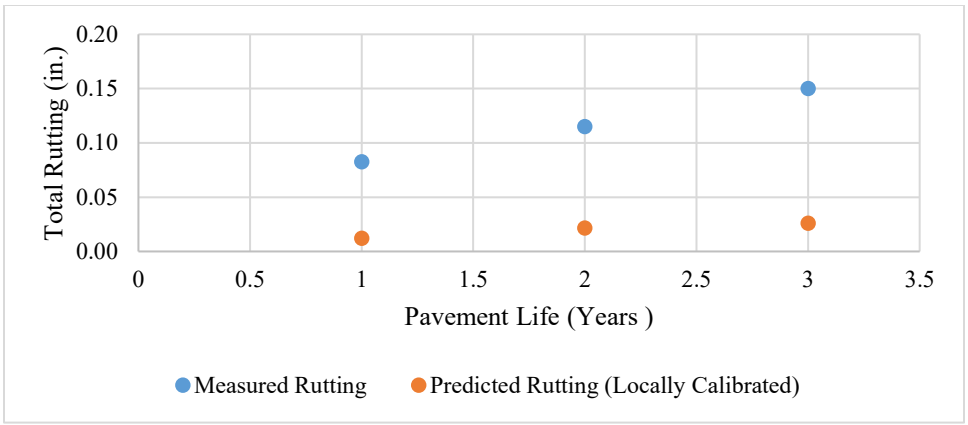


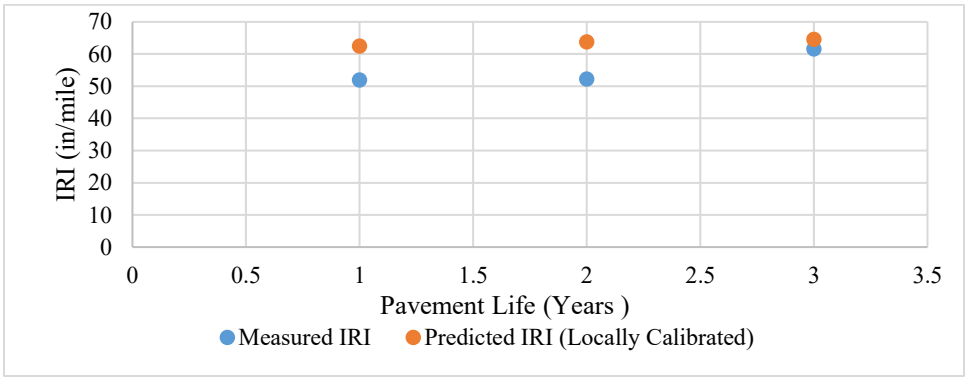


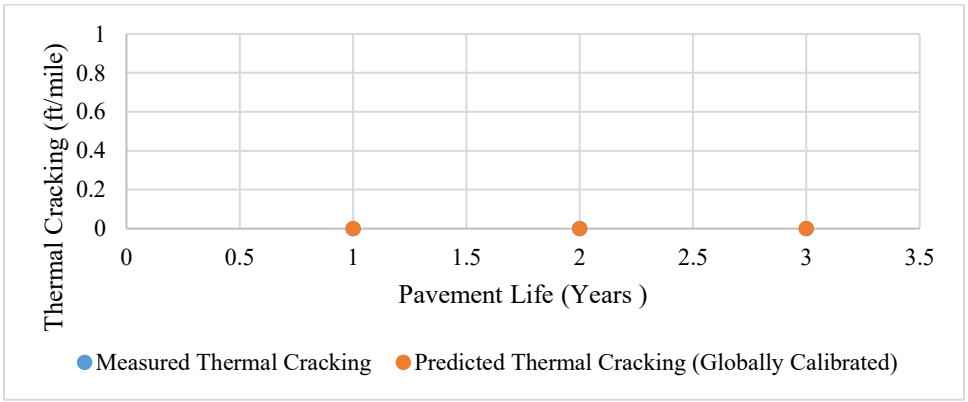


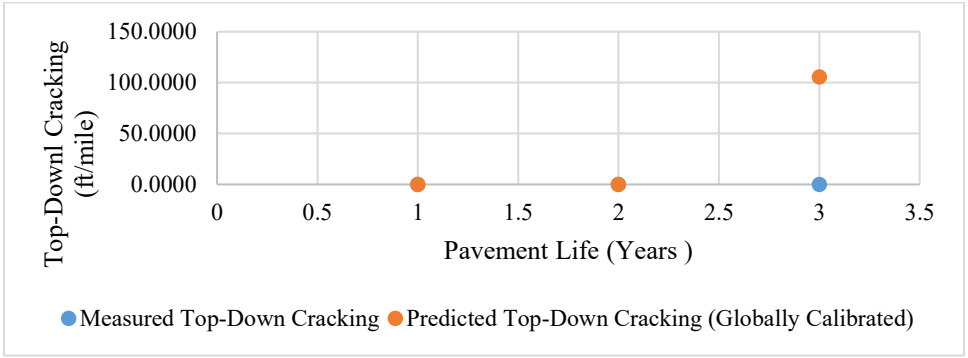


**Figure C-7: Measured and Predicted Performance Data for Project 011U0006900-NB**

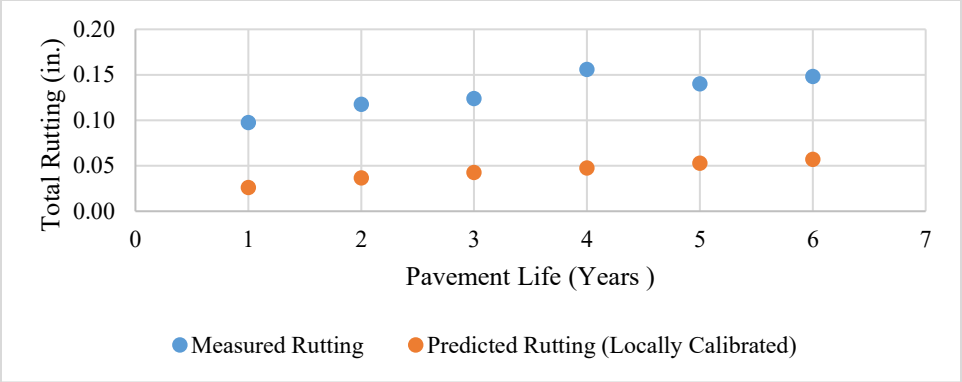


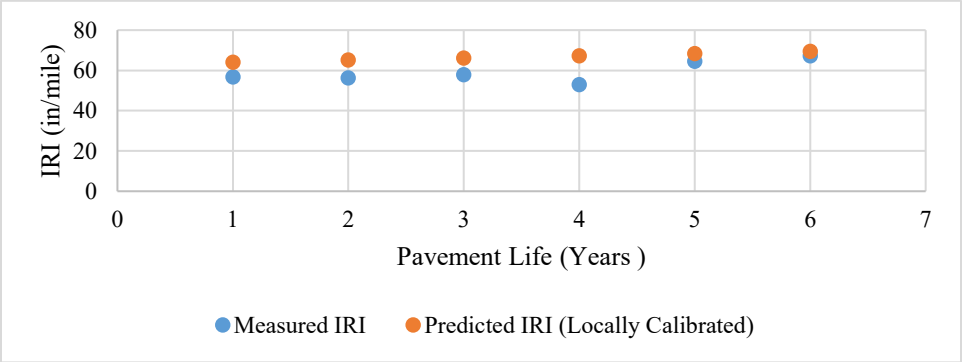


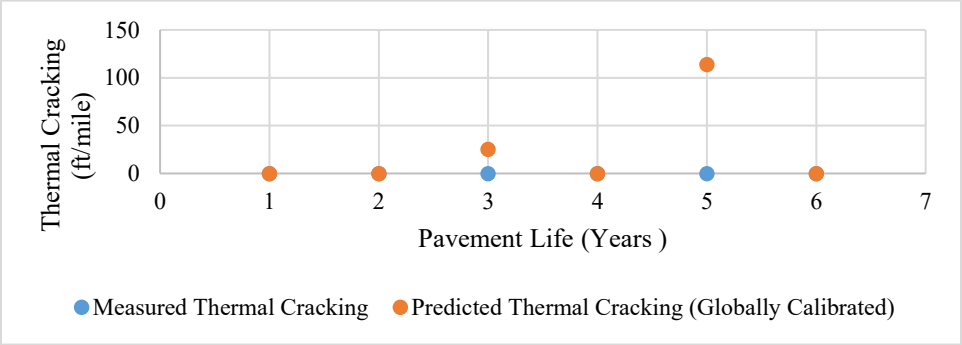


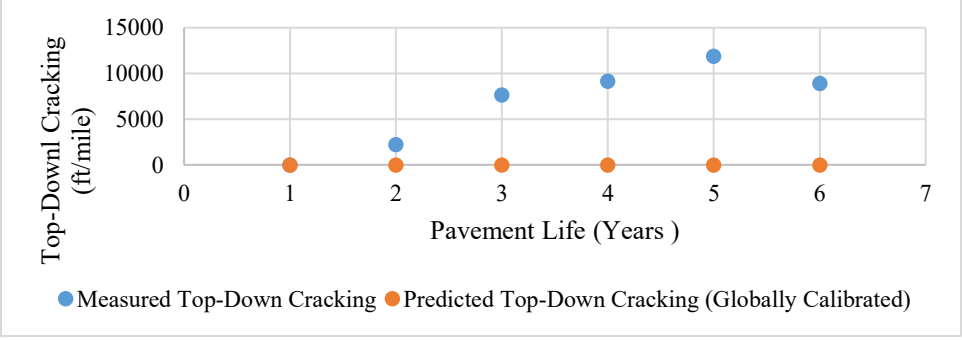


**Figure C-8: Measured and Predicted Performance Data for Project 019K0000700-NB-1**

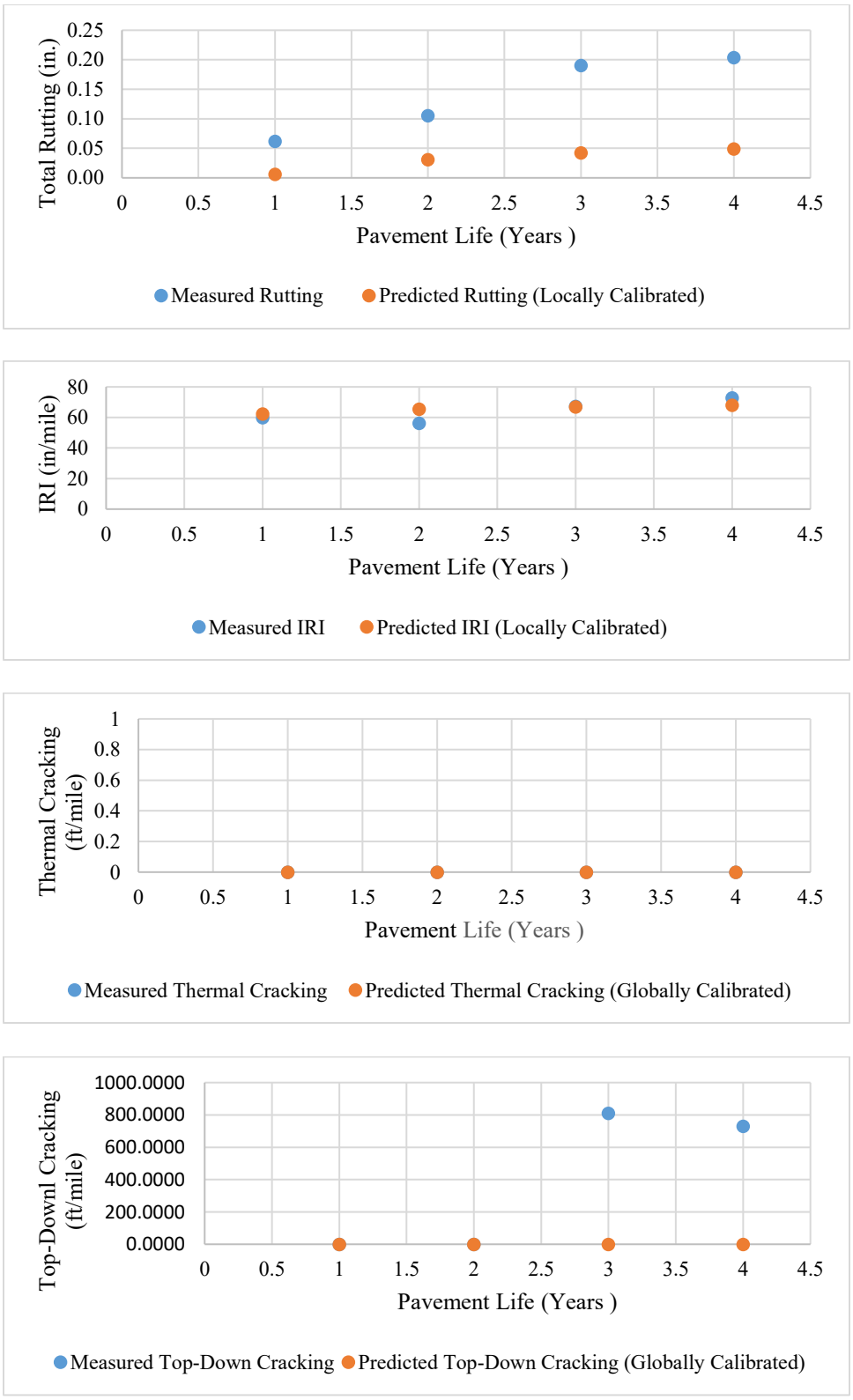


**Figure C-9: Measured and Predicted Performance Data for Project 019K0000700-NB-2**

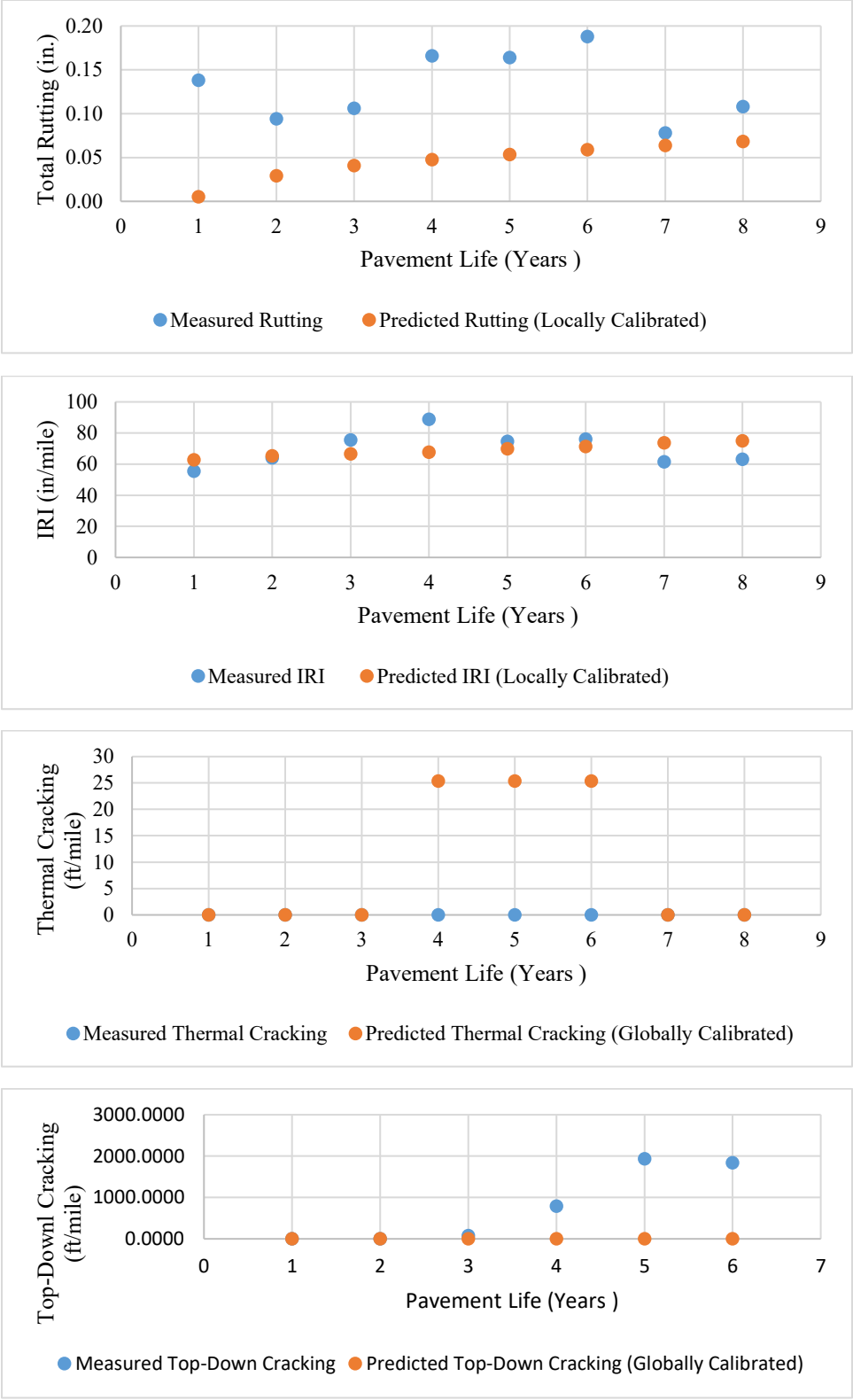


**Figure C-10: Measured and Predicted Performance Data for Project 019U0016000-EB**

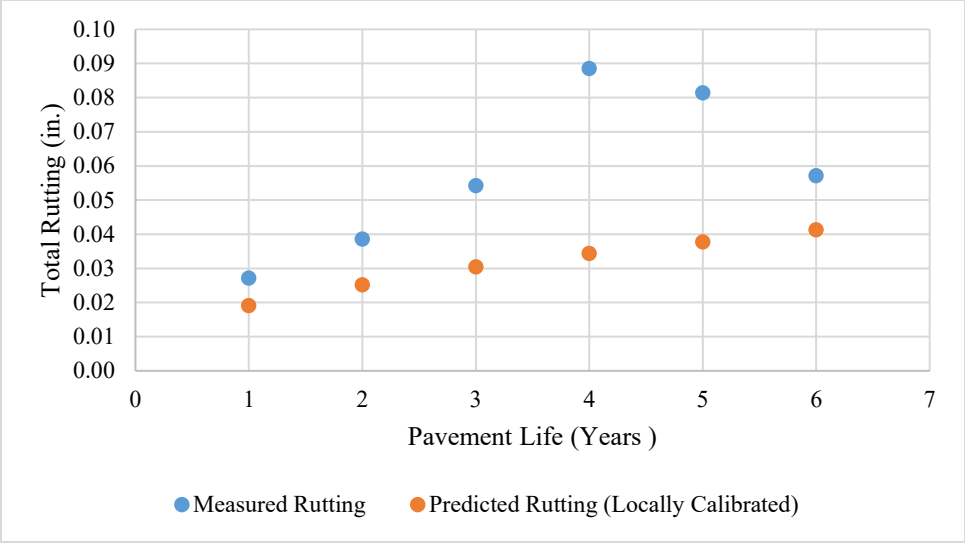


**Figure C-11: Measured and Predicted Performance Data for Project 022K0000700-NB**

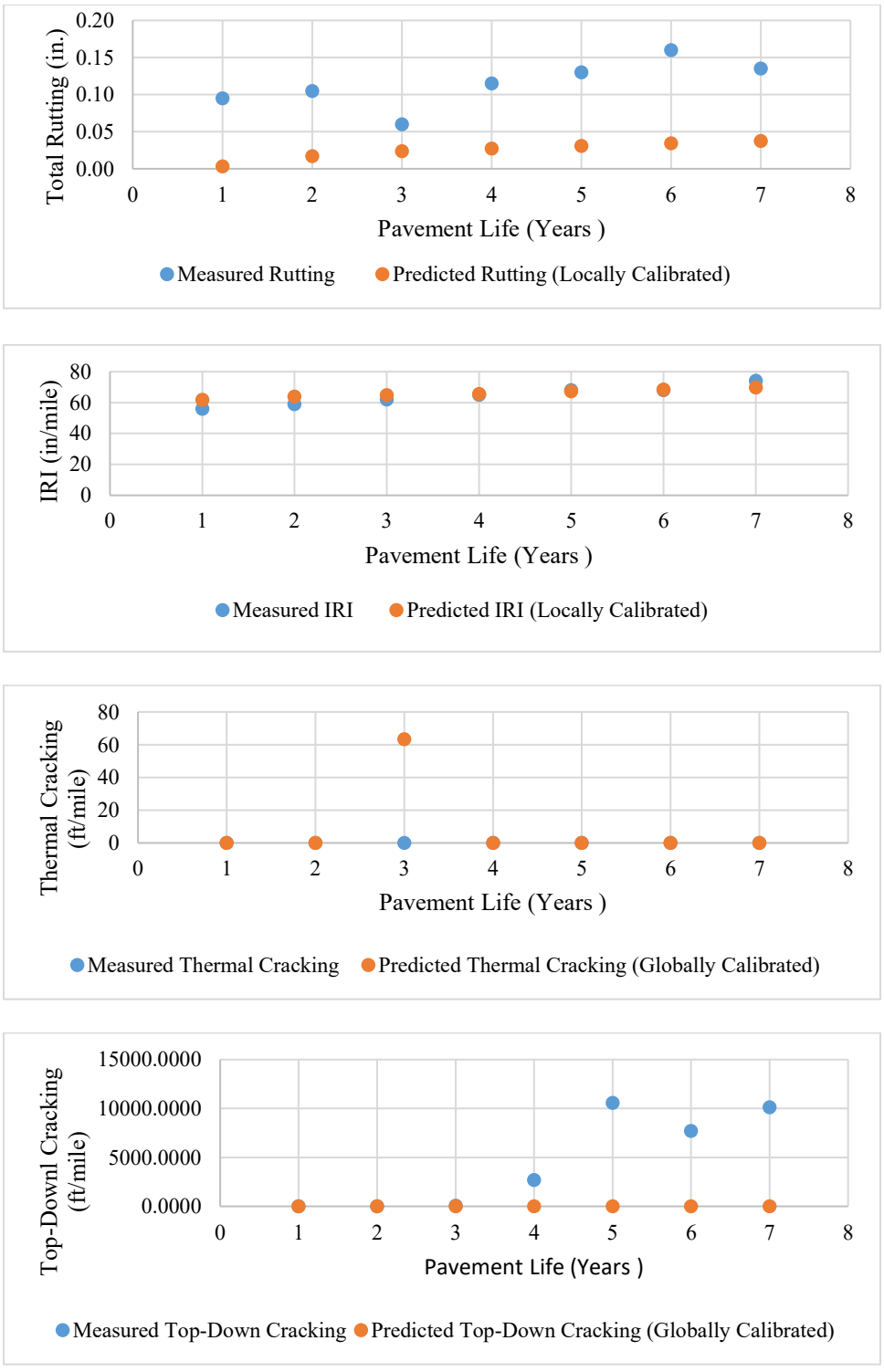


**Figure C-12: Measured and Predicted Performance Data for Project 023U0004000-EB**

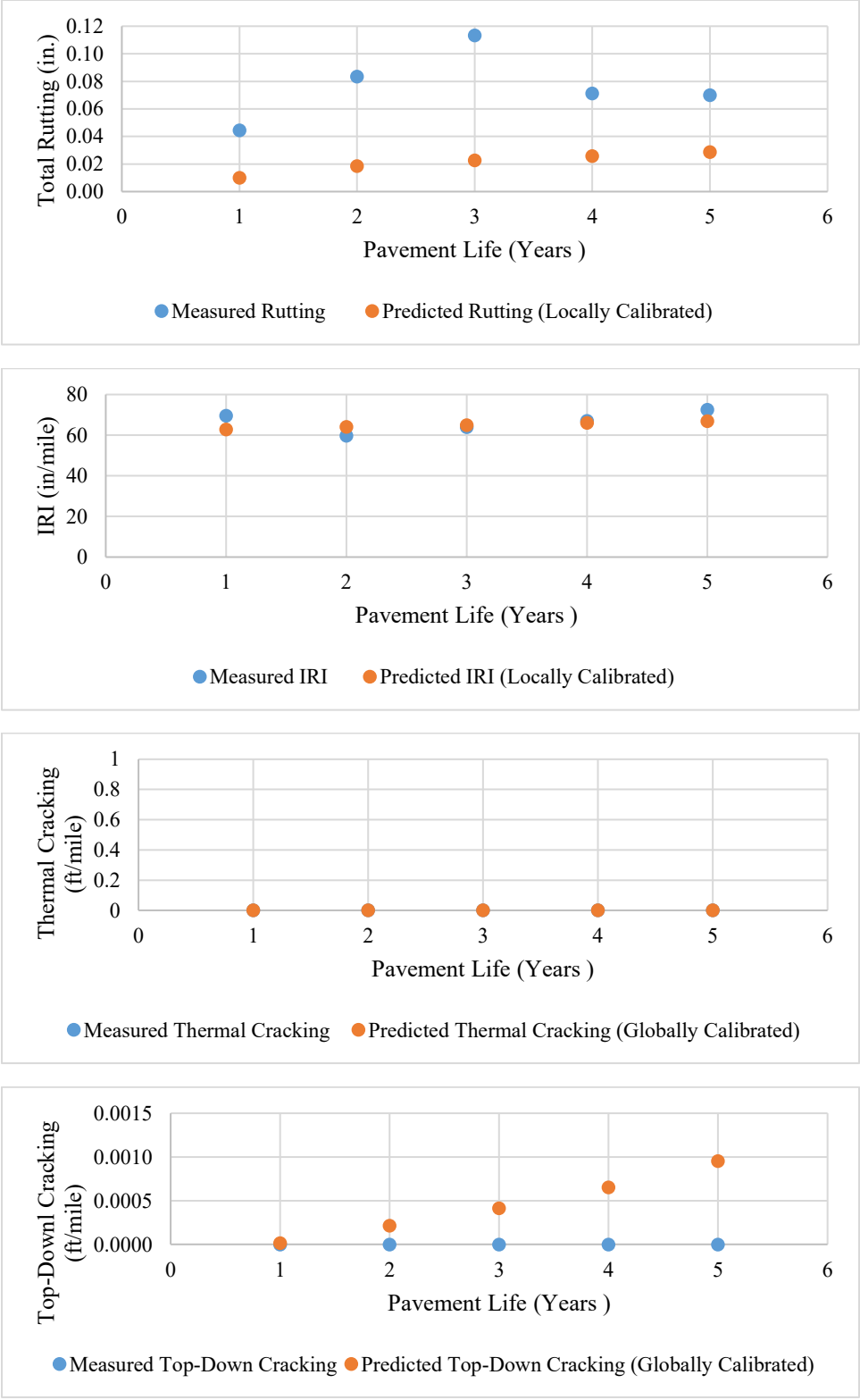


**Figure C-13: Measured and Predicted Performance Data for Project 025K0009900-NB**

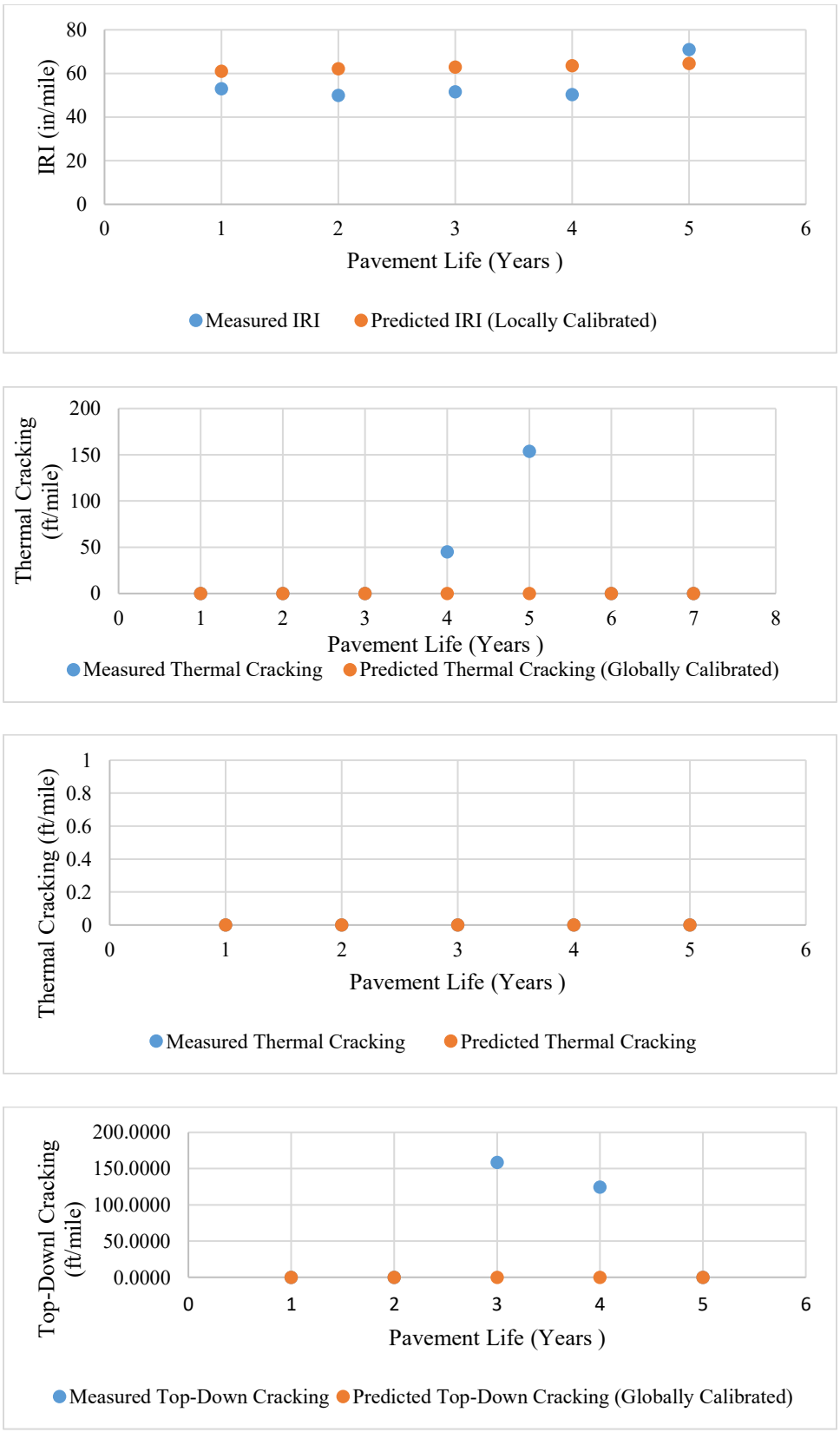


**Figure C-14: Measured and Predicted Performance Data for Project 027K0015600-EB**

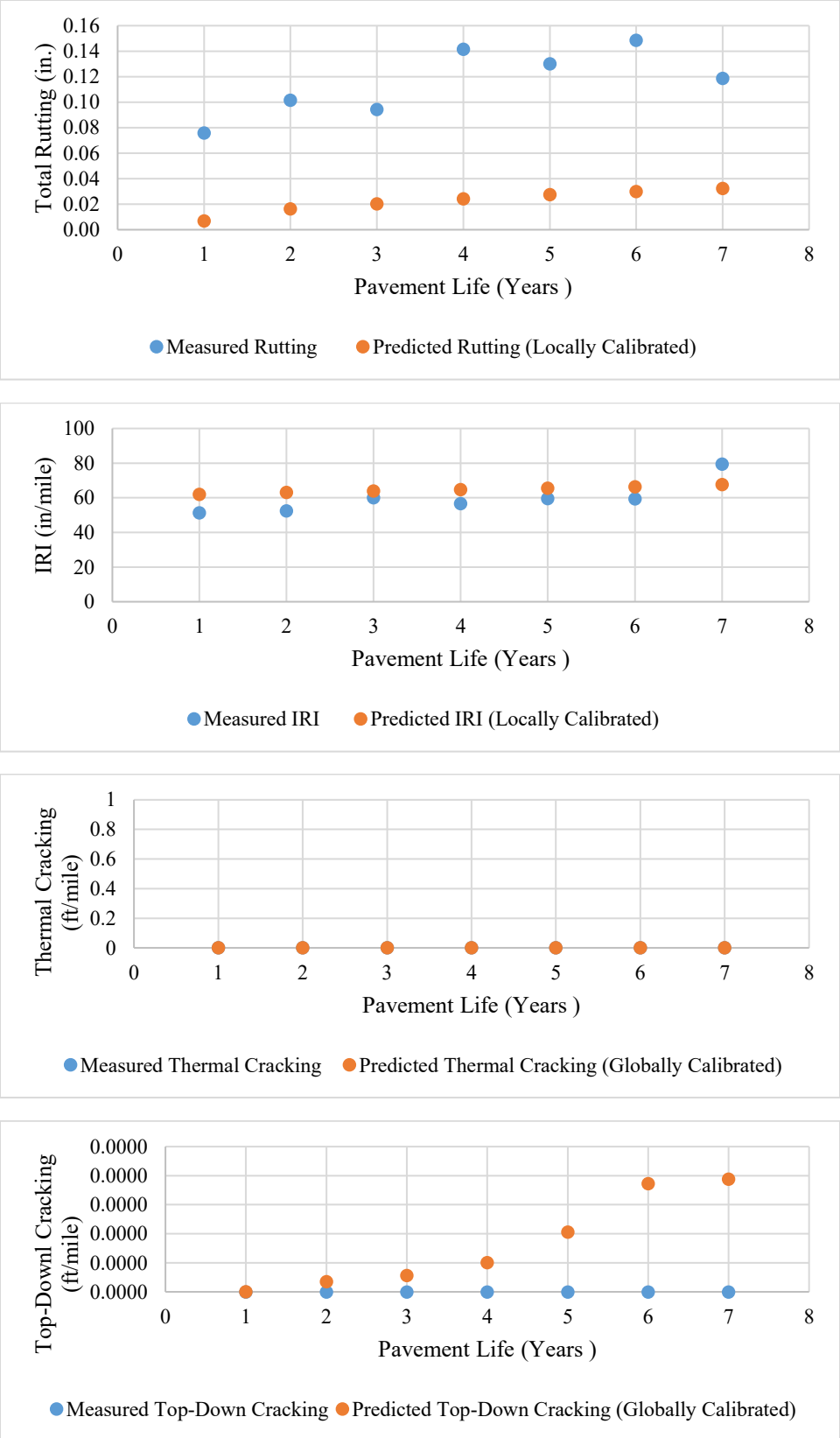


**Figure C-15: Measured and Predicted Performance Data for Project 028U0005000-EB**


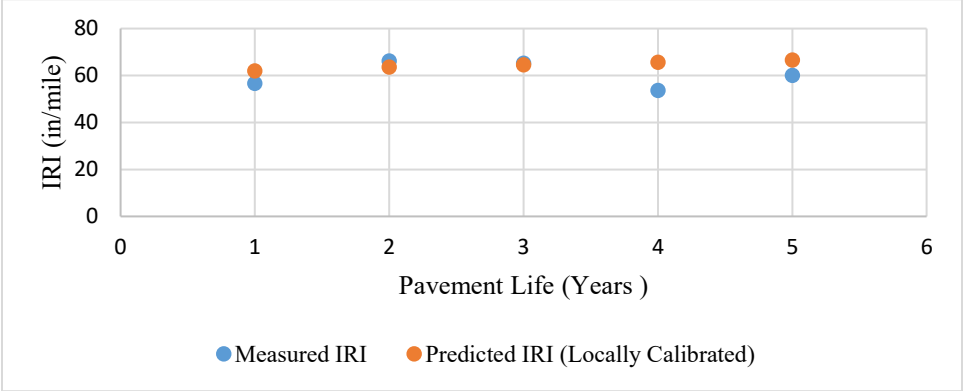


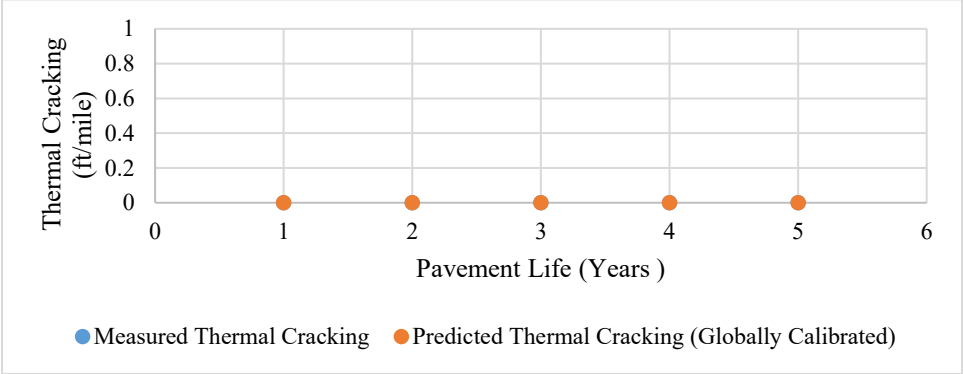


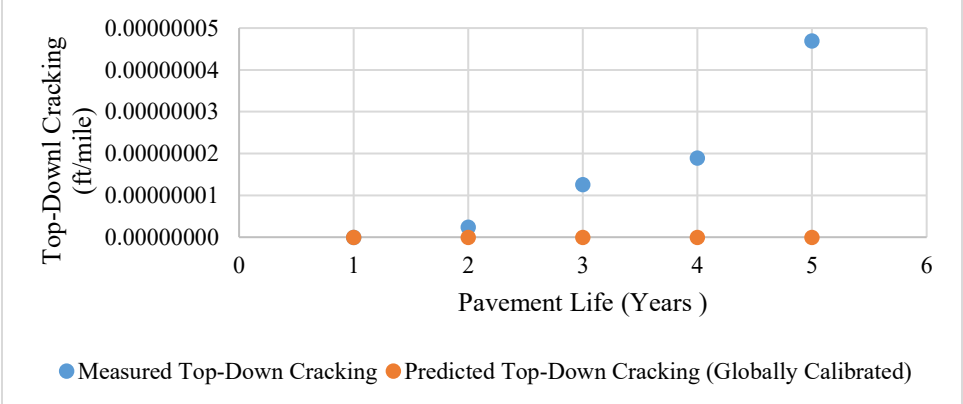


**Figure C-16: Measured and Predicted Performance Data for Project 031K0001800-WB**

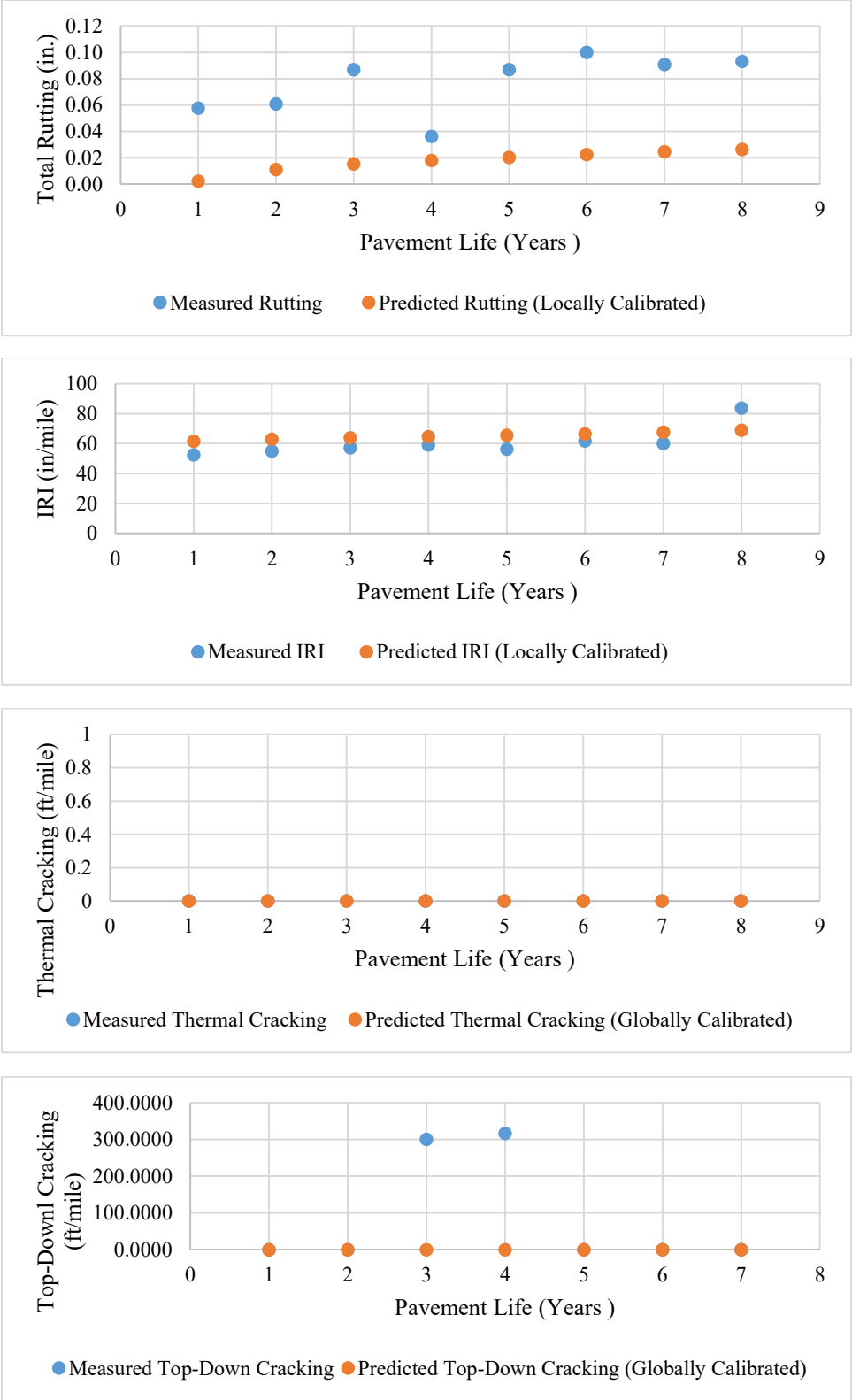


**Figure C-17: Measured and Predicted Performance Data for Project 033U0028300-NB**

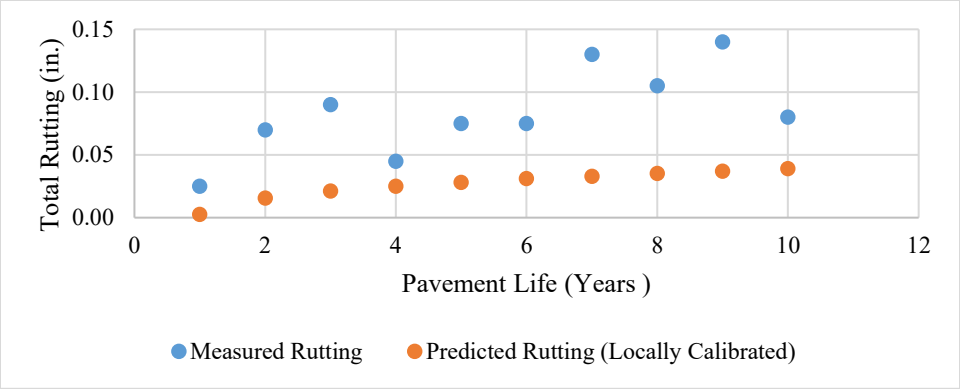


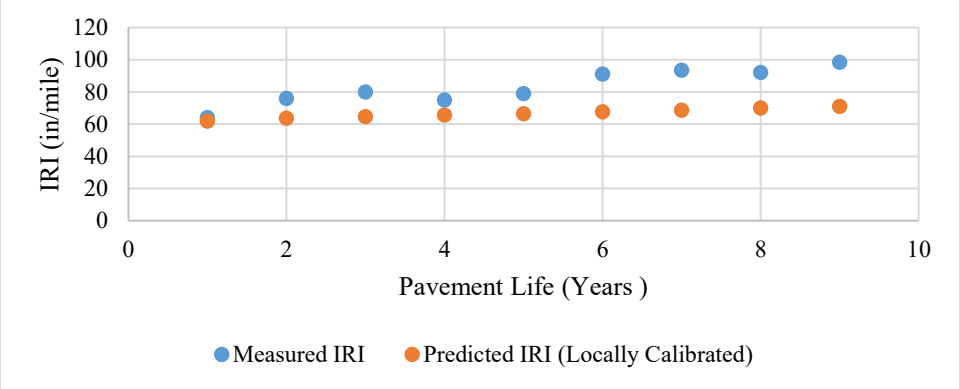


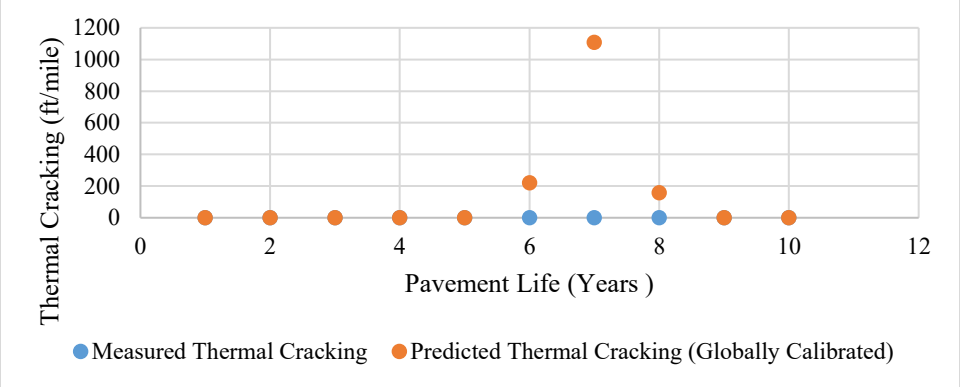


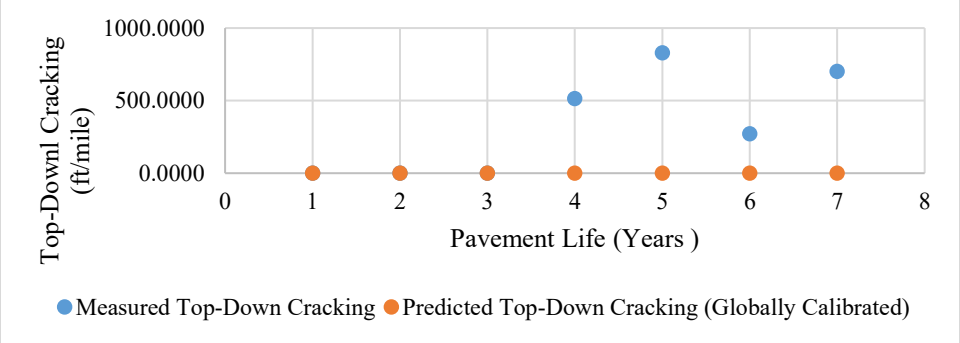


**Figure C-18: Measured and Predicted Performance Data for Project 052U0007300-NB**

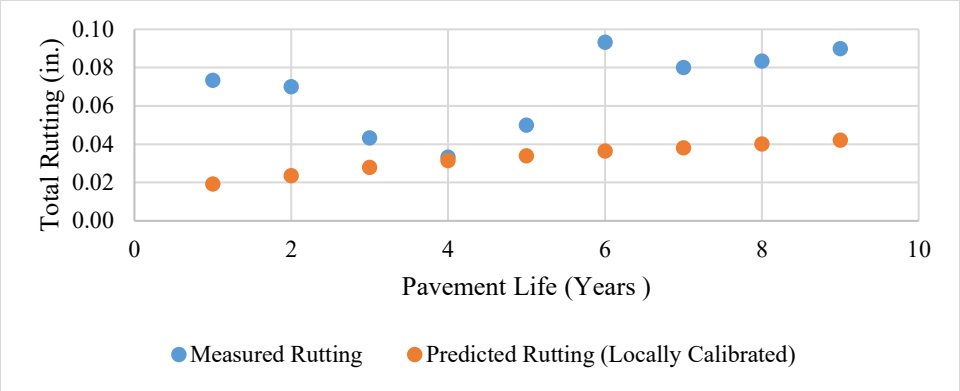


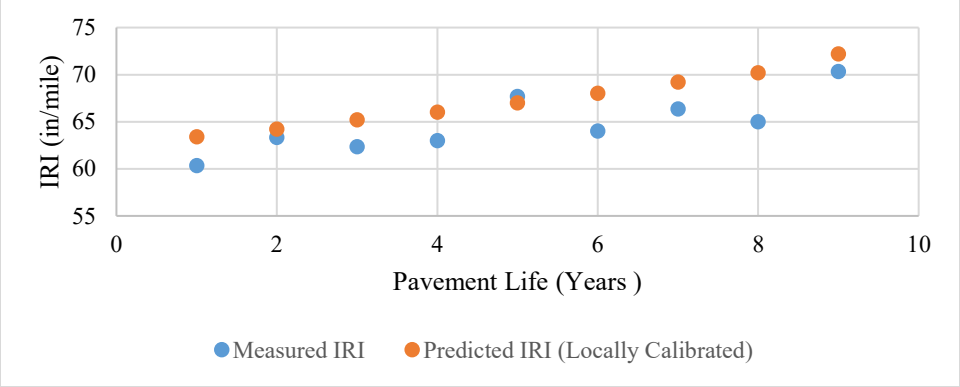


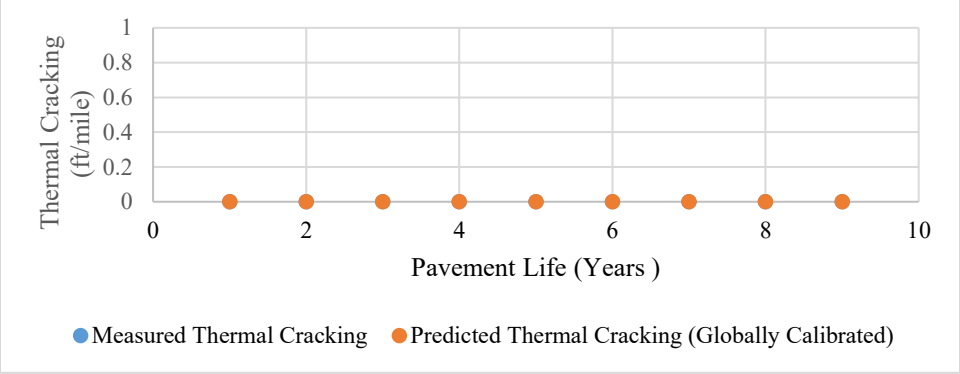


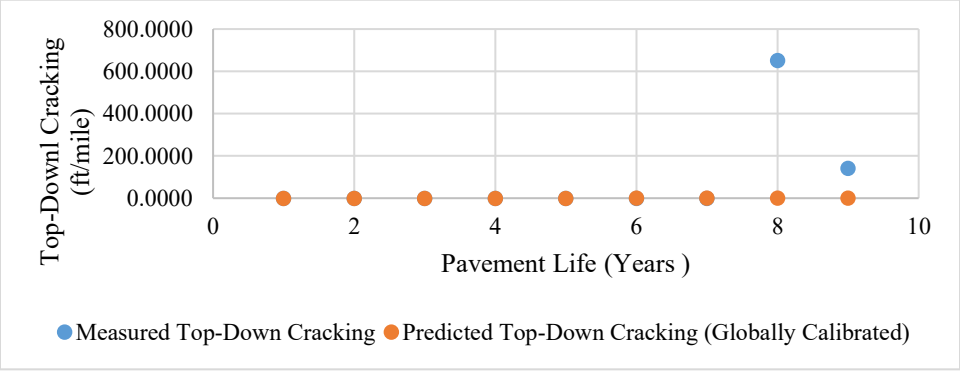


**Figure C-19: Measured and Predicted Performance Data for Project 065K0002700-NB**

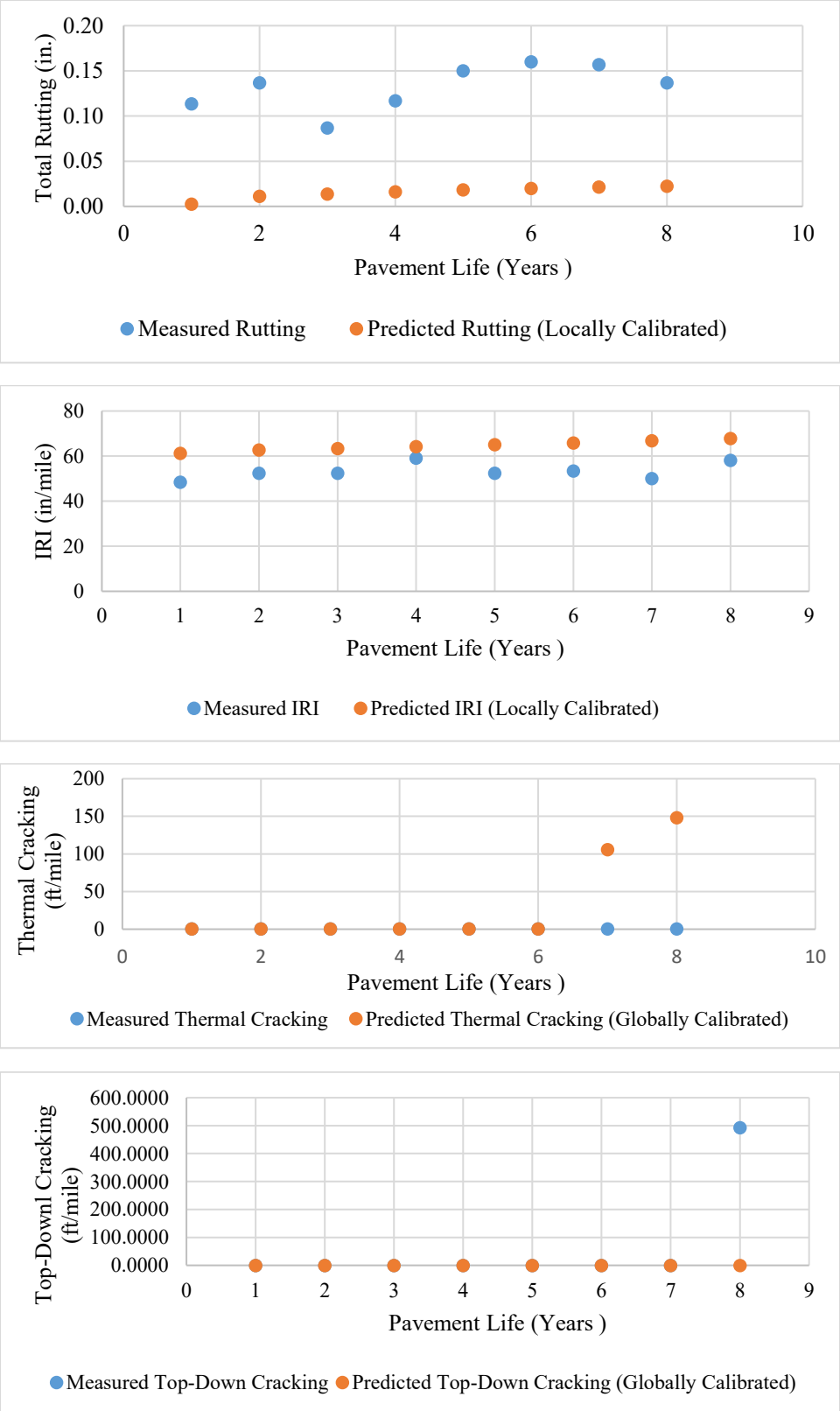


**Figure C-20: Measured and Predicted Performance Data for Project 065U0005600-EB**

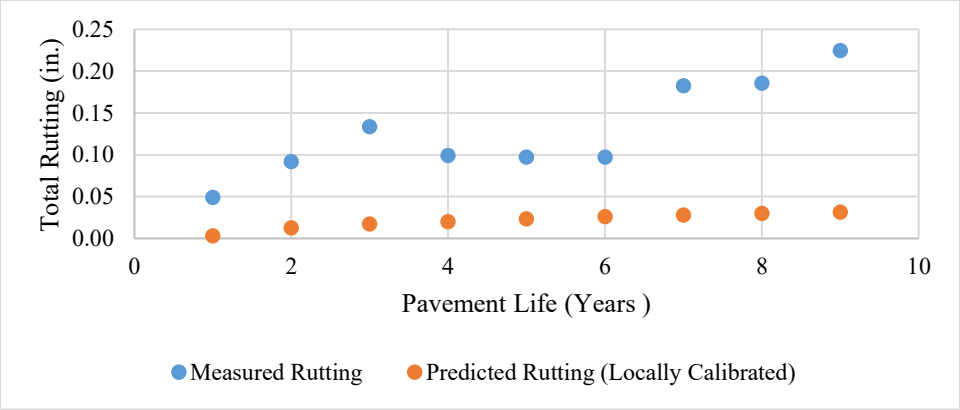


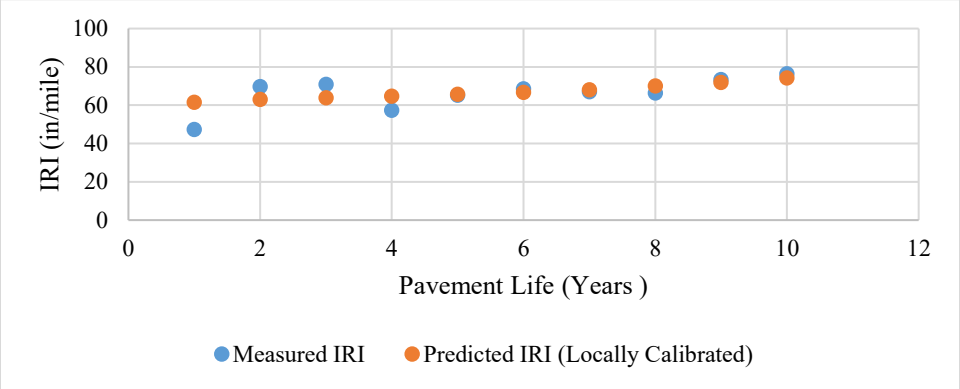


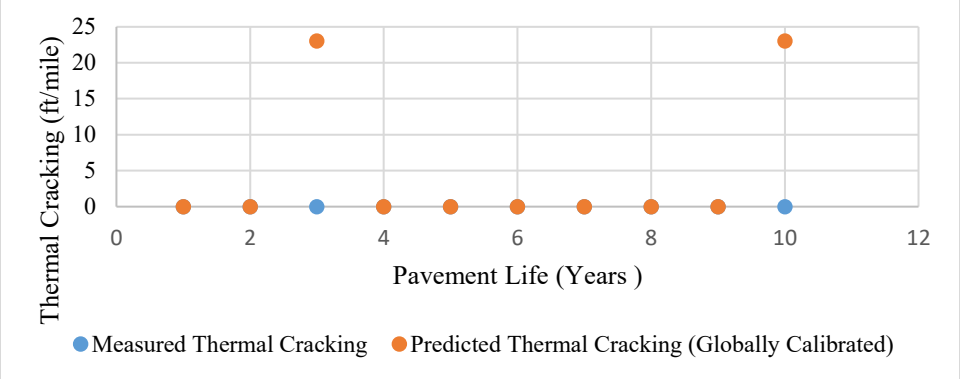


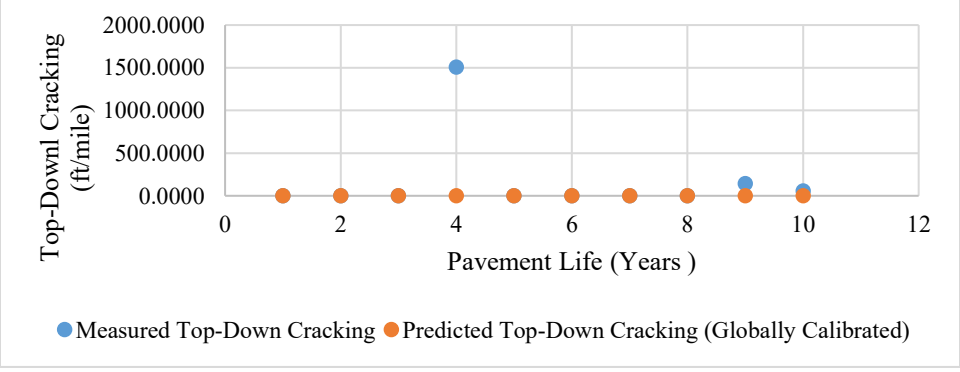


**Figure C-21: Measured and Predicted Performance Data for Project 069U0028300-NB**

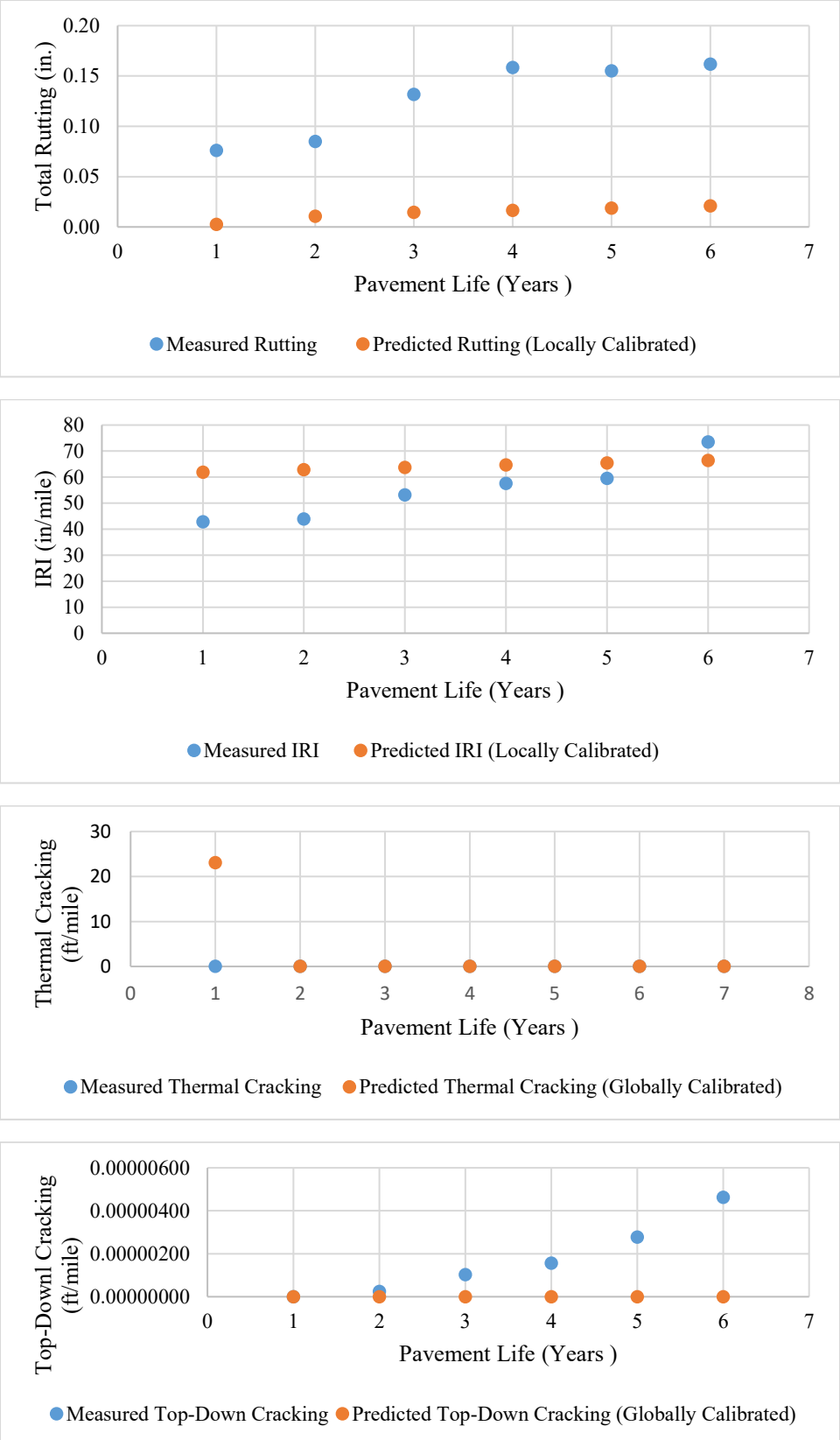


**Figure C-22: Measured and Predicted Performance Data for Project 082U0018300-NB**

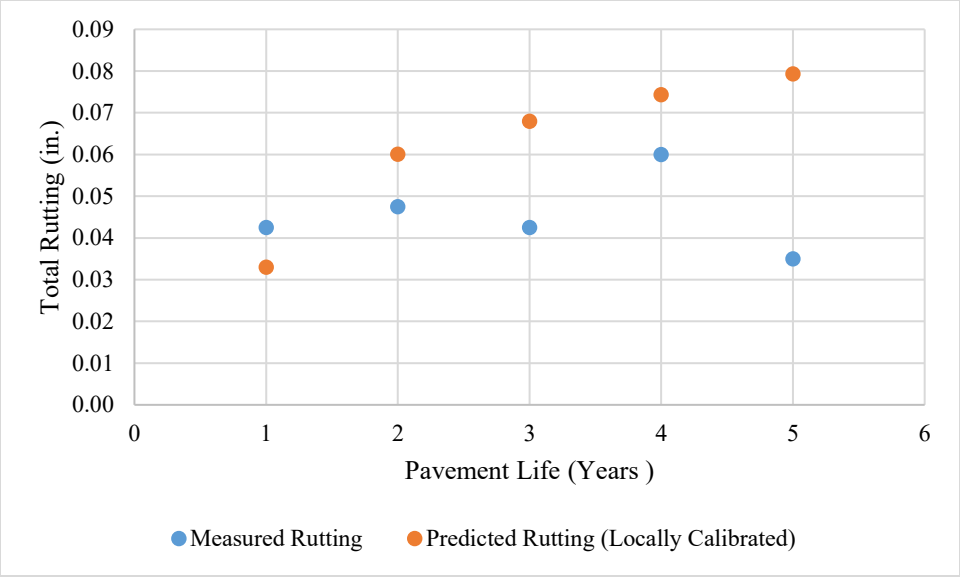


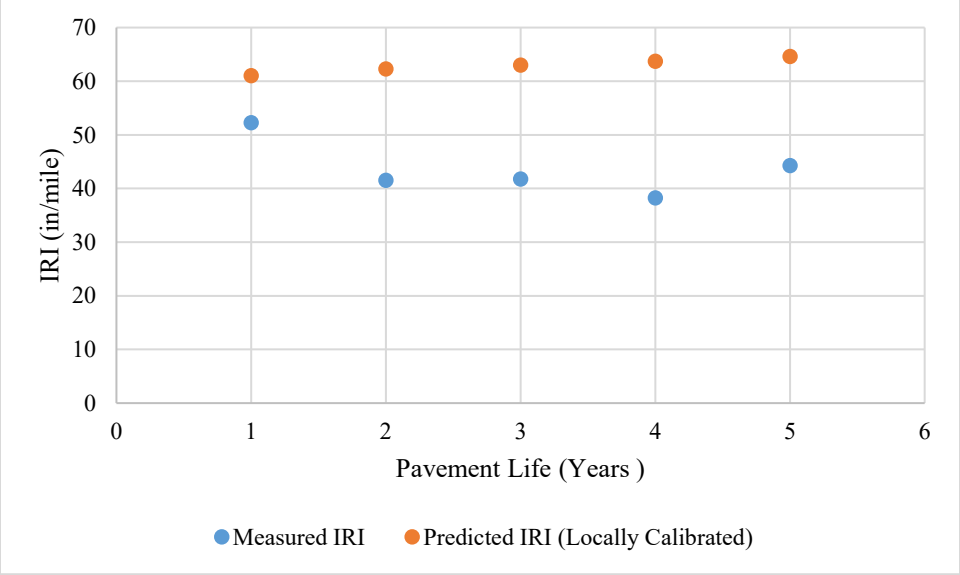


**Figure C-23: Measured and Predicted Performance Data for Project 088U0005400-WB**

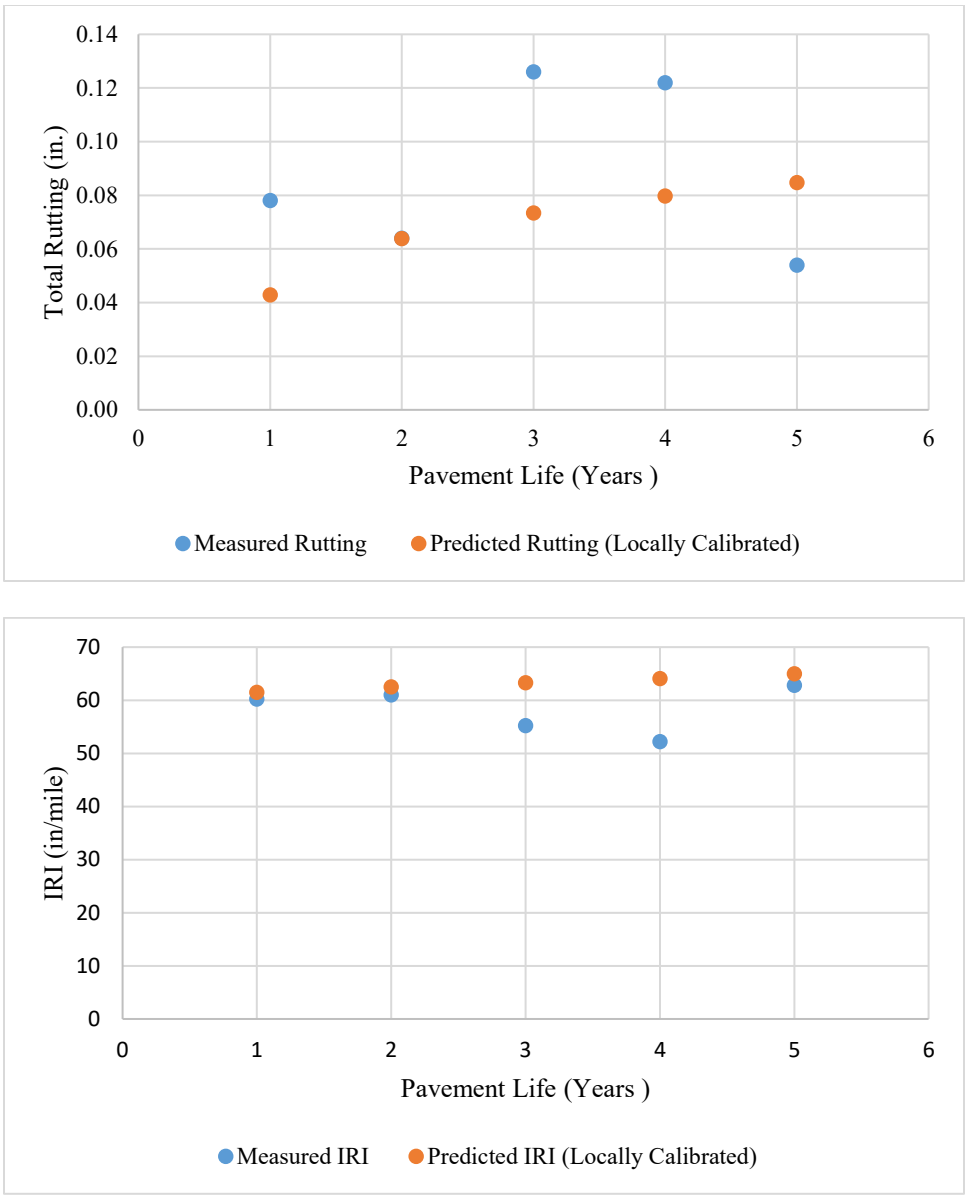


**Figure C-24: Measured and Predicted Performance Data for Project 091K0002700-NB**

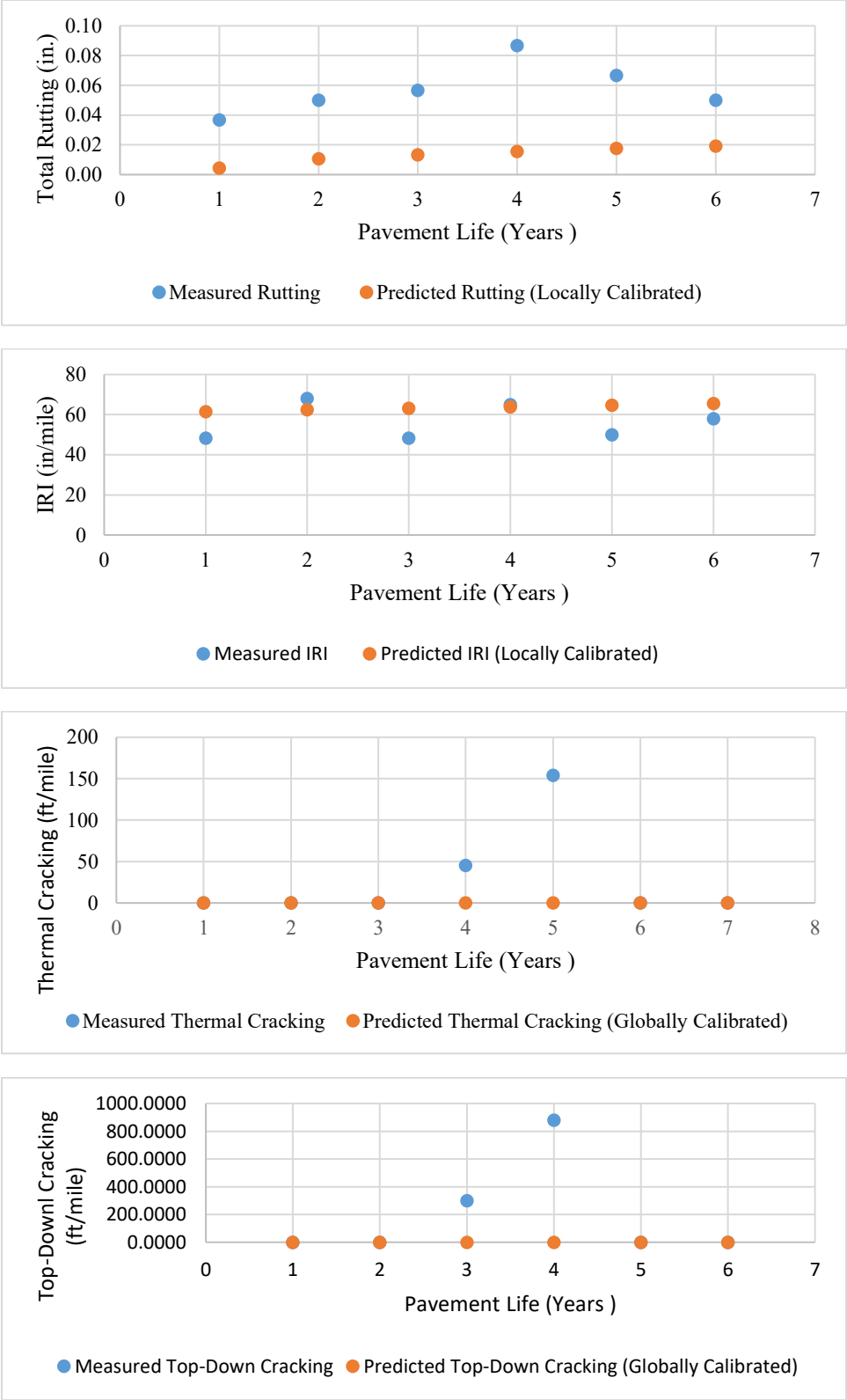


**Figure C-25: Measured and Predicted Performance Data for Project 095U0005600-EB**

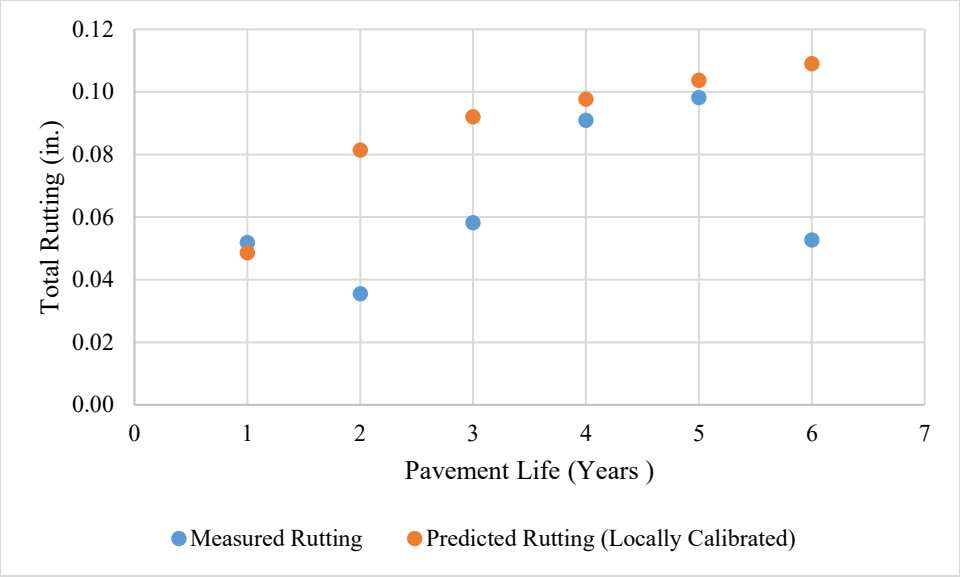


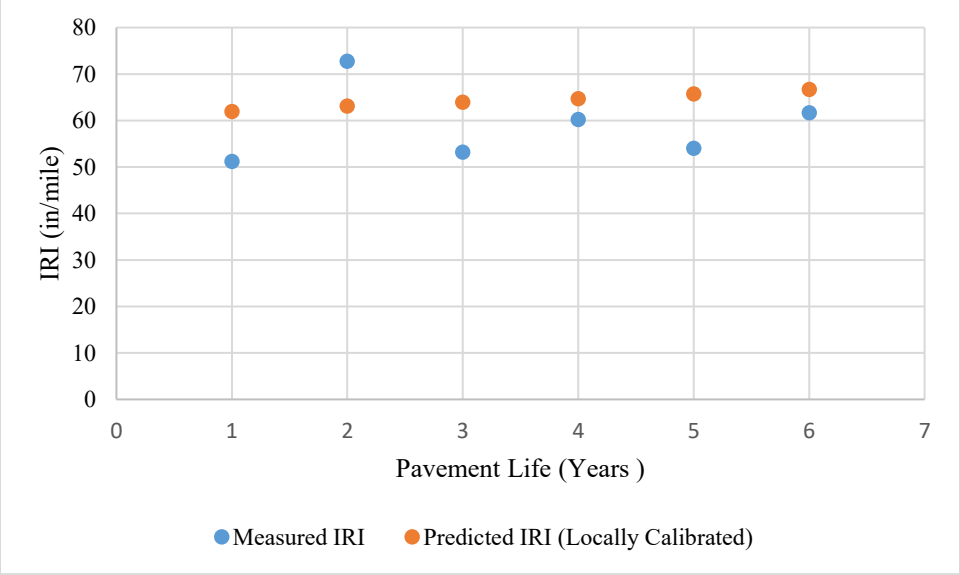


**Figure C-26: Measured and Predicted Performance Data for Project 098U0028300-NB**

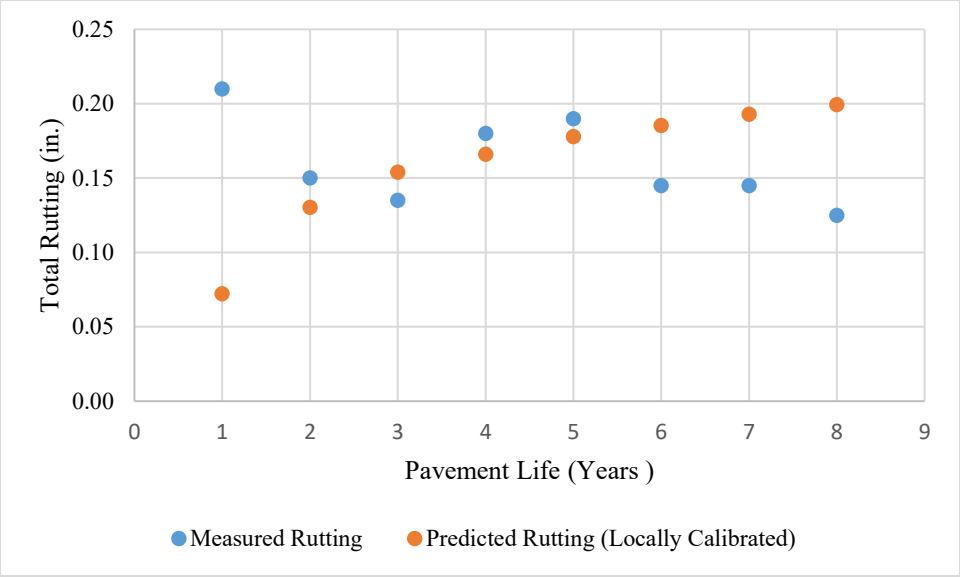


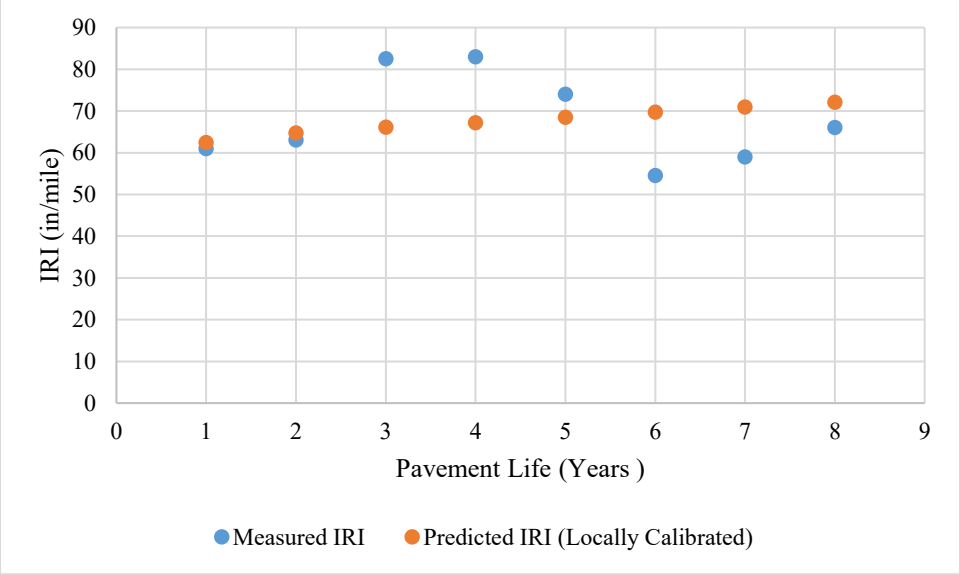


**Figure C-27: Measured and Predicted Performance Data for Project 103K0003900-NB**

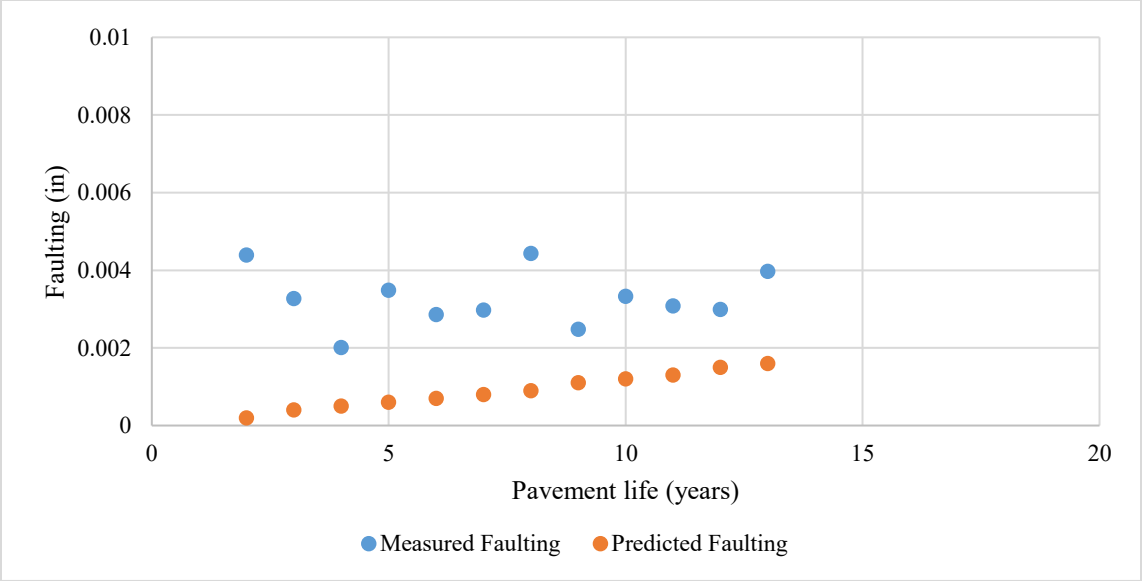


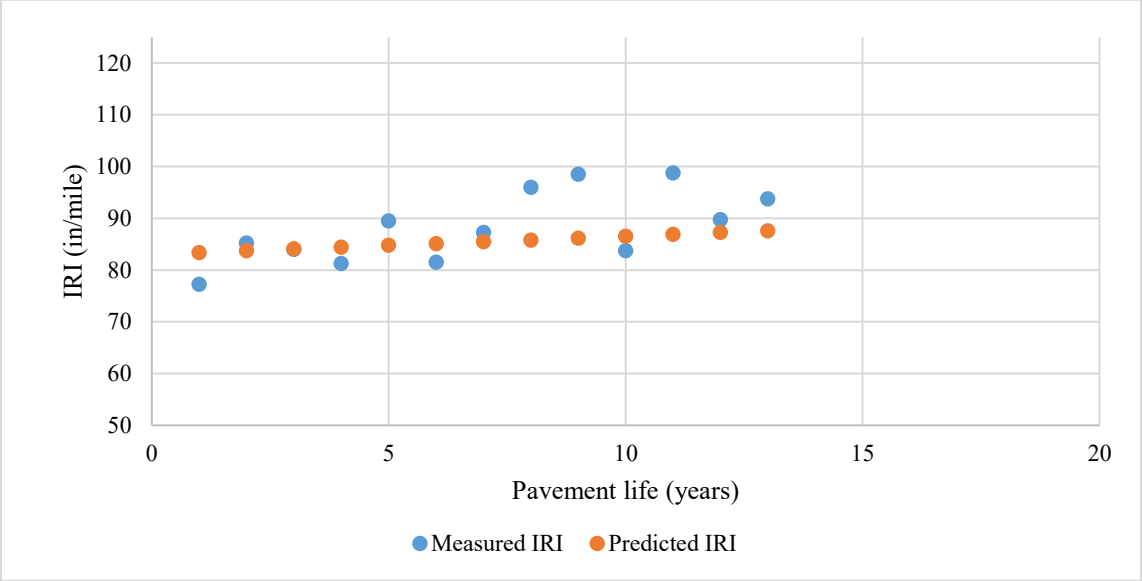


**Figure C-28: Measured and predicted data (locally calibrated) for transverse joint faulting and IRI for Project 018U0007700-NB**

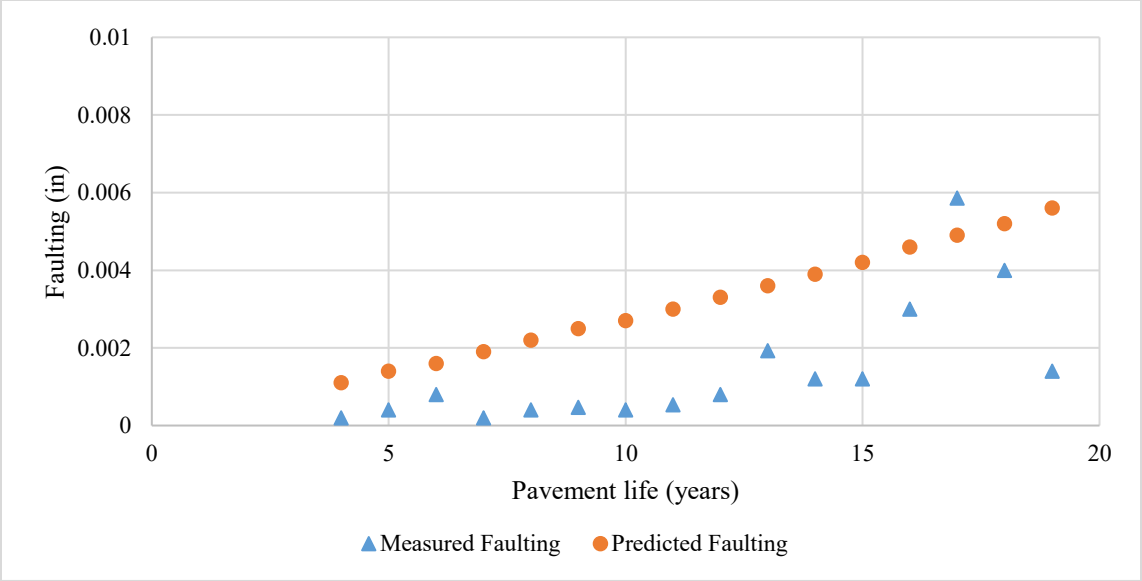


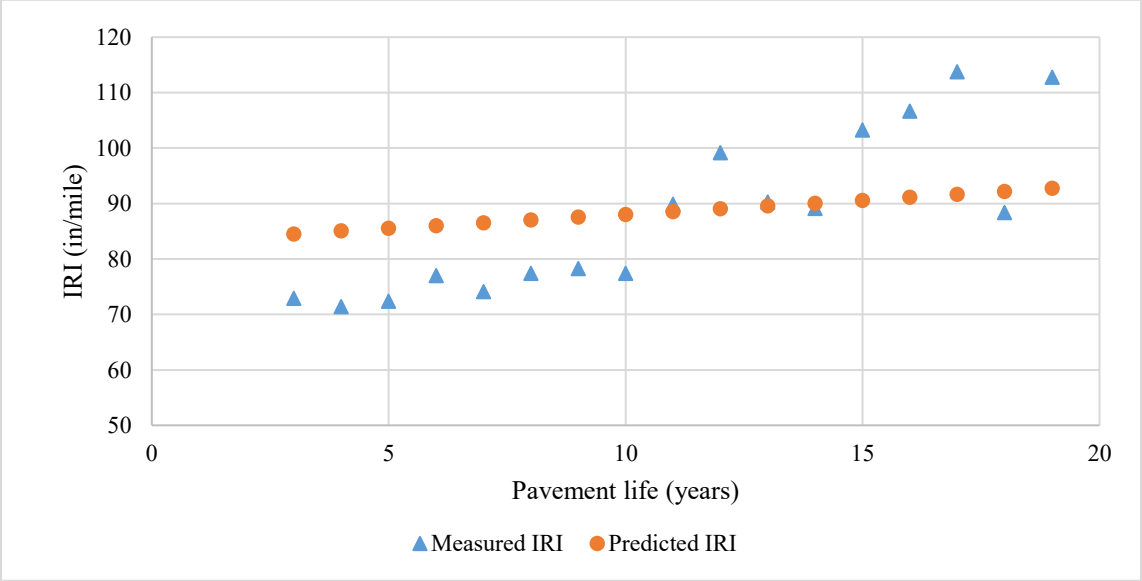


**Figure C-29: Measured and predicted data (locally calibrated) for transverse joint faulting and IRI for Project 043U0007500-NB-1**

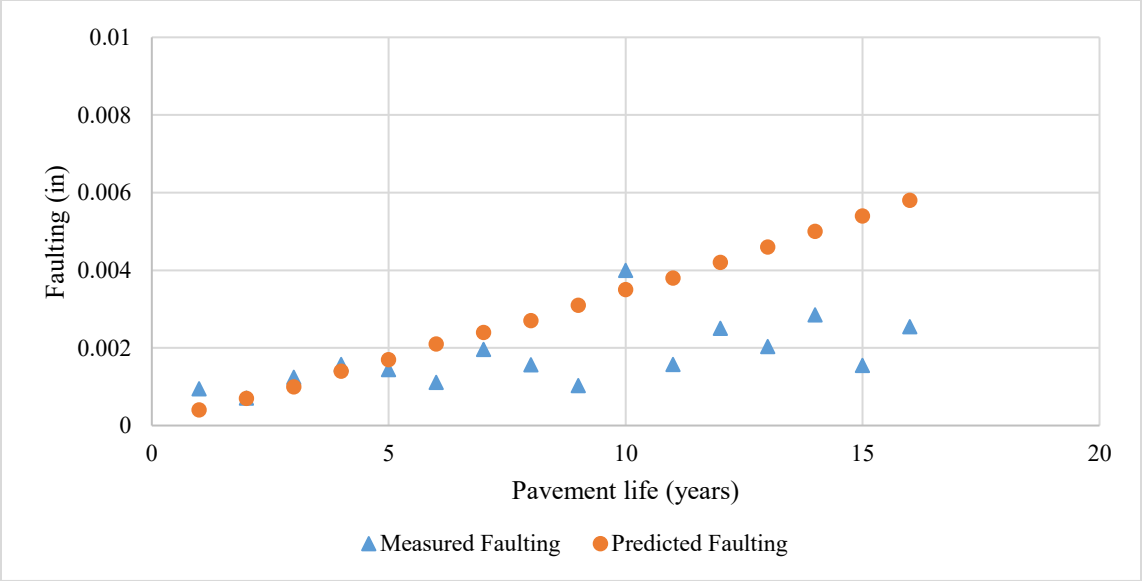


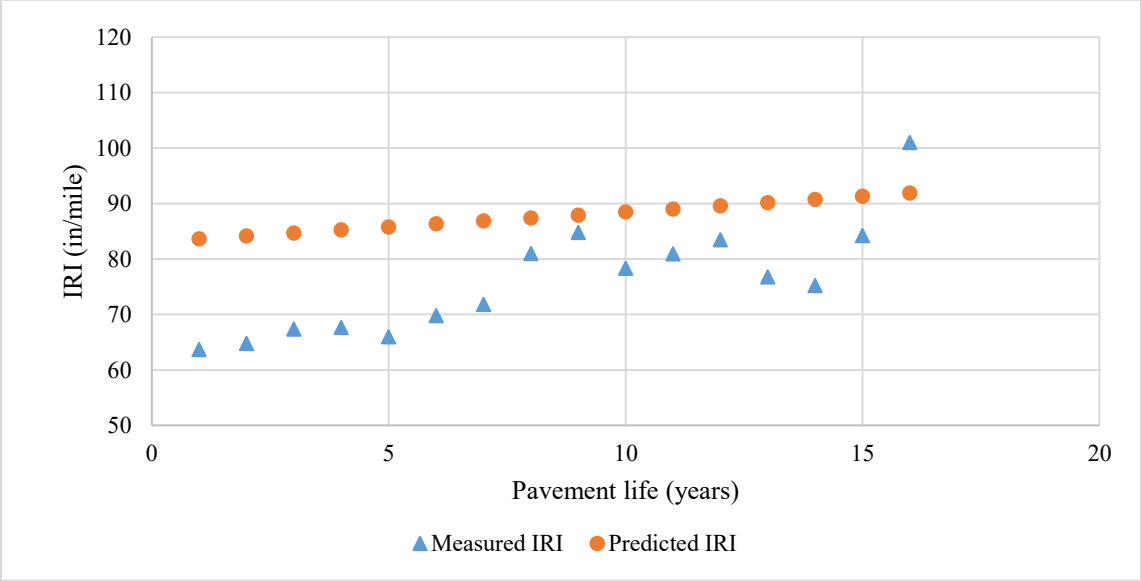


**Figure C-30: Measured and predicted data (locally calibrated) for transverse joint faulting and IRI for Project 043U0007500-NB-2**

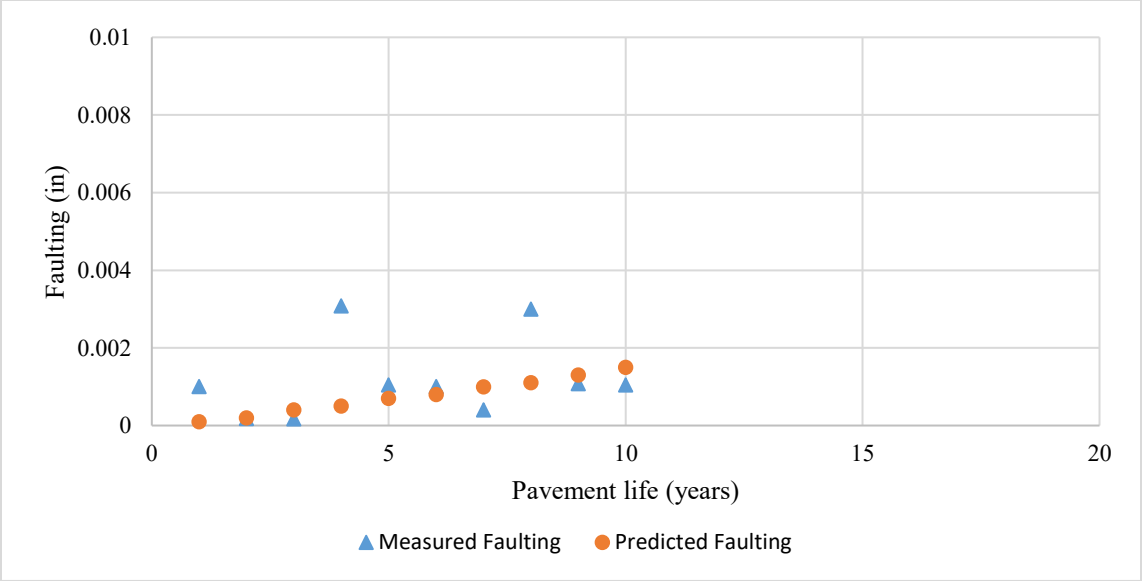


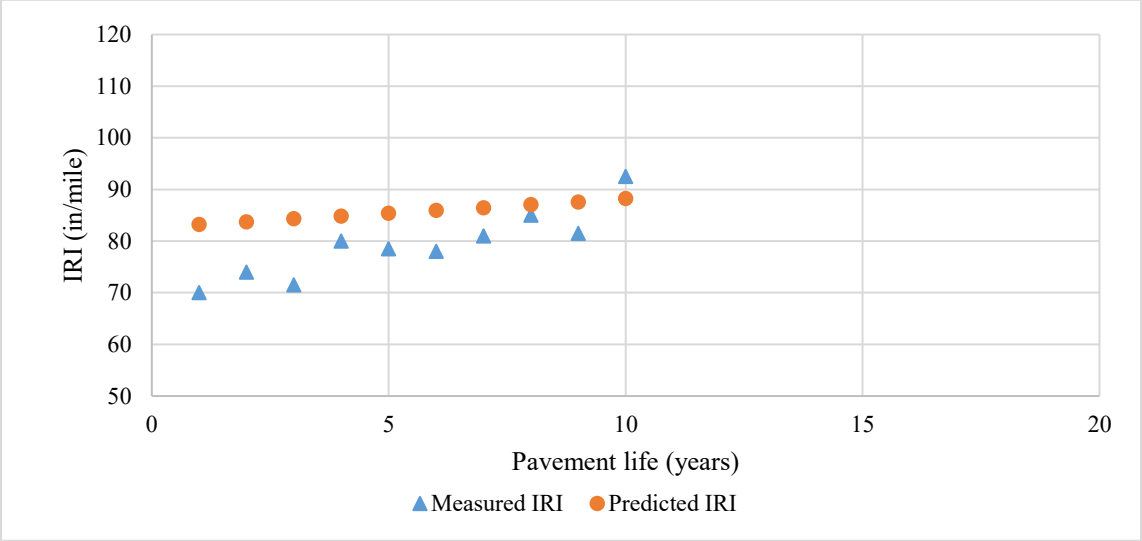


**Figure C-31: Measured and predicted data (locally validated) for transverse joint faulting and IRI for Project 055U0004000-WB**

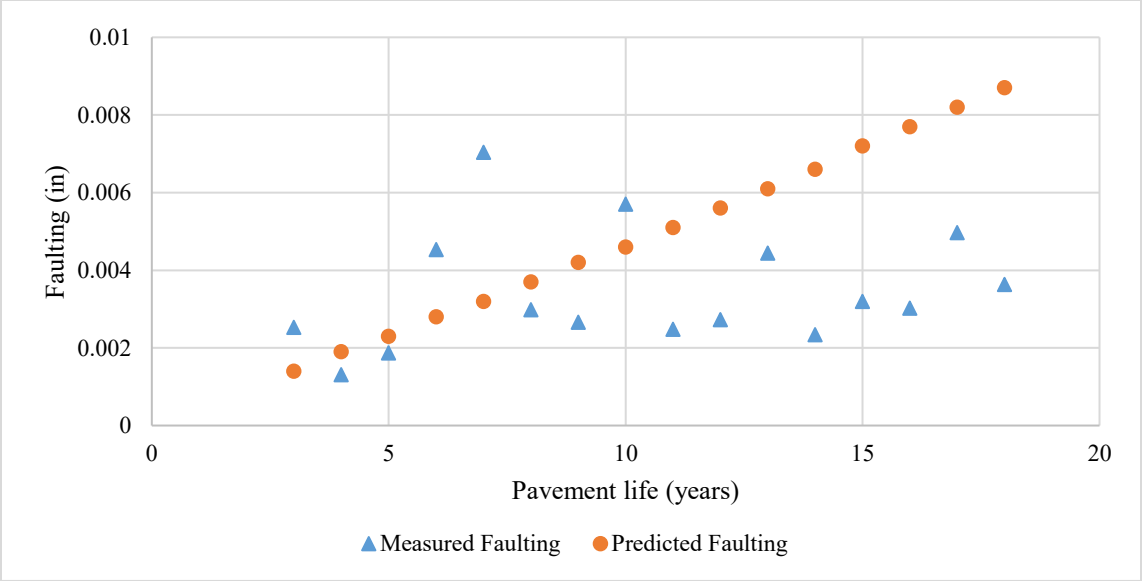


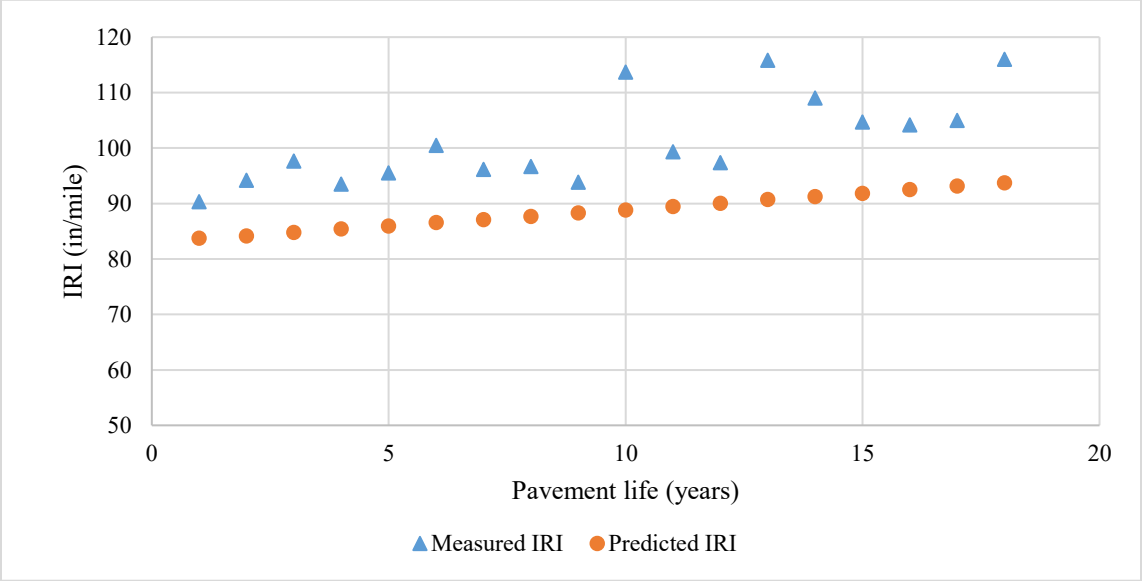


**Figure C-32: Measured and predicted data (locally calibrated) for transverse joint faulting and IRI for Project 056I0003500-SB-1**

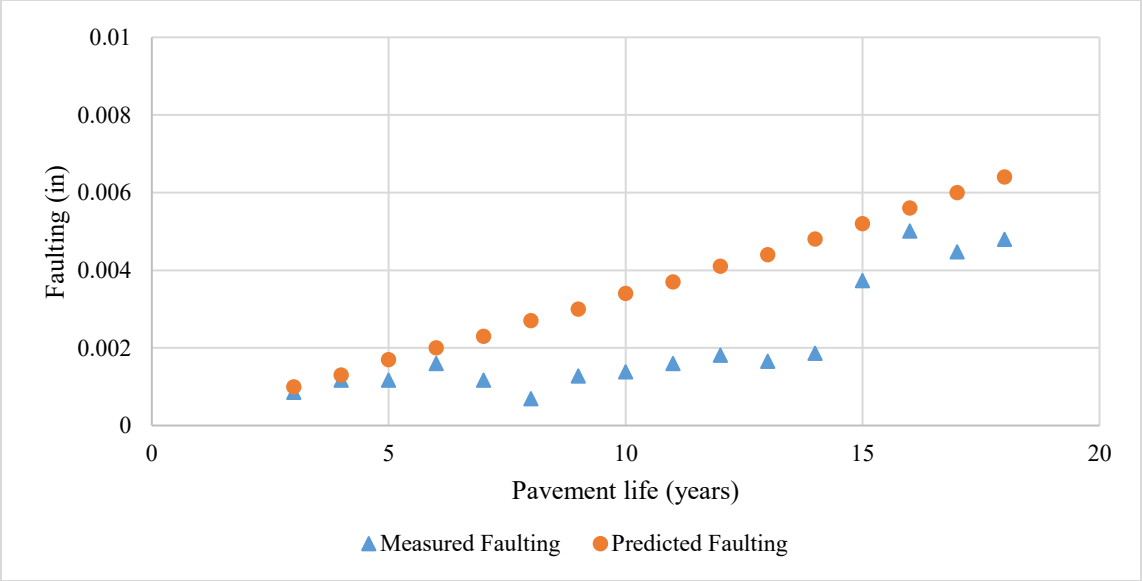


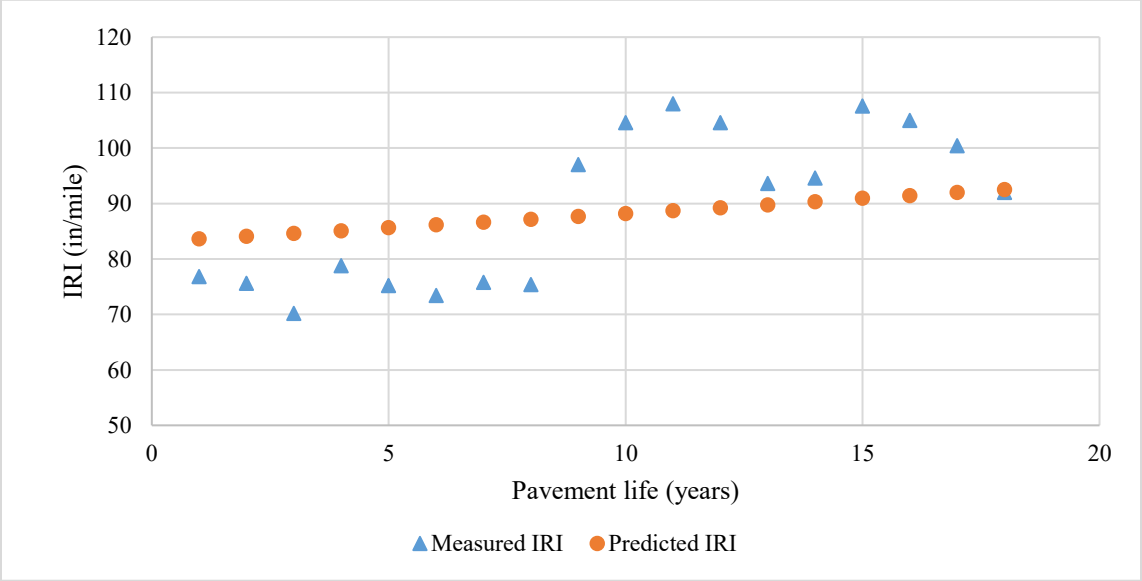


**Figure C-33: Measured and predicted data (locally calibrated) for transverse joint faulting and IRI for Project 056U0005000-EB-1**

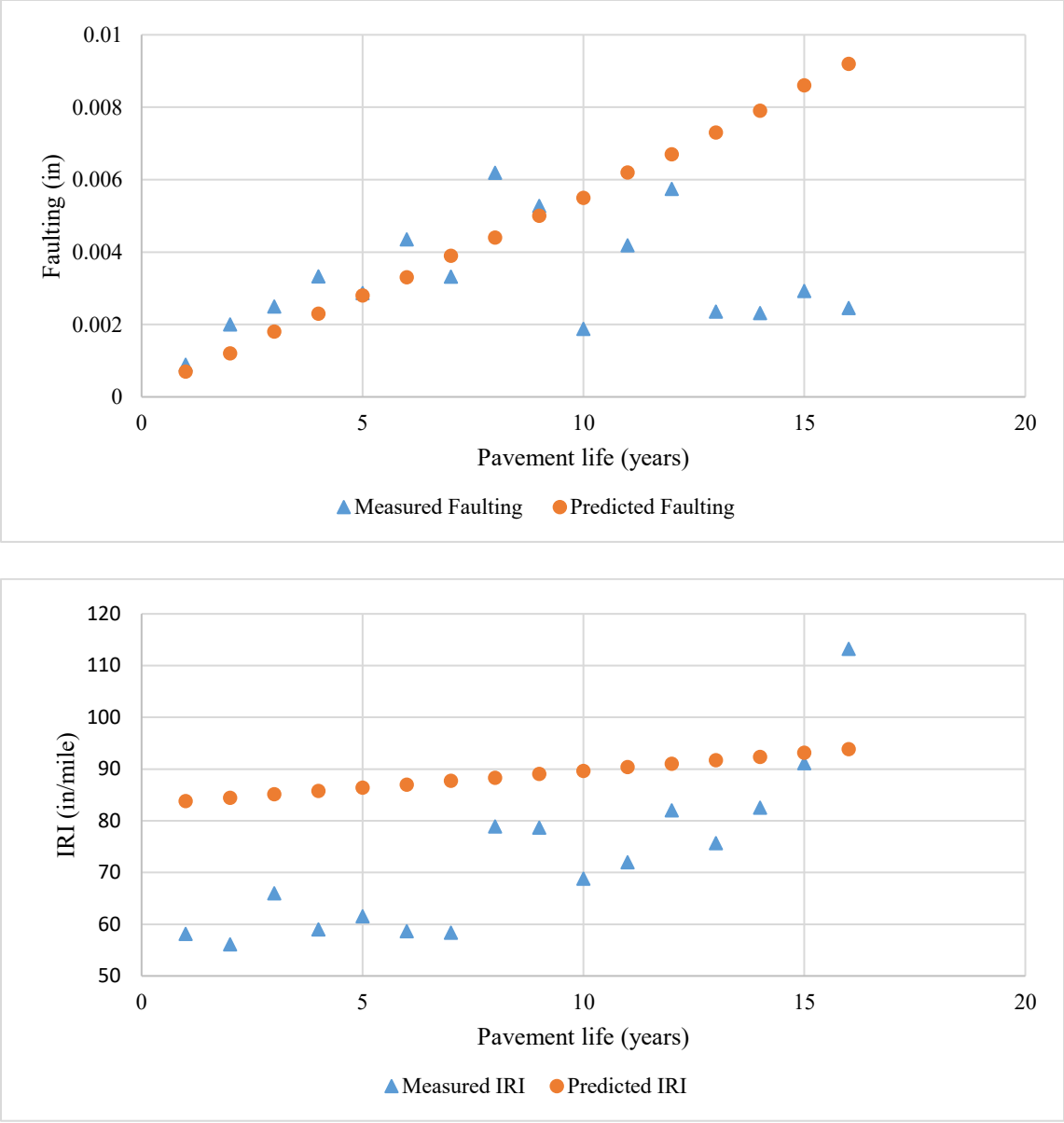


**Figure C-34: Measured and predicted data (locally calibrated) for transverse joint faulting and IRI for Project 059I0003500-NB**

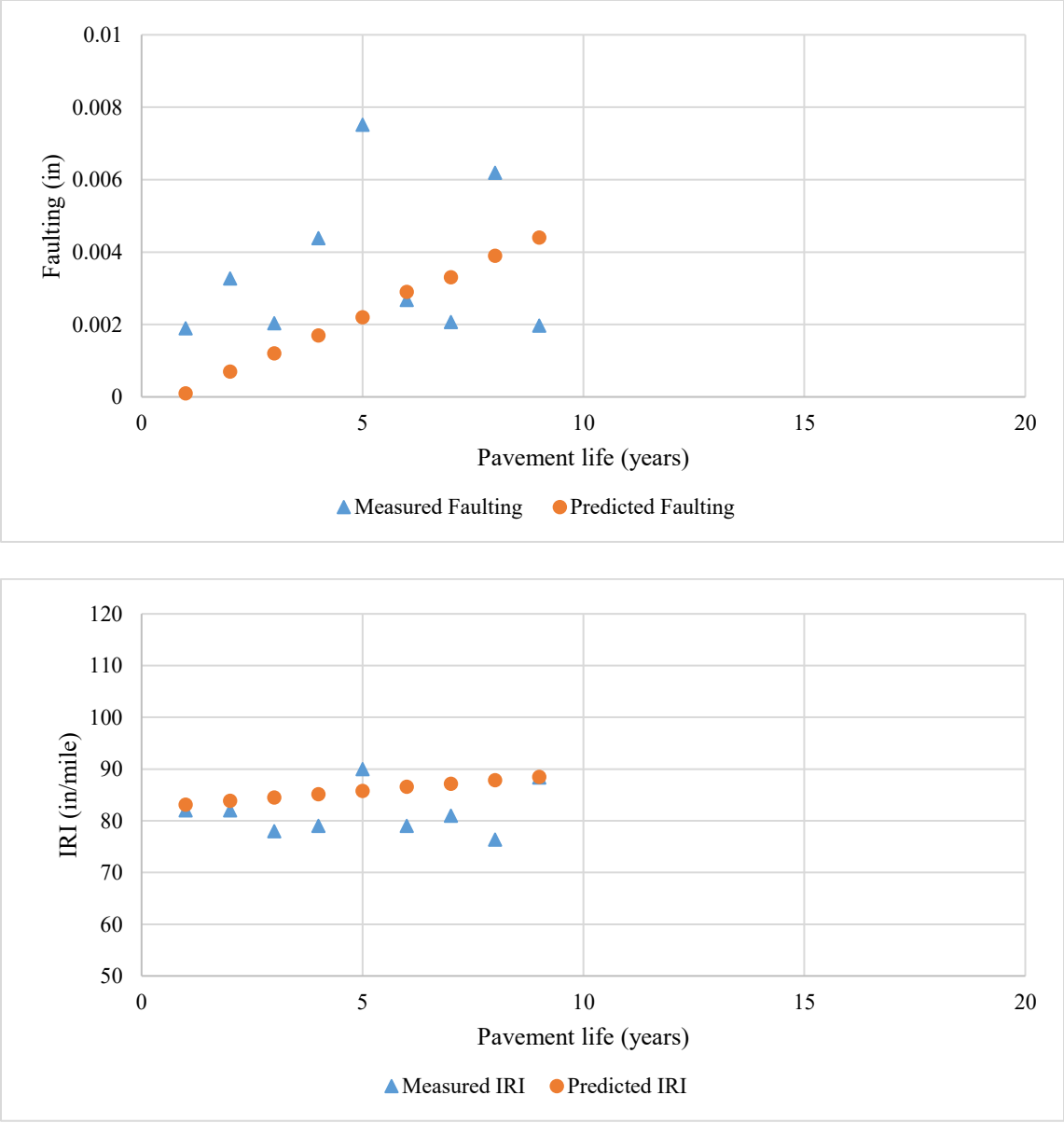


**Figure C-35: Measured and predicted data (locally calibrated) for transverse joint faulting and IRI for Project 061I0003500-NB**

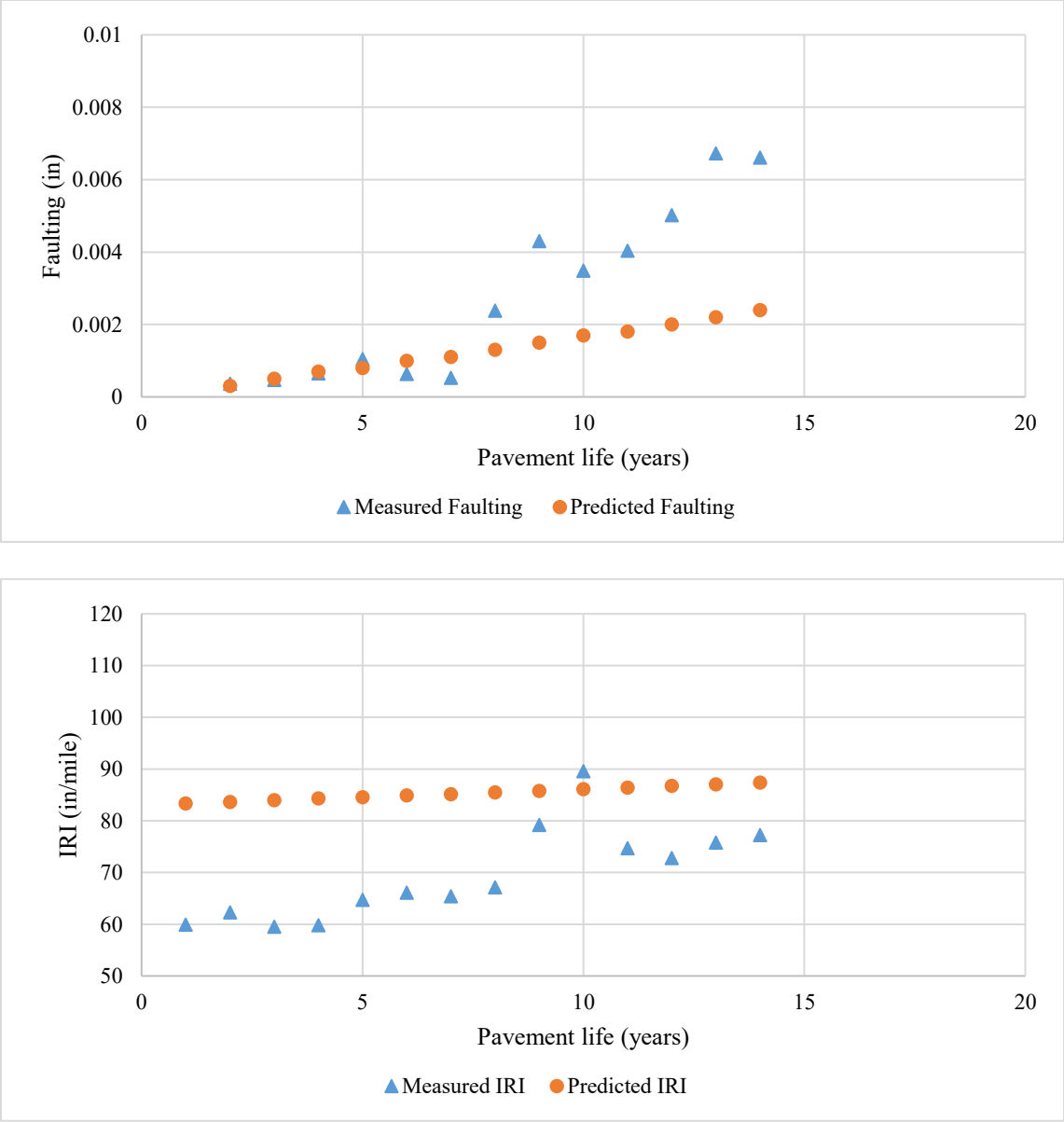


**Figure C-36: Measured and predicted data (locally calibrated) for transverse joint faulting and IRI for Project 063U004000-EB**

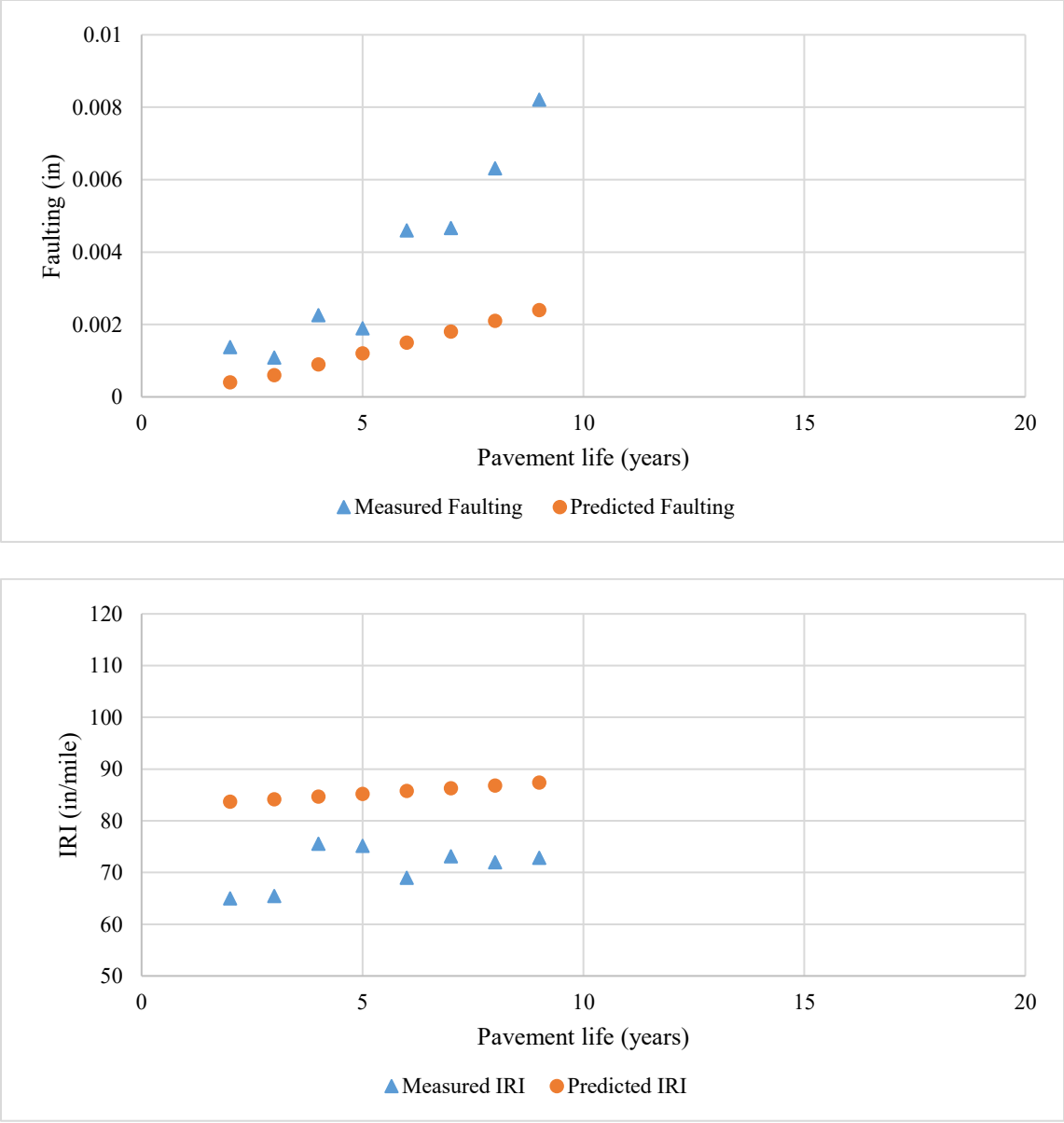


**Figure C-37: Measured and predicted data (locally calibrated) for transverse joint faulting and IRI for Project 067U0016900-NB**

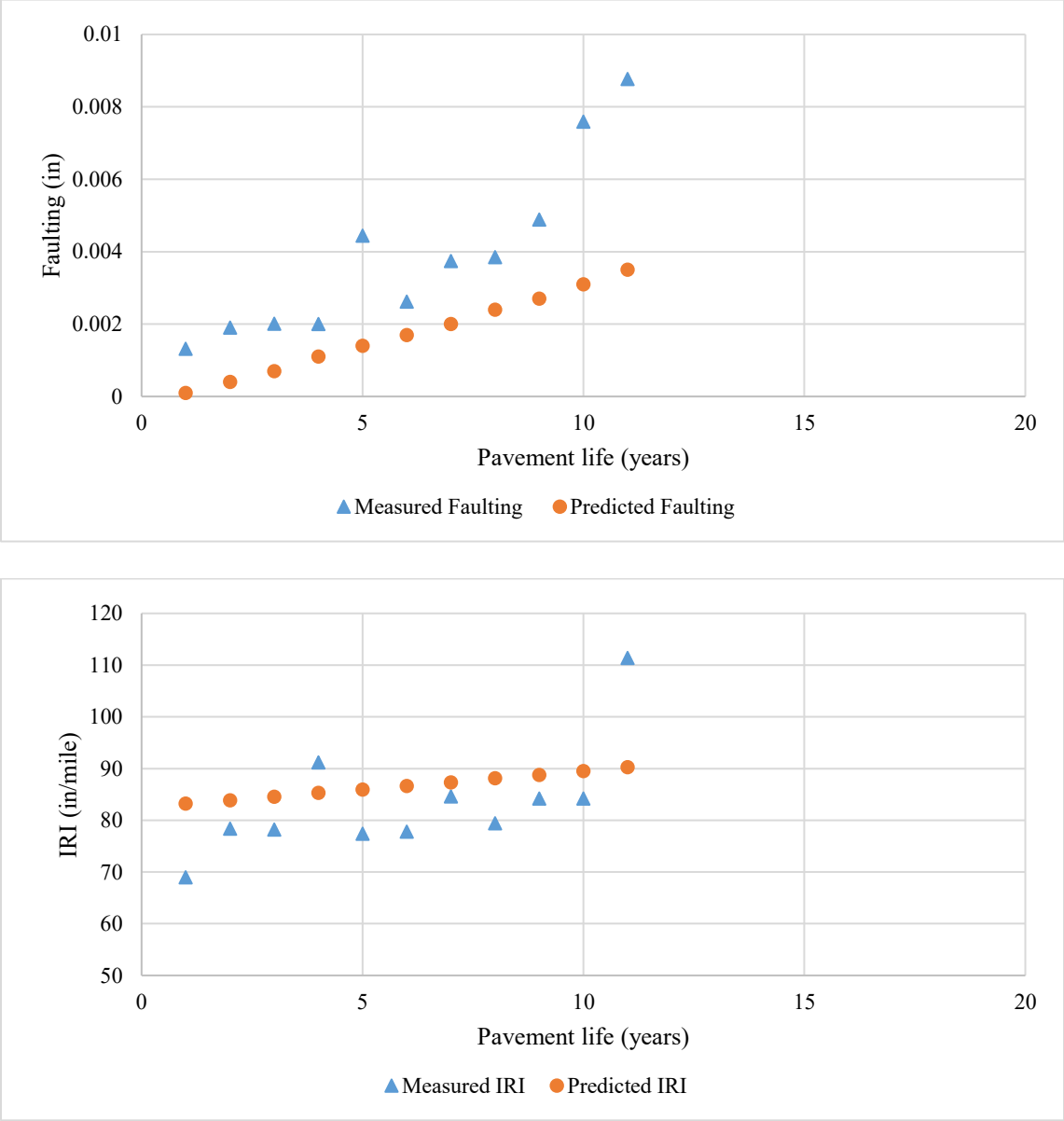


**Figure C-38: Measured and predicted data (locally calibrated) for transverse joint faulting and IRI for Project 079U008100-NB**

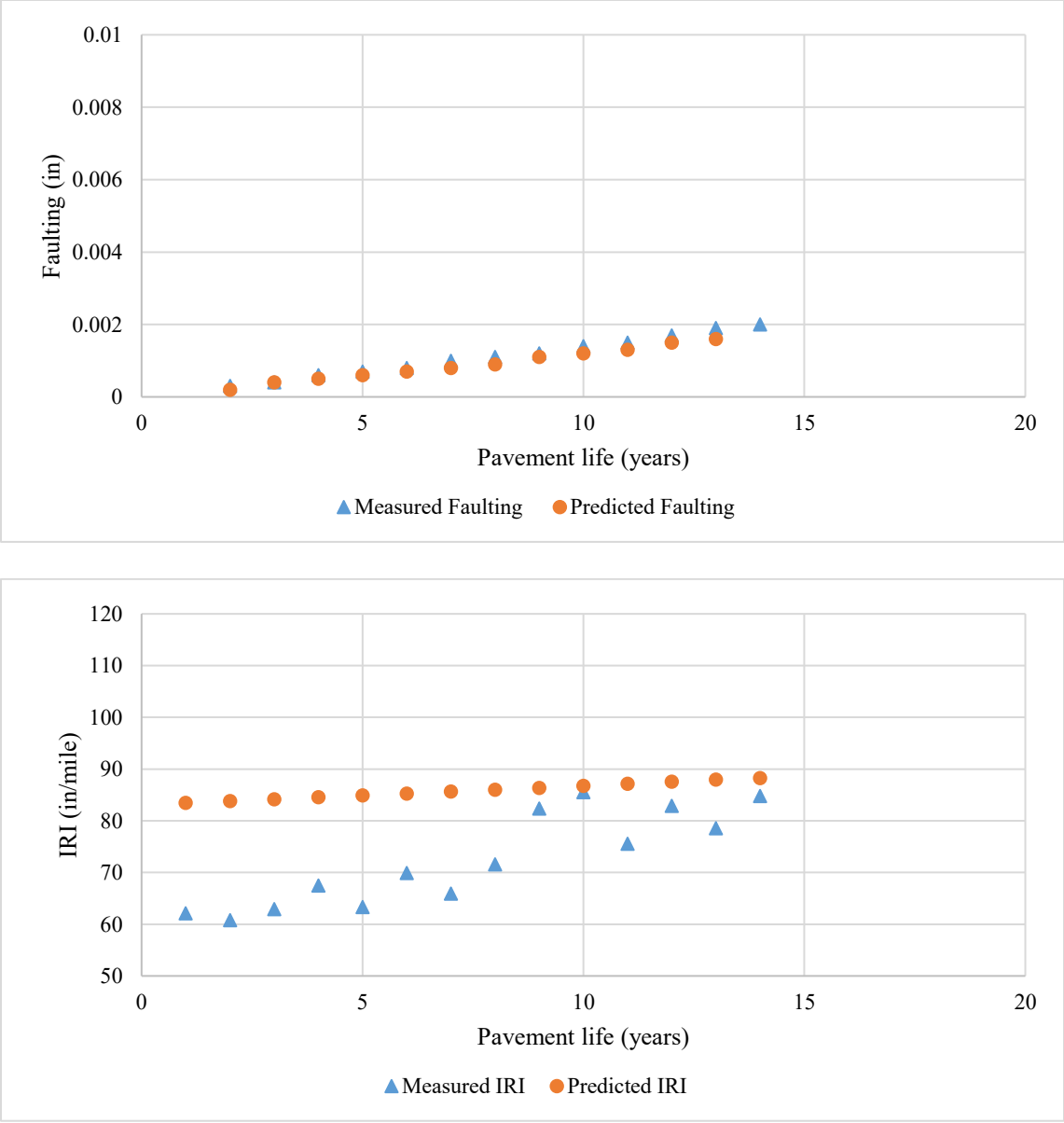


**Figure C-39: Measured and predicted data (locally calibrated) for transverse joint faulting and IRI for Project 103U0040000-EB**

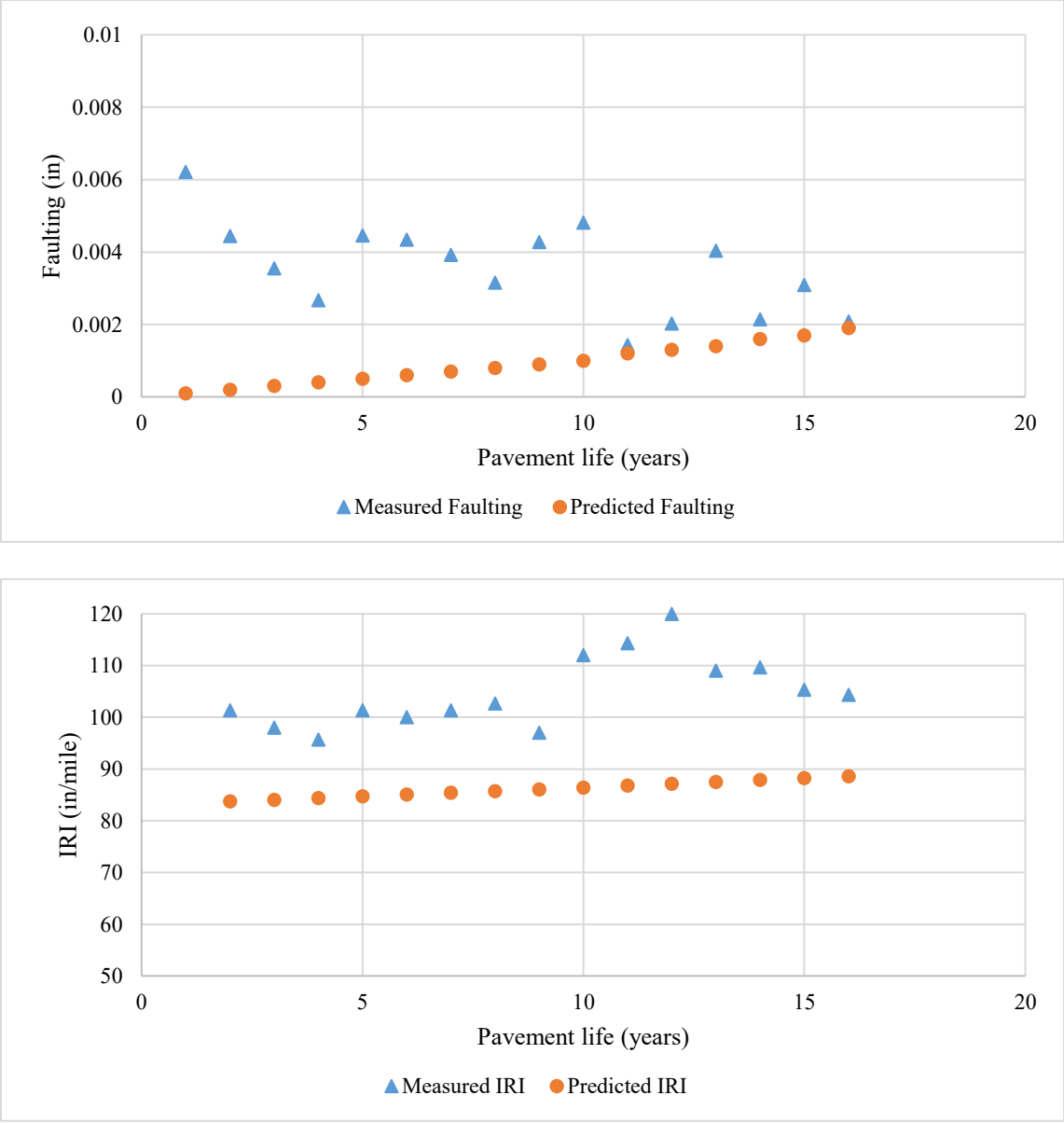


**Figure C-40: Measured and predicted data (locally calibrated) for transverse joint faulting and IRI for Project 018K0036000-EB**

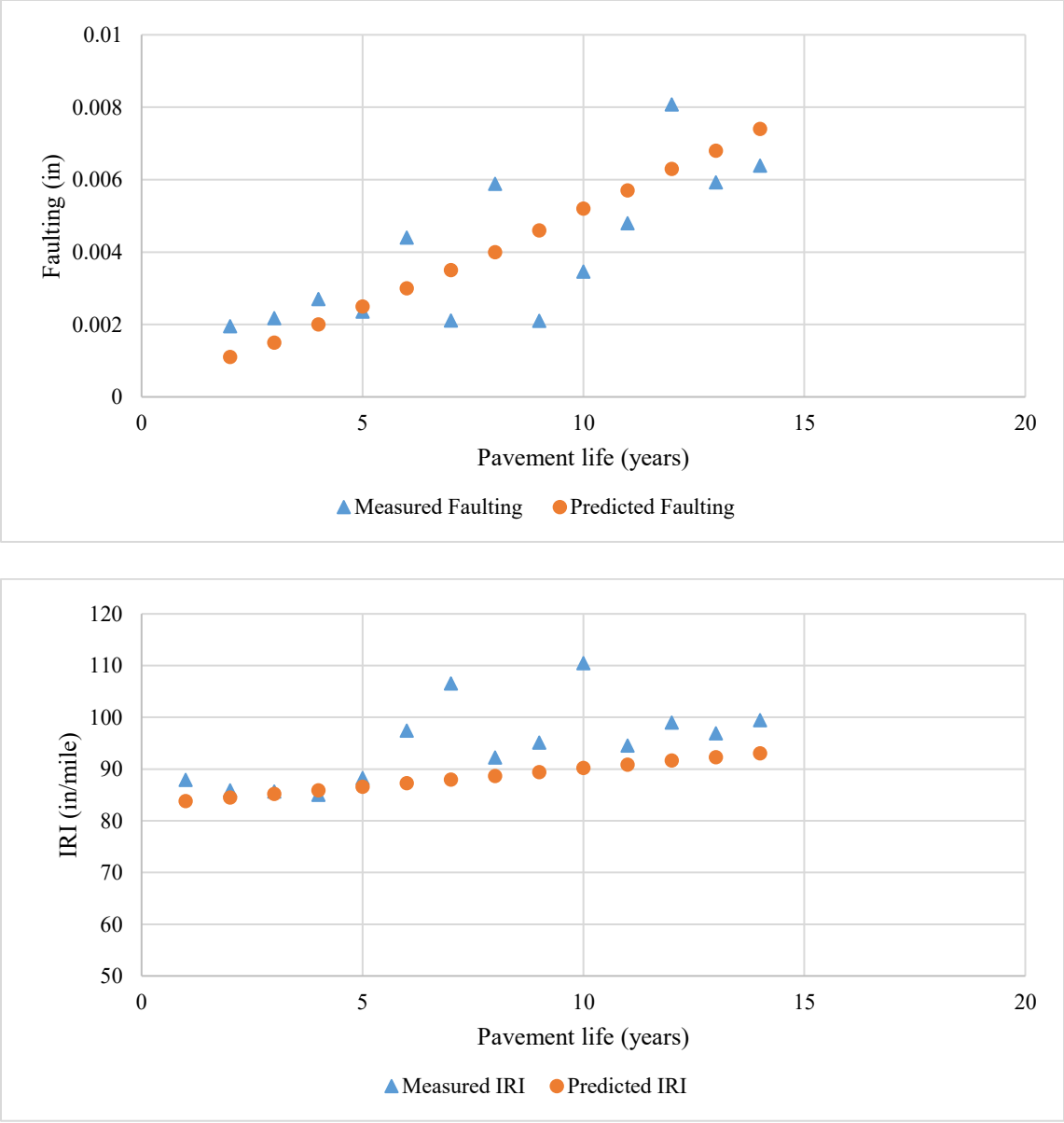


**Figure C-41: Measured and predicted data (locally calibrated) for transverse joint faulting and IRI for Project 031I0007000-EB**

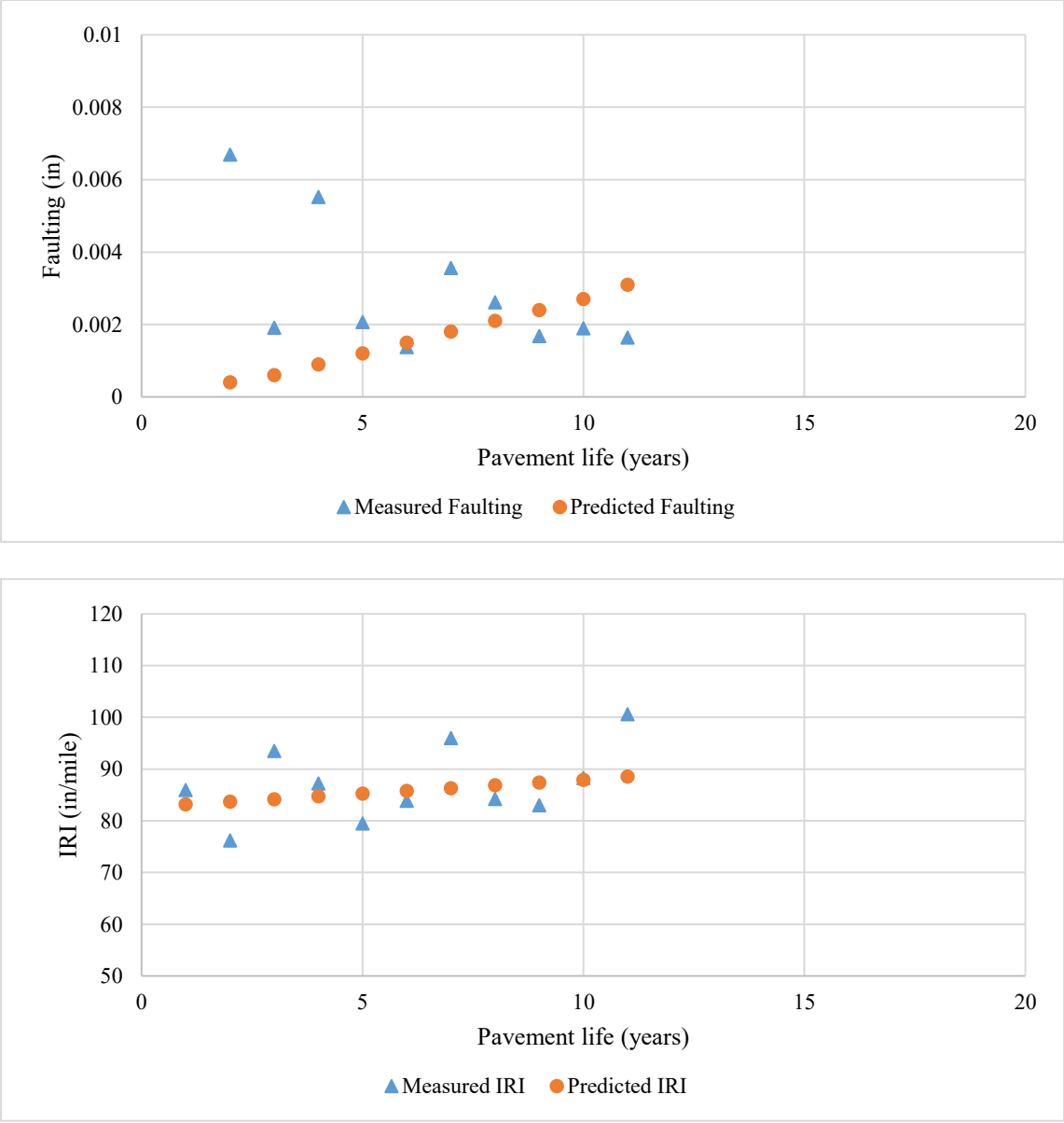


**Figure C-42: Measured and predicted data (locally calibrated) for transverse joint faulting and IRI for Project 040I0013500-NB-1**

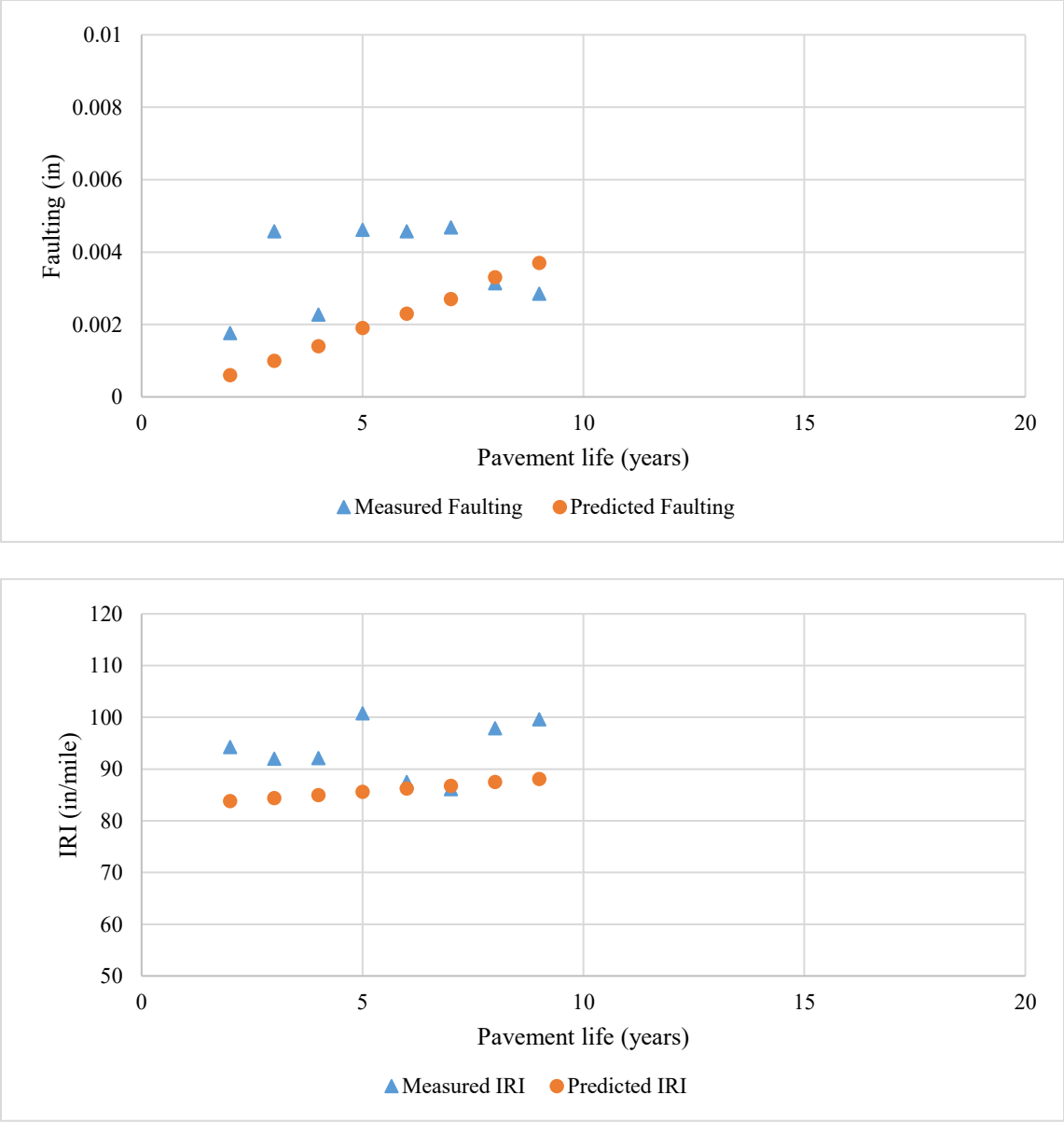


**Figure C-43: Measured and predicted data (locally calibrated) for transverse joint faulting and IRI for Project 040I0013500-NB-2**

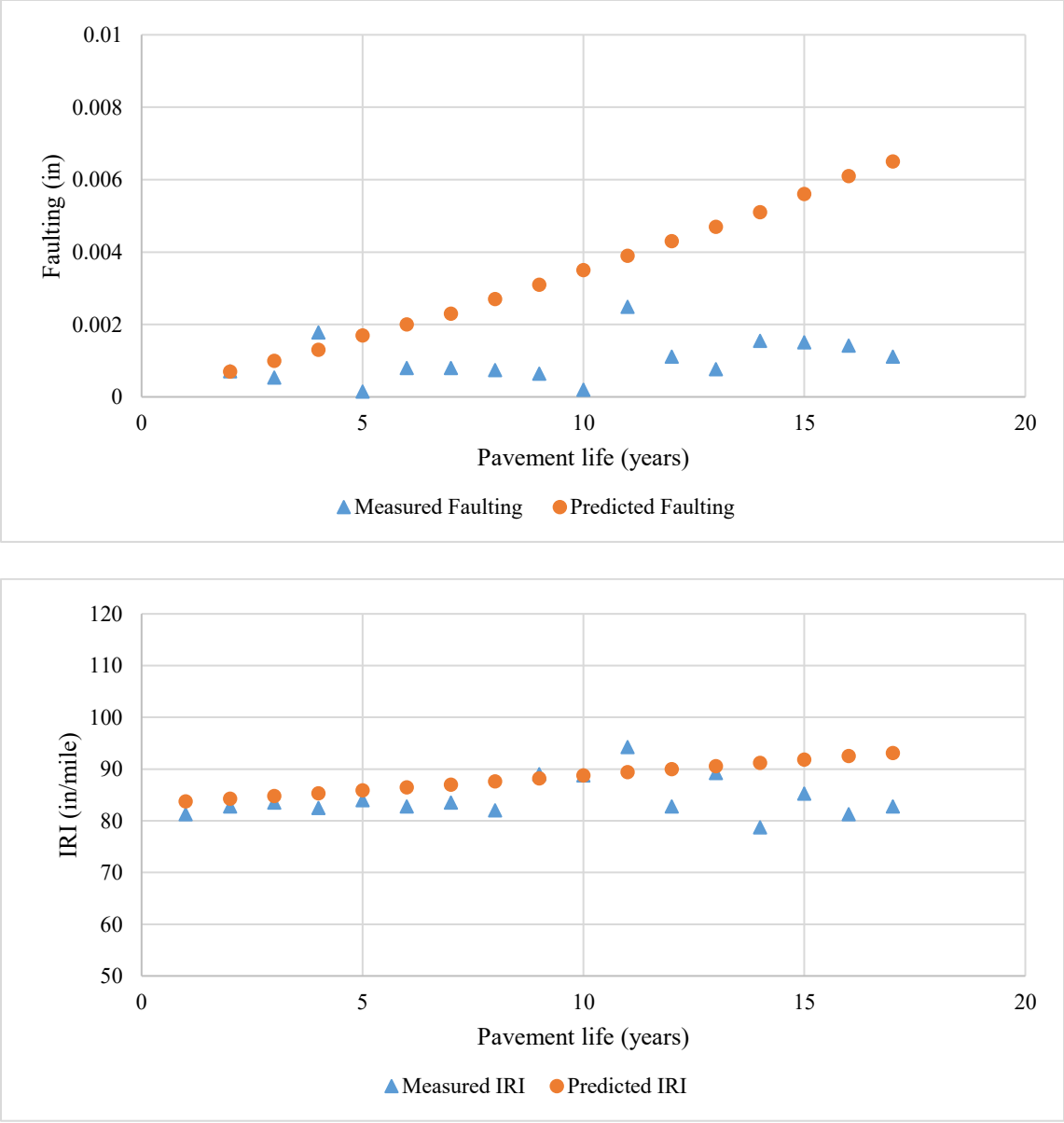


**Figure C-44: Measured and predicted data (locally calibrated) for transverse joint faulting and IRI for Project 046K0000700-SB**

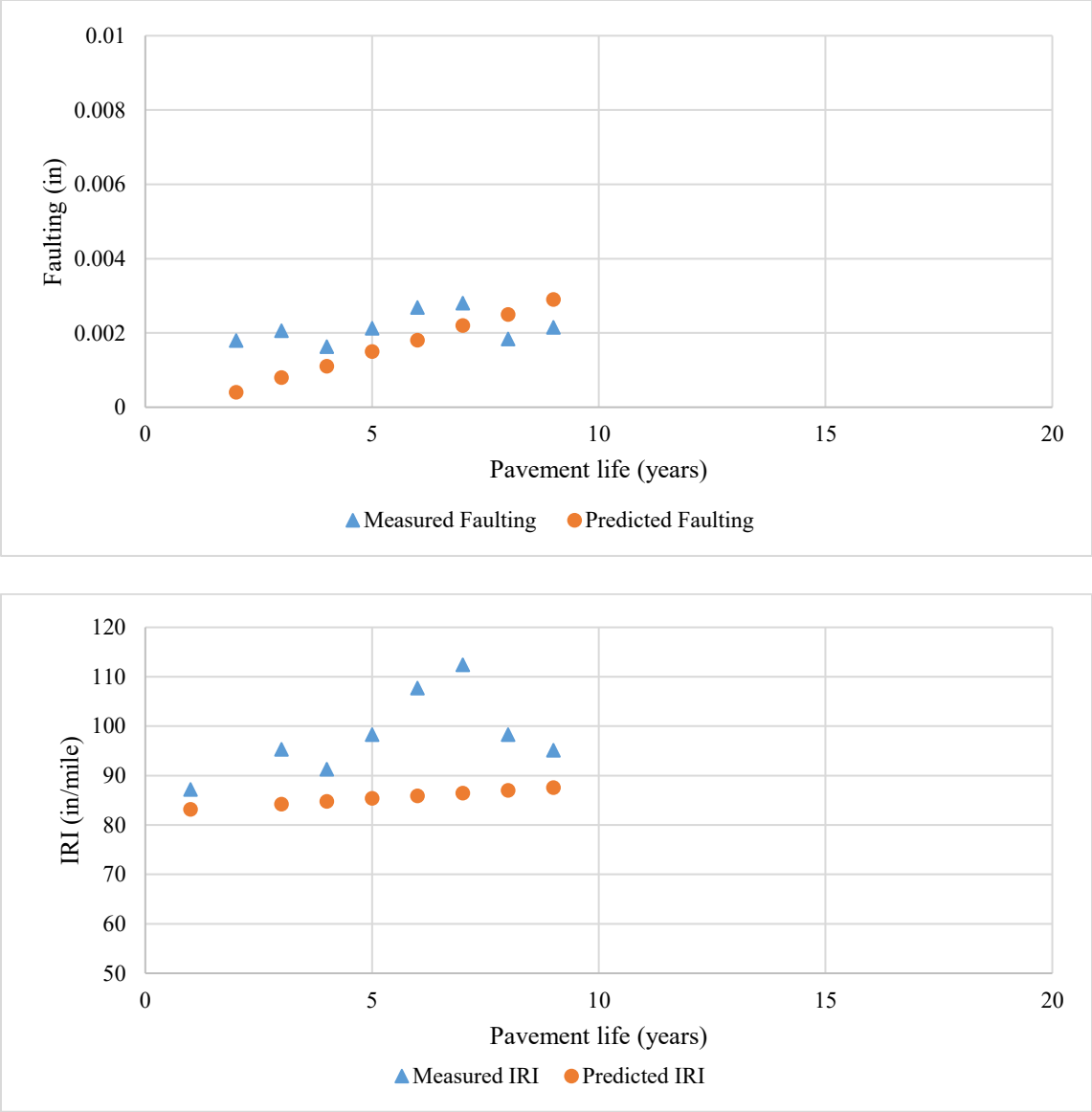


**Figure C-45: Measured and predicted data (locally calibrated) for transverse joint faulting and IRI for Project 085I0007000-EB**

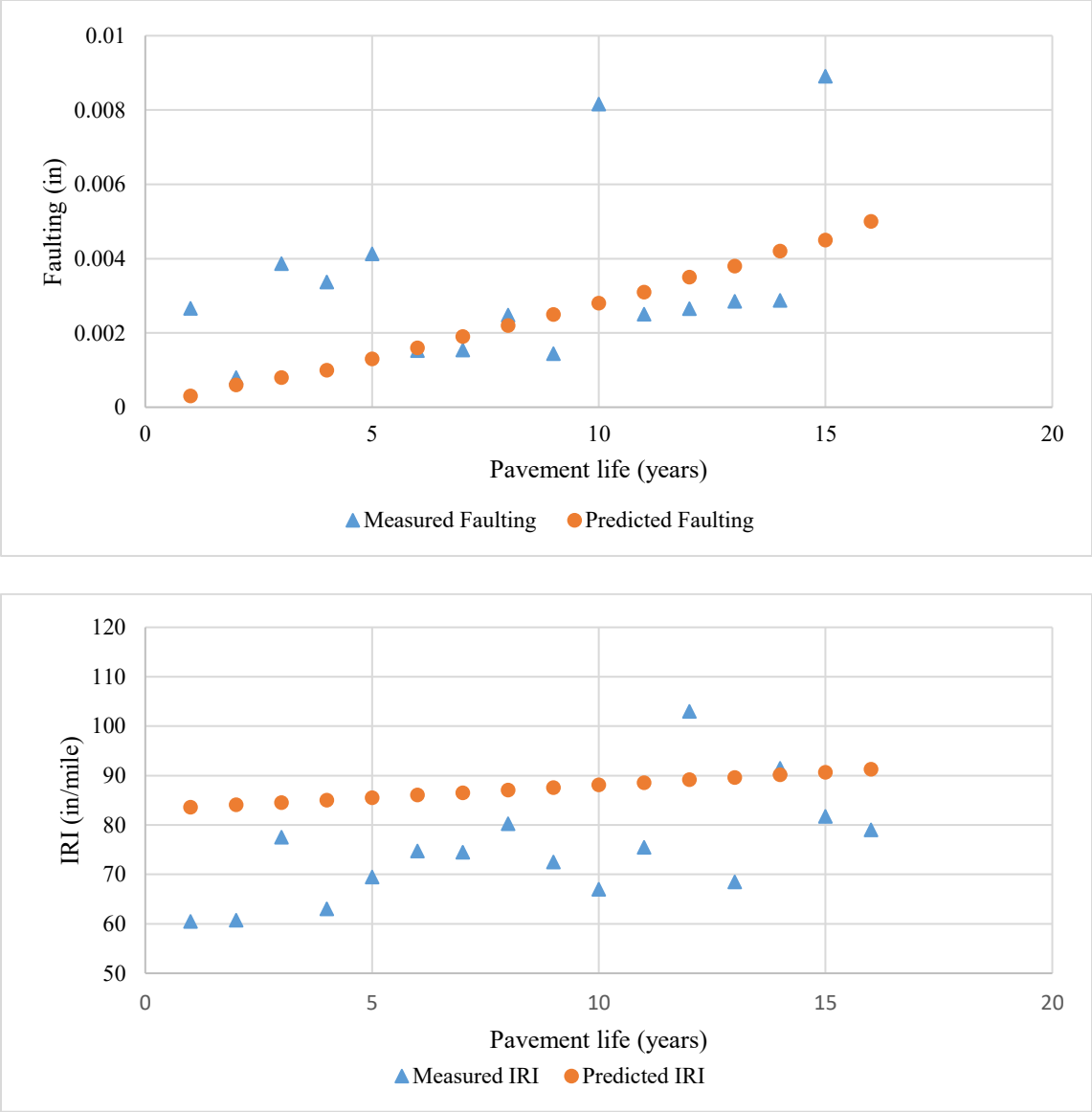


**Figure C-46: Measured and predicted data (locally validated) for transverse joint faulting and IRI for Project 029U000560000-EB**

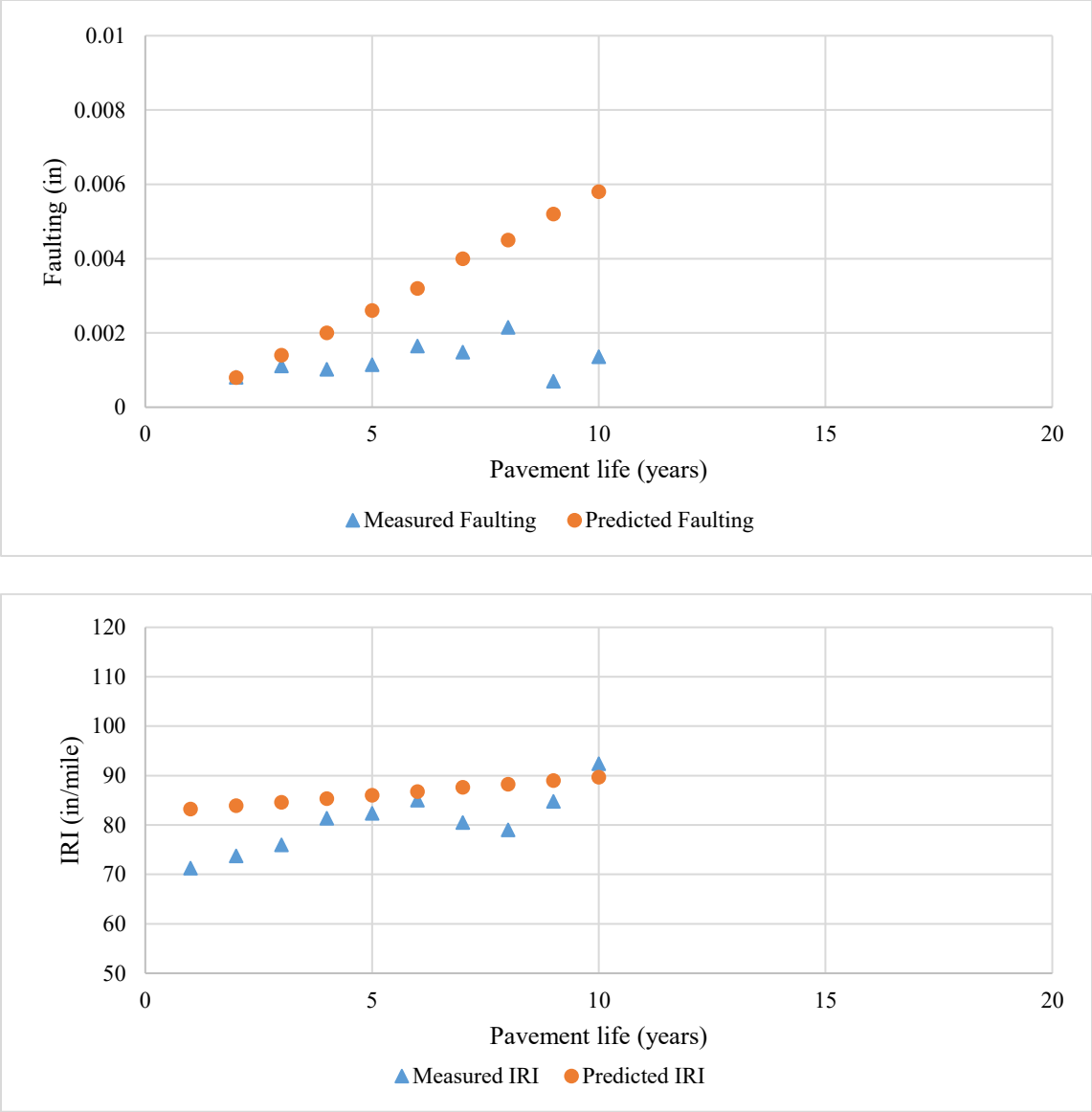


**Figure C-47: Measured and predicted data (locally validated) for transverse joint faulting and IRI for Project 030I0003500-NB-3**

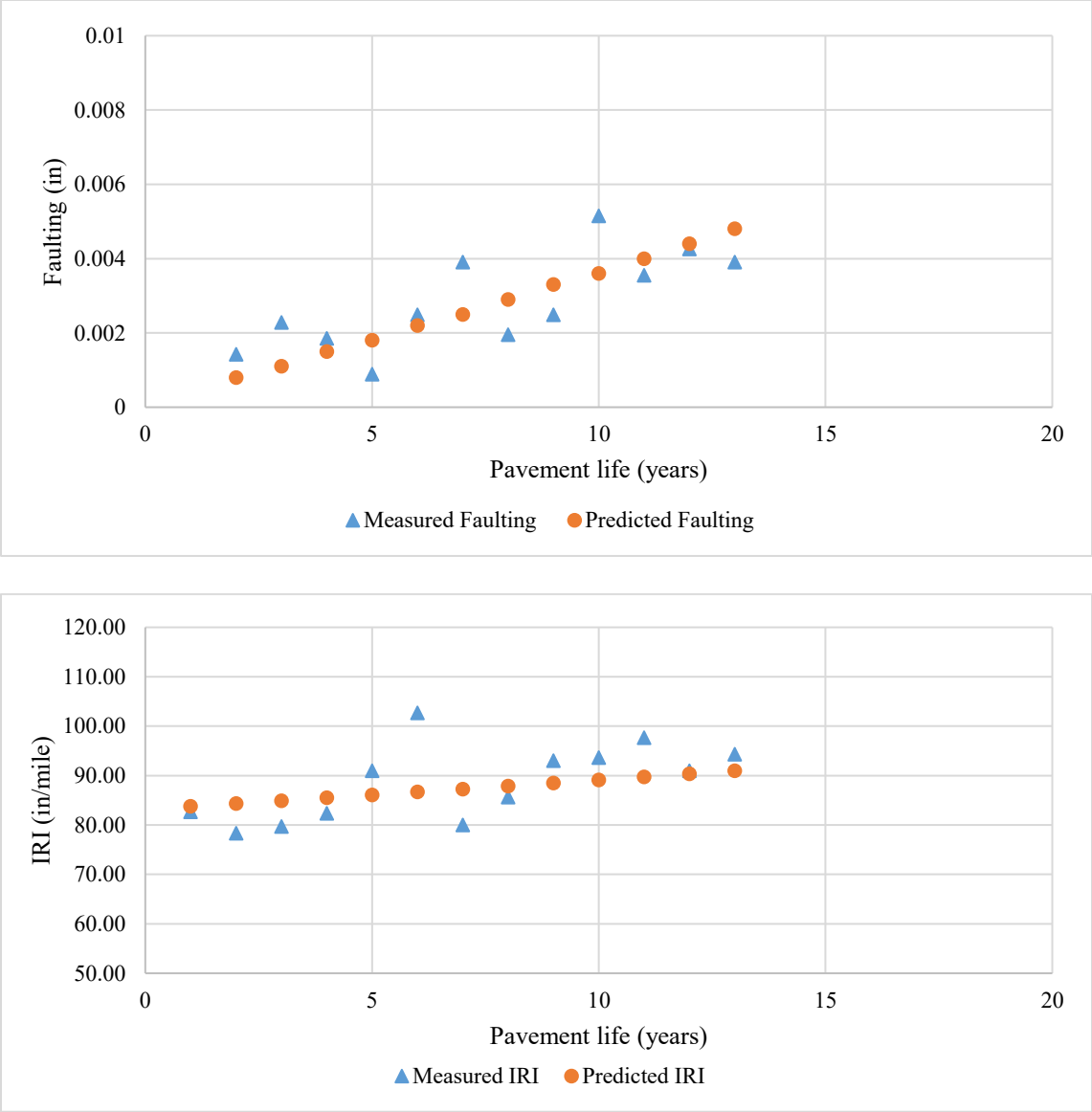


**Figure C-48: Measured and predicted data (locally validated) for transverse joint faulting and IRI for Project 099I0007000-EB-2**